NASA
Contractor Report 179643

AVSCOM
Technical Report 87-C-23

An Investigation of the Dynamic Response of Spur Gear Teeth With Moving Loads

C.E. Passereilo and L.W. Shuey
Michigan Technological University
Houghton, Michigan

August 1987

Prepared for
Lewis Research Center
Under Grant NAG3-344

National Aeronautics and
Space Administration

TABLE OF CONTENTS

1. INTRODUCTION

(1.1) Background

The topics of dynamic loading of gear teeth and the deflections of gear teeth due to dynamic loads have been treated extensively.

One such work, presented by Cornell and Westervelt [1], utilizes an improved version of a model developed by Richardson [4]. The model generates the dynamic loads for a meshing gear using a cantilever beam with a cam moving along it, simulating the engagement and disengagement of the adjacent tooth (see Figure 1-1). These dynamic loads are then used in a dynamic model of meshing gear teeth where the two gear hubs act as rigid inertia and the teeth as variable stiffness springs as shown in Figure 1-2. Of significant importance in this investigation is the claim made by the authors that the effect of variable tooth stiffness is small, changing the dynamic load response slightly compared to a system with constant tooth stiffness.

Another dynamic load response algorithm was developed by Wang and Cheng [2-3], where they reported that both the dynamic load and the induced dynamic response are highly dependent on the speed of the moving load. In slow speed regions, the dynamic load response is composed of a static response which varies with the stiffness of the tooth. Superimposed on the static is an oscillatory response caused by the excitation of the system at the resonant frequency. Wang states that as the speed of

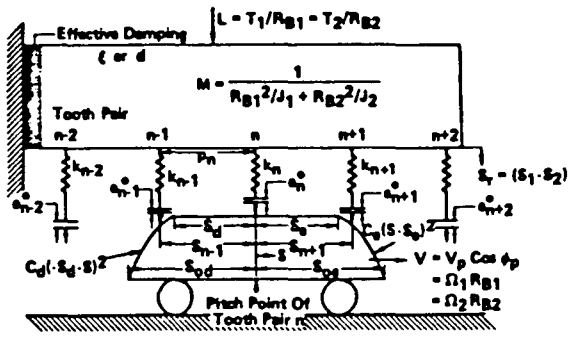

Figure 1-1: Dynamic load model

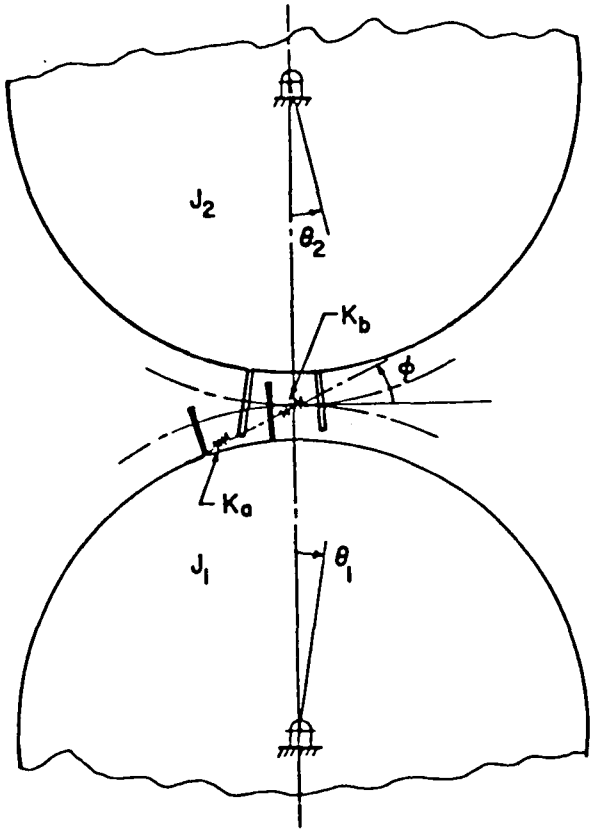

Figure 1-2: Dynamic model of meshing gears

the moving load increases and the resonant frequency of the system is approached, the dynamic load response becomes so abrupt that tooth separation occurs. A much smoother response is generated when the speed of the moving load is increased and becomes out of phase with the system resonance. Here the peak response is reduced significantly and actually becomes less than that for a static load. Examples of the dynamic load variation obtained by Wang and Cheng are included in Figure 1-3.

Kasuba [5] presents an algorithm which analyzes spur gearing under static and dynamic loading conditions. In his analysis, the stiffness of the teeth are determined by solving the statically indeterminant problem of multi-pair contacts, changes in contact ratio, and meshing gear deflections. in general, Kasuba states that to decrease the dynamic load response, increased damping and/or contact ratio can be used. He also noted that, in a general sense, high contact ratio gears have lower dynamic loads than low contact ratio gears.

Up to now, the discussion of models developed to determine the dynamic response of gear teeth has been limited to theoretical cases. Wallace [9] in his investigation, uses finite element analysis in conjunction with experimental techniques to study the deflection of gear teeth. He subjects a single tooth to both Hertzian impact and general dynamic loads, hoping to define a procedure for predicting deformation distributions due to dynamic loads. The finite element method shows good correlation with experimental results obtained using a short

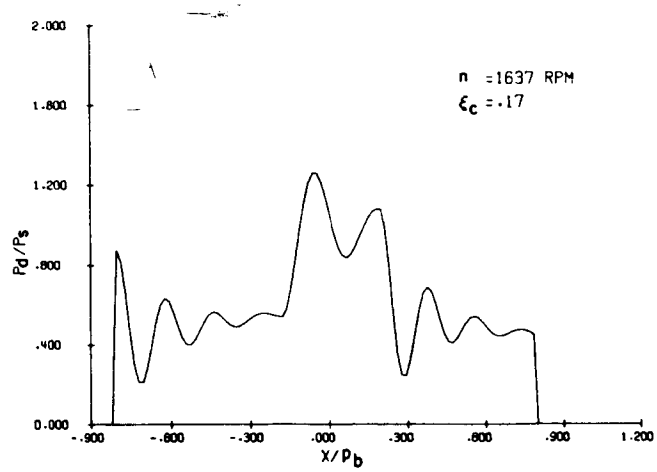

(a) Dynamic Load Variation, $r_G = 1$, $N_T = 28$, $D_p = 8$, D = .254 cm (.1 in.) *(a)* n = 1637 RPM, *(b)* n = 7640 RPM, and *(c)* n = 16370 RPM

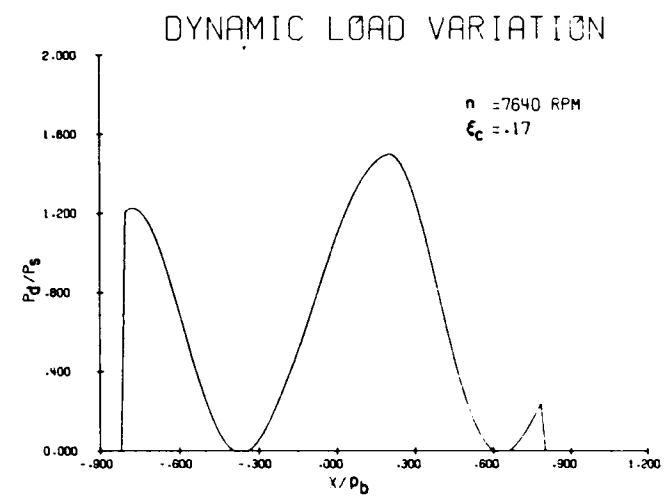

(b) Dynamic Load Variation, $r_G = 1$, $N_T = 28$, $D_p = 8$, $D = .254$ cm (.1 in.) *(a)* n = 1637 RPM, *(b)* n = 7640 RPM, and *(c)* n = 16370 RPM

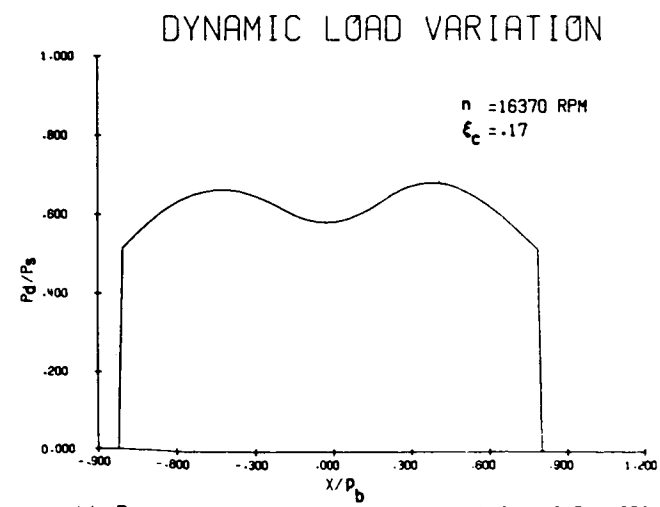

(c) Dynamic Load Variation, $r_G = 1$, $N_T = 28$, $D_p = 8$, $D = .254$ cm (.1 in.) *(a)* n = 16370 RPM, *(b)* n = 7640 RPM, and *(c)* n = 16370 RPM

Figure 1-3

cantilever beam subjected to impact loadings at different positions.

Another important contribution to the subject of gear dynamics was made by Attia [6]. He studied the effects of including the rim when performing a static analysis to determine tooth spring constants. He concluded that the stiffness of teeth with the rim included is significantly less compared to a variable cross-section cantilever beam rigidly fixed to the gear body. With the added flexibility, the initial conditions of two meshing teeth are highly dependent on the deflections of the two previously engaging teeth. This fact is very significant, as it will definitely affect the type of load experienced by the upcoming gear pair.

Many of the theoretical models used to predict the deflections of gear teeth, such as those presented by Cornell [1], Wang [2-3] and Kasuba [5], make use of tooth stiffness variations obtained from a static deflection analysis. The equations of motion are expressed as functions of the load position only.

Nagaya and Uematsu [7] state that because the contact point moves along the involute, the dynamic load response should be considered as a function of both the position and speed of the moving load. In their analysis, they approximate the deflections of actual gear teeth due to moving loads by modelling the tooth as a tapered Timoshenko beam. They present plots of normalized centerline deflections for different moving load speeds, and claim that dynamic stiffness variations can be

derived from their results. However, as illustrated later, this claim turns out to be false.

In order to make the theoretical developments of models used to determine the dynamic response of gear teeth more practical, some assumptions are made. One such assumption made by the first three authors presented, is that the mass of the gear tooth compared to the gear body is small and can be neglected. Literature gives no hints to whether this assumption has been thoroughly investigated.

(1.2) Problem Statement

In this study, two basic problems are investigated. The first phase is to determine whether the dynamic response of a single spur gear tooth is dependent on the speed of a moving load acting on the tooth.

The second phase is an investigation to determine the significance of omitting the inertia of the gear tooth from the dynamic deflection model due to the small mass relative to the gear body.

(1.3) Scope of Work

A model based on involute geometry is developed to automatically generate a spur gear tooth profile and finite element mesh, including the rim, using a minimum of input parameters. This model is then used to determine the effects of the speed of a moving load on the deflection of a single gear tooth. Two constraint configurations are tested; one where only the involute profile and fillet regions are allowed to deform, the

other with the entire rim included. The results are first represented as normalized deflections of the tooth centerline. Then the tooth tip deflection time histories are studied for the entire load cycle.

The second phase of the work is to model a meshing gear tooth pair using two cantilever beams attached to moveable foundation masses. Relative displacements of the foundation masses as well as beam deflections are determined for moving load speeds bracketing the system resonant frequency.

2. MODEL DEVELOPMENT

In order to effectively perform a static and dynamic analysis of spur gear teeth using finite element techniques, a model is needed to automatically generate a tooth profile and the accompanying finite element mesh for different size gear teeth. Also, the geometry of the tooth should be defined using a minimum of parameters corresponding to those most generally specified when generating a tooth profile. One such list of parameters is:

Pressure Angle	= θp
Pitch Radius	= RP
Addendum	= AD
Dedendum	= DED
Circular Pitch	= CIRP
Backlash	= BACKL
Fillet Radius	= RF
Rim Thickness	= RTH

With these parameters, the profile of any spur gear tooth can be generated including the rim.

In the proceeding sections, the equations necessary to construct the tooth profile using the preceeding parameters are developed, including the implementation of these relationships in a profile generation algorithm. The topic of finite element mesh generation is also discussed, along with an overview of the mesh generation algorithm used to generate the grid.

Later in this chapter, a brief discussion of the plane strain finite element type used to model the gear is included. Also, a general treatment of a linear quadrilateral element is used to help develop equations describing the moving loads used on the gear teeth. These relations are then implemented in a moving load generation algorithm using idealized load time history equations for a spur gear tooth.

(2.1) Profile Generation

The profile generation sequence is divided into three sections; determining relationships, first for the involute, then for the fillet, and finally for the rim.

(2.1.1) Involute Generation

An involute curve is generated by unwrapping an inextensible cord from a cylinder. Figure 2-1 illustrates that as the cord is unwrapped from the cylinder, point B on the cord traces an involute curve AC. The radius of curvature of the involute varies continuously, being a zero at point A and increasing towards C. At the instant shown, the radius is equal to BE, as point E corresponds to the instantaneous center of rotation about point B. When generating the involute of a spur gear tooth, the cylinder from which the cord is unwrapped corresponds to the base circle. This concept is further developed as shown in Figure 2-2. Here the local coordinate system X-Y, fixed to the hub at the base circle, is used to determine relative coordinates along the involute. The parameters shown are; the base

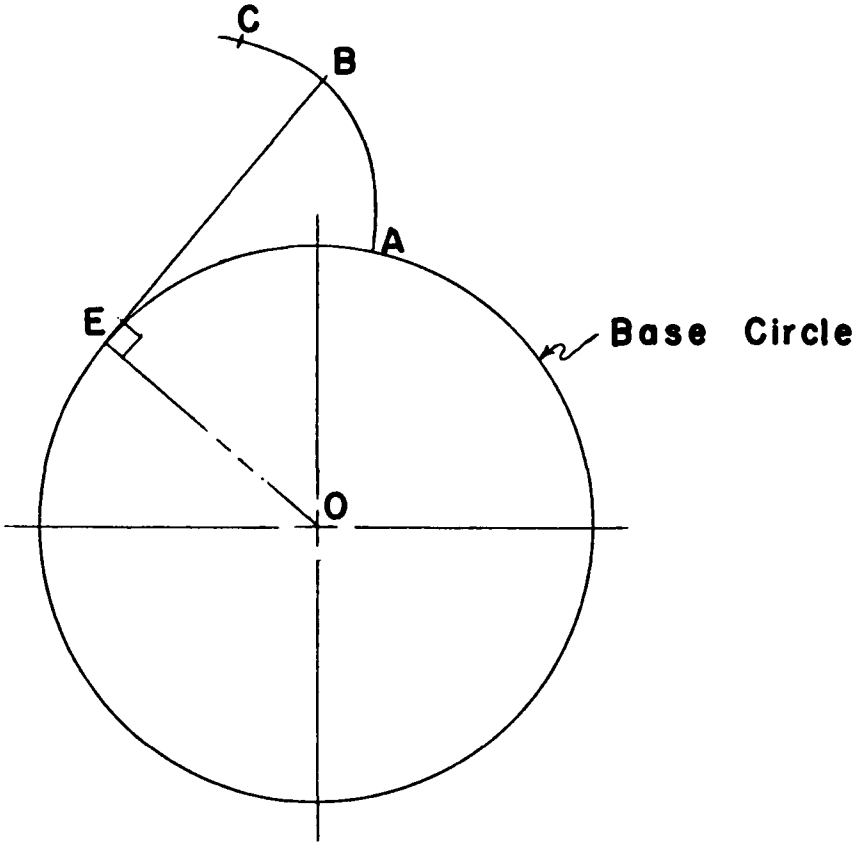

Figure 2-1: Generation of an involute

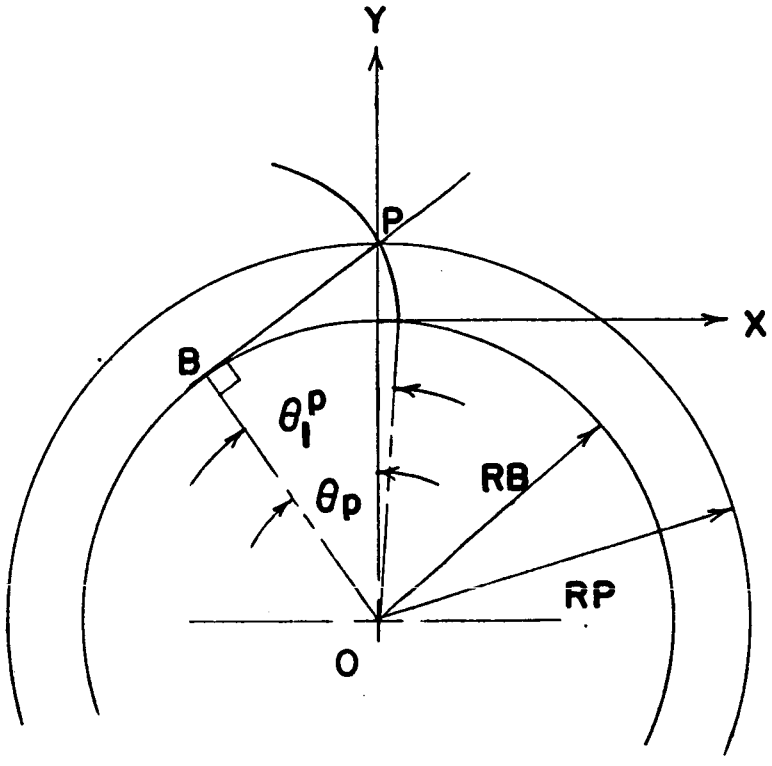

Figure 2-2: Elements of involute geometry

circle radius RB, the pitch circle radius RP, the roll angle θ_1^p and the pressure angle θp. The pressure angle is defined by drawing a line perpendicular to the base circle and passing through the point P. This line corresponds to the pressure line or line of action of forces between meshing gear teeth. The point P being the pitch point. From the triangle OBPO, the base circle radius is defined in terms of the pitch radius as:

$$RB = RP\cos\theta_p \qquad (2\text{-}1)$$

In order to generate discrete points along the involute, θ_i is used in place of θ_1^p and allowed to vary from zero to a maximum, $\theta_{max} = \sum\theta_i$; i=1,2,3,...,n, corresponding to the desired height of the involute, as shown in Figure 2-3. The maximum value of θ, corresponding to the point B_n on the tip of the tooth, is found by writing the equation for the triangle OA_nB_nO;

$$(RB\,\theta_{max})^2 + RB^2 = RO^2$$

Solving for θ_{max} gives;

$$\theta_{max} = \left(\frac{RO^2 - RB^2}{RB^2}\right)^{\frac{1}{2}} \quad \text{(rad)} \qquad (2\text{-}2)$$

where RO is the outer radius defined as the sum of the pitch radius and the addendum. Each increment of θ_i produces a point on the involute progressively further from the base circle. In terms of the local axis system, X-Y, the coordinates of the points Bi are determined from the geometry shown in Figure

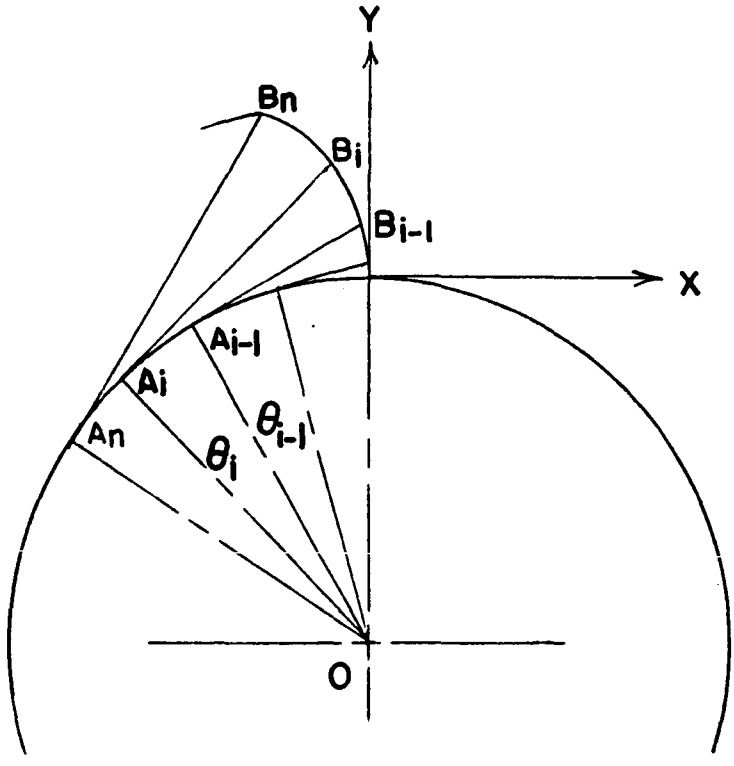

Figure 2-3: Construction of an involute curve

2-4. In simplified form the equations for the X and Y coordinates are:

$$XB_i = -RB(\sin\theta_i - \theta_i\cos\theta_i) \qquad (2\text{-}3)$$

$$YB_i = RB(\cos\theta_i + \theta_i\sin\theta_i - 1) \qquad (2\text{-}4)$$

where $RB\theta_i$ is the arc length from the origin of the X-Y system to point A_i.

Next, those equations defining the overall geometry or size of the tooth are presented. From Figure 2-5, it can be seen that;

$$(RB\,\theta_1^p)^2 + RB^2 = RP^2$$

from which;

$$\theta_1^p = \left(\frac{RP^2 - RB^2}{RB^2}\right)^{\frac{1}{2}} \text{(rad)} \qquad (2\text{-}5)$$

Also from Figure 2-5, it is obvious that;

$$\theta_p = \tan^{-1}\left(\frac{RB\theta_1^p}{RB}\right)$$

which can also be written as;

$$\theta p = \tan^{-1}(\theta_1^p) \qquad (2\text{-}6)$$

where θ_1^p is expressed in radians. During the process of calculating actual tooth dimensions, equation (2-6) serves as a useful derivational check on θ_1^p. With θ_1^p and θp the angle ϕ is written as the difference of the two previous angles;

$$\phi = \theta_1^p - \theta p \qquad (2\text{-}7)$$

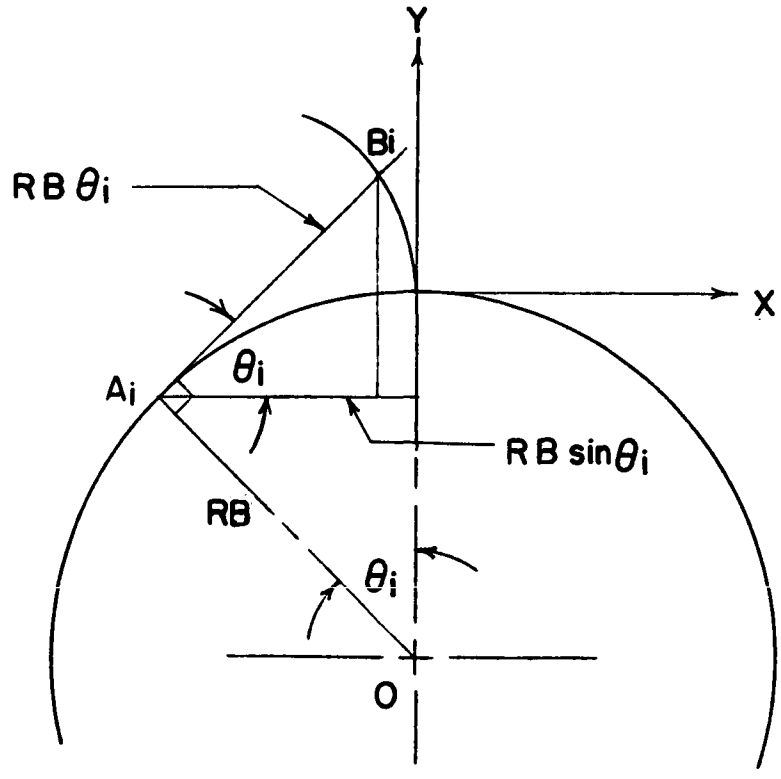

Figure 2-4: Roll angle geometry

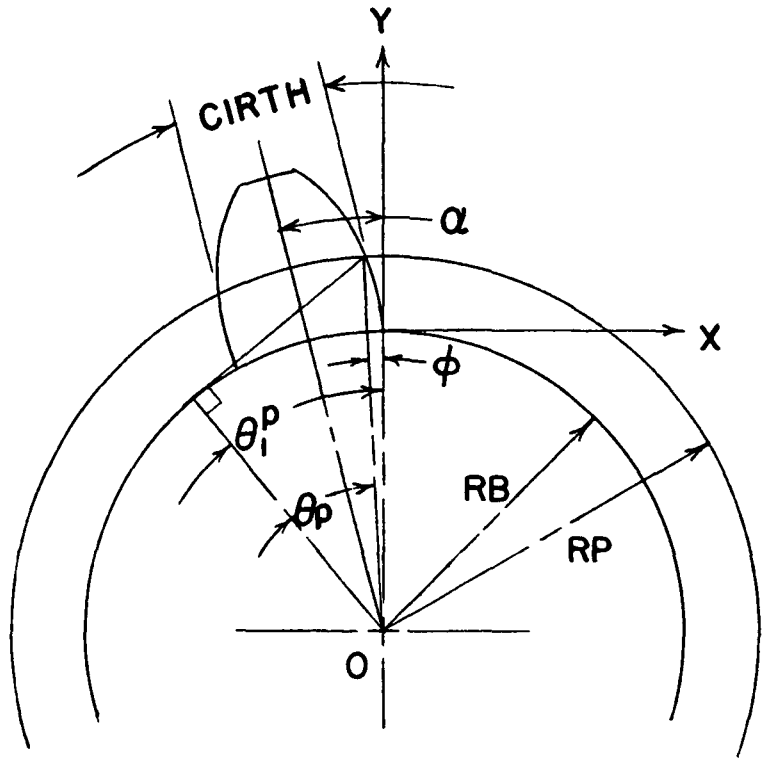

Figure 2-5: Spur gear tooth geometry

And finally, from Figure 2-5, α is found to be;

$$\alpha = \theta_1^P - \tan^{-1}(\theta_1^P) + \frac{CIRTH}{2RP} \qquad (2\text{-}8)$$

where CIRTH is the circular thickness measured on the pitch circle, given by;

$$CIRTH = \frac{CIRP}{2} - BACKL \qquad (2\text{-}9)$$

Since one leg of α passes through the tooth center, this angle is well suited for transforming the involute coordinates from the X-Y axis system to a system whose Y axis passes through the center of the tooth, such as Y' shown in Figure 2-6.

When analyzing a gear tooth to determine stresses, deflections, etc., it is very advantageous to make full use of the axisymmetric properties of the tooth. The involute points generated relative to the X-Y axis system are, therefore, transformed into another system X'-Y', taking full advantage of these properties.

Using the pitch point on one side of the tooth as a reference, as seen in Figure 2-6, a vector $\bar{r}'$ is drawn from the pitch point, Bp, to the gear center, O, which defines the origin of the X'-Y' coordinate system. The vector, $\bar{r}'$, is composed of two vectors, $\bar{R}$ and $\bar{r}$;

$$\bar{r}' = \bar{R} + \bar{r} \qquad (2\text{-}10)$$

where;

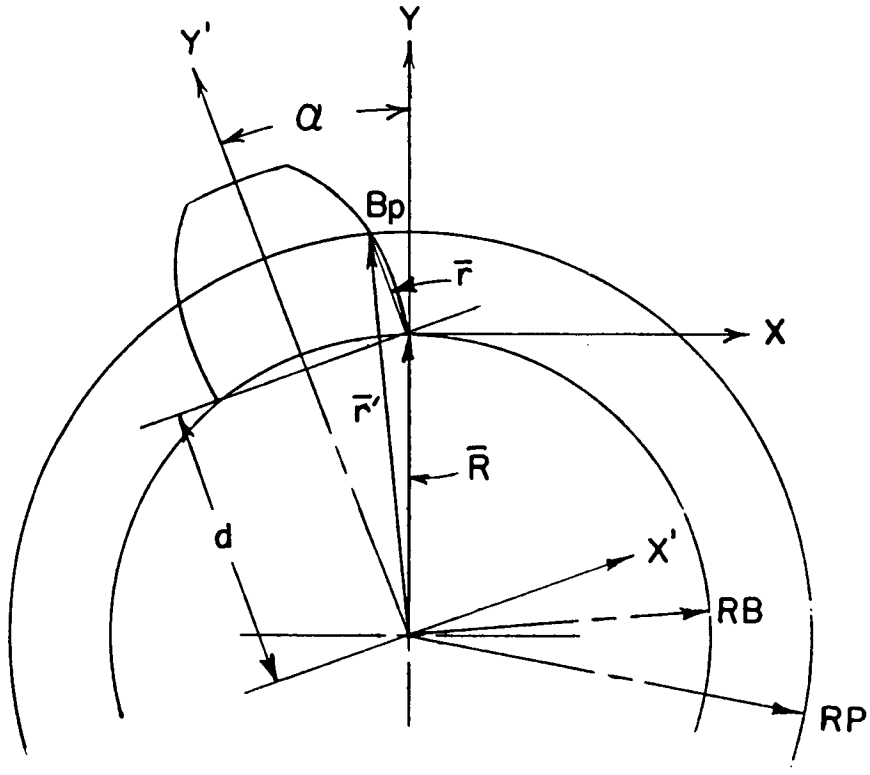

Figure 2-6: Definition of axisymmetric coordinate system

$$\bar{R} = d\bar{j}' + RB\sin\alpha\bar{i}' \qquad (2\text{-}11)$$

with;

$$d = RB\cos\alpha$$

and;

$$\bar{r} = x\bar{i} + y\bar{j} \qquad (2\text{-}12)$$

(x and y are the coordinates of point Bp calculated in terms of X-Y using equations (2-3) and (2-4)).

In the new coordinate system, the coordinates of point Bp are now defined as;

$$X' = RB\sin\alpha + x\cos\alpha + y\sin\alpha \qquad (2\text{-}13)$$

$$Y' = d - x\sin\alpha + y\cos\alpha \qquad (2\text{-}14)$$

Figure 2-7 illustrates more clearly the elements comprising equations (2-13) and (2-14).

In the profile generation algorithm, included in Appendix 1, eleven points are calculated along the involute. Equations (2-2), (2-3), (2-4), (2-5), (2-8), (2-13), and (2-14) are used directly to calculate the point coordinates in the X'-Y' axis system.

(2.1.2) Fillet Generation

In the present work, two different spur gear tooth geometries are considered; low contact ratio gearing (LCRG) and high contact ratio gearing (HCRG). By definition, the contact ratio is the length of the path of contact of mating gears

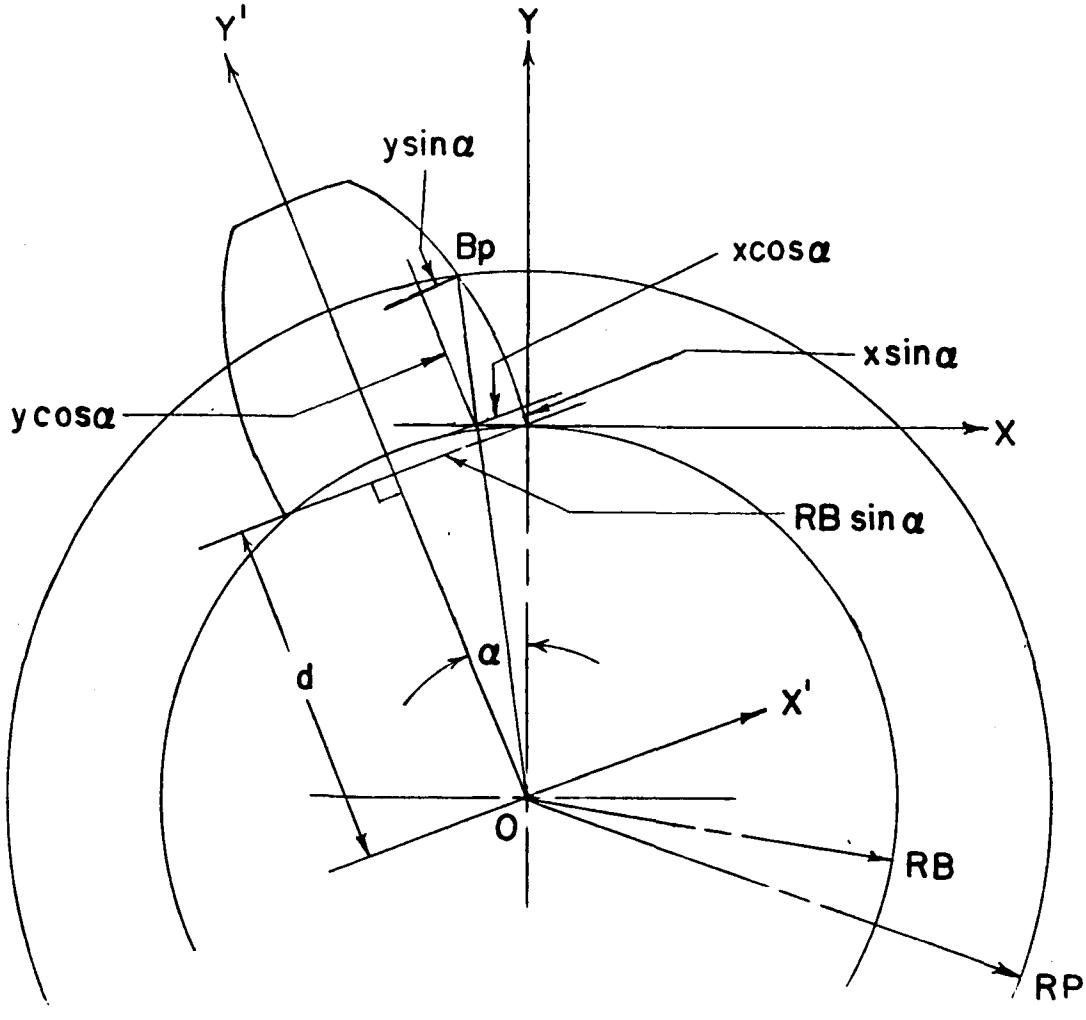

Figure 2-7: Coordinate transformation geometry

divided by the base pitch. More practically, it can be thought of as the average number of teeth in contact during the meshing cycle. A high contact ratio gear is one which has at least two teeth in contact at all times.

One of the main differences between the two forms (LCRG and HCRG) is the fillet transition (see Figure 2-8). For an actual low contact ratio gear, the fillet radius is placed tangent to the involute and the root circle as shown in Figure 2-8a. The amount of overlap of the involute may be different for any given tooth design. In the current model, however, the fillet radius is calculated to fit tangent to the involute at the base circle and tangent to the root circle, as shown in the modified case (see Figure 2-8b).

When designing the high contact ratio gears, the fillet region is undercut to provide additional clearance for the engaging teeth. Also, the HCRG tooth is generally longer due to addendum or other profile modifications, thus the radial distance between the base and root circles is also extended as shown in Figure (2-8c).

Given the gear parameters defined for a particular gear, the following equation can be used to determine whether the gear is a low or high contact ratio gear [10].

$$RR^2 + 2RF\ RR \geq RB^2 \qquad (2\text{-}15)$$

In equation (2-15) RF is the fillet radius specified for a given tooth. If this inequality is satisfied, the tooth is

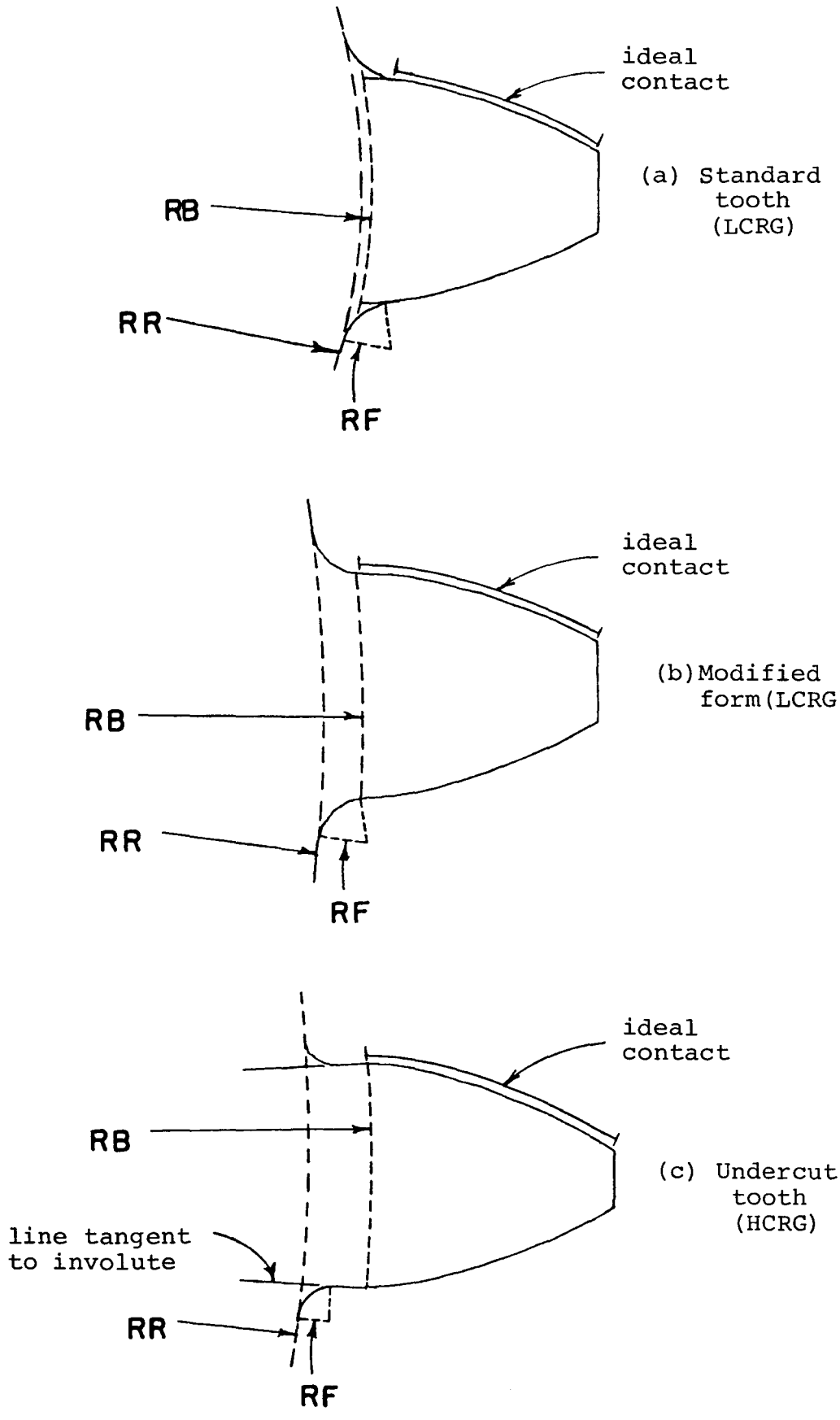

Figure 2-8: Fillet radius geometries

classified as LCRG. This means that the specified fillet radius will overlap the involute, and thus must be changed to fit the modified form as described in Figure 2-8b.

Figure 2-9a illustrates the geometry used in developing the LCRG fillet radius relations. From Figure 2-9a it is obvious that the fillet radius needed to make the transition from the base circle to the root circle will have to be larger than the radial distance DD as shown. The equation of the given triangle is;

$$(RF + RR)^2 = (RR + DD)^2 + RF^2 \qquad (2\text{-}16)$$

By expanding and rearranging terms, equation (2-16) can be written for RF as;

$$RF = \frac{2RR\ DD + DD^2}{2RR} \qquad (2\text{-}17)$$

This then gives the equation of the fillet radius which will fit tangent to the involute at the base circle, and tangent to the root circle.

Rewriting equation (2-15) with the inequality reversed gives the equation defining a HCRG. For HCRG the transition is

$$RR^2 + 2\ RF\ RR < RB^2 \qquad (2\text{-}18)$$

divided between a radial line tangent to the involute and a fillet radius from the end of the tangent line to the root circle (see Figure 2-8c). Instead of calculating a new fillet radius, as done for LCRG, equation (2-16) is used, along with

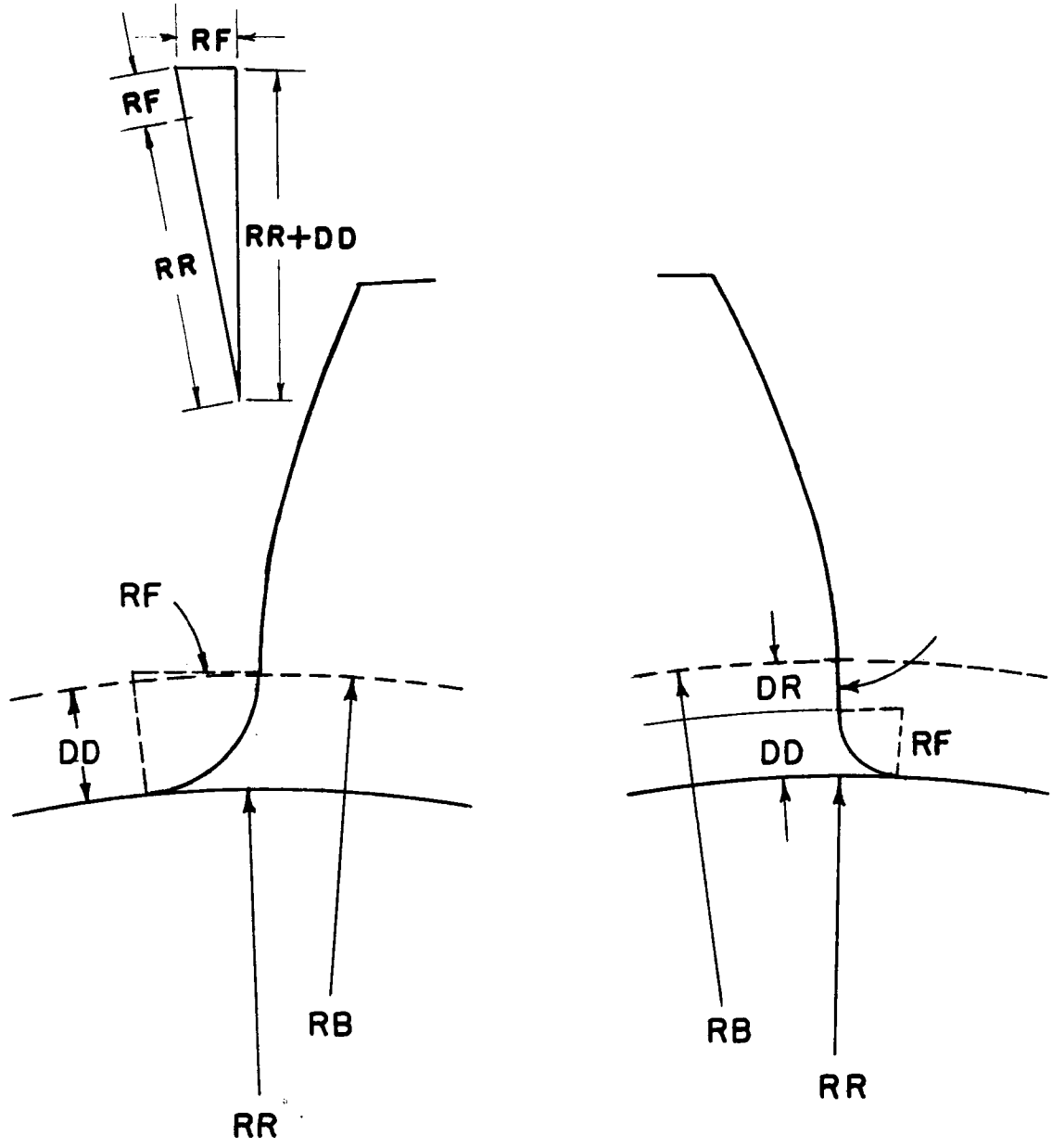

a. Low contact ratio

b. High contact ratio

Figure 2-9: Fillet geometry

the specified fillet radius, to calculate the length of the radial line DR (see Figure 2-9b). Rewritten in another form, equation (2-16) becomes;

$$DD^2 + 2RR\ DD - 2RF\ RR = 0 \qquad (2\text{-}19)$$

and can be used to determine the radial distance DD spanned by the fillet radius. Using the positive root of the quadratic equation (2-19) for DD yields;

$$DD = \frac{-2RR + (4RR^2 + 8RF\ RR)^{\frac{1}{2}}}{2} \qquad (2\text{-}20)$$

DD is then subtracted from the difference between the base and root radii to give the length of the radial tangent line.

$$DR = (RB - RR) - DD \qquad (2\text{-}21)$$

When programming the preceeding equations to calculate the fillet coordinates, eight equally spaced points are used. For LCRG, the arc AOB is divided up into eight equal angles, θ_i (see Figure 2-10a). Coordinates of successive points are calculated by adding θ_i's together for i=1,2...,8 until the arc from A to B is generated. The coordinates of B_i in Figure 2-10b are found from;

$$X_{Bi} = X_A - RF\cos\theta$$

$$Y_{Bi} = Y_A - RF\sin\theta$$

For HCRG, the radial distance required for the fillet radius, and the radial distance of the tangent line may vary

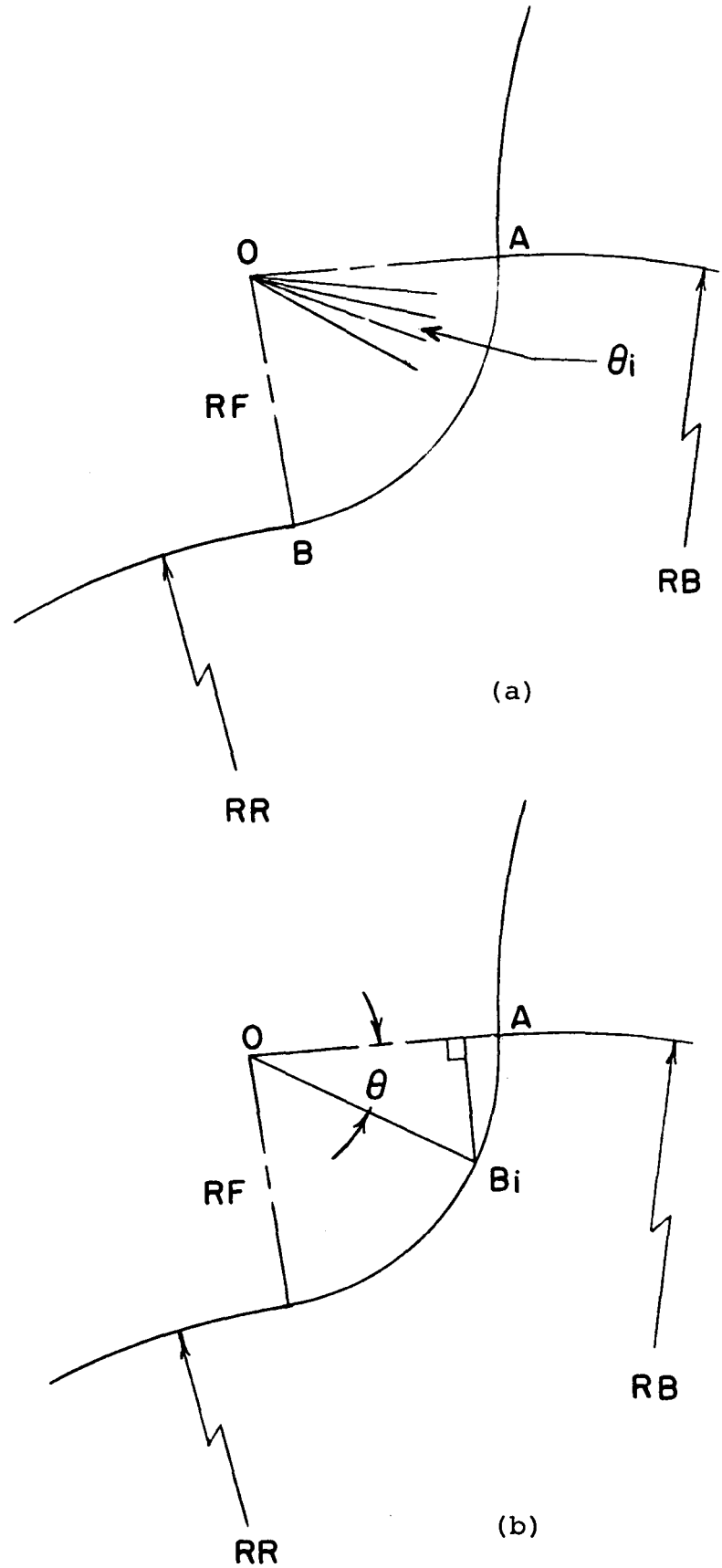

Figure 2-10: Fillet radius generation

from one gear design to another. To insure equal point spacing, integer arithmetic is used to weight the number of points between the radial portion and the fillet radius according to their respective sizes. This is done to facilitate the finite element mesh generation routine discussed later. As in the involute profile generation scheme, the points for the fillet are calculated in the X-Y coordinate system, and then transformed to the X'-Y' system.

(2.1.3) Rim Generation

With the involute and fillet defined, the rim is then generated. As stated previously, the fillet radius is placed such that it is tangent to the root circle for both LCRG and HCRG. From this tangent point, the rim of the gear is added by drawing an arc on the root circle. The distance the arc is extended on either side of the gear is approximately equal to the circular thickness of the gear as shown in Figure 2-11.

The angle ADA is determined from;

$$ADA = \sin^{-1}\left(\frac{XP+CIRTH}{RR}\right) - \sin^{-1}\left(\frac{XP}{RR}\right) \qquad (2\text{-}22)$$

This angle is then divided into six equal segments and the coordinates of points on the rim are calculated using a method similar to that shown in Figure 2-10. From the last point on the root circle, coordinates for a radial line extending inward a distance equal to the specified rim thickness RTH are calculated. To complete the tooth profile, coordinate points on the inner portion of the rim are calculated using a technique similar to that used for the outer rim.

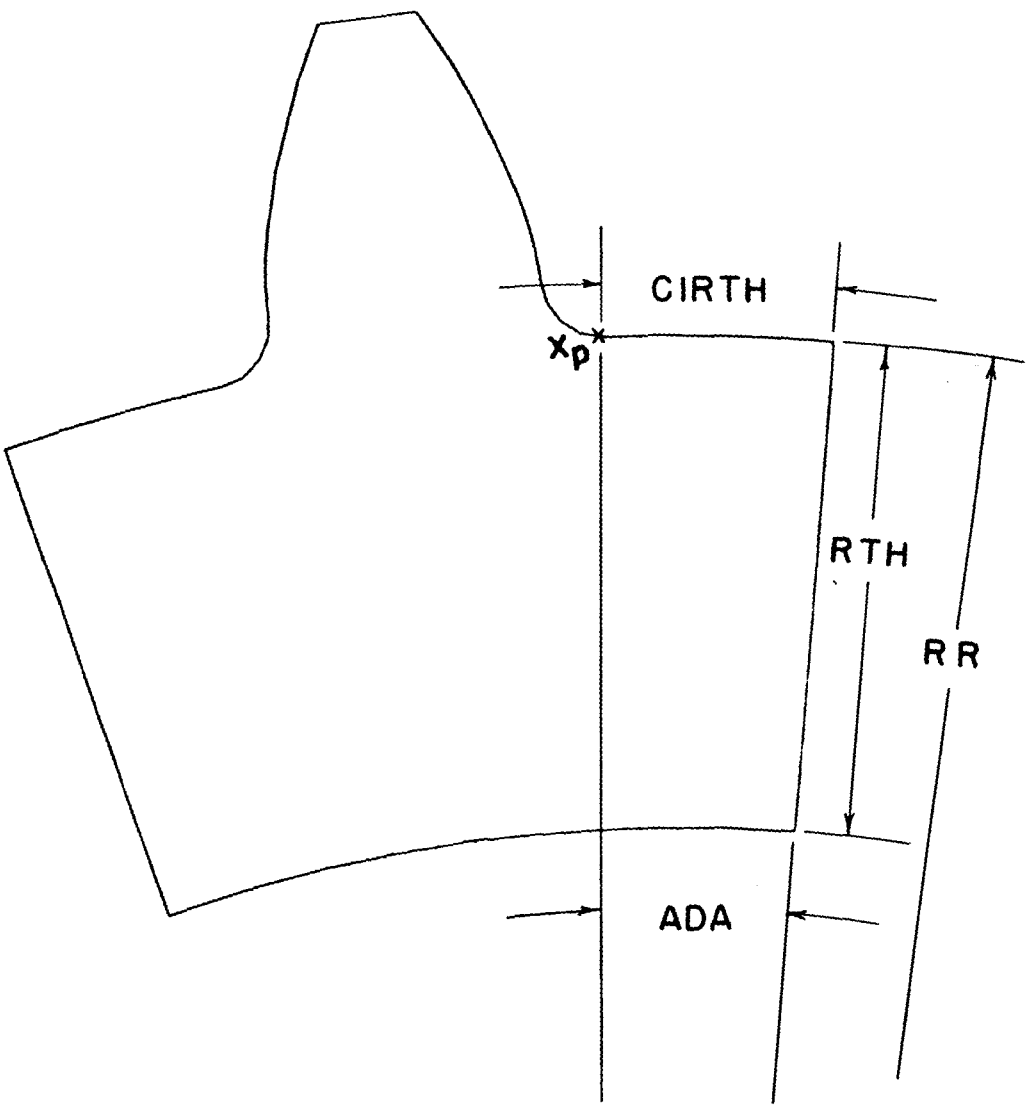

Figure 2-11: Completed profile and rim geometry

(2.2) Finite Element Mesh Generation

No absolutely correct method has been found to model a system using a finite element mesh, even though the topic of mesh development has been treated quite extensively. With different element types and solution techniques, several equally valid methods are available for any particular application.

Indeed, Cook [14] states that although an optimum mesh can be determined by requiring that element boundaries follow lines of constant strain, this optimum condition only exists for one set of loading conditions. As the load changes, so does the optimum mesh configuration, and for problems involving other than static loading, the difficulties are compounded.

However, when developing a mesh, simple guidelines can be followed which will produce a well enough refined mesh to obtain more than satisfactory results. To mention a few; element boundaries should be aligned with structural or geometric boundaries and principal load trajectories, element aspect ratios should be kept low (less than 7), and when different element sizes are used transitions between different size elements must be gradual (mesh grading).

The finite element mesh generation algorithm used for this analysis was developed in accordance with the preceeding rules, as well as maintaining computational efficiency. Figures 2-12 and 2-13 show the nodes and elements, respectively, for a low contact ratio gear, and Figures 2-14 and 2-15 illustrate the high contact ratio geometry and also the varying rim thickness.

The grid consists of 319 nodes and 276 quadrilateral ele-

MODEL DEVELOPEMENT : GEAR #1
UNDEFORMED SHAPE

JUNE 30, 1983 09:36:57
IAXIS= 3 ALPHA= 0.00 BETA= 0.00

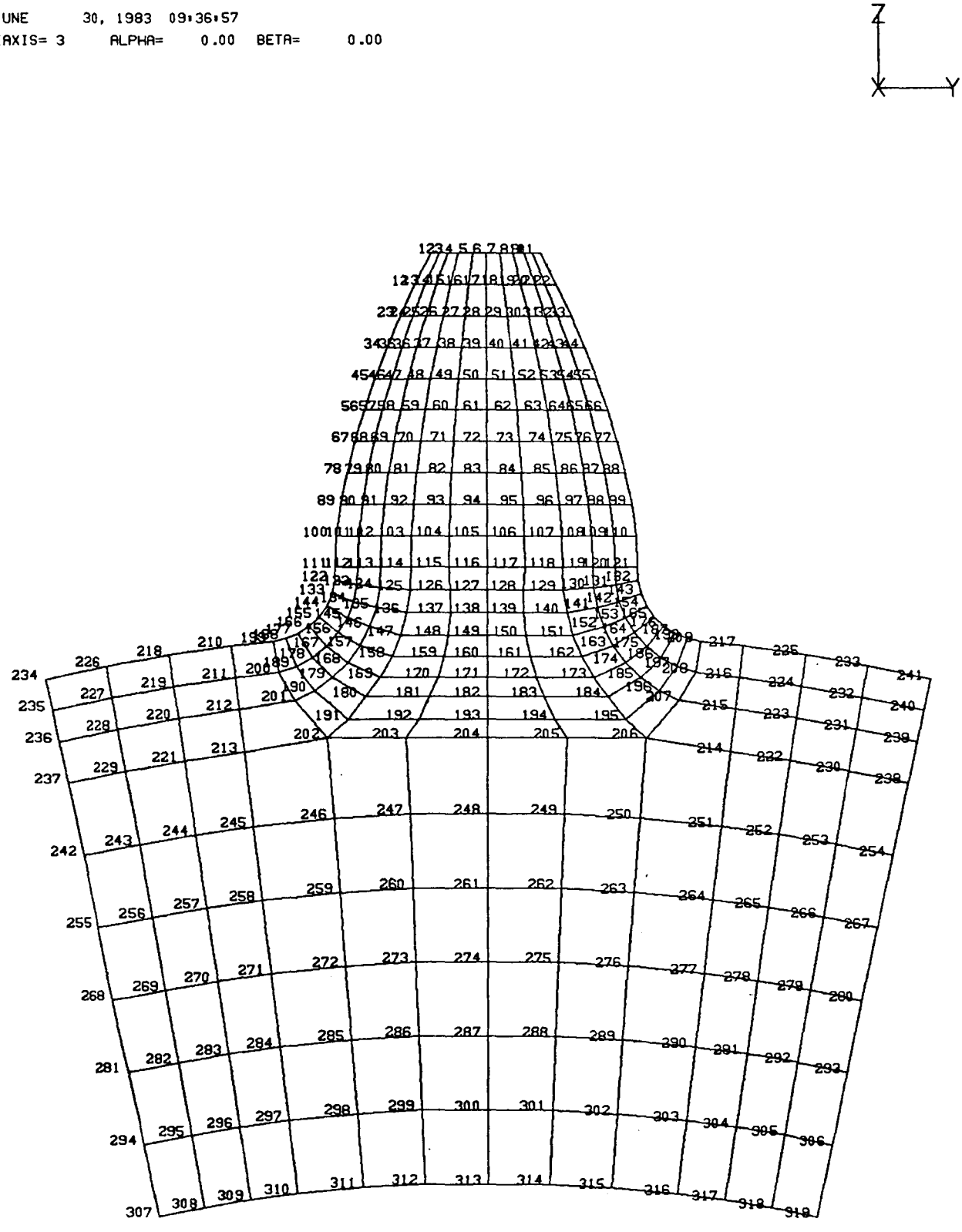

Figure 2-12: Nodal points

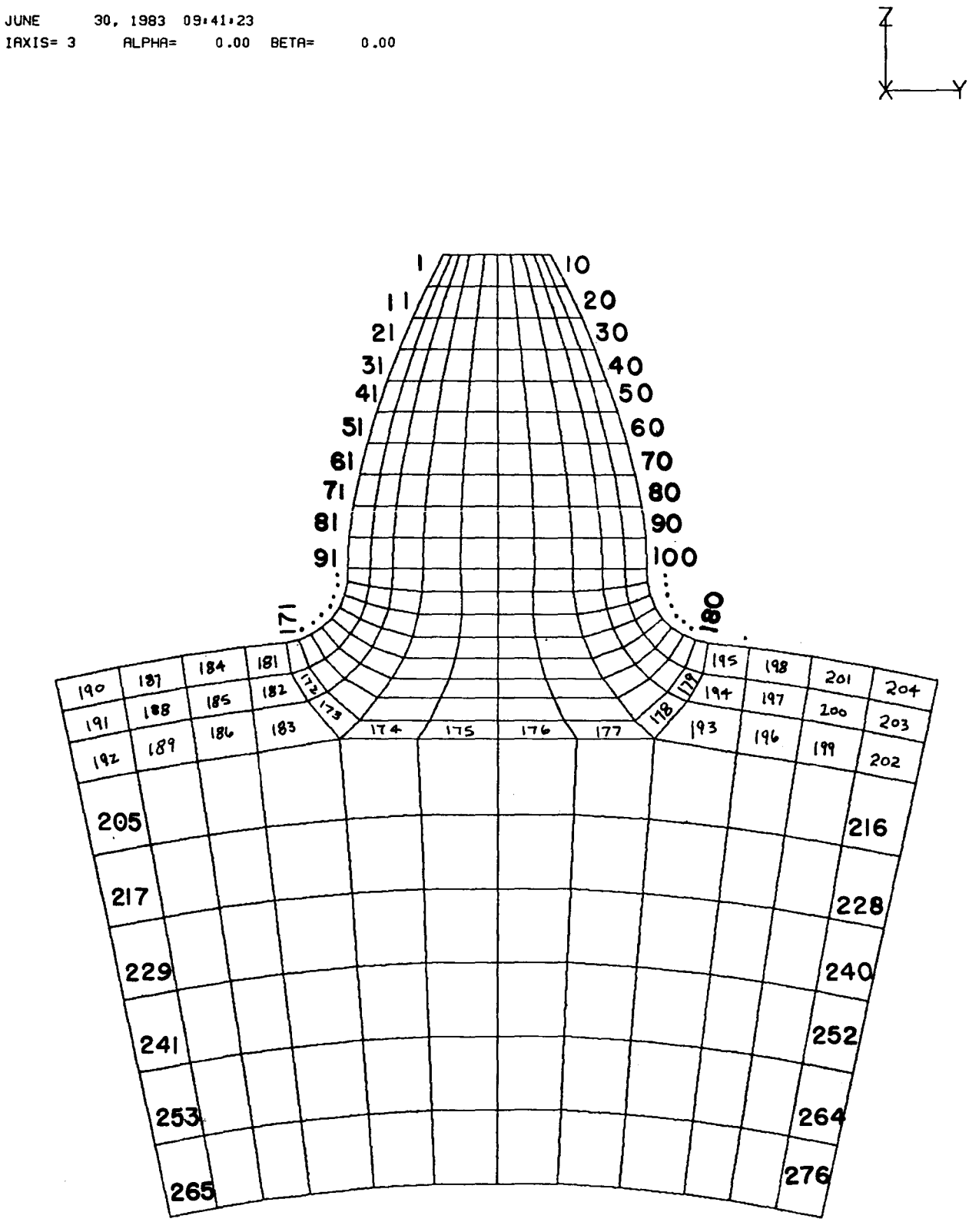

Figure 2-13: Elements

MODEL DEVELOPEMENT : GEAR #2
UNDEFORMED SHAPE

JUNE 29, 1983 17:09:03
IAXIS= 3 ALPHA= 0.00 BETA= 0.00

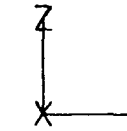

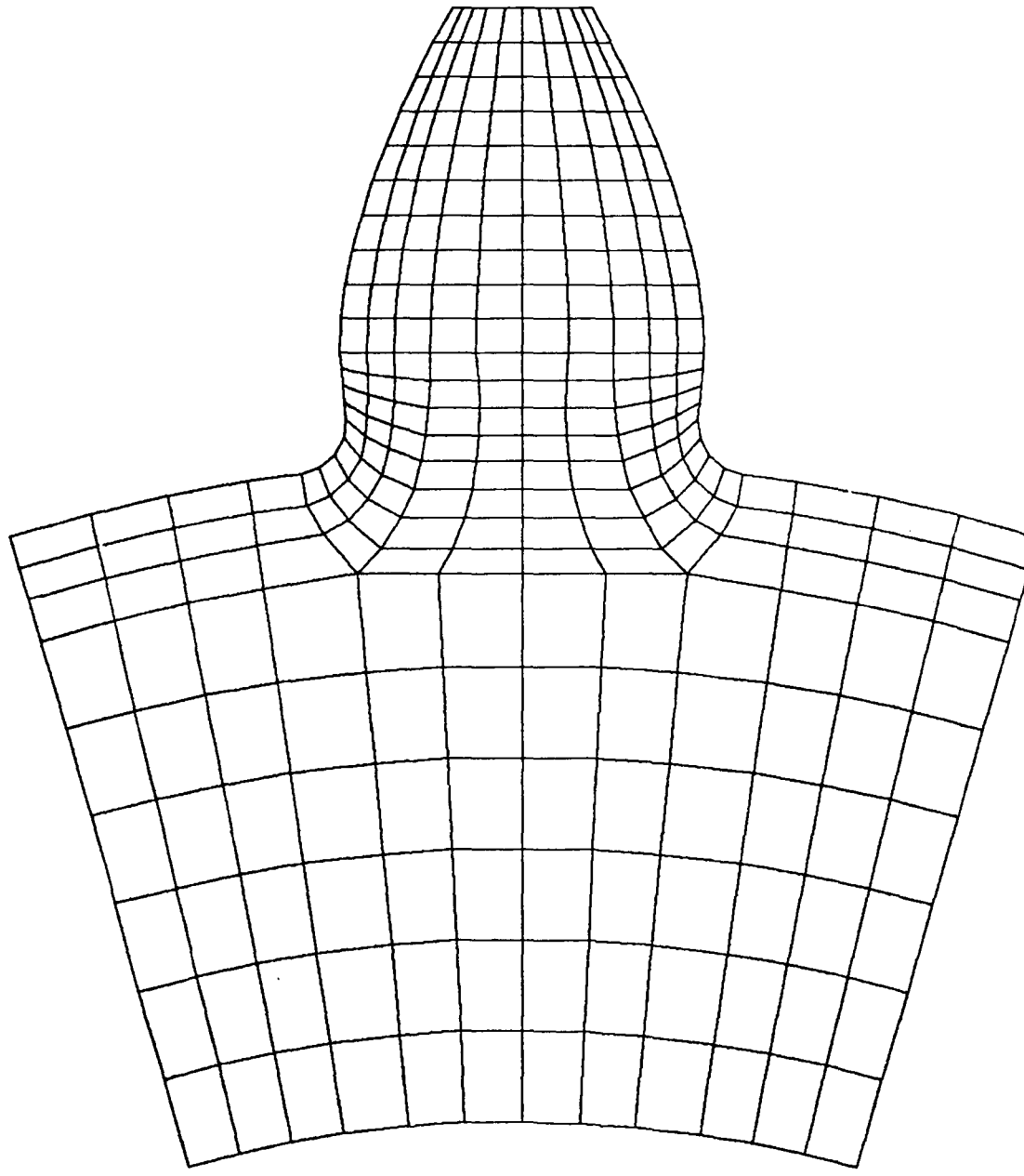

Figure 2-14: (HCRG)

MODEL DEVELOPEMENT : GEAR #2
UNDEFORMED SHAPE

JUNE 29, 1983 15:14:15
IAXIS= 3 ALPHA= 0.00 BETA= 0.00

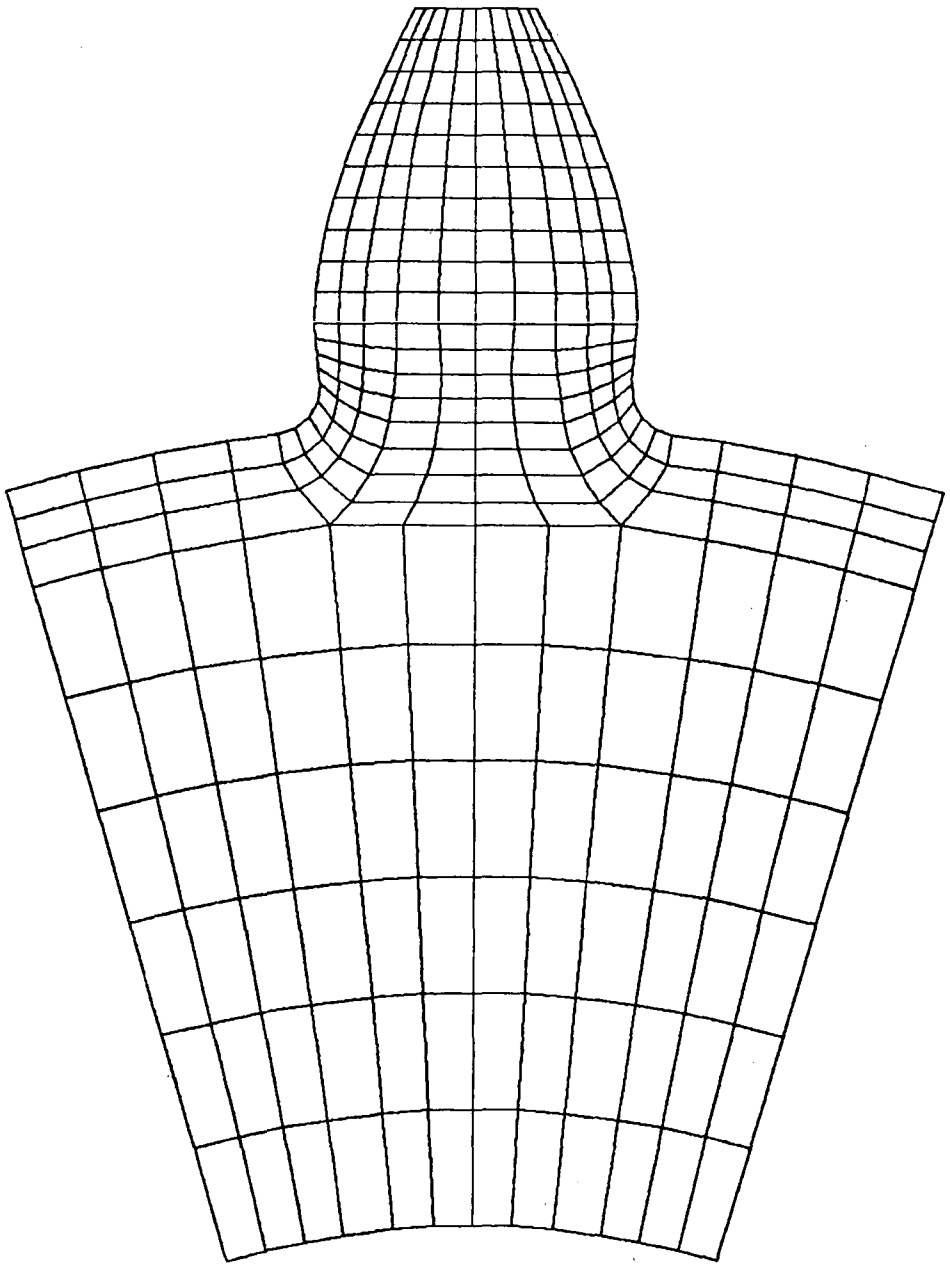

Figure 2-15: (HCRG)

ments. Ten equally divided vertical rows are used to form the involute portion of the gear (elements 1-100). Nodes on the surface of the involute correspond to the actual coordinate points calculated in the profile generation routine. Close to the surface of the involute, the element spacing is small providing additional stiffness for the application of the load. Towards the center of the tooth the element spacing is greater where less stiffness is needed.

The transition from the end of the involute to the root circle is accomplished using one of the two techniques described in section (2.1.2). For both LCRG and HCRG, eight equally spaced rows of elements are used for the transition, again using the actual coordinate points calculated in the profile generation section as surface nodes. When using the HCRG transition, with the radial line and fillet radius, the eight surface nodes are divided between the two sections keeping nodal spacing as even as possible.

In order to maintain continuity between different gear geometry finite element meshes, elements 1 through 204 remain the same size relative to the actual tooth sizes. In other words, no changes are made in the grid geometry during the generation of a particular gear model. The exception to this rule is that elements 205 through 276 do vary in size depending on the rim thickness. Figures 2-14 and 2-15 show this variation.

The algorithm containing the equations developed for the profile geometry, as well as those relationships used to create the finite element mesh is included in Appendix 1.

(2.3) Element Description

(2.3.1) Planar Elements

Two element types are considered for this analysis; plane strain and plane stress. Due to the geometry and loading conditions of the tooth, it is modelled as a plane elastic problem. A plane body is a region of uniform thickness contained within two parallel planes. When the thickness of the body is large compared to the lateral dimensions, the problem is considered to be plane strain. If the thickness is small, it is considered to be plane stress. The difference between plane strain and plane stress elements is evidenced in the material property matrices. For isotropic materials, the material property matrix for the case of plane strain is;

$$[D]=\frac{E(1-\mu)}{(1+\mu)(1-2\mu)}\begin{bmatrix} 1 & \mu/(1-\mu) & 0 \\ \mu/(1-\mu) & 1 & 0 \\ 0 & 0 & (1-2\mu)/2(1-\mu) \end{bmatrix}$$

When plane stress exists

$$[D]=\frac{E}{1-\mu^2}\begin{bmatrix} 1 & \mu & 0 \\ \mu & 1 & 0 \\ 0 & 0 & (1-\mu)/2 \end{bmatrix}$$

where E=30.E6 is the elastic modulus and μ=0.3 is Poisson's ratio. The matrix multiplication factor is larger for plane strain than for plane stress.

plane strain: $\frac{E(1-\mu)}{(1+\mu)(1-2\mu)}$ = 4.0385E7

plane stress: $\frac{E}{1-\mu^2} = 3.2967E7$

The matrix elements are also larger (except for element 3,3) for plane strain. When combined with the strain displacement relations to form the stiffness matrix, these differences result in an increase in the stiffness for plane strain compared to plane stress.

The thickness of the tooth used in the analysis is 0.25 inches. Comparatively, the largest and smallest planar dimensions on the actual tooth (not including the rim) are 0.224 and 0.081 inches, respectively. Based on the dimensions it is difficult to make a judgement on the correct element type for this analysis.

Figure 2-16 shows representative static deflection curves for the plane strain and plane stress element types. The additional stiffness of the plane strain element is noted. Since the difference in deflections between the two element types is small, the plane strain element type is chosen for this analysis.

(2.3.2) General Element Description

The plane strain element described earlier can be represented by a linear quadrilateral element similar to that shown in Figure 2-17a. The intersection of the lines which bisect the sides of the element form a normalized coordinate system $\xi\eta$, where;

$$\xi = \frac{x}{b} \qquad \eta = \frac{y}{a}$$

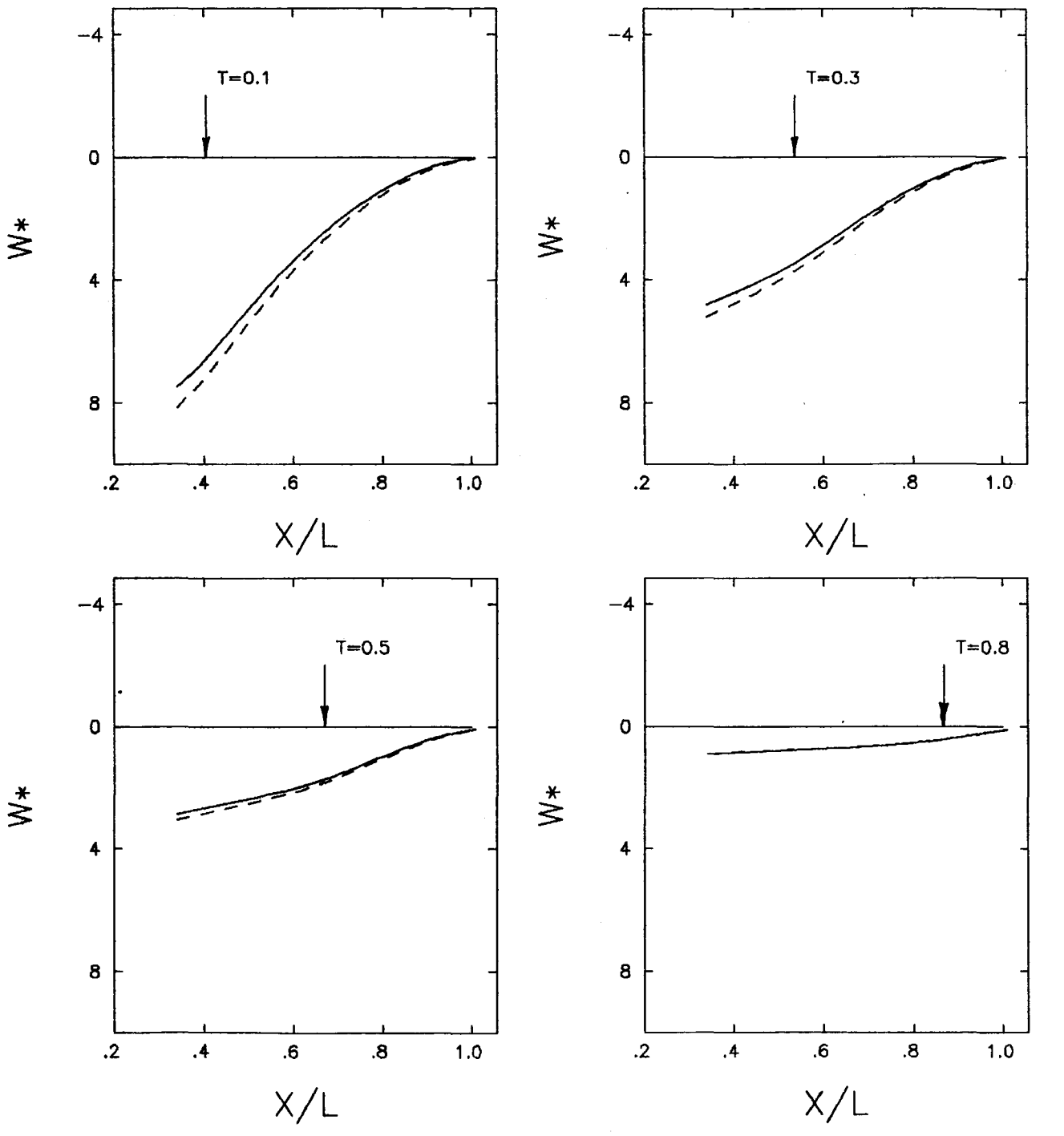

STATIC DEFLECTION CURVES: COMPARISON OF DIFFERENT ELEMENT TYPES

Figure 2-16:

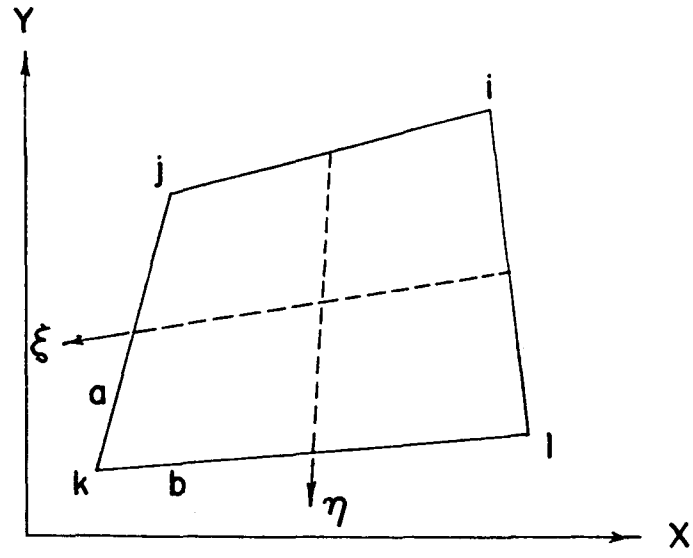

(a) General linear quadrilateral element

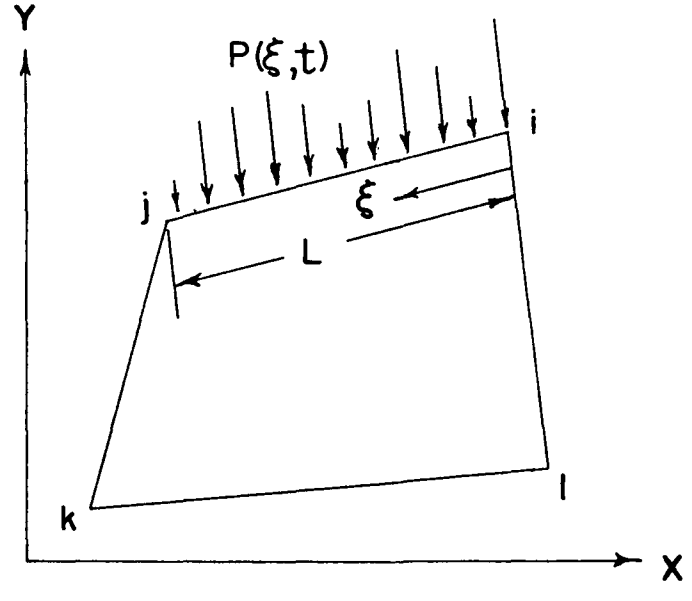

(b) Generalized force application

Figure 2-17:

Between element corners, ξ and η vary from -1 to +1. The displacements within the elements can be written in terms of the shape functions for each node, Ni, Nj, Nk and Nl as;

$$U = UiNi(x,y) + UjNj(x,y) + UkNk(x,y) + UlNl(x,y) \quad (2\text{-}23)$$

where Ui, Uj, etc. define the magnitudes of the displacements. If all nodal displacements are zero except for the coefficient of Ni(x,y), which is defined as unity, the displacement from node i to the other nodes will decrease from unity to zero. Using the parameters shown in Figure 2-17b the shape function for node i going from i to j is;

$$Ni(x,y) = \left(\frac{L-\xi}{L}\right) \quad (2\text{-}24)$$

where L is the length between nodes i and j in the direction of ξ.

(2.3.3) Moving Loads

An arbitrary load, $P(\xi, t)$, normal to ξ is introduced whose components are; $Px(\xi,t)$, $Py(\xi,t)$ (see Figure 2-17b). The effect of the force $P(\xi,t)$ on node i can be represented by the integral of the load times the shape function and thickness in the direction of from 0 to L. Component wise;

$$Fx^i = \Delta t \int_0^L Px(\xi,t)\ Ni(x(\xi), y(\xi))d\xi \quad (2\text{-}25)$$

$$Fy^i = \Delta t \int_0^L Py(\xi,t)\ Ni(x(\xi), y(\xi))d\xi \quad (2\text{-}26)$$

where; Δt is the element thickness (assumed to be unity). Inserting the shape function for node i into equations (2-25) and (2-26) yields;

$$Fx^i = \int_0^L Px(\xi,t)\ (\frac{L-\xi}{L})d\xi \qquad (2\text{-}27)$$

$$Fy^i = \int_0^L Py(\xi,t)\ (\frac{L-\xi}{L})d\xi \qquad (2\text{-}28)$$

Equations (2-27) and (2-28) give the load history at node i as a function of $\xi(t)$, resulting from the arbitrary load $P(\xi,t)$.

Conversely, the load history at node j is determined by considering the shape function obtained when going from node j to i with j at zero and i at unity. Here the shape function starts at zero and increases to unity as;

$$Nj(x,y) = \frac{\xi}{L} \qquad (2\text{-}29)$$

Substituting equation (2-29) into equations (2-25) and (2-26) yields the force in the x and y directions experienced at node j, resulting from $P(\xi,t)$.

$$Fx^i = \int_0^L Px(\xi,t)\ (\frac{\xi}{L})d\xi \qquad (2\text{-}30)$$

$$Fy^i = \int_0^L Py(\xi,t)\ (\frac{\xi}{L})d\xi \qquad (2\text{-}31)$$

Equations (2-27), (2-28), (2-30) and (2-31) can be used to represent a moving load by introducing the Dirac Delta Function. When used in an integral, it translates a given function to the origin and gives the value of a function at a given time at the origin. The argument of the delta function

takes the form of the variation in the position variable. For a moving load with constant velocity, the change in position is given by the velocity times the time. The arbitrary moving load then takes the form;

$$P(\xi,t) = P(t)\,\delta(\xi - Vot)$$

where Vo is the velocity and t the time. Using the delta function in the integrand results in all occurences of being replaced by Vot. Thus, the four force equations become;

$$Fx^i = Px(t)\left(\frac{L-Vot}{L}\right) \qquad (2\text{-}32)$$

$$Fy^i = Py(t)\left(\frac{L-Vot}{L}\right) \qquad (2\text{-}33)$$

$$Fx^j = Px(t)\left(\frac{Vot}{L}\right) \qquad (2\text{-}34)$$

$$Fy^j = Py(t)\left(\frac{Vot}{L}\right) \qquad (2\text{-}35)$$

Plotting these equations as a function of time where the magnitude of P(t) is constant, yields to general force histories (see Figure 2-18) for a load moving from i to j.

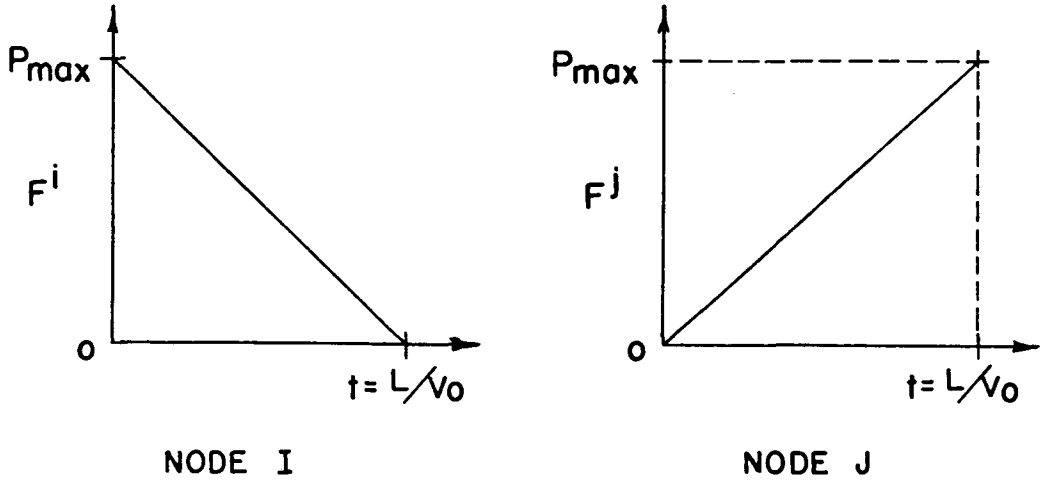

Figure 2-18: Linear force histories

For an actual meshing gear set, the speed of the moving load on a single tooth is not constant, but varies linearly with time. The time varying speed can be seen to be (see Appendix 2);

$$V(t) = RB\ \omega^2 t$$

Now, the force equations take a different form with β being replaced by the displacement resulting from the above velocity;

$$S(t) = \frac{RB\omega^2 t}{2}$$

where A can replace the quantity $RB\omega^2/2$;

$$S(t) = At^2$$

For the time varying load the force equations then become;

$$F^i = P(t)\ \left(\frac{L-At^2}{L}\right) \qquad (2\text{-}36)$$

$$F^j = P(t)\ \left(\frac{At^2}{L}\right) \qquad (2\text{-}37)$$

where the x and y subscripts are assumed.

3. DISCUSSION OF NAGAYA ANALYSIS

Although the problem of theoretically analyzing dynamic gear tooth deflections has been treated extensively [1-5][10], models addressing the problem assume that the variation in tooth stiffness can be approximated using a static deflection analysis. These models assume that the gear hubs act as rigid bodies and that the teeth act as variable stiffness springs. The stiffness of the teeth varies with the contact position along the tooth and is generally arrived at using a static deflection analysis such as the one developed by Weber [12]. Recently, K. Nagaya and S. Uematsu [7] proposed that since the contact point moves along the tooth during the meshing cycle, the dynamic load response should be considered as a function of both the position and the speed of the moving load. In their paper they generate plots of normalized gear tooth centerline deflection curves from which they claim the equivalent spring constant of gear teeth can be determined.

(3.1) Approximating A Gear Tooth with a Timoshenko Beam

In Nagaya's analysis, the differential equations for a tapered Timoshenko beam are written and solved, in the form of an eigenvalue problem, from which a modal response analysis is used to determine tooth deflections due to moving loads. Nagaya assumed a load of constant magnitude moving along the beam at a constant velocity from the tip to the base of the tooth (see Figure 3-1).

Using Kara's [8] assumption for the profile of gear

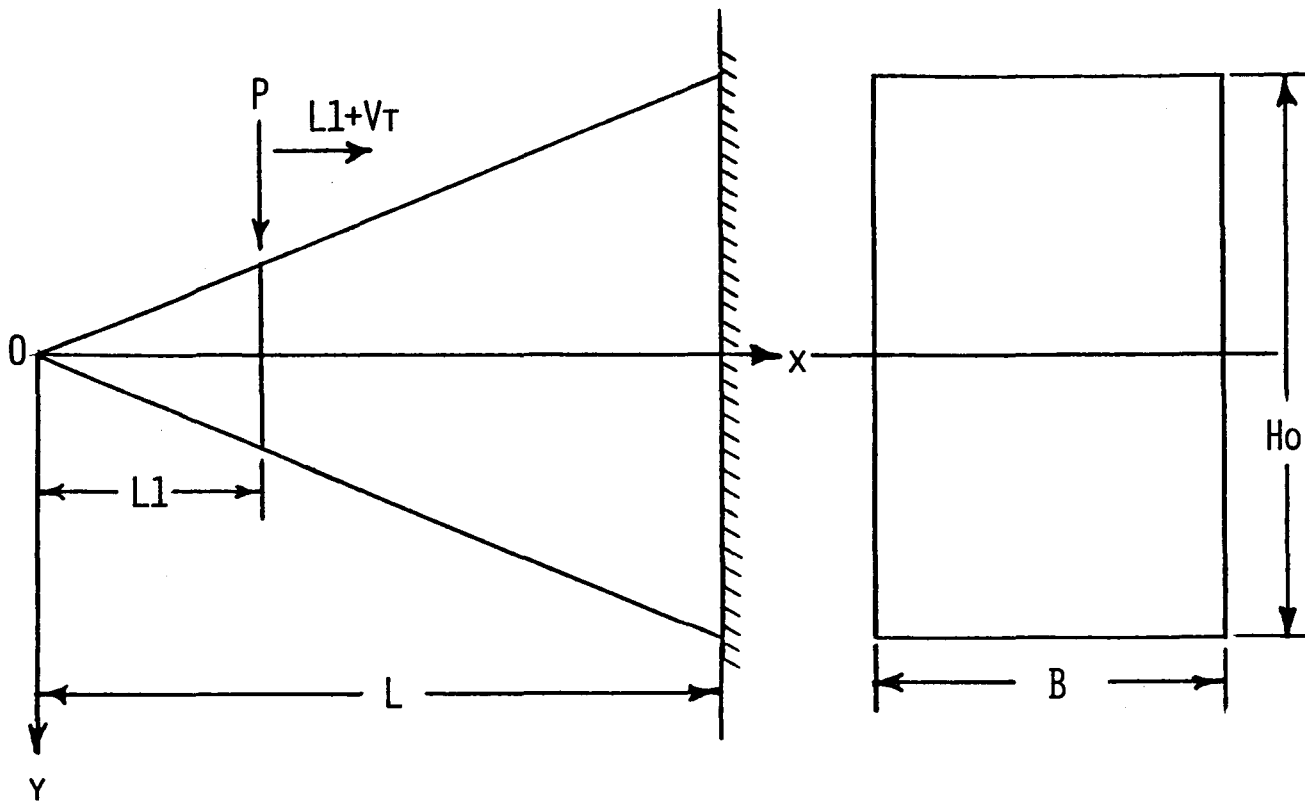

$$\theta_P = 20^\circ$$

$$L - L1 = 2.25M$$

$$Ho = 2.48M$$

$$L1/L = .34$$

$$S = (AoL^2/Io)^{\frac{1}{2}} = 4.76$$

Figure 3-1: Tapered Timoshenko beam

teeth, Nagaya claimed that the deflections obtained using the beam approximation were applicable to any spur gear defined by the parameters

$$\text{Pressure Angle} = 20°$$

$$L - L1 = 2.25\ m$$

$$Ho = 2.48\ m$$

$$L1/L = .34$$

$$S = (AoL^2/Io)^{1/2} = 4.76$$

where m is the module, L, L1, Ho are shown in Figure 3-1, and S is the slenderness ratio. The module, m, is the pitch diameter divided by the number of teeth, measured in inches. When analyzing a gear tooth the above parameters are used to describe the Timoshenko beam used for the approximation. An example of such a comparison is shown in Figure 3-2 where the approximating Timoshenko beam is shown superimposed onto the gear tooth used in the finite element analysis of Chapter 4. Instead of the beam lying tangent to the involute of the actual test gear as shown, it should have passed through the tip of the involute as illustrated by the inset figure. The inset is a correct representation of Kara's assumption for the profile of spur gear teeth. This discrepancy, is solely attributable to the use of backlash when defining the gear geometry. Backlash effectively decreases the width of the tooth. In order to better compare the finite element analysis to Nagaya's work, the tooth, when analyzed, is constrained so that only the

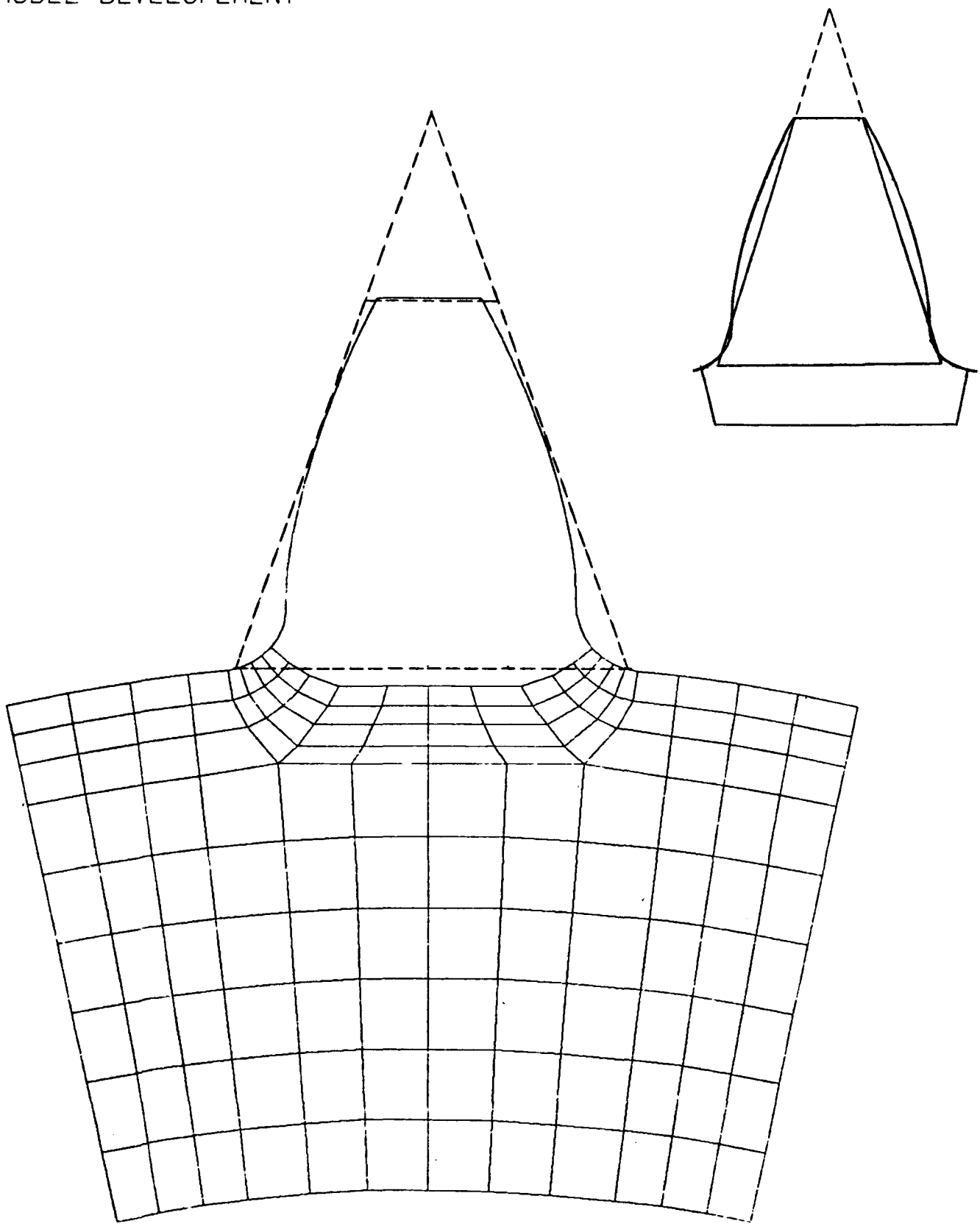

Figure 3-2: Karas' assumption for profile of gear teeth

portion void of interior elements is allowed to deform (see Figure 3-2). The foundation and rim are constrained against motion. Later on, the deflection of the gear tooth is again analyzed with the tooth, foundation, and rim allowed to deform.

(3.2) Interpretation of Nagaya Results

When presenting his findings, Nagaya plotted normalized tooth centerline deflections versus normalized load position for different moving load speeds. Figure 3-3, taken directly from reference [7], illustrates these results. The solid curves in the figure represent normalized tooth centerline deflections, each one for a different normalized velocity, V*. The vertical arrows labelled T represent the load position relative to the length of the tooth, where X/L is the ratio of the position of the load on the tooth relative to the total length L. The dotted lines are the static curves obtained from the Karas analysis. By normalizing these parameters; deflection, load position, and velocity, the results then become applicable to any size gear tooth.

Non-dimensional deflections can be represented by;

$$W^* = AoEW/PL$$

where

Ao = Area of the base of the tooth (in^2)

E = Elastic modulus (Psi)

W = Actual tooth deflection in direction of applied load (in)

P = Applied load (lbs)

L = Extended tooth length (in)

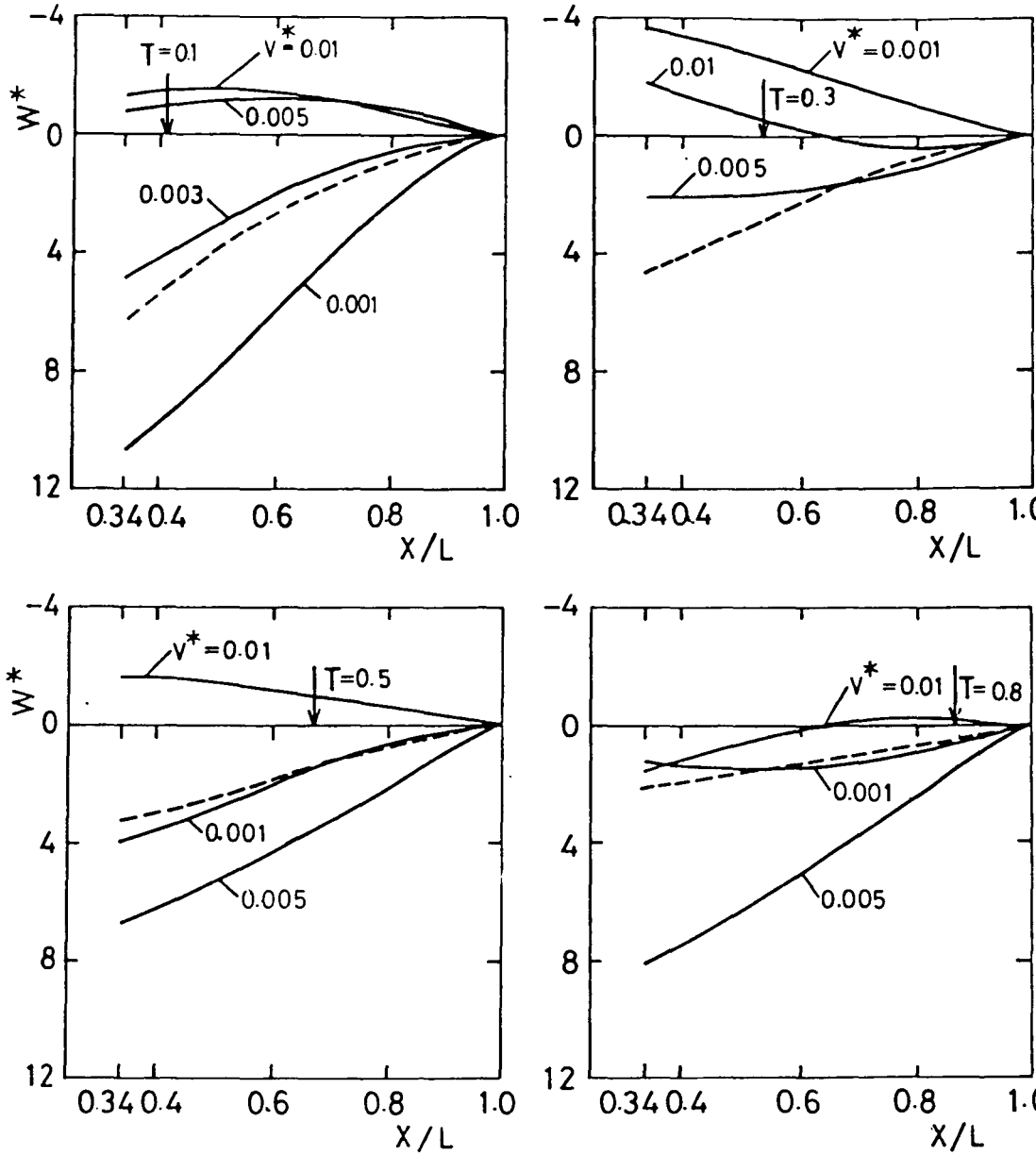

Dynamic deflection curves for the gear teeth with various moving loads

Figure 3-3

The velocity in normalized form is written as;

$$V^* = V/\sqrt{E/\rho}$$

where;

V = Speed of moving load (in/sec)

E = Elastic modulus (Psi)

ρ = Material density (lb/in^3)

In this equation the denominator represents the wave velocity in bars. Finally, the position of the moving load is given by;

$$T = Vt/(L-L1)$$

where;

V = Speed of the moving load (in/sec)

t = Elapsed time (sec)

(L-L1) = Actual tooth height (in)

From the plots shown in Figure 3-3, Nagaya claims that the deflections of gearteeth, subjected to moving loads, vary with the speed of the moving load. That is, for the same values of T, the displacements are directly related to the speed of the load. He states that for slowly moving loads, the dynamic response reduces to the case of a step function impact load for small values of T (see T=0.1, V*=0.001 in Figure 3-3). Since Figure 3-3 indicates that the dynamic response is dependent on the moving load speed (due to effects of inertia forces of the mass of the tooth), Nagaya states that the stiffness of the tooth must also depend on the moving load speed. he then claims that the varying tooth stiffnesses can be determined

from these plots. However, as later demonstrated, Nagaya's claim that the response, and therefore the stiffness, is dependent on the speed of the moving load is a false one.

A major portion of the present work is directed towards substantiation of this conclusion.

4. FINITE ELEMENT ANALYSIS

The deflections of single spur gear teeth with moving loads acting on them are determined using finite element analysis. A single gear tooth is used for six different moving load cases. First, the same moving load scheme used by Nagaya [7] (constant magnitude and speed) is applied to the tooth, which is constrained according to the Timoshenko beam approximation. Then the load application on the tip of the tooth is changed slightly and the test repeated on the tooth with the same constraints. The two preceeding load cases are then applied to a tooth allowing the entire model to deform, including the rim. Finally, an idealized load function, with variable load magnitude and speed, is applied to the tooth using both constraint cases.

(4.1) Description of Test Gear

The gear used as the model for this analysis was selected at random. The parameters used to define the geometry of the gear are;

θ_p = Pressure angle = 20°

RP = Pitch radius = 1.75 (in)

AD = Addendum = 0.125 (in)

DED = Dedendum = 0.175 (in)

CIRP = Circular pitch = 0.3927 (in)

BACKL = Backlash = 0.01 (in)

RF = Fillet radius = 0.05 (in)

RTH = Rim thickness = 0.6 (in)

Δt = Tooth thickness = 0.25 (in)

Figure 4-1 shows the finite element model of the tooth. The test gear is a low contact ratio gear (contact ratio = 1.74).

(4.2) Determination of Normalized Plotting Parameters and Their Application to the Gear Tooth

As stated previously, the normalized deflections of the gear tooth are calculated using those parameters specified in Kara's assumption for the profile of gear teeth. Thus, when the deflections are plotted, the only term in the normalized deflection equation taken directly from the gear analysis is the deflection of the tooth centerline in the direction of the applied load which is perpendicular to the centerline of the tooth.

In Chapter 3.1 the equations needed to define the tooth profile approximation, according to Karas, are given. The physical dimensions, length, area, etc. are defined in terms of the module, m. For a standard spur gear the module is defined as the pitch diameter per tooth measured in inches, and is usually represented by the inverse of the diametral pitch;

$$\text{Module} = M = 1/DP \text{ (in)} \qquad (4\text{-}1)$$

where the diametral pitch is;

$$\text{diametral pitch} = DP = \frac{\pi}{CIRP} = \frac{\pi}{.3927} = 8 \qquad (4\text{-}2)$$

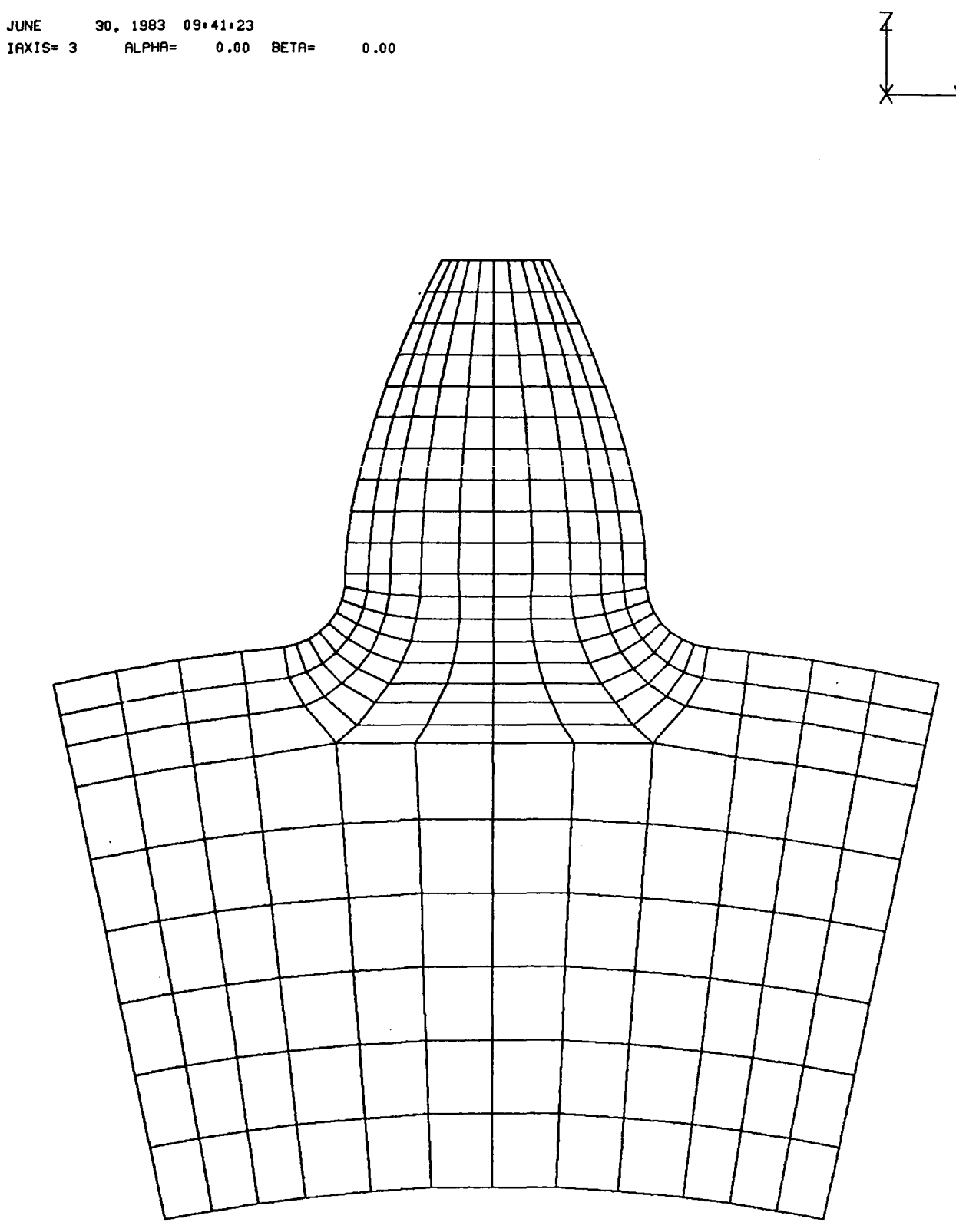

Figure 4-1: Test gear

To further define the test gear, the number of teeth can be calculated from;

$$\text{number of teeth} = N = 2RP*DP = 2(1.75)(8) = 28 \quad (4\text{-}3)$$

Given either the diametral pitch or the number of teeth, the module can easily be obtained.

$$m = 0.125 \text{ (in)}$$

Using the value for the module and the relations of Chapter 3.1, the dimensions of the approximating Timoshenko beam are determined. The height of the corresponding beam becomes;

$$(L\text{-}L1) = 2.25m = 0.28125 \text{ (in)} \quad (4\text{-}4)$$

and the extended length;

$$L = \left(\frac{L\text{-}L1}{0.66}\right) = 0.42614 \text{ (in)} \quad (4\text{-}5)$$

At the base, the beam thickness is;

$$Ho = 2.48m = 0.31 \text{ (in)}$$

and thus the area at the base;

$$Ao = Ho\,\Delta t = (0.31)(0.25) = 0.775 \text{ (in)} \quad (4\text{-}6)$$

Given the above parameters, the non-dimensional deflections can be plotted using;

$$W^* = AoEW/PL \quad (4\text{-}7)$$

Again, it should be emphasized that although the beam approximation (shown in Figure 3-2) does not match the tooth exactly,

the dimensions just determined in equations (4-5) and (4-6) are still used in the normalized deflection equation when plotting results for the actual tooth.

Nagaya defines the normalized velocity of the moving load to be;

$$V^* = V/\sqrt{E/\rho} \qquad (4\text{-}8)$$

and plots four speeds corresponding to V* equal to; 0.01, 0.005, 0.003, and 0.001. Using equation (4-8), the actual velocities, V, are;

V*	V(in/sec)
0.01	2025
0.005	1012
0.003	607
0.001	203

Table 4-1: Actual Velocities

When the load moves along the involute at a constant speed, the values shown in the preceeding table are used directly. However, for a meshing gear set, the velocity along the involute changes from zero to a maximum velocity, V_{max}, according to equation (A2-6). When the speed of the moving load is modelled using this relation, the maximum velocity is defined to be the velocity given in Table 4-1. Therefore, the speed starts at zero and increases to a maximum speed corresponding to those given in the table. By choosing the previously determined velocities of Table (4-1) to occur at the base circle

where the velocity is maximum, the RPM of the gear for each non-dimensional velocity can be determined. From equations (A2-6) and (A2-7) the load cycle time for a meshing tooth can be shown to be;

$$TF = 2S/V_{max} \qquad (4\text{-}9)$$

where S is the distance along the involute from the tip to the base circle, and V_{max} is the velocity at the base circle. Equation (A2-6) can then be used to calculate the angular velocity of the gear;

$$OMEGA = \frac{Vmax}{TF*RB} \text{ (rad/sec)} \qquad (4\text{-}10)$$

For each non-dimensional velocity, load cycle times, TF, and the RPM's of the test gear are found to be;

V*	V_{max} (in/sec)	TF(sec)	RPM
0.001	2025	.2436E-3	21470
0.005	1012	.4875E-3	10730
0.003	607	.8127E-3	6435
0.001	203	.2436E-2	2147

Table 4-2: Variable Velocity Parameters

To reiterate, the times TF included in Table 4-2 are those for which the velocity starts at zero at the tip and increases linearly to a maximum value, V_{max}. For a load moving with constant velocity, the time for the load to move over the involute is simply the distance, S, divided by the velocity.

Returning now to the non-dimensional parameters plotted by

Nagaya, for a constant speed moving load the position of the load along the involute is given by;

$$T = \frac{Vt}{L-LI} \qquad (4\text{-}11)$$

where T varies from 0.0 at the tip, to 1.0 at the root circle. A value T=0.8 correponds to a point near the base circle radius between nodes 110 and 121 (see Figure 2-12). Equation (4-11) is valid only for constant speeds, V.

(4.3) Description of Dynamic Loading Cases

The dynamic deflections of single spur gear teeth are generated using three loading cases; a constant speed constant magnitude load with impact engagement, a constant speed constant magnitude load using a finite load engagement rise time (for these two loading cases the load is applied normal to the tooth centerline), and a load with varying speed and magnitude. In this last case the load is applied normal to the involute.

The first of these three loading cases is designed to imitate exactly the forcing function used by Nagaya. At time equal to zero, a load of 1000 lbs, simulating an impact load, is applied to the tip of the tooth, and maintained until the end of the load cycle (i.e. from the tip to the base circle). (Whenever the terms "impact loading" are used, the author is describing a step function). To simulate this loading condition for the finite element analysis, time functions representing nodal load histories are calculated for each node on

the involute. For the load moving between nodes i and j, the force histories are described by equations (2-36) and (2-37);

$$F^i = P(t)\left(\frac{L-Vt}{L}\right) \qquad (4\text{-}12)$$

$$F^j = P(t)\left(\frac{Vt}{L}\right) \qquad (4\text{-}13)$$

where; L is the distance between nodes, V is the velocity of the moving load, and t the time. With several load value data points defined along the involute, the finite element code uses these points and linearly interpolates between them to define the time functions. The time functions for this loading case are shown in Figure 4-2. In Figure 4-2 the node numbers correspond to the first eleven nodes on the right involute surface of the tooth.

To determine the effect of impact load engagement, another test is run using a finite rise time for the load on the first node. Instead of the load applied all at once at time equal to zero, it starts at zero and gradually increases to the maximum value (see Figure 4-3). Here the magnitude of the load is zero

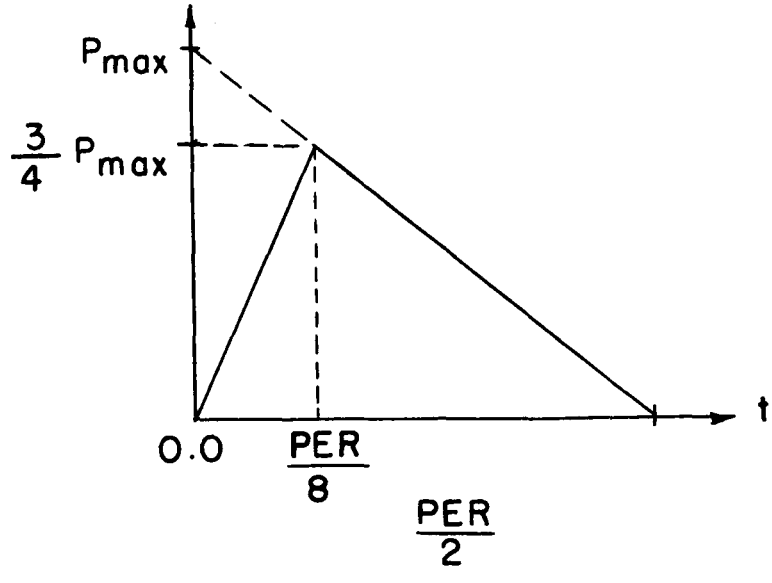

Figure 4-3: Finite rise time

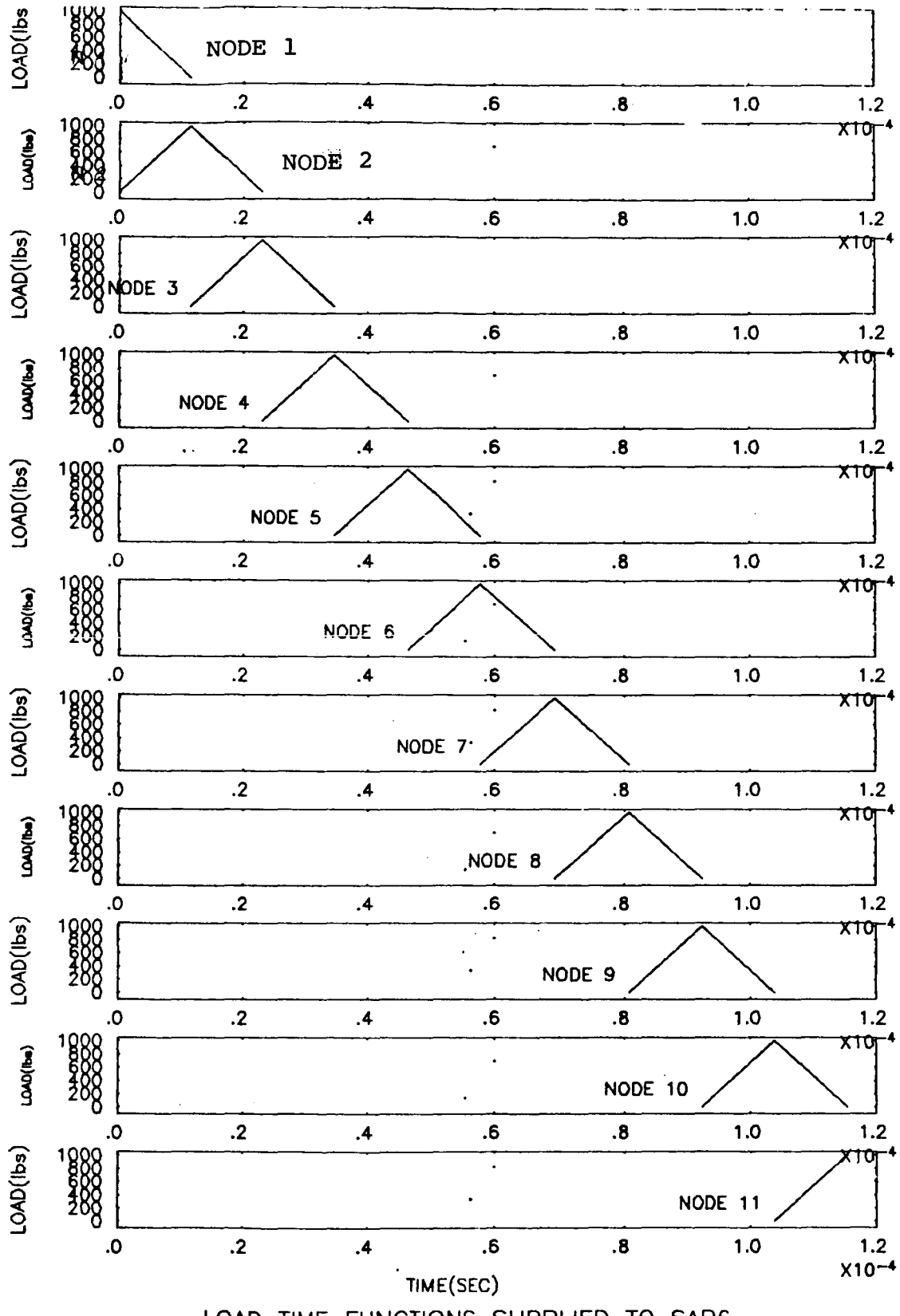

Figure 4-2: Impact load engagement

at t equal to 0.0 and goes up to 3/4 of P_{max} by PER/8. The rise time is defined as a fixed fraction (PER/8) of the time function period. As the speed of the moving load increases, the rise time decreases. Therefore, the rise time for V*=0.001 is ten times greater than for V*=0.01. The time functions for this loading case are shown in Figure 4-4. Only the first time function is different between Figures 4-2 and 4-4.

The last loading case tested is one in which the speed and the magnitude of the load vary with time. Wallace and Seireg [9] give idealized relationships for the magnitude of the load on a gear tooth as a function of time and the contact ratio. They are;

$$P(t) = \tfrac{1}{2}\, Pmax\left(1-\cos\left(\frac{\pi t}{\alpha TF}\right)\right) \qquad \text{for: } 0.0 < t < \alpha TF$$

$$P(t) = Pmax \qquad \text{for: } \alpha TF < t < (1-\alpha)TF \qquad (4\text{-}14)$$

$$P(t) = \tfrac{1}{2}\, Pmax\left(1-\cos\left(\frac{\pi (TF-t)}{\alpha TF}\right)\right) \qquad \text{for: } (1-\alpha)TF < t < TF$$

where; TF is the load cycle time, t is the time along the involute, and α is a factor dependent on the contact ratio. A value of 0.28 for α is used, corresponding to a contact ratio of 1.56. The force history described by equations (4-14) is plotted in Figure 4-5. By applying equations (2-36) and (2-37) with the load replaced by equations (4-14), the time functions generated for this loading case are like those shown in Figure 4-6. Note that the time function period decreases as the load moves down the involute due to increasing speed.

Equation (4-12) and (4-13), along with equation (4-14) are

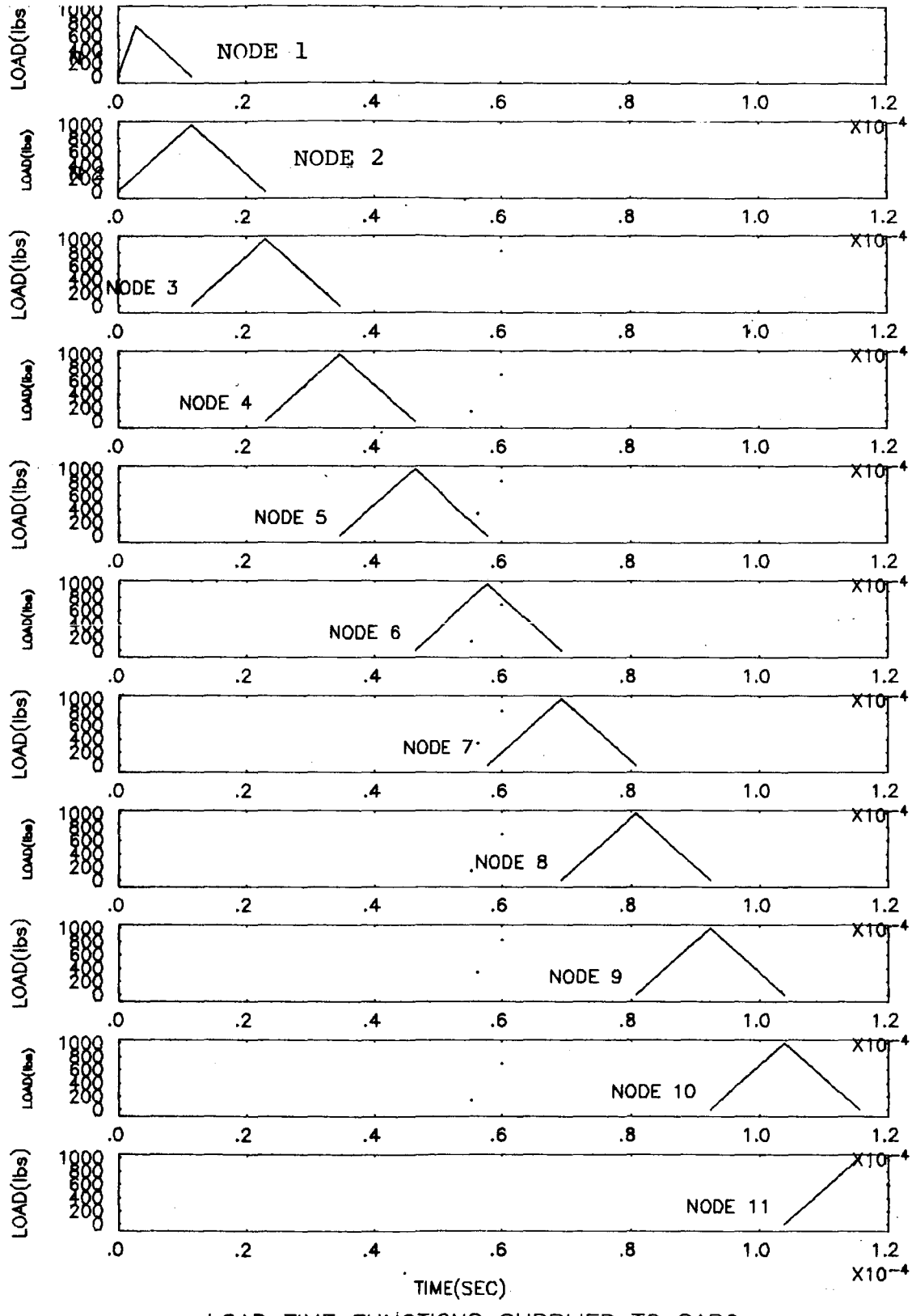

Figure 4-4: Gradual load engagement

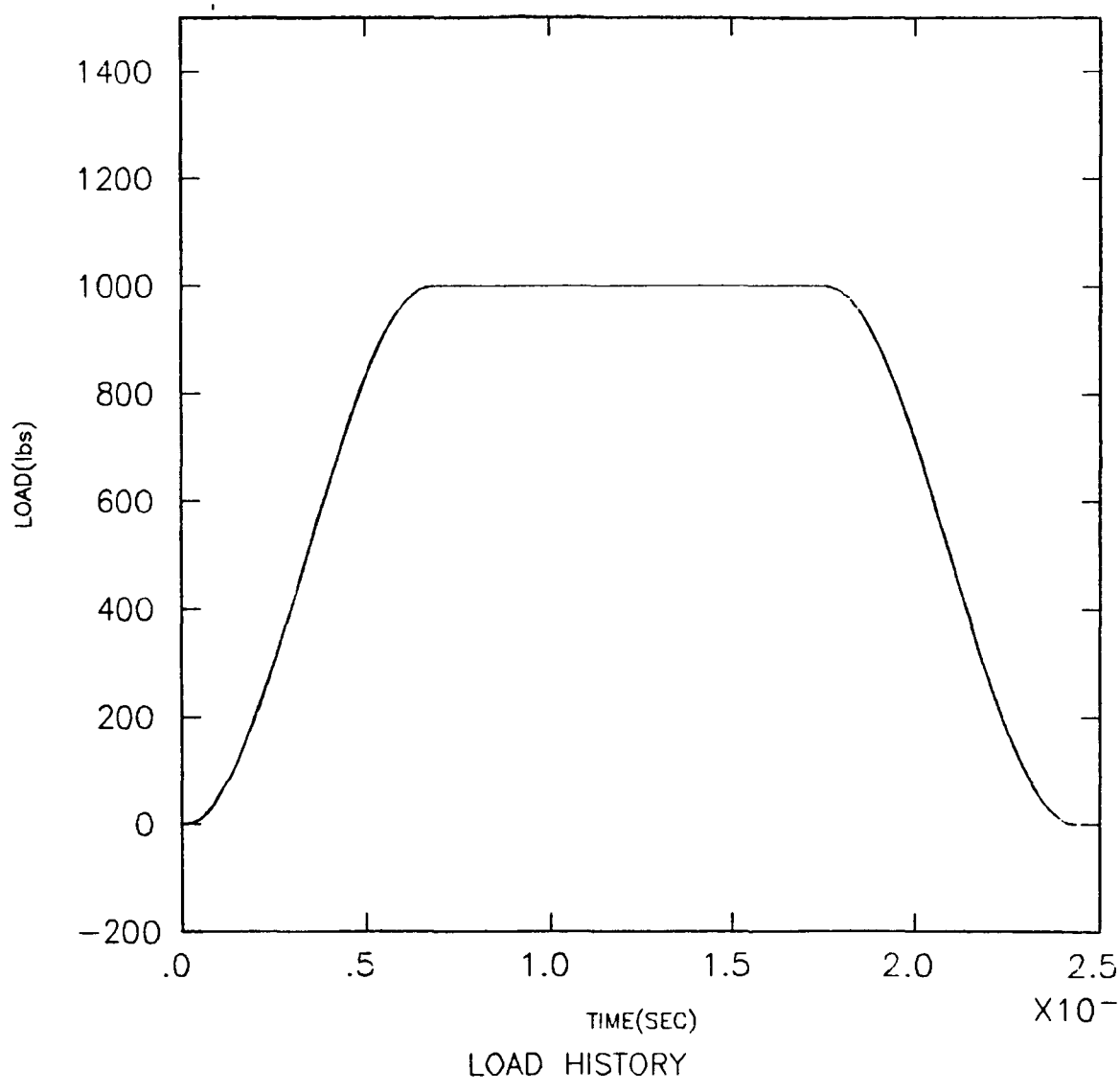

Figure 4-5: Wallace - Seireg loading

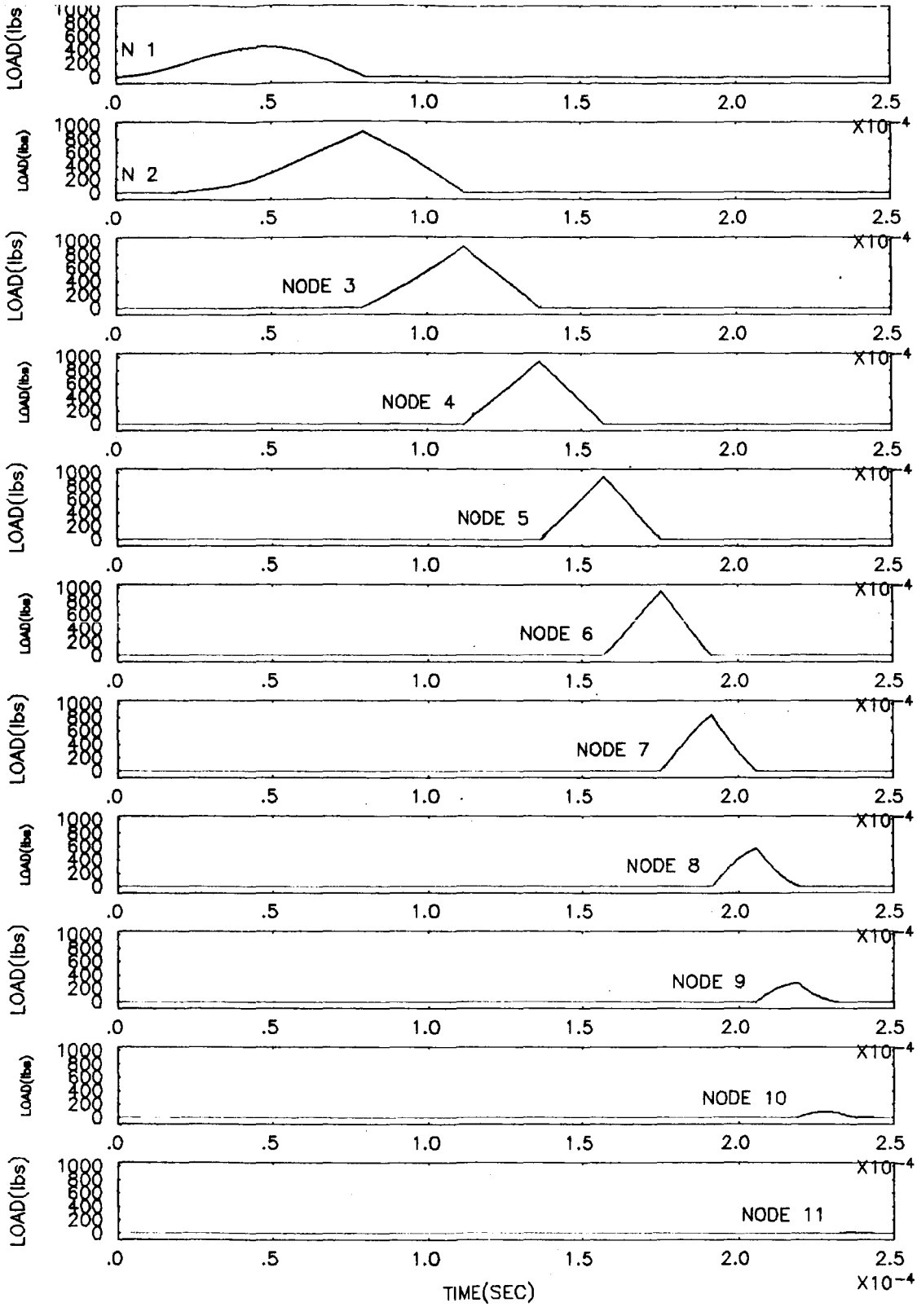

LOAD TIME FUNCTIONS SUPPLIED TO SAP6

Figure 4-6: Wallace- Seireg loading

used in a time function generation algorithm which is included in Appendix 1.

(4.4) Finite Element Test Results

The results contained in the proceeding sections were obtained using the SAP6 finite element code, implemented on the UNIVAC 1100/80 computer facility at Michigan Technological University.

(4.4.1) Comparison of Static Results

As a preliminary check on the accuracy of the finite element analysis technique applied to gear teeth, static-deflections obtained using finite elements are compared to those calculated by Nagaya using Kara's assumption for the profile of gear teeth. Comparisons are made with and without the rim included in the analysis. Figure 4-7 shows the plots of the normalized centerline deflections obtained using Timoshenko beam constraints. The dashed lines are the static deflections calculated by Nagaya. From the figure it is apparent that the Timoshenko beam (used to produce the dashed lines) is stiffer than the tooth. Going back to Figure 3-2, it is seen that the beam is considerably larger than the tooth, especially towards the base. Thus one would expect the beam to be stiffer. As the load is applied closer to the base of the tooth the difference between the static deflection curves becomes less exaggerated. For T=0.8 the centerline of the tooth actually deflects less than the beam. The reasons for this are not completely clear. One possible explanation, however, is the

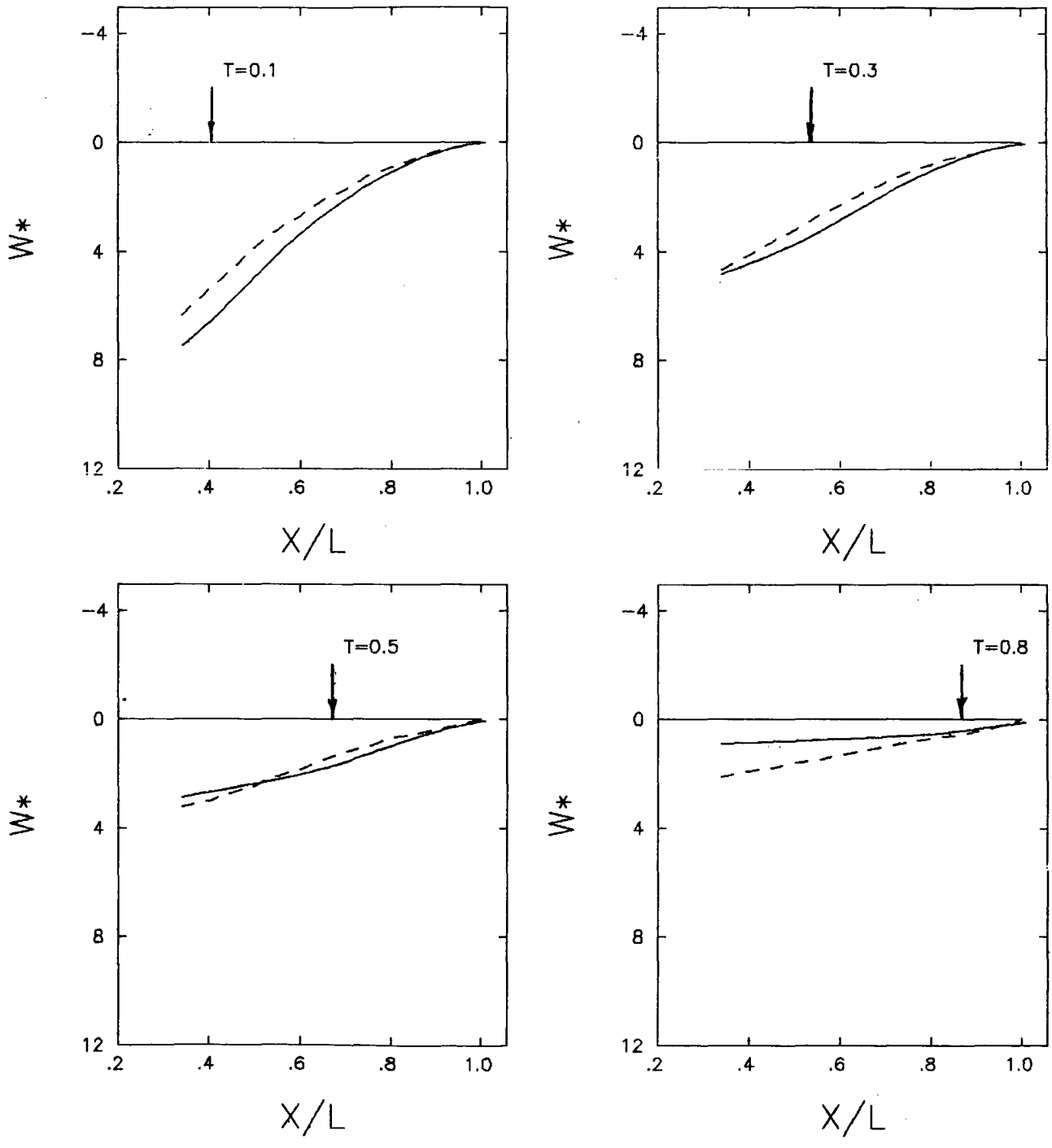

STATIC DEFLECTION CURVES: COMPARISON OF FEM AND KARAS' TECHNIQUES

Figure 4-7: Timoshenko beam constraints

fact that as the load is applied closer to the base, the amount of local deformation around the point of load application increases due to increased nodal spacing. This causes the tooth centerline to deform around the local deformation, thus decreasing the overall deflection of the gear tooth. (Appendix 3 includes the actual tooth in the statically deformed condition, illustrating the increase in local deformation). In these figures, the compatibility of the element is not violated. The deformation scale factor causes element overlap.

With the rim included in the analysis, the centerline deflections are considerably more severe (see Figure 4-8). The curves obtained by Nagaya, represented by the dashed line, are exactly those pictured on Figure 4-7. The purpose of this set of plots (Figure 4-8) is to emphasize the added flexibility afforded by the rim material. (Appendix 3 also contains the tooth in the deflected state with the rim included).

(4.4.2) Modal Analysis - Determination of Mode Shapes and Natural Frequencies

In Nagaya's paper, the differential equation for the non-dimensional deflection, W*, is derived and then solved numerically. The solution to the differential equation (eigenvalue problem) includes an infinite number of natural frequencies (eigenvalues) and an infinite number of mode shapes (eigenvectors). However, he included only the first three eigensolutions in the dynamic response analysis. It should also be mentioned that the differential formulation is done for transverse vibration so only bending modes are included.

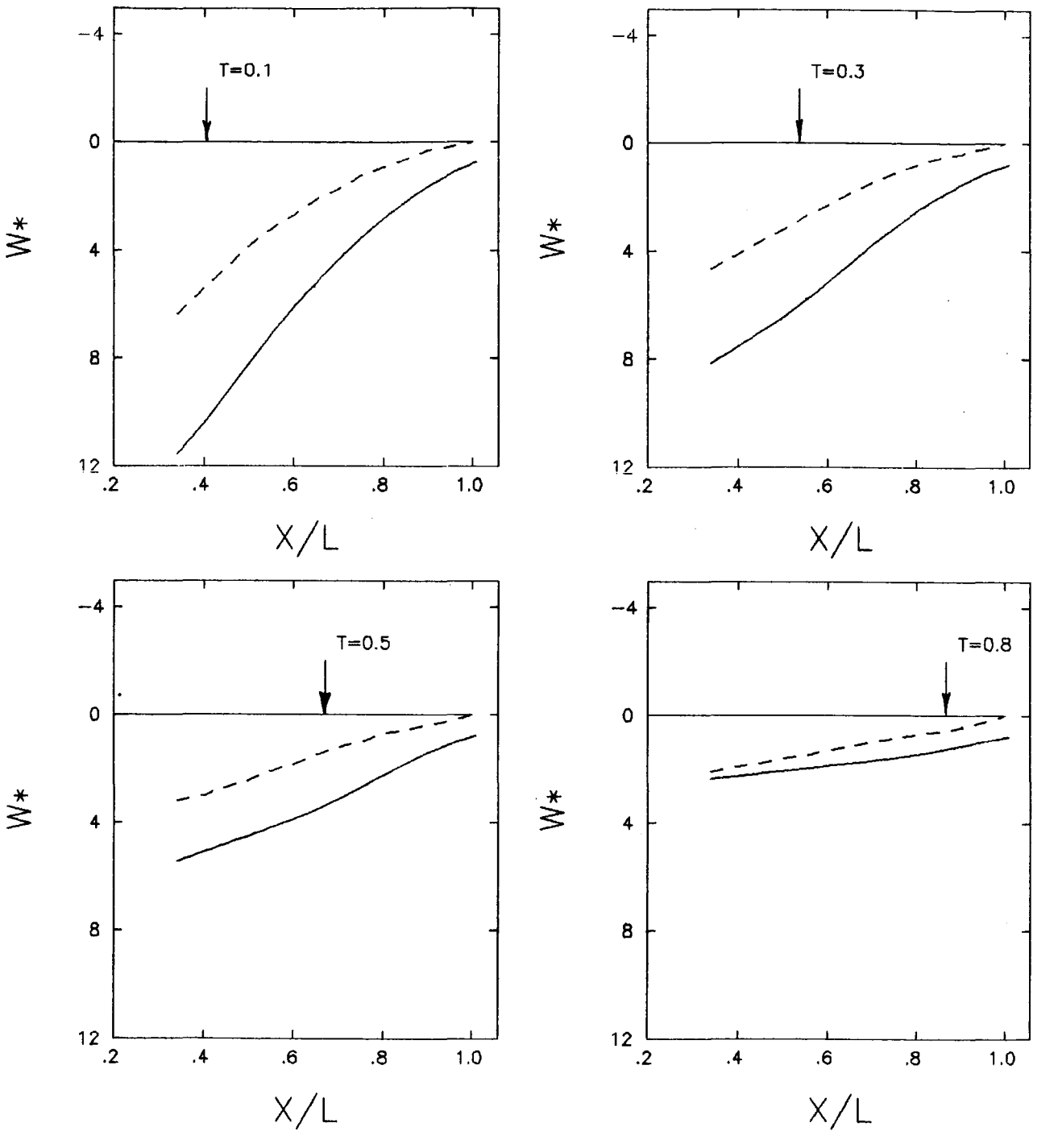

STATIC DEFLECTION CURVES: COMPARISON OF FEM AND KARAS' TECNIQUES

Figure 4-8: Rim included

For the present analysis the mode shapes and natural frequencies are determined from the finite element model by solving the general equation;

$$([K] - \lambda[M])\{D\} = 0 \quad \text{for} \quad \lambda = \omega^2$$

for pairs of λ and $\{D\}$. These results are then used in a modal response analysis to determine the response of the tooth to the moving loads. For this analysis ten modes are included, with both transverse and axial vibration. Appendix 3 includes the first few mode shapes and natural frequencies of the tooth for both constraint cases. Again, note the difference in flexibility between the two models (with and without the rim).

The first three natural frequencies from Nagaya's work are compared with those found for the actual tooth. Both bending and axial modes are included in the finite element analysis, so the first three bending modes from this analysis are used for comparison (modes 1,3,4) (see Table 4-3).

NAGAYA		FEM	
Mode	FREQ (rad/sec)	Mode	FREQ (rad/sec)
1	1.092E6	1	5.718E5
2	3.764E6	3	1.436E6
3	9.488E6	4	2.650E6

Table 4-3 Comparison of Modal Results

As expected, the natural frequencies of the beam approximation are somewhat higher than those of the tooth (beam constraints),

partly due to the additional material toward the base of the beam.

(4.4.3) Dynamic Deflections: Timoshenko Beam Constraints

(4.4.3.1) Impact Loading

Shown in Figures 4-9a and 4-9b are the normalized centerline deflections obtained using the impact engagement loading case (see Figure 4-2). Results are obtained for load positions of T=0.1,0.2,...,0.8. Each solid line represents the non-dimensional centerline deflection;

$$W^* = AoEW/PL$$

due to the applied moving load. Remember also that the deflections are plotted as a function of position;

$$T = \frac{Vt}{L-L1}$$

and not as a function of time. So for T=0.1 the solid lines show the normalized centerline deflections for the different speeds with the load one tenth the distance between the tip and the root. Remember also that the time for the load to move from T=0 to T=0.1 is different for all velocities, V*. The dashed lines correspond to the static deflections obtained for the tooth with the load in the position shown.

Initial examination of these plots suggests that the displacements are indeed dependent on the speed of the moving load. For slow speeds and low values of T (V*=0.001, T=0.1), the deflection is approximately twice the static as Nagaya

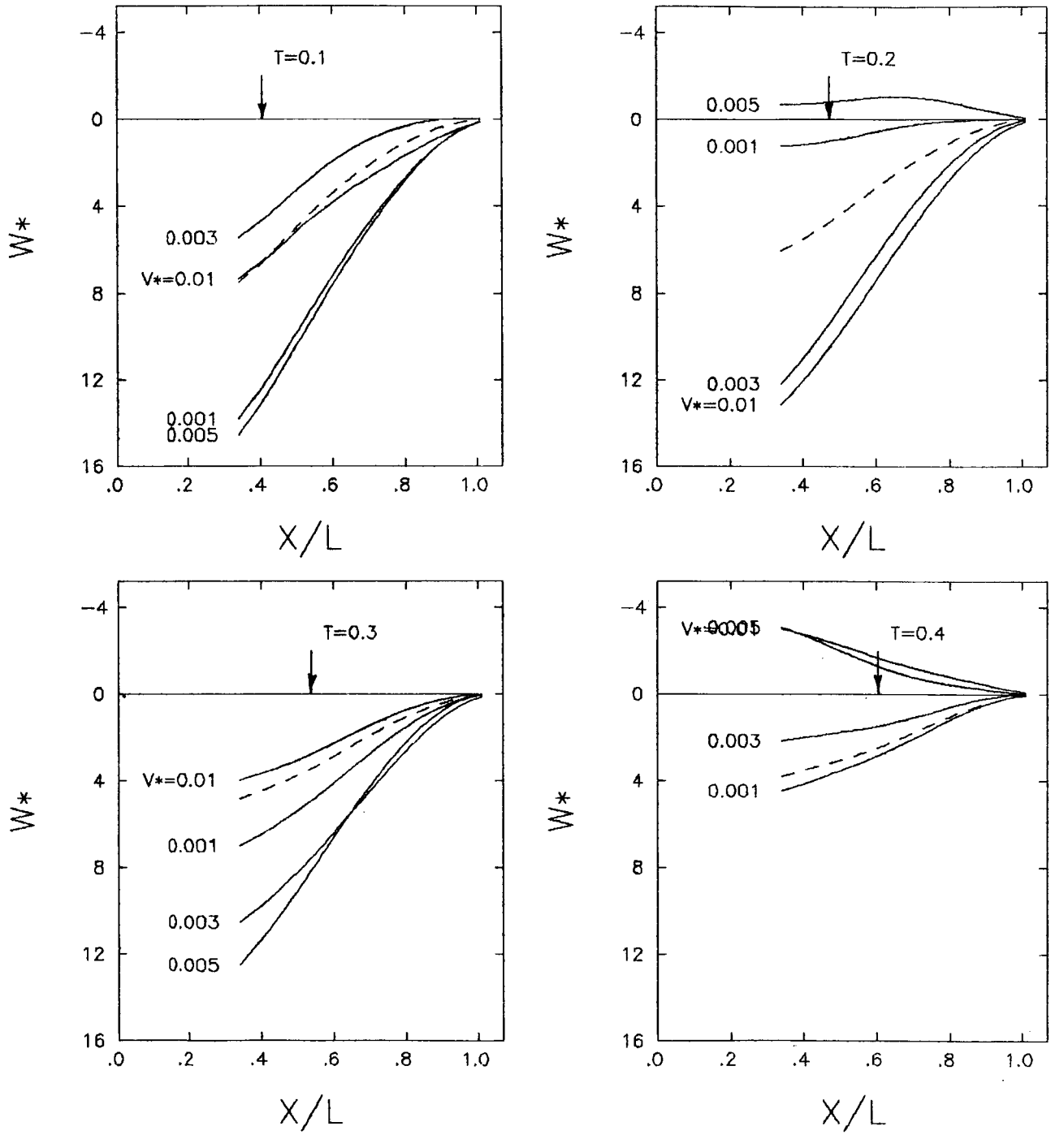

DYNAMIC DEFLECTION CURVES OF SPUR GEAR TEETH WITH MOVING LOADS

Figure 4-9a: Timoshenko beam constraints, impact load engagement

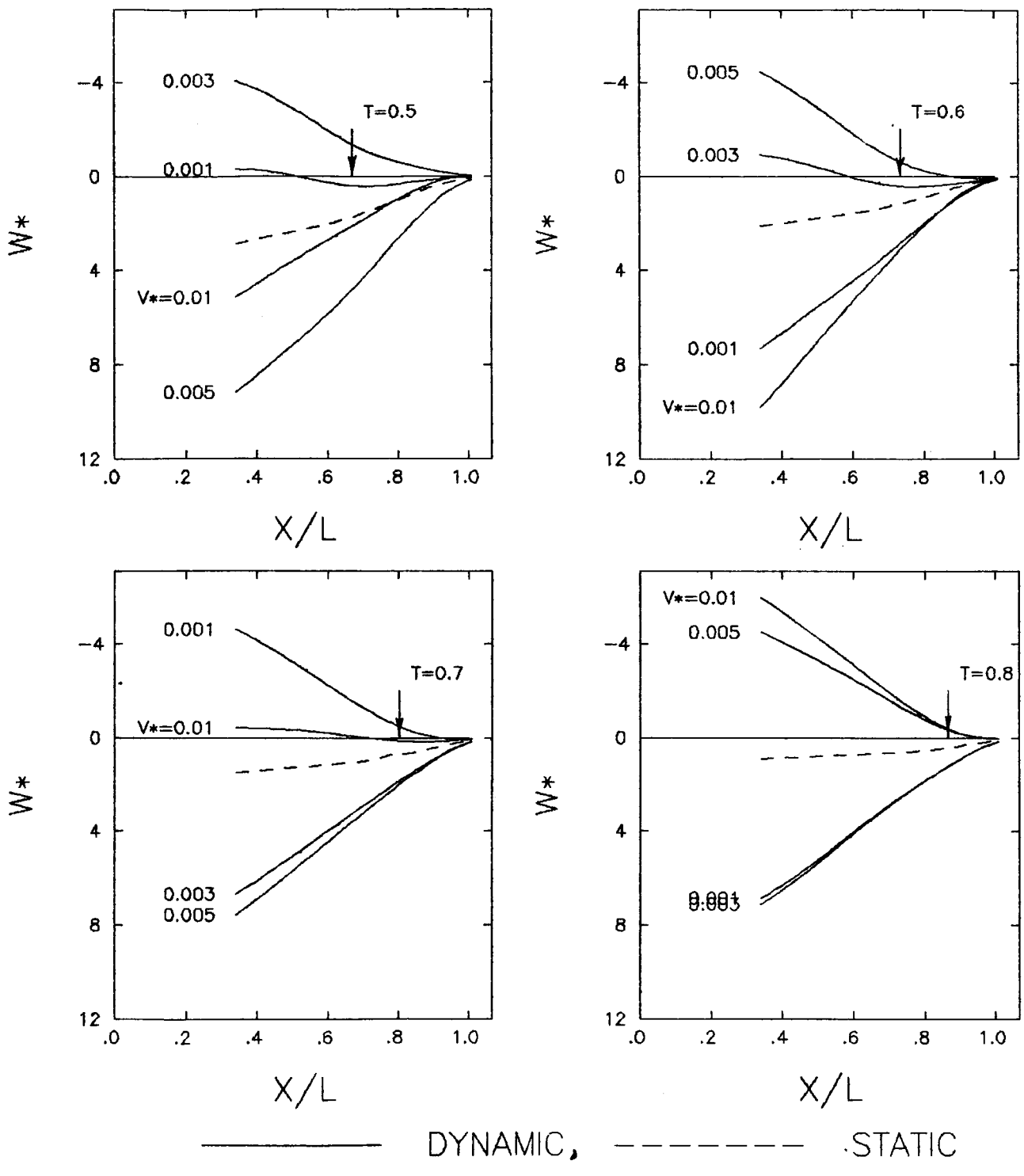

DYNAMIC DEFLECTION CURVES OF SPUR GEAR TEETH WITH MOVING LOADS

Figure 4-9b: Timoshenko beam constraints, impact load engagement

claimed. However, these plots do not give an accurate description of the dynamic deflections.

A much more representative picture is obtained when the actual deflection of the tooth tip is examined over the load cycle using small sampling intervals, (T=0.001 for V*=0.01). Figure 4-10 shows the true time history of the tooth tip as the load moves from the tip to the base of the tooth. Instead of the tooth being in a particular deformed state at load position T, dependent completely on the speed, it actually oscillates about a datum with constant amplitude and frequency. By assuming that the tip oscillates about the static position, the amplitude of oscillation is approximately twice the static, and is initiated by the impact load at the beginning of the load cycle. The only effect the speed of the moving load has is to change the number of oscillations per load cycle. Recall that the time for the load to move from T=0.1 to T=0.8 is ten times greater for V*=0.001 than for V*=0.01. Therefore, approximately ten times more oscillations occur for the slower of the two speeds.

From Figures 4-9 and 4-10 we can then conclude that the deflections of the tooth do not depend so much on the speed of the moving load, but on the tooth position at the instant the deflection sample is taken. By roughly lining up the position and deflection on the tip deflection curves, the position of the tip of the tooth shown in Figures 4-9a and b can easily be duplicated.

The datum about which the tooth oscillates is determined

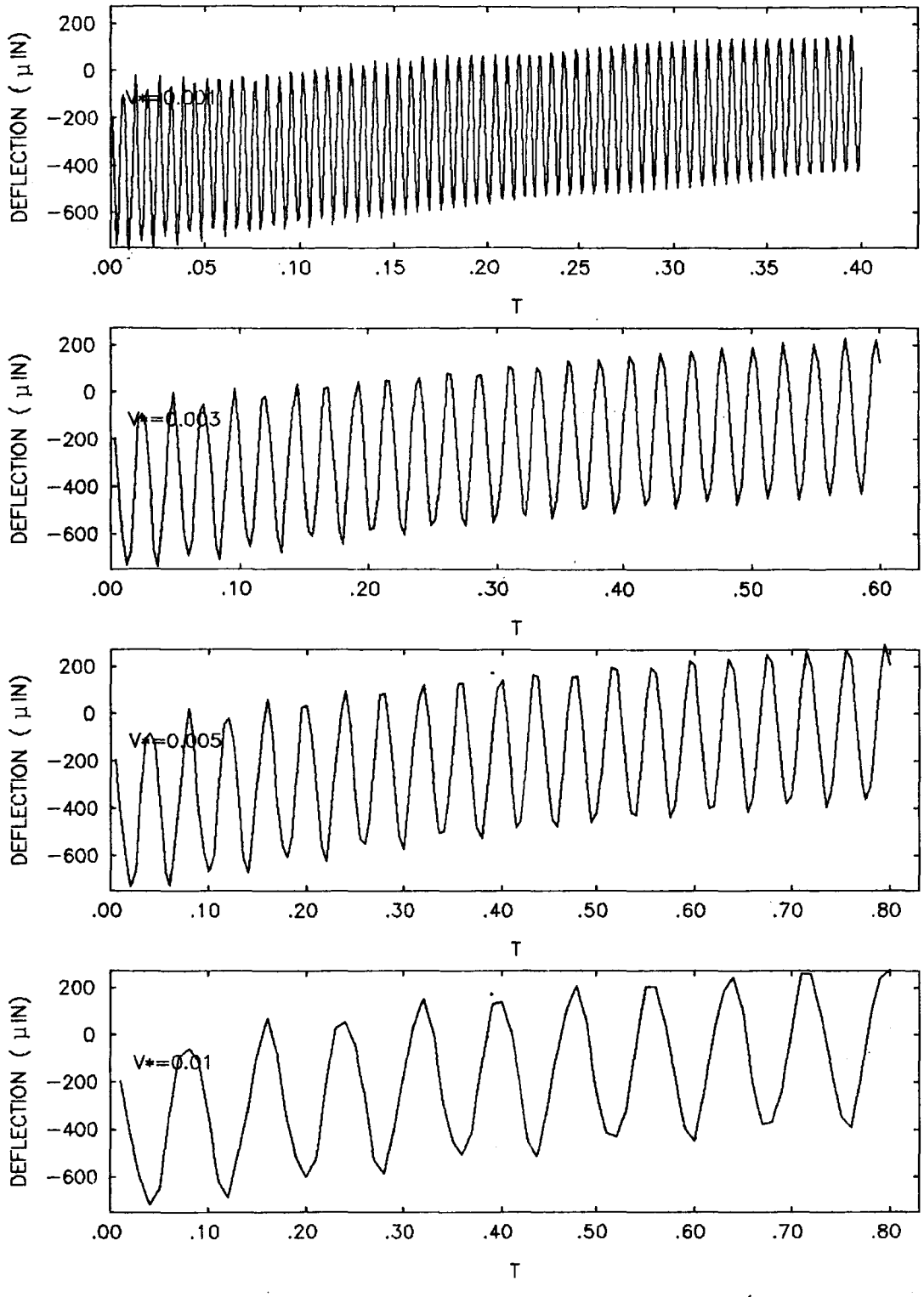

TOOTH TIP DEFLECTION TIME HISTORY;BEAM CONSTRAINTS (RISE TIME=0.0)

Figure 4-10

by repeating the previous analysis with the system critically damped. The transient caused by the impact load is then "filtered" out with only the steady state response remaining. Figure 4-11 shows the non-dimensional centerline deflections for all four moving load speeds. From the figure it is apparent that all centerline deflections lay over the static curve. To verify this claim, the tooth tip deflection histories are again plotted. In Figure 4-12 the plots show the tip following the static curve.

(4.4.3.2) Finite Engagement Rise Time Loading

In this test the tooth is subjected to the moving load conditions illustrated in Figure 4-4 where the load on the first node is gradually applied over a time of PER/8. This loading case produces significantly different results compared to the impact load test. (Since the normalized centerline deflection curves do not accurately represent the dynamic deflection phenomenon, they are not included). Figure 4-13 gives the tooth tip deflection history for this loading condition. The tooth still oscillates about the static position with constant frequency, but the amplitude varies significantly with speed. The reason for this change, from the previous load case, is best explained by again considering the load engagement rise time.

In Chapter 4.3, Figure 4-3, the rise time is defined as a fixed fraction of the time function nodal period (PER/8). For V*=0.01, the rise time is ten times less than for V*=0.001.

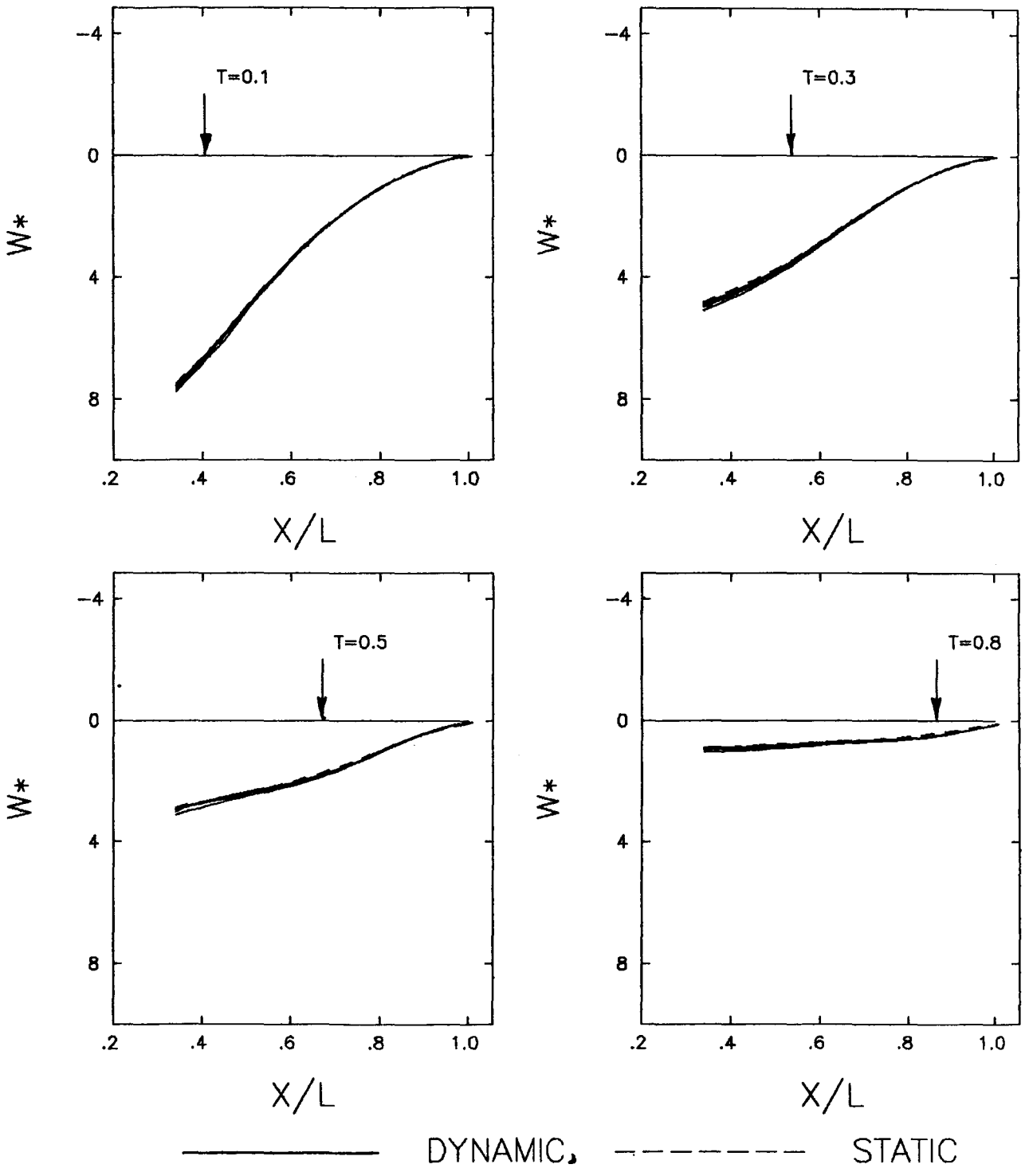

DYNAMIC DEFLECTION CURVES WITH MOVING LOADS: DAMPING $\zeta = 1.0$

Figure 4-11

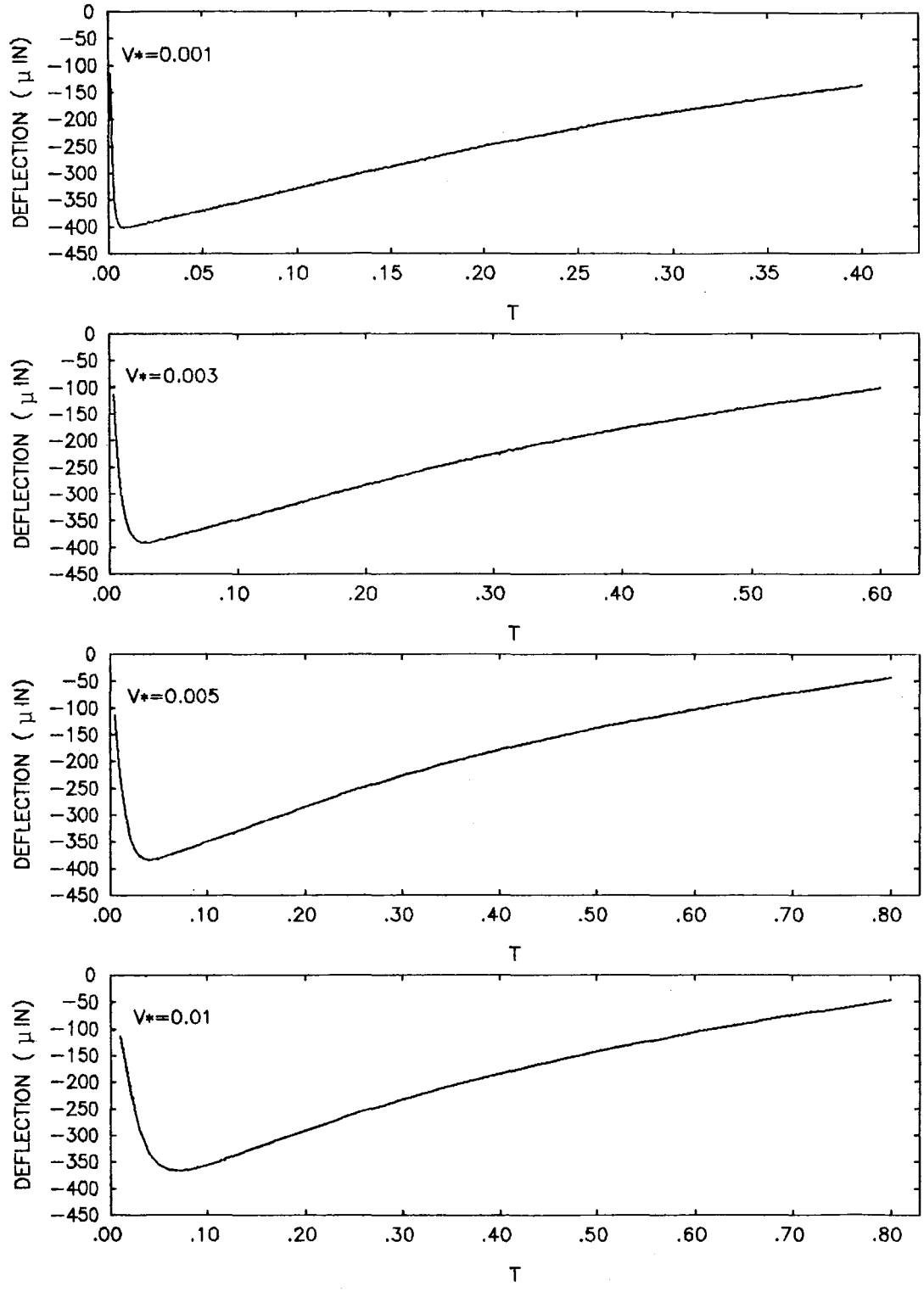

TOOTH TIP DEFLECTION TIME HISTORY: BEAM CONSTRAINTS, DAMPING $\zeta = 1.0$

Figure 4-12

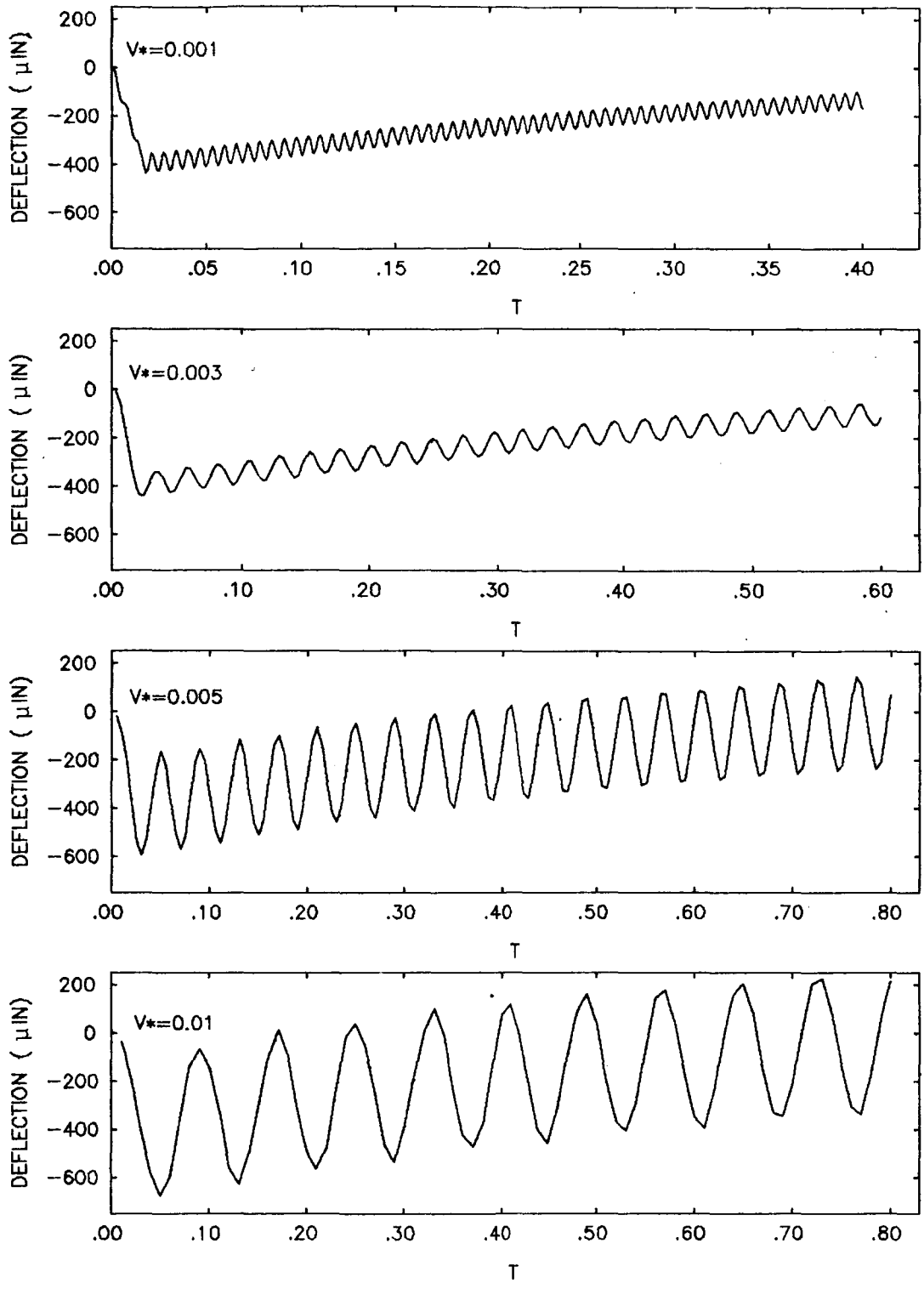

TOOTH TIP DEFLECTION TIME HISTORY: BEAM CONSTRAINTS(RISE TIME=PER/8)

Figure 4-13

It should then be obvious, that as the speed of the load increases, the time function for the first node begins to approximate the step function impact load of Figure 4-2. Examination of the deflection amplitude for V*=0.01 of Figure 4-13 shows it to be nearly the same as V*=0.01 of Figure 4-10.

(4.4.3.3) Wallace - Seireg Loading

For this loading case (time function shown in Figure 4-6) both the speed and magnitude of the load vary with time. With a contact ratio of 1.56, the load doesn't reach the maximum value of 1000 lbs until it is between the second and third nodes. Since the magnitude increases smoothly and gradually, no abrupt load changes are encountered.

The tooth tip deflection history curves for this loading case are included in Figure 4-14. Due to the nature of the speed variation, the deflections are plotted as a function of time instead of position as done previously. Here it can be seen that the tip of the tooth follows the static deflection curve for each of the speeds. This is again due to the slow and gradual engagement of the load.

(4.4.4) Dynamic Deflections: Rim Included

Including the rim adds flexibility to the system as already mentioned. The tooth tip deflection history for the impact loading case, shown in Figure 4-15, illustrates this fact. As before, the amplitude and frequency of vibration are the same for each of the four speeds. However, compared to the beam constraint case of Figure 4-10, the amplitude is con-

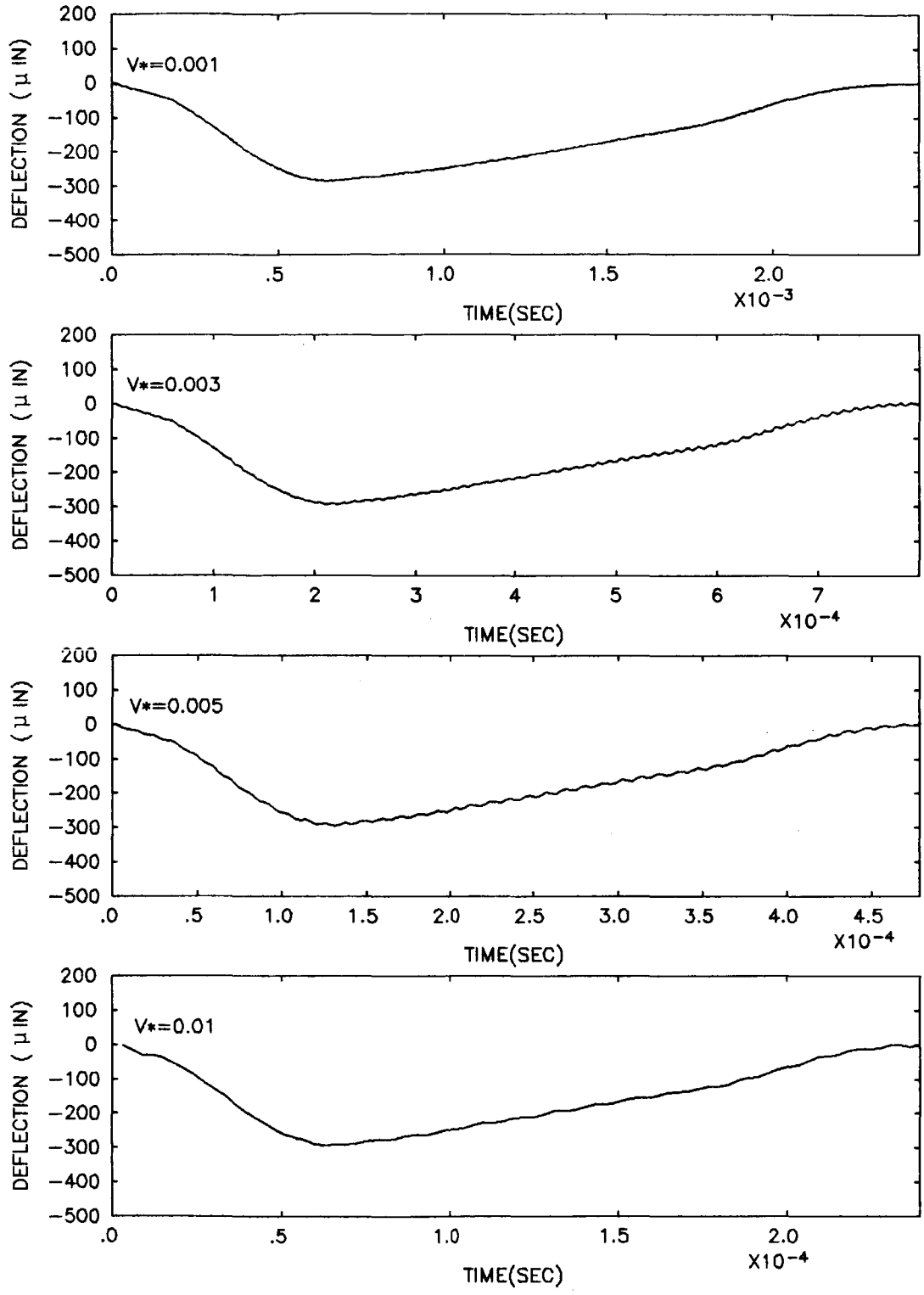

TIP DEFLECTION TIME HISTORY: BEAM CONSTRAINTS (VARIABLE SPEED)

Figure 4-14: Wallace- Seireg loading

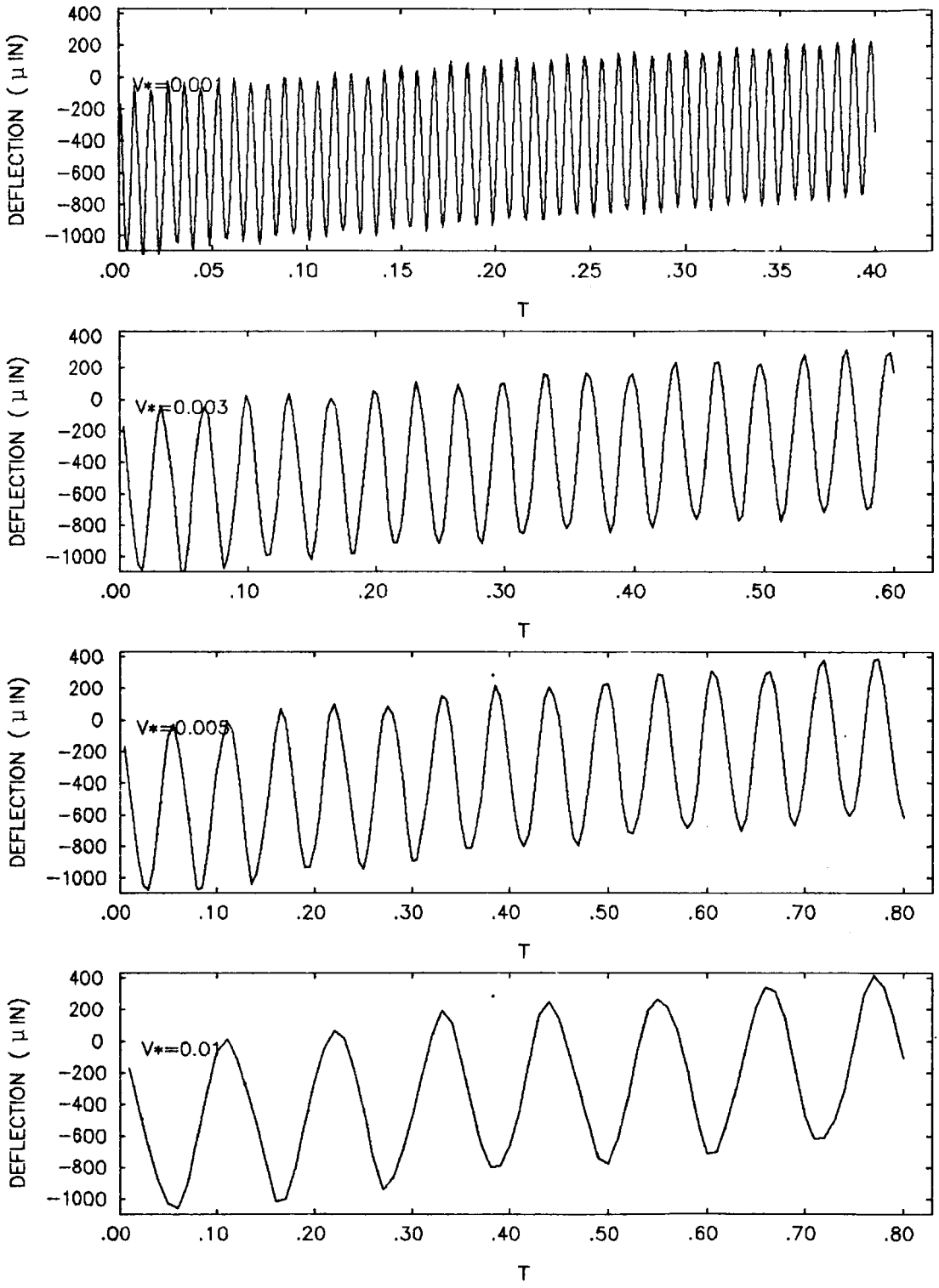

TOOTH TIP DEFLECTION TIME HISTORY: RIM INCLUDED (RISE TIME=0.0)

Figure 4-15

siderably larger and the frequency slower.

When the finite engagement rise time loading case is used the same general results are noted as before. That is, as the speed of the moving load increases, the rise time approaches impact conditions for V*=0.01 (see Figure 4-16).

Application of the Wallace-Seireg load history equations to the rim constraint case produces results which behave exactly as before. In Figure 4-17 the tip of the tooth deflects in proportion to the magnitude of the applied load. The oscillations about the static curve are evident but do not contribute significantly to the overall response.

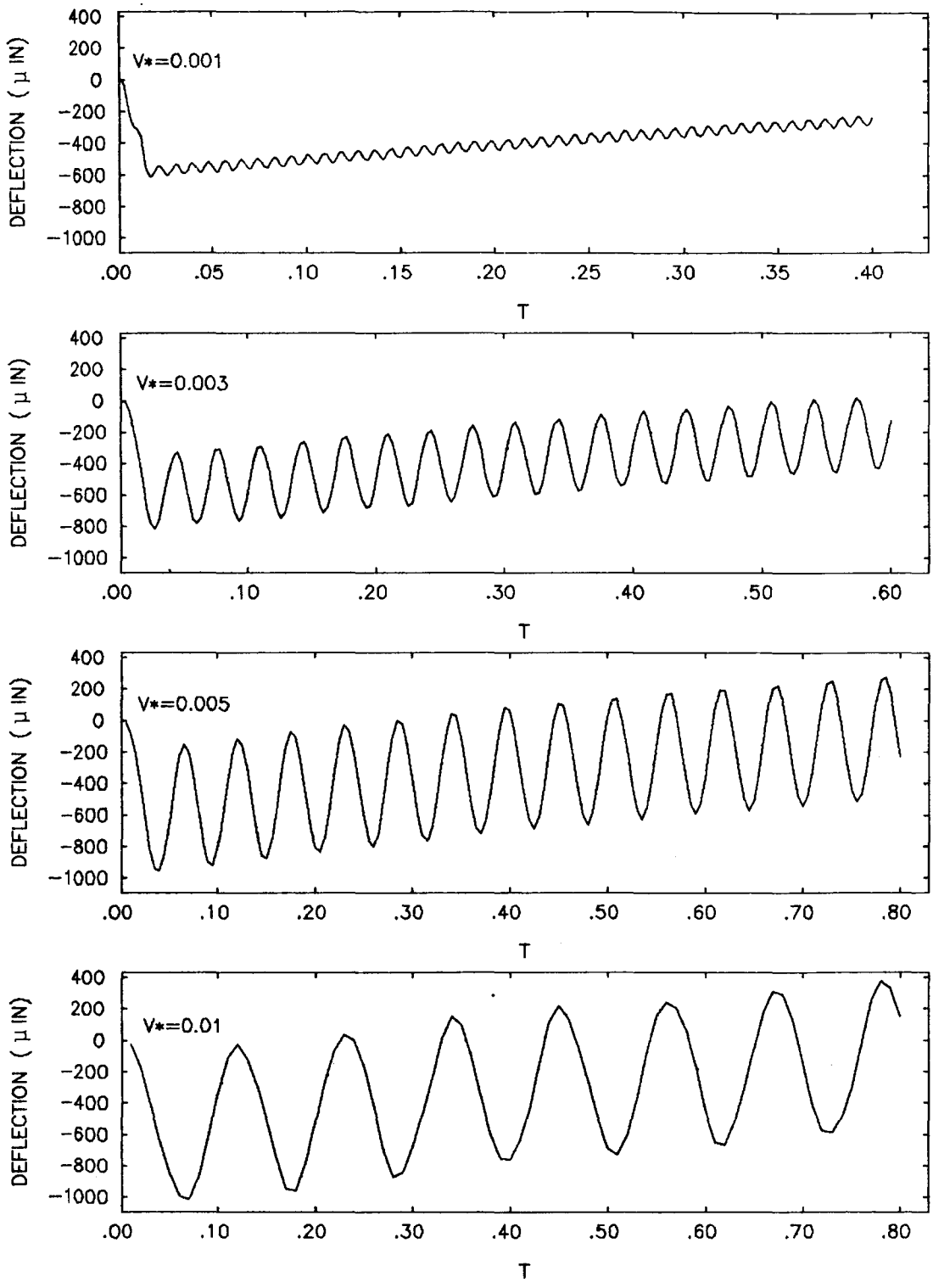

TOOTH TIP DEFLECTION TIME HISTORY: RIM INCLUDED (RISE TIME=PER/8)

Figure 4-16

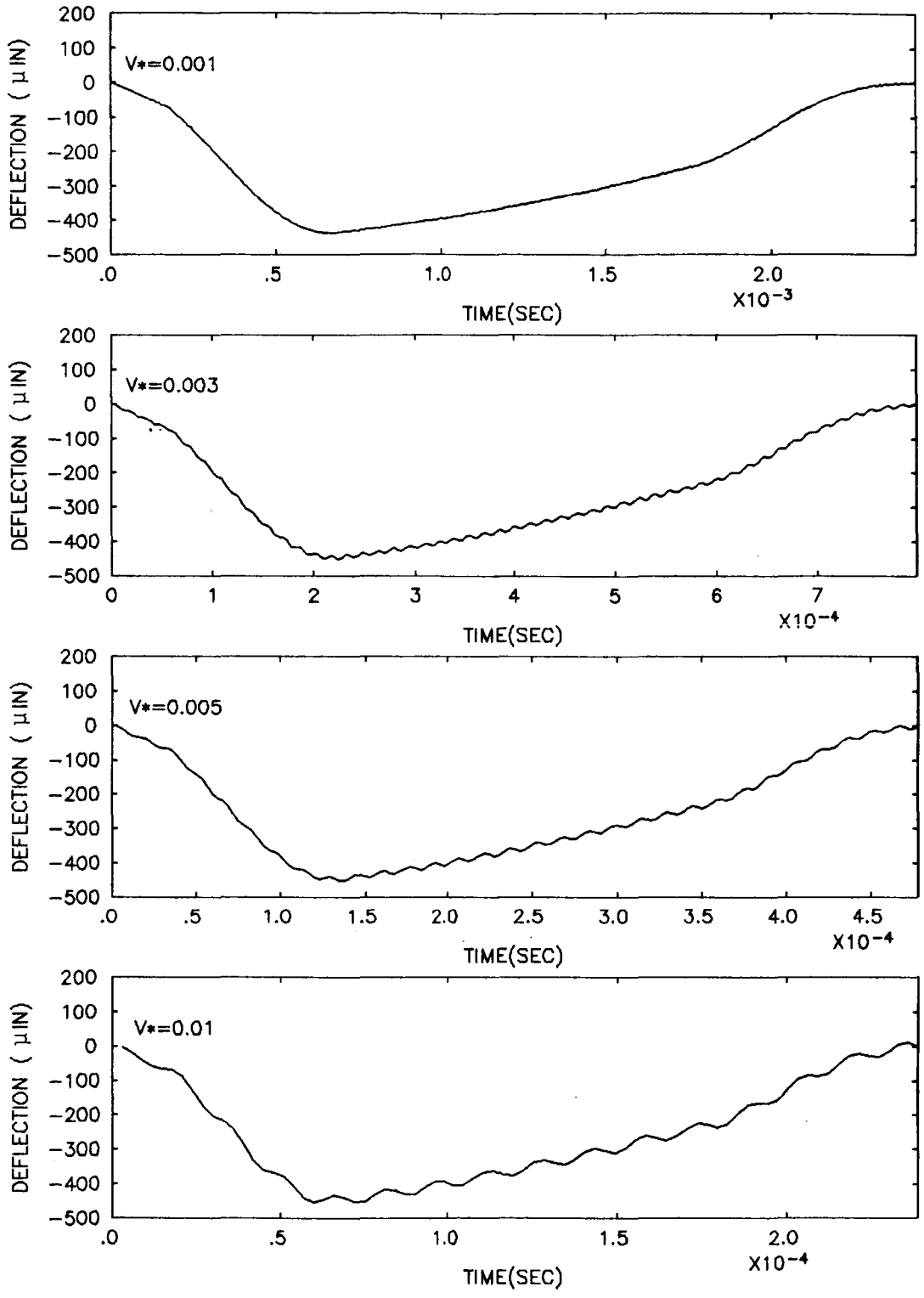

TIP DEFLECTION TIME HISTORY: RIM CONSTRAINTS (VARIABLE SPEED)

Figure 4-17: Wallace- Seireg loading

5. DETERMINING THE EFFECTS OF INERTIA ON THE DYNAMIC RESPONSE OF MESHING GEAR TEETH

In most theoretical models developed to determine the dynamic response of meshing gear teeth [1-5], the mass (inertia) of the tooth is neglected in the analysis. This simplification is based on the claim that the mass of the tooth is small compared to the mass of the hub.

To determine the effect of the inertia of the tooth on the dynamic response of a meshing gear pair, a simplified model of two cantilever beams attached to foundation masses is used.

The system analyzed is illustrated in Figure 5-1.

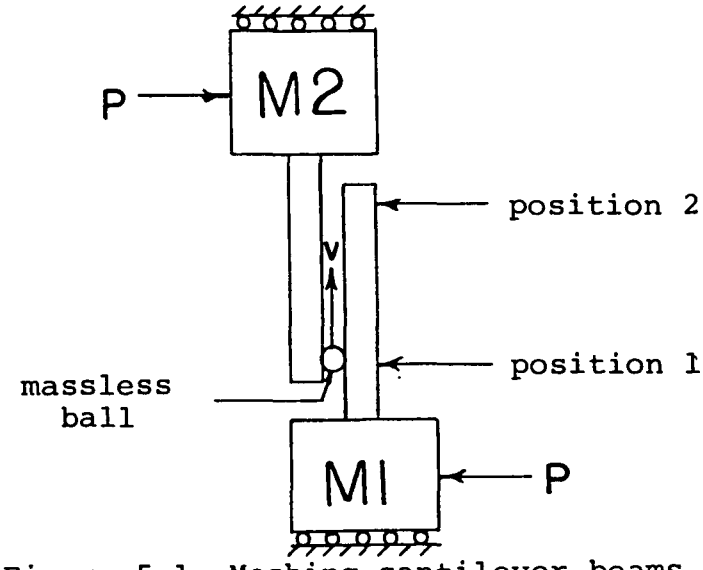

Figure 5-1: Meshing cantilever beams

Two cantilever beams with identical geometric and material properties are rigidly fixed to two foundation masses, M1 and M2. In this analysis, the masses of the foundations are defined to be the same. The two beams are held together by opposing forces, P, acting on the masses M1 and M2. A massless ball acts as the contact point between the beams and moves along the

beams at a prescribed speed. As the contact point moves from position 1 to position 2 at a velocity V, the change in stiffness of the beams causes the masses to oscillate in the direction of P at the system resonant frequency. To simplify the problem, movement only in the direction of P is allowed.

The dynamic response of the meshing cantilever beams is determined for two loading cases; one where the beams are assumed massless, the other where the masses of the beams are included. The system is analyzed using constant and variable speed moving loads of constant magnitude. Both impact and smooth load engagement responses are examined by changing the initial conditions of the system. These loading cases are analyzed using two values for the foundation masses of 1.0 and 1.0E-4 lbs.

(5.1) Analysis Using Massless Beams

Figure 5-2 shows the system used when the beams are assumed massless. As the contact point, represented by a

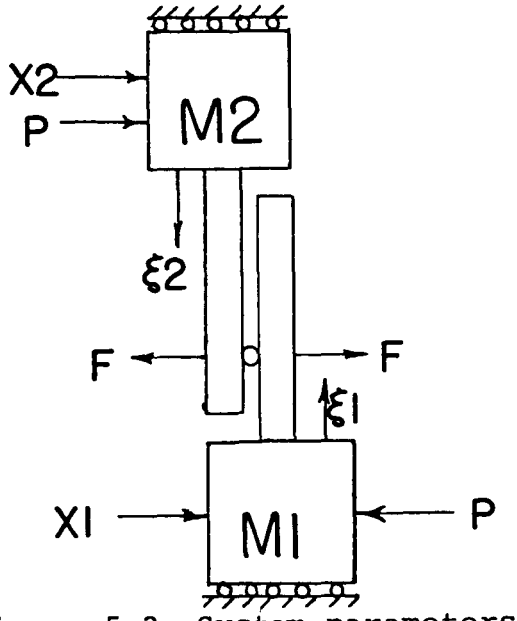

Figure 5-2: System parameters

massless ball, moves along the beams, the deflection of the beams will change due to the variation in stiffness. The stiffness of each beam varies with the local coordinate, ξ . Since the beams are massless, they do not affect the system resonant frequency, but follow the oscillations of M1 and M2 exactly. To determine the dynamic response for the massless beam configuration, the differential equations of motion are written and solved for this system.

(5.1.1) Equations of Motion

The equations of motion for this system are determined by first considering each beam-mass configuration as a free body (see Figure 5-3). Writing Newton's Second Law as the sum of

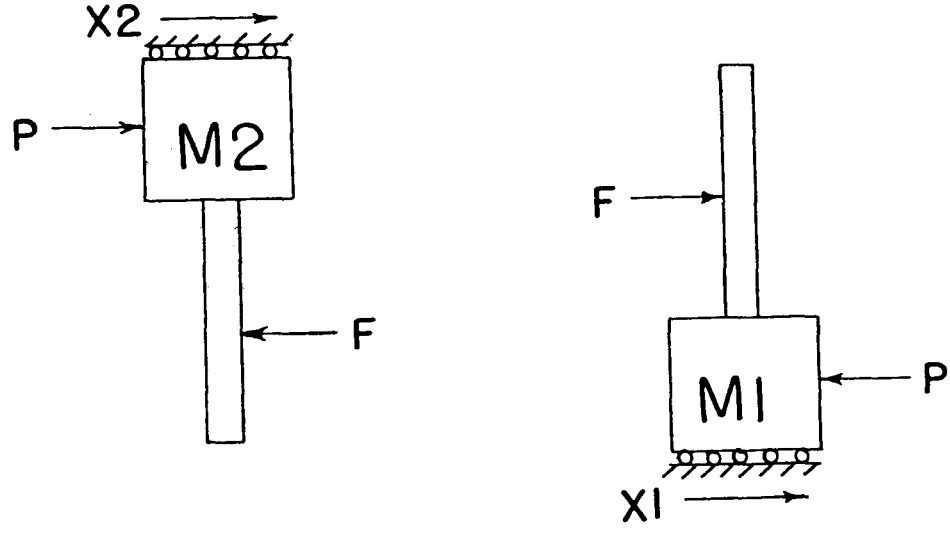

Figure 5-3: Free body diagrams

the forces acting on each body we have;

$$M1\ \ddot{X}1 = F - P \qquad \text{body 1} \qquad (5\text{-}1)$$

$$M2\ \ddot{X}2 = -F + P \qquad \text{body 3} \qquad (5\text{-}2)$$

(Here it is assumed that X1 and X2 define the positive displacement direction). Dividing through by the coefficient of the

second derivative term, and subtracting (5-1) from (5-2) yields;

$$\ddot{X}2 - \ddot{X}1 = -F(\frac{1}{M1}+\frac{1}{M2}) + P(\frac{1}{M1}+\frac{1}{M2}) \qquad (5\text{-}3)$$

To further simplify equation (5-3), the right hand side is combined and a common denominator is determined. This gives;

$$\ddot{X}2 - \ddot{X}1 = (P-F)\frac{M1+M2}{M1M2} \qquad (5\text{-}4)$$

where;

$$\frac{1}{M1}+\frac{1}{M2} = \frac{M1M2}{M1M1}\ (\frac{1}{M1} + \frac{1}{M2}) = \frac{M1+M2}{M1\ M2}$$

Making simple substitutions, equation (5-4) can then be written as;

$$M\ddot{X} = P-F \qquad (5\text{-}5)$$

where;

$$M = \frac{M1M2}{M1+M2}$$

and;

$$\ddot{X} = \ddot{X}2-\ddot{X}1$$

From beam theory, the static deflections of each beam at the point of contact of the load, are given by;

$$\delta 1 = \frac{F\xi_1^3}{3EI} \quad ; \quad \delta 2 = \frac{F\xi_2^3}{3EI} \qquad (5\text{-}6)$$

as illustrated in Figure 5-4. Equations (5-6) are written in

Figure 5-4: Beam deflection configuration

terms of the beam stiffness as;

$$\delta 1 = \frac{F}{K1} \quad ; \quad \delta 2 = \frac{F}{K2} \tag{5-7}$$

where;

$$K1 = \frac{3EI}{\xi_1^3} \quad ; \quad K2 = \frac{3EI}{\xi_2^3}$$

represent the stiffnesses of the beams.

As the load moves along between the beams, the varying stiffness causes M1 and M2 to oscillate at the resonant frequency of the system. To insure constant contact between the beams while the masses are vibrating, the following relationship, termed the constraint equation, must be satisfied;

$$X2 - X1 = \delta 1 + \delta 2 \tag{5-8}$$

where $\delta 1$ and $\delta 2$ assume orientations as shown in Figure 5-4. Substituting equations (5-7) into (5-8) gives the constraint equation in terms of the beam stiffnesses as;

$$X2 - X1 = \frac{F}{K1} + \frac{F}{K2} \qquad (5\text{-}9)$$

Combining the right hand terms in equation (5-9),

$$X2 - X1 = F(\frac{K1 + K2}{K1K2})$$

multiplying through by

$$K = \frac{K1K2}{K1+K2}$$

and letting X=X2-X1, yields a familiar form of the constraint equation, describing the deflection of a spring;

$$F = KX \qquad (5\text{-}10)$$

Inserting F from equation (5-10) into equation (5-5) gives the equation of motion for the massless beam system;

$$M\ddot{X} + KX = P \qquad (5\text{-}11)$$

where;

$$\ddot{X} = \ddot{X}2 - \ddot{X}1$$

$$X = X2 - X1$$

$$M = \frac{M1M2}{M1+M2}$$

$$K = \frac{K1K2}{K1+K2}$$

Initially, the system deflection is determined by assuming that static equilibrium is satisfied. Thus, at time equal to zero, the initial deflection is the applied load divided by the total stiffness (the combined deflections of the beams);

$$X(0) = X2(0)-X1(0) = P/K$$

With the initial deflections, equation (5-11) is solved using a fourth order Runge-Kutta integration algorithm. Since the Runge-Kutta algorithm used is designed for systems of first order equations, the second order differential equation (5-11) must be converted to first order. This is done by defining;

$$Y1 = \dot{X} \quad \text{and} \quad Y2 = X$$

Substituting these relations into (5-11), we then have;

$$M\dot{Y}1 + KY2 = P \qquad (5\text{-}12)$$

where at t=0.0,

$$Y1(0) = 0.0$$

$$Y2(0) = P/K$$

Given these initial values, the relations;

$$\dot{Y}1 = (P-KY2)/M$$

$$\dot{Y}2 = Y1 = \dot{X}$$

are used as input for Runge-Kutta and integrated to determine the displacement, X=X2-X1 during the load cycle. (See Appendix 7 for solution algorithm).

(5.1.2) Static Analysis

Before any dynamic analysis is performed, a static deflection test is done to provide a reference for dynamic deflection comparisons. Solving the relationship;

$$X2 - X1 = P/K$$

at different load positions produced the plots shown in Figure 5-5. The three blocks represent the components comprising the constraint equation (5-8). Deflections are determined between load positions 1 and 2 illustrated in Figure 5-6. The load position is measured relative to beam 1 as labelled on the abscissa of Figure 5-5.

(5.1.3) Dynamic Response Results

The dynamic response of the massless beam system is determined for two loading cases; a constant speed 1000 lb load, and a variable speed 1000 lb load. For each of these loading cases, two sets of initial conditions are considered; those defined for static equilibrium in equation (5-11), and another set where the initial deflection, X2 - X1, is equal to zero. The second of these initial conditions will cause the load P to be experienced as an impact load since the beams initially will have no deflection and will attempt to return to static equilibrium.

For loads moving with constant speed, speeds of; 1.0, 5.0, 10.0, 20.0, and 40.0 inches per second are used. This range of speeds is chosen in order to bracket the cycle period associated with the fundamental frequency of the system. The frequency of vibration of the system is constantly changing with the position of the load. However, a representative fundamental frequency is calculated when the load is halfway through the load cycle. At this position the beam stiffnesses are

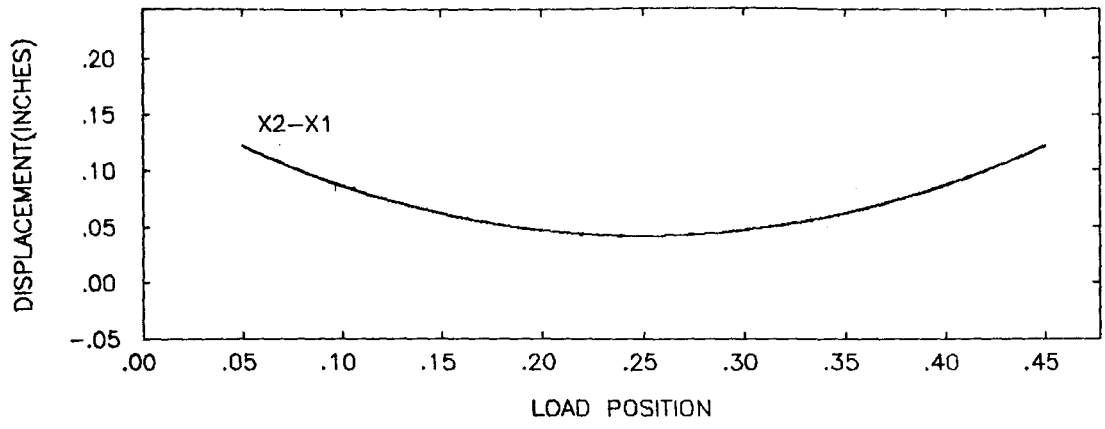

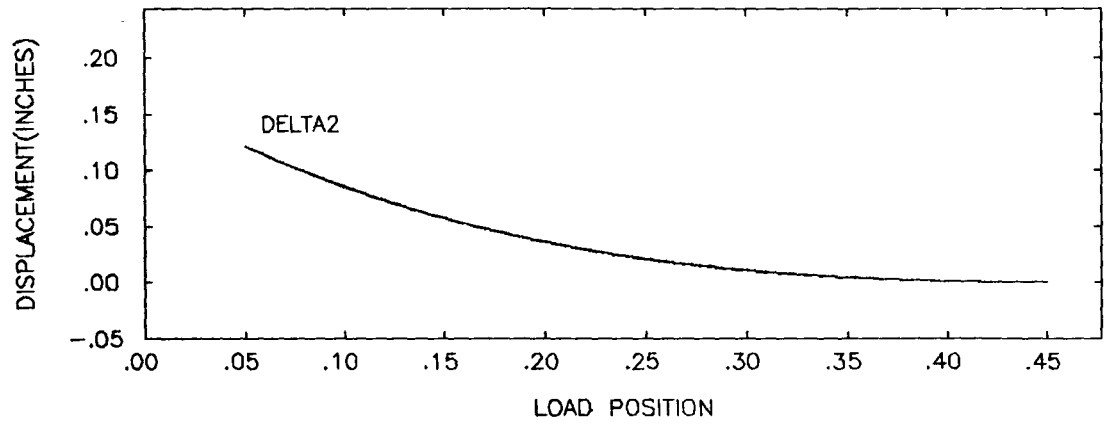

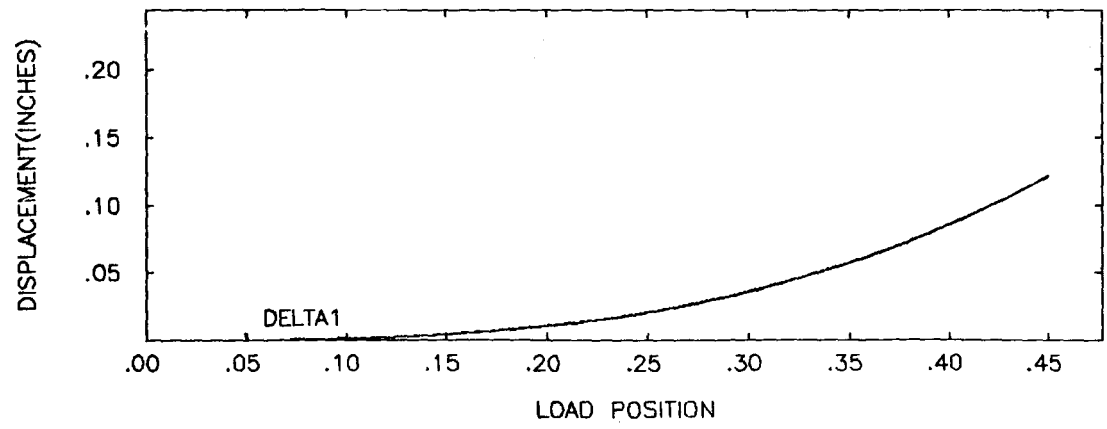

BEAM LENGTH = 0.5 IN; APLLIED LOAD = 1000. lbs

STATIC DEFLECTION OF MASSLESS CANTILEVER BEAMS

Figure 5-5

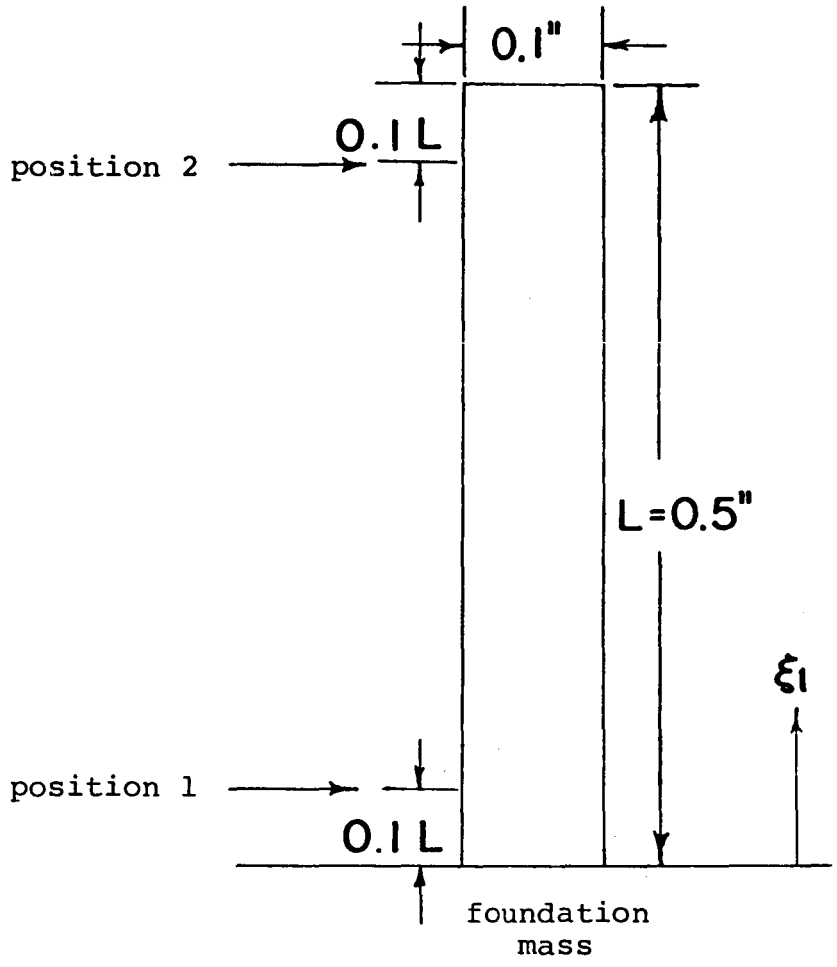

Figure 5-6: Beam dimensions and load cycle definition

equal. Then, we simply have a spring mass system whose undamped natural frequency is defined as;

$$\omega = \sqrt{\frac{K}{M}} \frac{1}{2\pi} \quad \text{(cycle/sec)}$$

With beam dimensions the same as those given in Figure 5-6 and the masses M1 and M2 equal to 1.0, the period of oscillation is approximately 0.03 seconds. Thus for a constant velocity of 7.0 in/sec, approximately two oscillations will occur during the load cycle.

When a variable speed moving load is used, the speed initially is zero and increases linearly to 1.0, 5.0, 10.0, 20.0, and 40.0 in/sec at the end of the cycle.

(5.1.3.1) Constant Speed Moving Loads

For slowly moving loads, relative to the fundamental period of the system, one would expect near static deflections. This is the case for a speed of 1.0 in/sec as shown in Figure 5-7. The figure gives the components of the constraint equation resulting from an initial deflection equal to the ratio of the load and stiffness. The only deviations from the static deflection curve are caused by small oscillations at the resonant frequency. As the speed of the moving load increases, one would expect an increase in the amplitude of oscillation as the period of the load cycle approaches the resonant period. Increasing to 5.0 in/sec produced larger deviations from static due to increased oscillation amplitudes (Figure 5-8). This trend continues until the deflection is

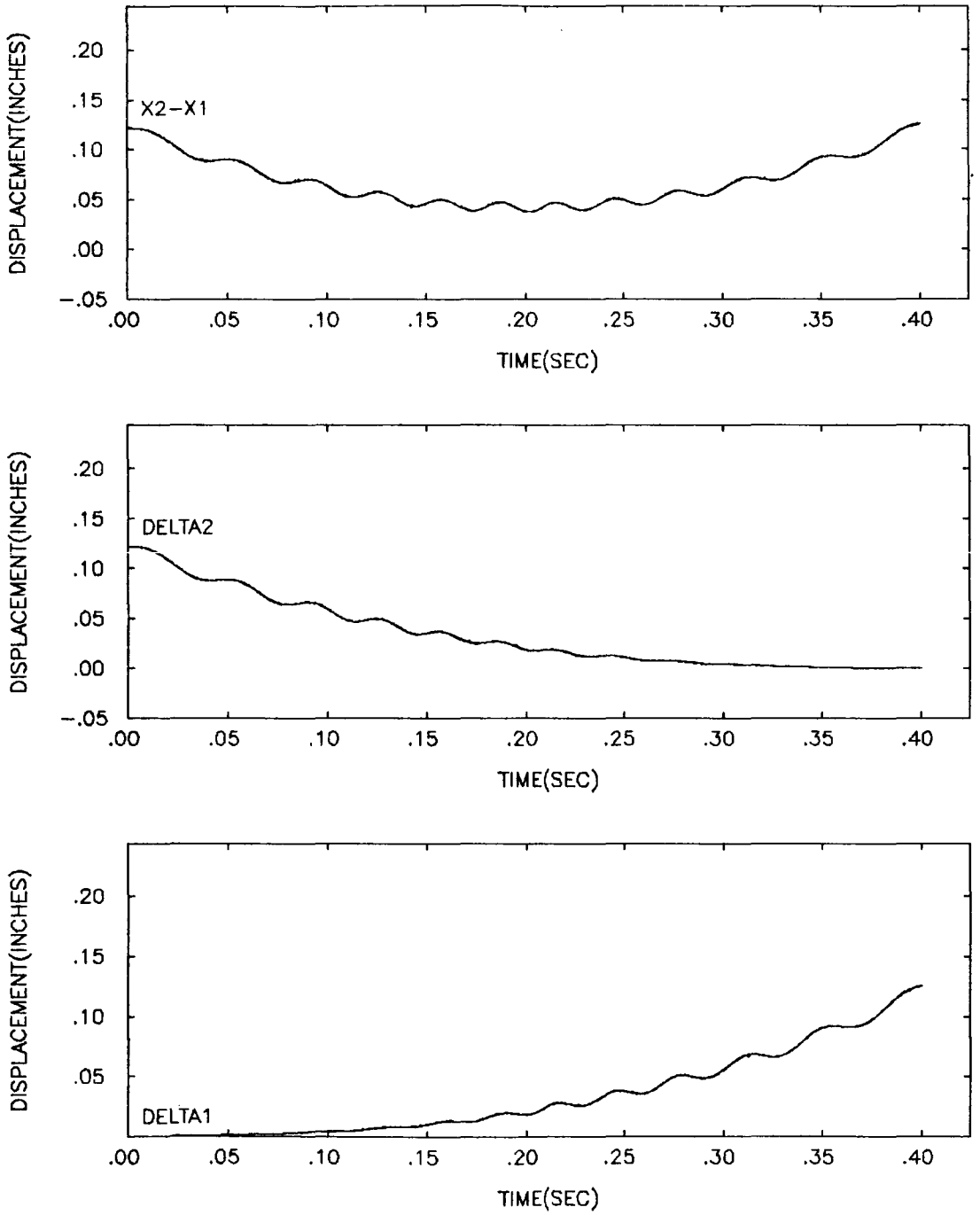

VEL= 1.0 IN/SEC ; MASS= 1.0 ; LENGTH= 0.5 IN

DYNAMIC RESPONSE OF MESHING MASSLESS CANTILEVER BEAMS

Figure 5-7

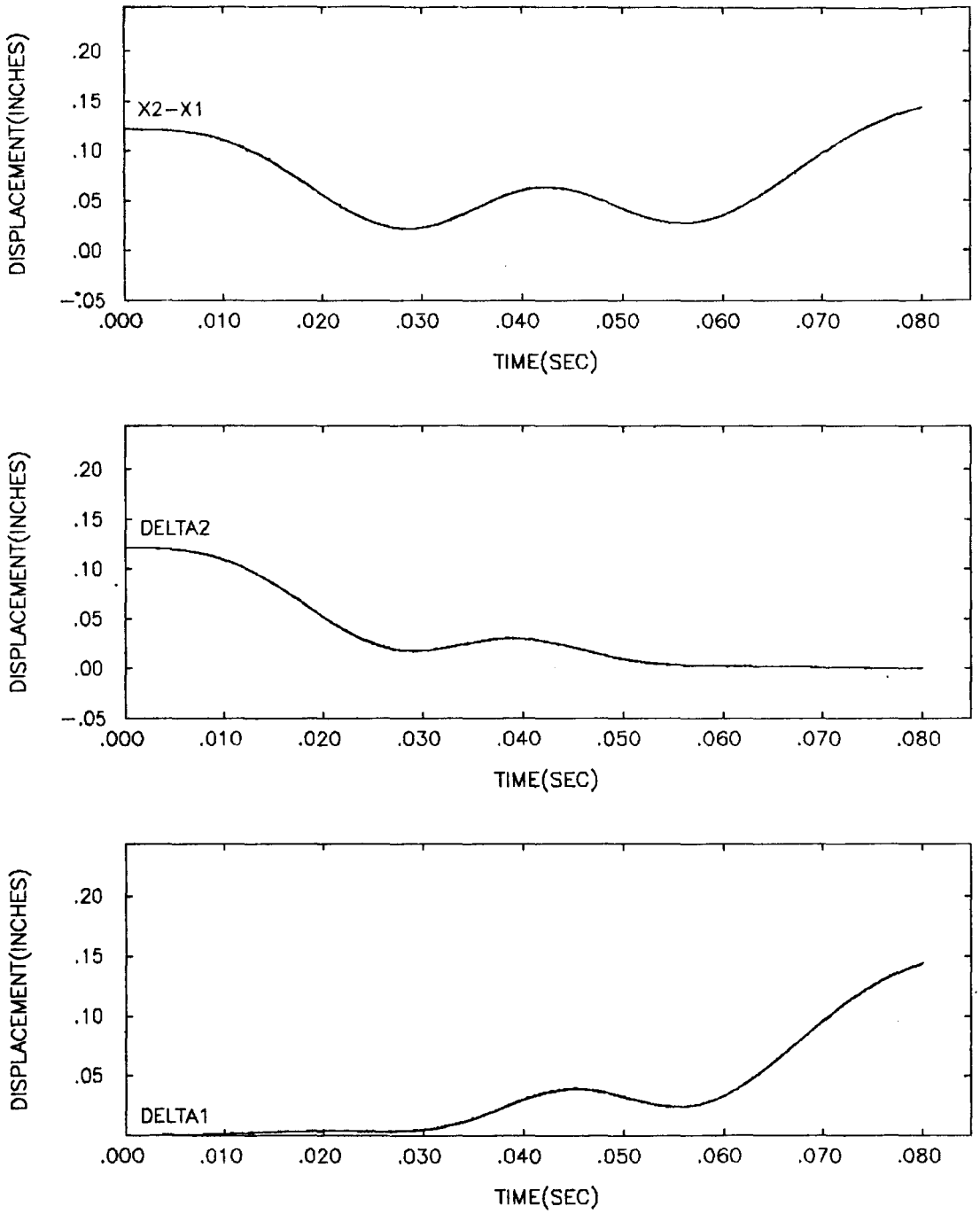

VEL= 5.0 IN/SEC ; MASS= 1.0 ; LENGTH= 0.5 IN

DYNAMIC RESPONSE OF MESHING MASSLESS CANTILEVER BEAMS

Figure 5-8

maximum for a speed of 20.0 in/sec. (See Figure 5-9 and 5-10). In both Figures 5-9 and 5-10, the value of X2-X1 goes negative. This means that the beams have separated. Notice also that the system at 20 in/sec, does not even begin to approach the initial conditions at the end of the cycle, as for the slower speeds. A further increase in speed to 40.0 in/sec, shows that although the beams themselves deflect appreciably (DELTA1 and DELTA2), the masses themselves are displaced very little because the load cycle is much shorter than the resonant period (see Figure 5-11).

In each case, the system strives toward the static deflection position. But due to the inertia of the foundation masses, this position may or may not be maintained depending on the speed of the moving load.

As discovered in the finite element analysis (see section 4.4.3), the type of load engagement significantly affects the response of the undamped gear tooth. This is also the case for the meshing beams configuration. By changing the initial conditions of X=X2-X1 to zero, the system reacts to restore itself to static equilibrium. Since the system is undamped, a high amplitude oscillation is set up due to the rapid movement of the foundation masses. This is best illustrated by examining Figure 5-12 where the components of the constraint equation are plotted for a velocity of 1.0 in/sec. As before, the system oscillates about the static deflection position, but with very large amplitude. Note also, that separation occurs during each oscillation. The same phenomenon occurs for

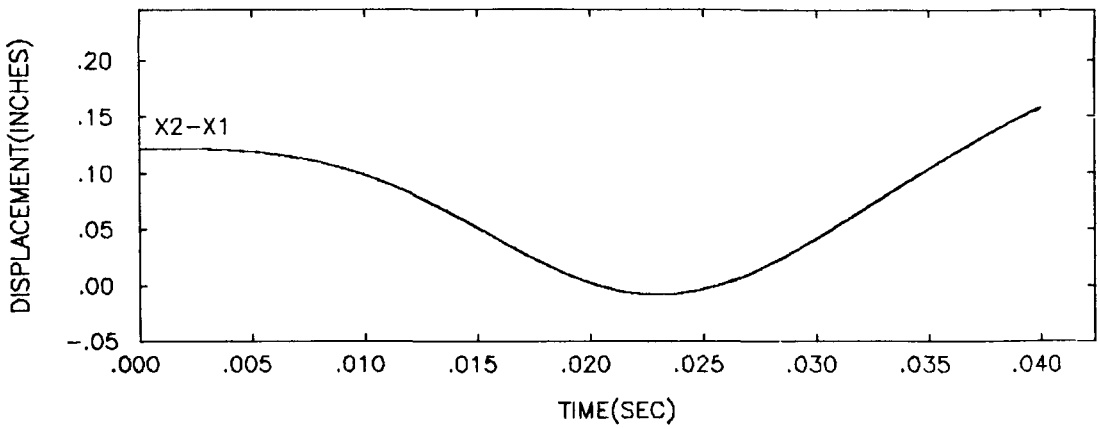

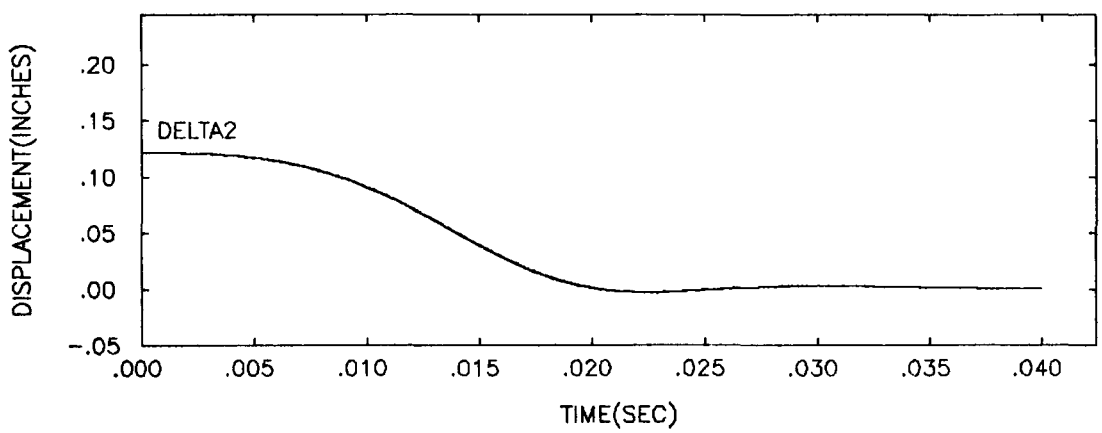

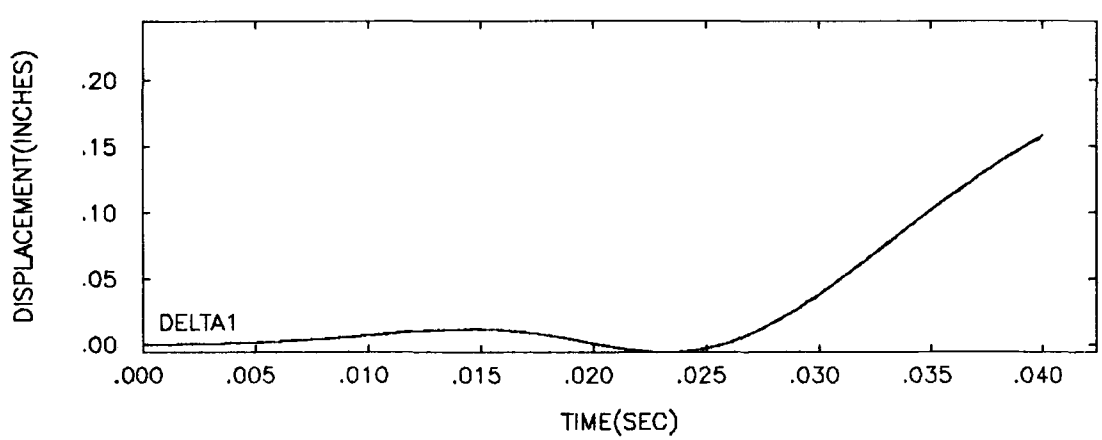

VEL= 10.0 IN/SEC ; MASS= 1.0 ; LENGTH= 0.5 IN

DYNAMIC RESPONSE OF MESHING MASSLESS CANTILEVER BEAMS

Figure 5-9

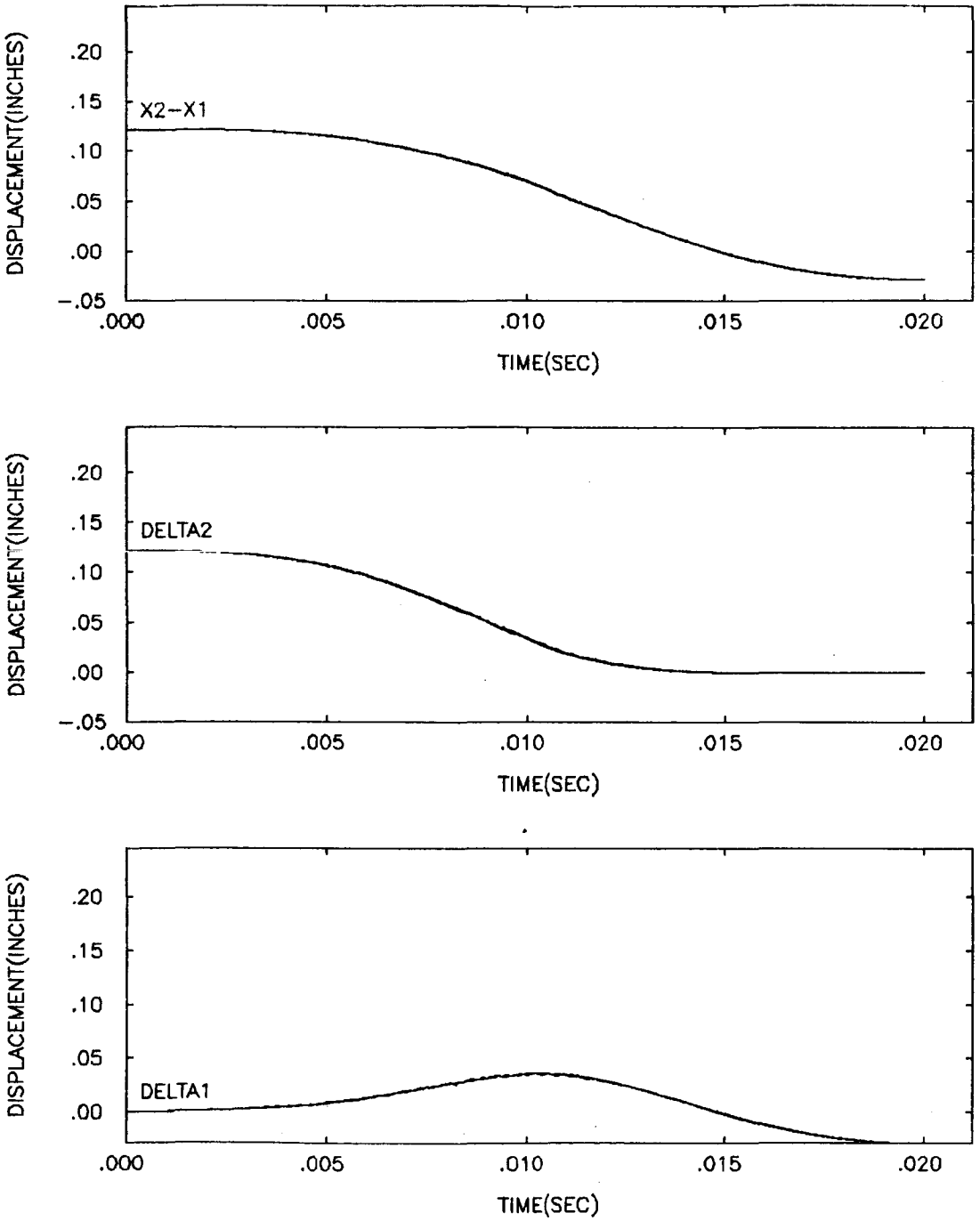

VEL= 20.0 IN/SEC ; MASS= 1.0 ; LENGTH= 0.5 IN

DYNAMIC RESPONSE OF MESHING MASSLESS CANTILEVER BEAMS

Figure 5-10

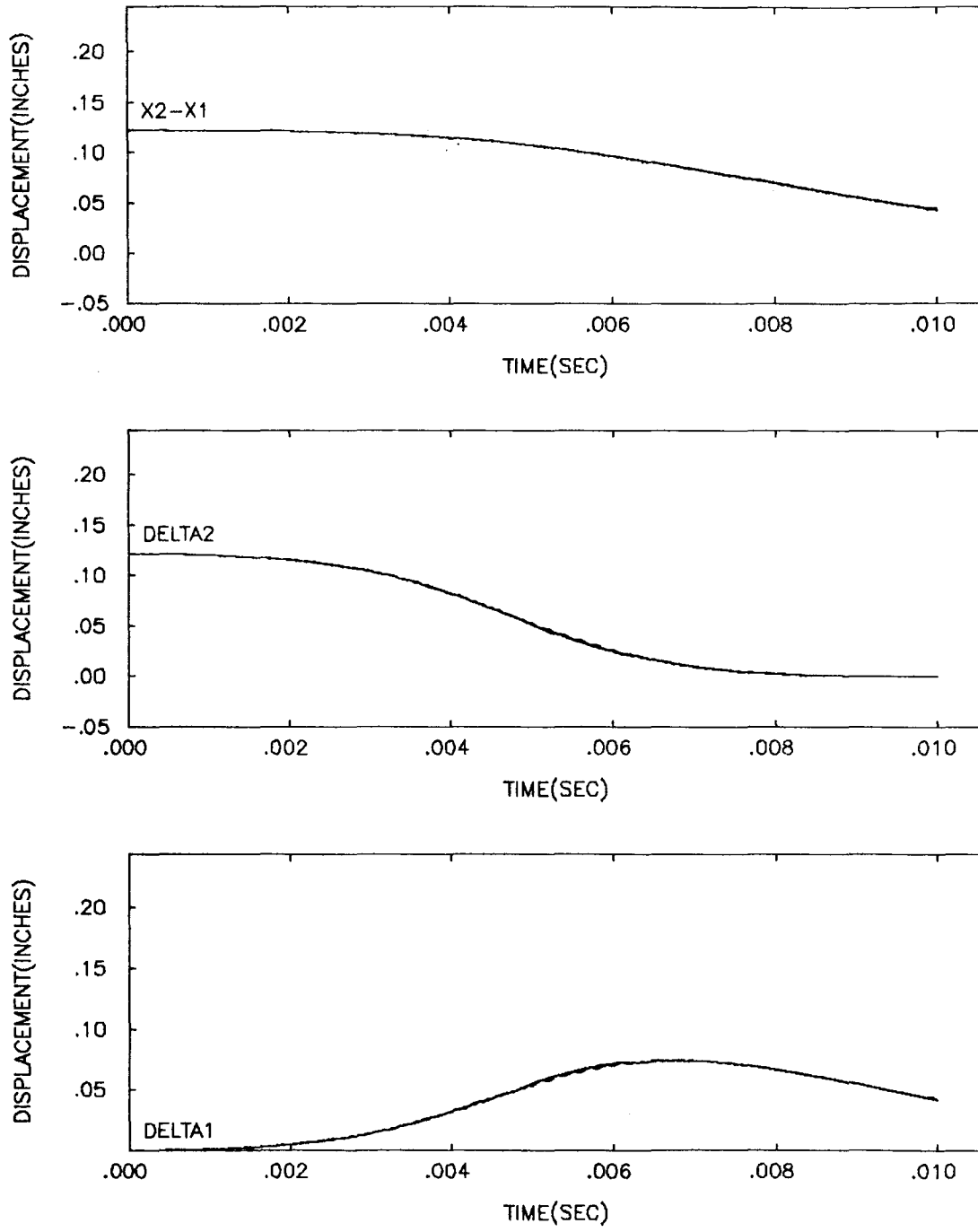

VEL= 40.0 IN/SEC ; MASS= 1.0 ; LENGTH= 0.5 IN

DYNAMIC RESPONSE OF MESHING MASSLESS CANTILEVER BEAMS

Figure 5-11

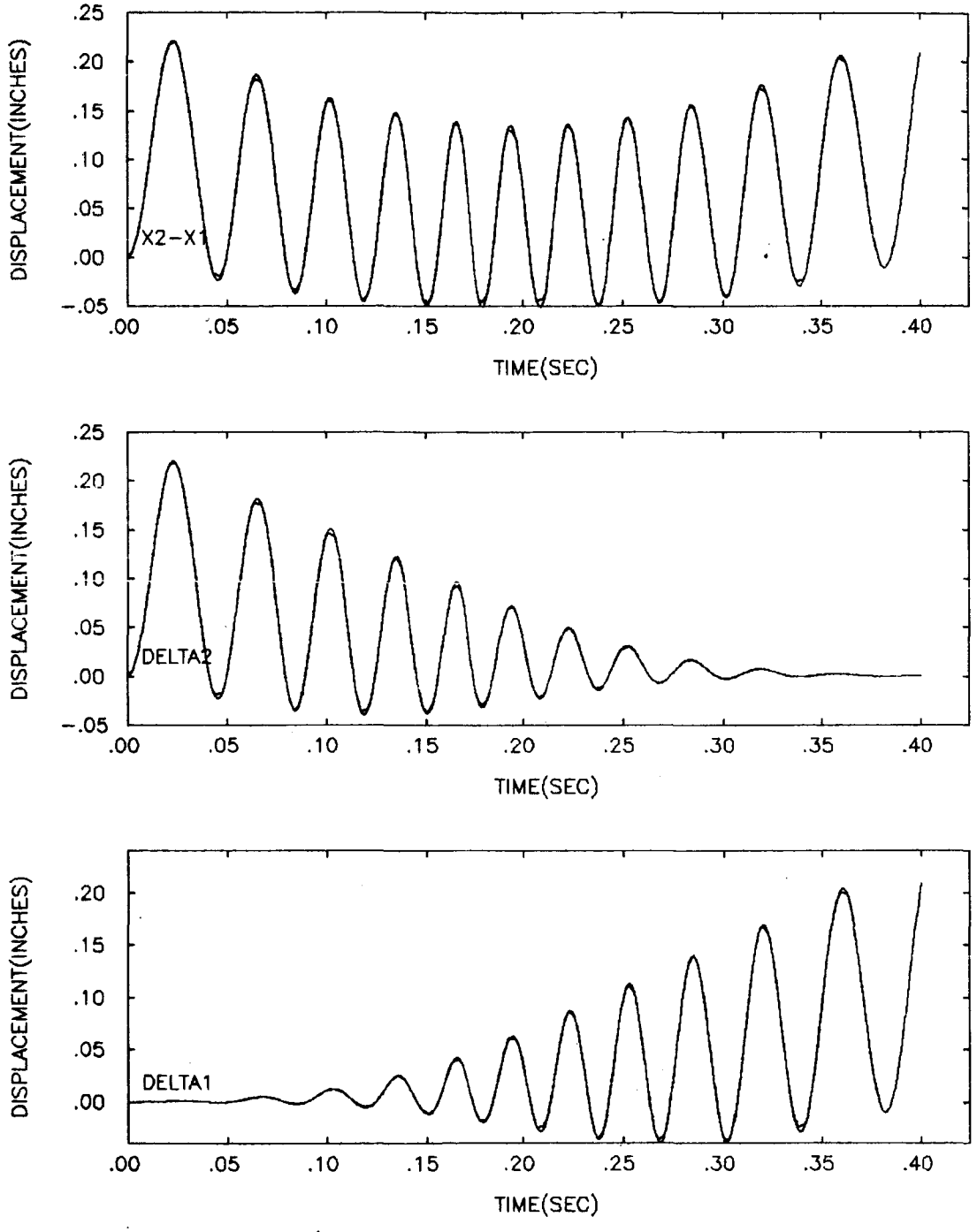

VEL= 1.0 IN/SEC ; MASS= 1.0 ; BEAM LENGTH= 0.5 IN

DYNAMIC RESPONSE OF MESHING MASSLESS CANTILEVER BEAMS

Figure 5-12

speeds of 5.0 and 10 in/sec (Figure 5-13 and 5-14). However, with a further increase in speed, the system does not have sufficient time to react and the oscillations become less significant (see Figure 5-15 and 5-16). One should not be led to believe that the separation occuring for these initial conditions is caused by the characteristics of the system. It is caused, however, by the application of a 1000 lb load to a beam which in the physical sense could not support it. However, since the system behaves linearly, the characteristics of the response are the same for whatever load is applied, and the 1000 lb load is used simply to exaggerate that response.

(5.1.3.2) Variable Speed Moving Loads

Introducing a variable speed moving load, versus constant speed, has little effect on the general behavior of the meshing massless cantilever beam system. The same conclusions can be drawn concerning the dynamic resonse trends due to increased moving load speed. As a reference, the dynamic response curves for both sets of initial conditions and the five different speeds, plotted as a function of position, are included in Appendix 4.

(5.2) Analysis Including Beam Inertia

Figure 5-17 illustrates the physical system used to determine the effects of including the inertia of the beams on the dynamic response due to moving loads. This system is exactly the same as the one used in Section 5.1 except the mass of the beams is included. First, the equations of motion for this system are developed.

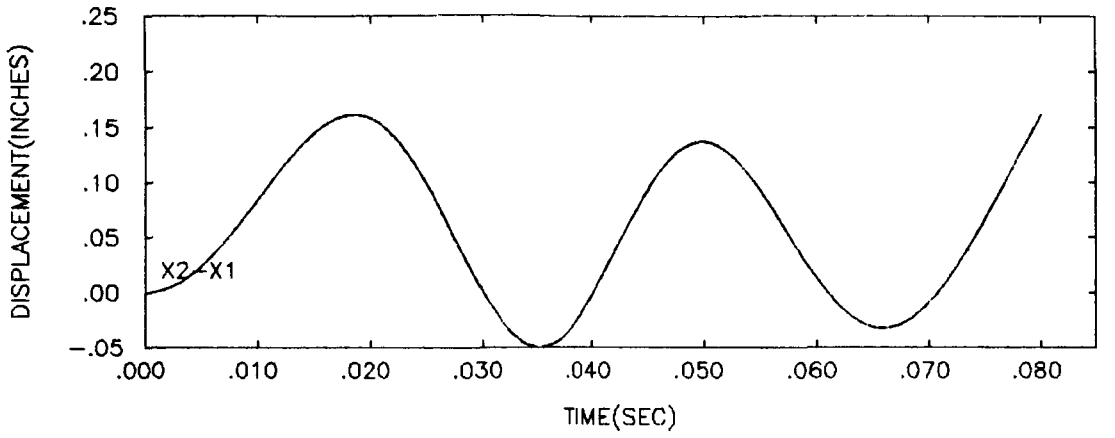

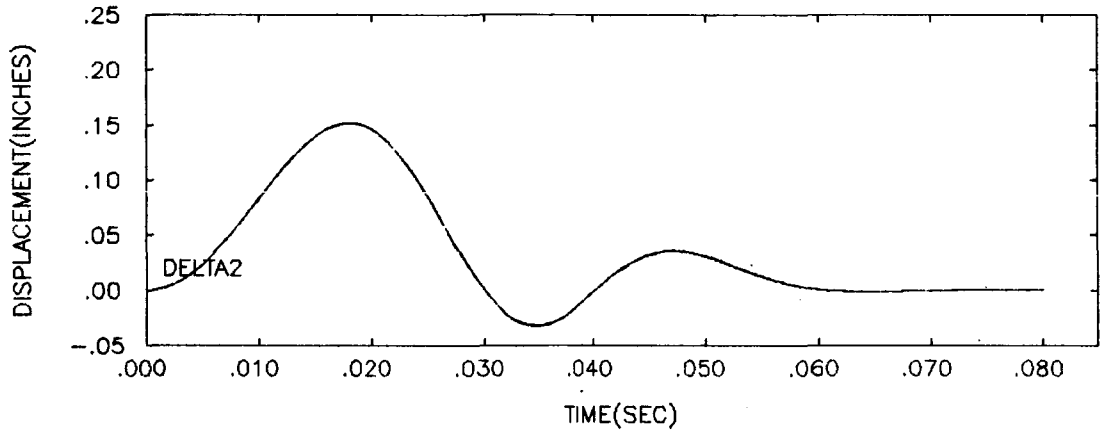

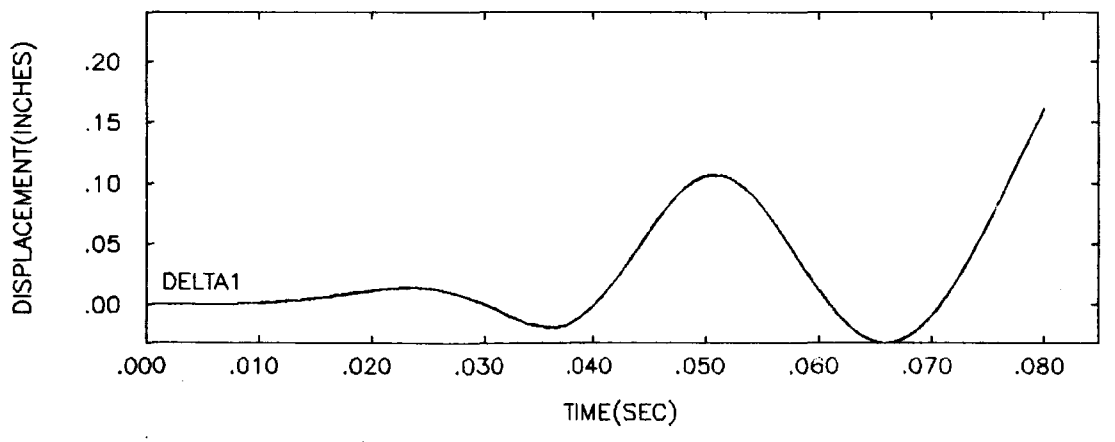

VEL= 5.0 IN/SEC ; MASS= 1.0 ; BEAM LENGTH= 0.5 IN

DYNAMIC RESPONSE OF MESHING MASSLESS CANTILEVER BEAMS

Figure 5-13

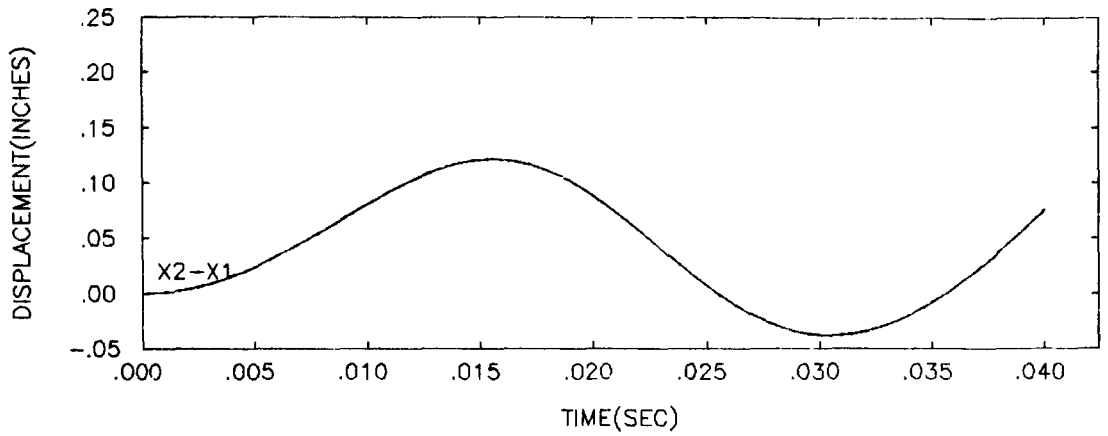

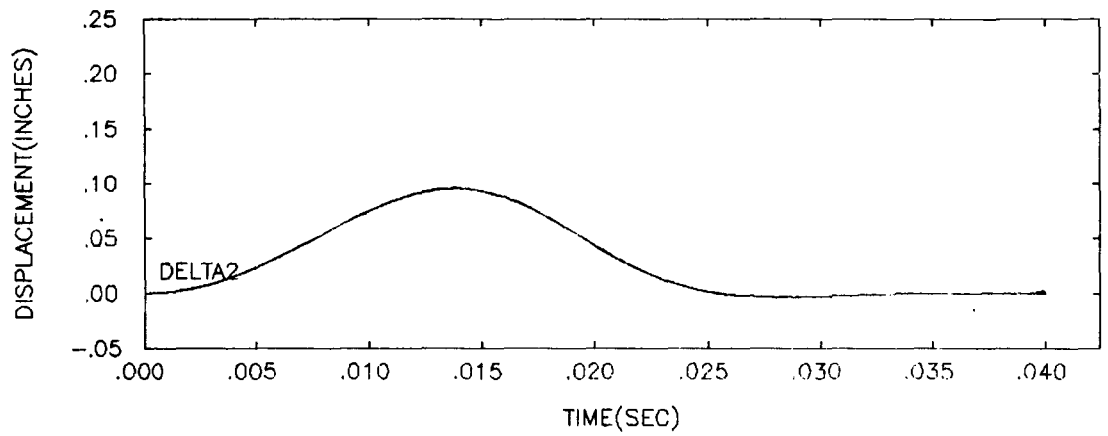

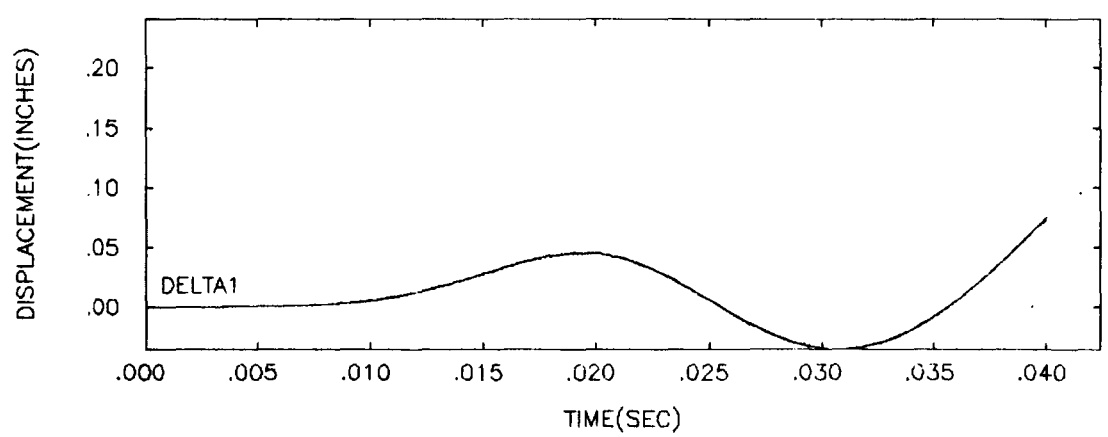

VEL= 10.0 IN/SEC ; MASS= 1.0 ; BEAM LENGTH= 0.5 IN

DYNAMIC RESPONSE OF MESHING MASSLESS CANTILEVER BEAMS

Figure 5-14

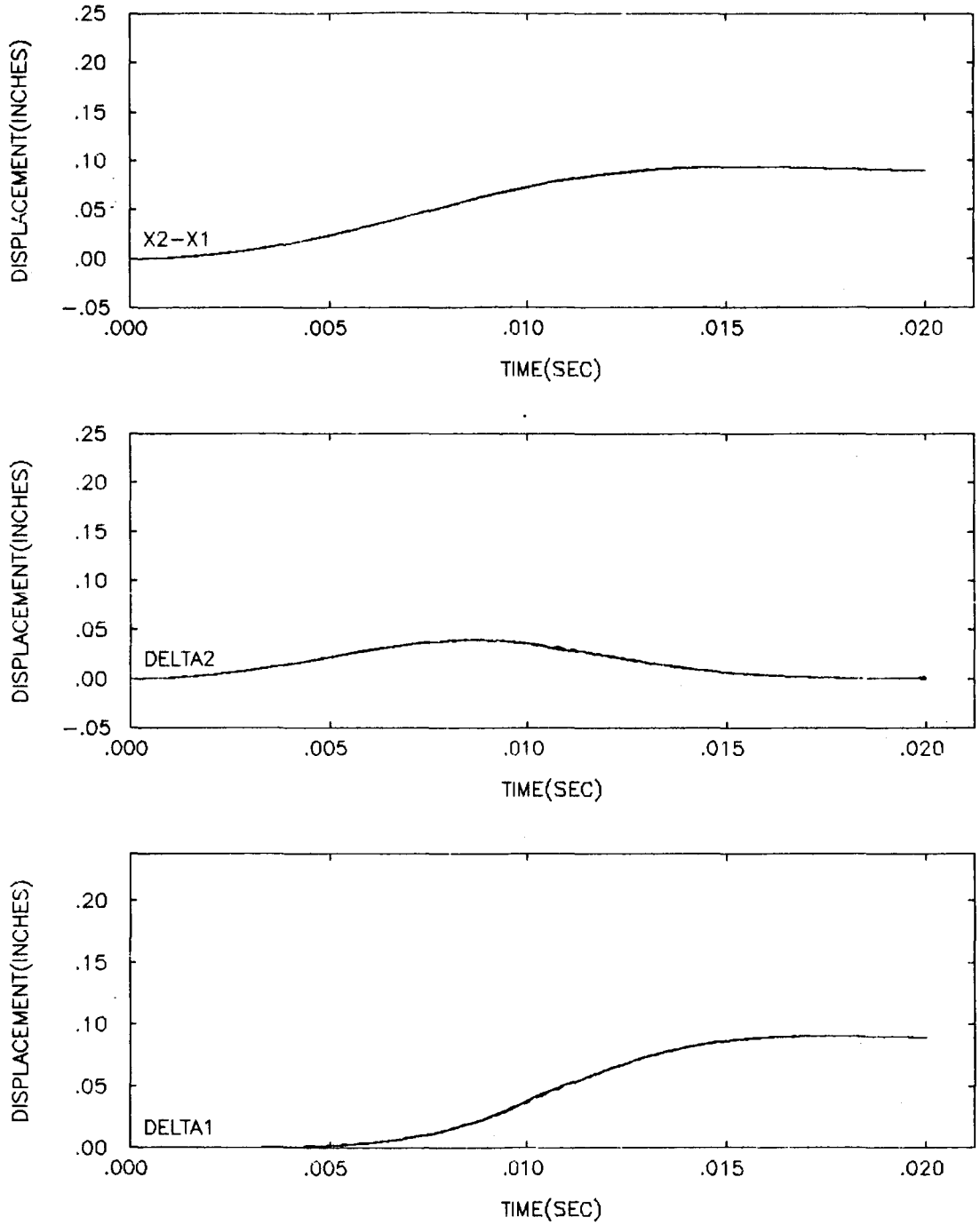

VEL= 20.0 IN/SEC ; MASS= 1.0 ; BEAM LENGTH= 0.5 IN

DYNAMIC RESPONSE OF MESHING MASSLESS CANTILEVER BEAMS

Figure 5-15

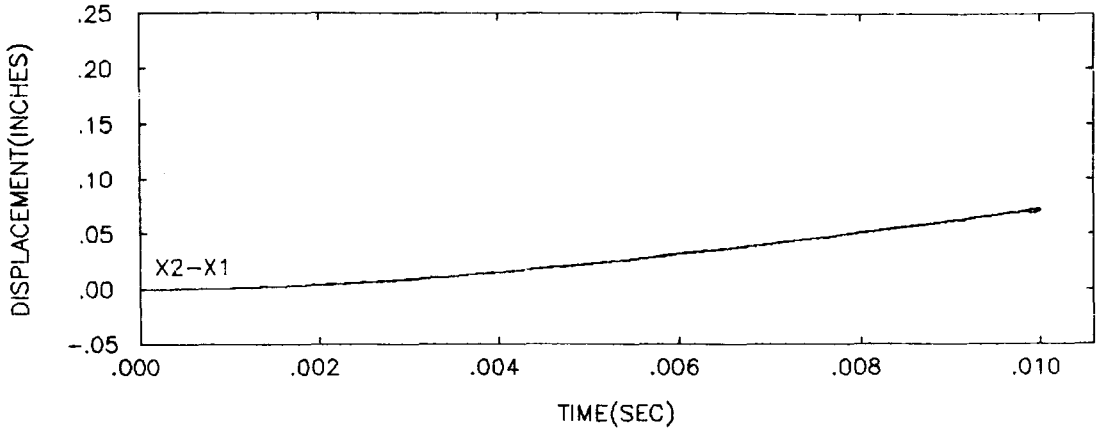

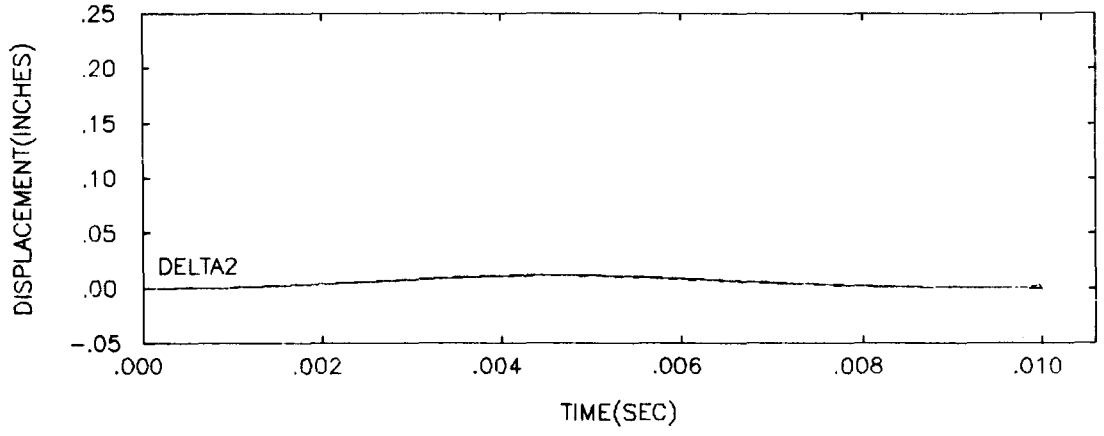

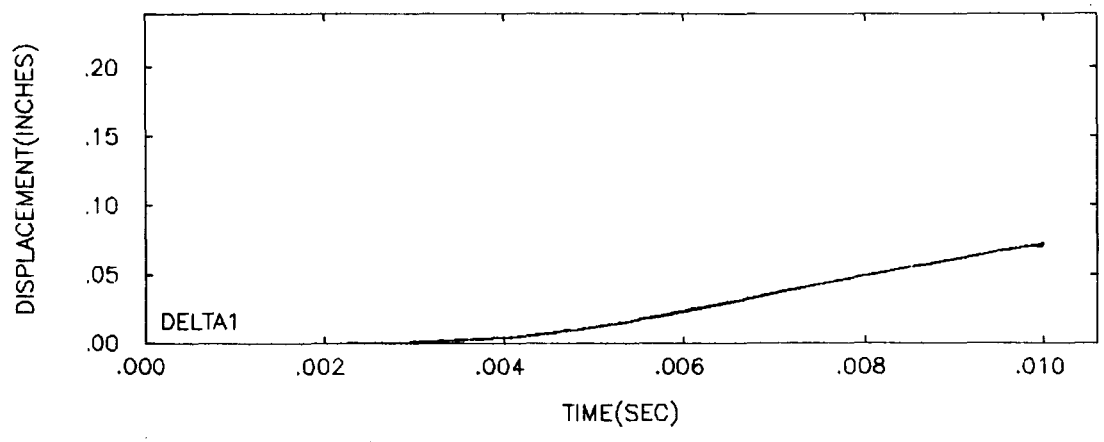

VEL= 40.0 IN/SEC ; MASS= 1.0 ; BEAM LENGTH= 0.5 IN

DYNAMIC RESPONSE OF MESHING MASSLESS CANTILEVER BEAMS

Figure 5-16

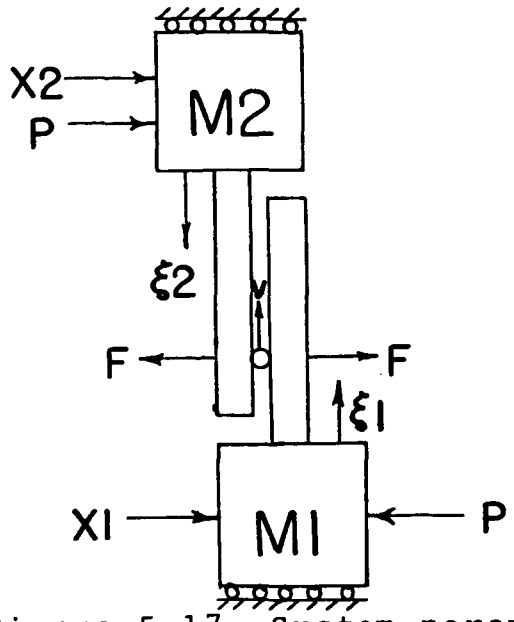

Figure 5-17: System parameters

(5.2.1) Equations of Motion

The equations of motion for this system are somewhat more difficult than those developed for the massless beam configuration. Instead of writing down the differential equation directly, a form of Lagange's Equation is used which takes into account the added mass of the beams.

The Lagrange Equation of motion, utilizing Lagrange multipliers is;

$$\frac{d}{dt}\left(\frac{\partial L}{\partial \dot{q}_i}\right) - \frac{\partial L}{\partial q_i} = Q_i + \sum_{k=1}^{m} \lambda_k a_{ki}$$

for: $i = 1,2,\ldots,n$ (5-13)

where;

$L = T - U$ = Lagrangian

T = System kinetic energy

U = System potential energy

q_i = Generalized coordinates

Q_i = Sum of non-potential forces

λ_k = Lagrange Multipliers

$$a_{ki} = \frac{\partial f(q1,q2,\ldots,qn)}{\partial qi} = \text{first partial}$$

derivative of the constraint equation with respect to the generalized coordinates

The last term on the right hand side of equation (5-13) represents the constraint forces which makes it possible to regard all generalized coordinates, q_i, as independent.

Four generalized coordinates are used to describe the system position, velocity, and acceleration. They are;

X1 - describing M1

X2 - describing M2

q1 - describing beam 2 relative to foundation mass M1

q2 - describing beam 2 relative to foundation mass M2

From the definition of generalized coordinates, these four quantities are assumed independent of each other, and when used together they describe the state of the dynamical system at any time.

The static deflection of a loaded cantilever beam is given by the applied load divided by the stiffness. When considering the dynamic deflection of a beam which has mass, this relationship is not valid. Instead, the superposition of the natural vibrational modes is used to describe the shape of the deformation, and when multipled by the generalized coordinate, q_i, the actual deflection is obtained.

The mode shapes are an infinite set of eigenvectors derived from the differential equation of the cantilever beam. To exactly duplicate the deflection obtained from elasticity theory, an infinite number of modes must be used. In practice, however, only the first few contribute significantly to the overall deflection, such as those illustrated in Figure 5-18.

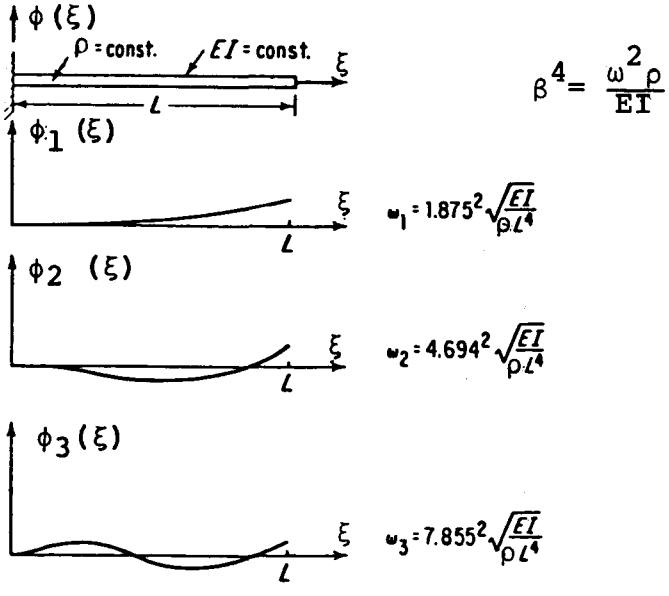

Figure 5-18: Natural Modes

In this analysis, only the first mode shape is used, the natural mode described by the equation;

$$\phi(\xi) = C[(\sin\beta L-\sinh\beta L)(\sin\beta\xi-\sinh\beta\xi)$$

$$+(\cos\beta L+\cosh\beta L)(\cos\beta\xi-\cosh\beta\xi)] \qquad (5\text{-}14)$$

where the parameters are defined in Figure 5-18.

We are now ready to develop the equations of motion for the mass-beam system of Figure 5-17. The kinetic energy of the system is determined by considering the velocity of the foundations M1 and M2, and the vibration of the beams with respect to the foundation masses. By defining the beam deflections to be positive as shown in Figure 5-19, the kinetic energy of the

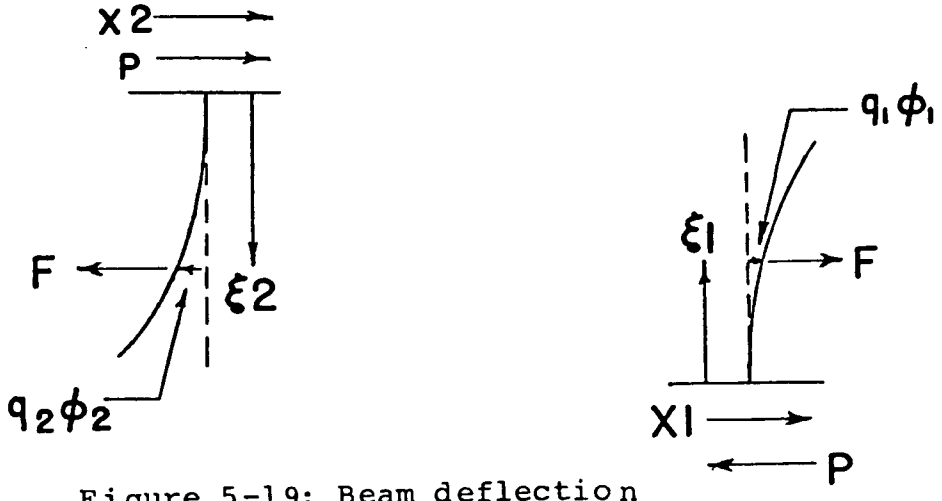

Figure 5-19: Beam deflection configuration

system can be written as;

$$T = \frac{1}{2}M1\ \dot{X}1^2 + \frac{1}{2}M2\ \dot{X}2^2 + \frac{1}{2}\rho\int_0^{L1}(\dot{X}1 + \phi_1\ \dot{q}_1)^2 d\xi_1$$

$$+ \frac{1}{2}\rho\int_0^{L2}(\dot{X}2 - \phi_2\ \dot{q}_2)^2 d\xi_1 \qquad (5\text{-}15)$$

The potential energy consists only of the strain energy due to the beam deflections;

$$U = \frac{1}{2}EI \int_0^{L1} (\phi_1'' q_1)^2 d\xi_1 + \frac{1}{2}EI \int_0^{L2} (\phi_2'' q_2)^2 d\xi_2 \qquad (5\text{-}16)$$

Where ϕ'' is the second derivative of the mode shape with respect to the length variable, ξ . In equations (5-15) and (5-16) the mass per unit length, ρ , the elastic modulus, E, and the moment of inertia, I, are constant over the length of the beams and can be left outside the integrals. Substracting (5-16) from (5-15) to form the Lagrangian we have;

$$L = T - U = \frac{1}{2}M1\ \dot{X}1^2 + \frac{1}{2}M2\ \dot{X}2^2$$

$$+ \frac{1}{2}\rho \int_0^{L1} (\dot{X}1 + \phi_1\ \dot{q}_1)^2 d\xi_1 + \frac{1}{2}\rho \int_0^{L2} (\dot{X}2 - \phi_2\ \dot{q}_2)^2 d\xi_2$$

$$- \frac{1}{2}EI \int_0^{L1} (\phi_1'' q_1)^2 d\xi_1 - \frac{1}{2}EI \int_0^{L2} (\phi_2'' q_2)^2 d\xi_2 \qquad (5\text{-}17)$$

For the meshing cantilever beam system there are four unknown parameters, X1, X2, q1, q2 and their derivatives, each dependent on time, describing the dynamical system. At any time, t, the position of the system can be described by the constraint equation;

$$X2\text{-}X1 - \phi_1 q_1 - \phi_2 q_2 = f(X1,X2,q1,q2) = 0 \qquad (5\text{-}18)$$

If the constraint equation is not satisfied, separation occurs between the beams at the point of contact.

A Lagrange Equation of motion is written for each degree

of freedom of the system corresponding to the four generalized coordinates. This gives four equations relating the generalized coordinates and λ . Including the constraint equation or its derivative gives a fifth equation necessary to determine .

In terms of X1, the equation of motion, term by term, becomes;

$$\frac{\partial L}{\partial \dot{X1}} = M1\dot{X1} + \rho \int_0^{L1} (\dot{X1} + \phi_1 \dot{q}_1)^2 d\xi_1$$

$$\frac{d}{dt}\left(\frac{\partial L}{\partial \dot{X1}}\right) = M1\ \ddot{X1} + \rho \int_0^{L1} (\ddot{X1} + \phi_1 \ddot{q}_1) d\xi_1 \qquad (5\text{-}19a)$$

and;

$$\frac{\partial L}{\partial X1} = 0.0 \qquad (5\text{-}19b)$$

On the right hand side, differentiation of the constraint equation with respect to X1 yields;

$$\frac{\partial f}{\partial X1} = -1.0 \qquad (5\text{-}19c)$$

Combining equations (5-19a) through (5-19c) along with the non-constraint force, P, acting on M1, in the form of equation (5-13) we have;

$$(M1 + \rho \int_0^{L1} d\xi_1)\ddot{X1} + \rho \int_0^{L2} (\phi_1\ \ddot{q}_1) d\xi_1 = P-\lambda \qquad (5\text{-}20)$$

The term $\rho \int_0^{L1} d\xi_1$ is simply the total mass of beam 1 which is defined as MB1. Similarly, with X2 as the generalized coordinate;

$$(M2 + MB2)\ddot{X}2 - \rho\int_0^{L2} \phi_2\ \ddot{q}_2\ d\xi_2 = P + \lambda \qquad (5\text{-}21)$$

Performing the required differentiation of the Lagrangian and constraint equation with respect to ql yields;

$$\frac{\partial L}{\partial \dot{q}_1} = \rho\int_0^{L1} (\phi_1\ \dot{X}1 + \phi_1^2\ \dot{q}_1)d\xi_1$$

$$\frac{d}{dt}\left(\frac{\partial L}{\partial \dot{q}_1}\right) = \rho\int_0^{L1} (\phi_1\ \ddot{X}1 + \phi_1^2\ \ddot{q}_1)d\xi_1 \qquad (5\text{-}22a)$$

$$\frac{\partial L}{\partial q_1} = -EI\int_0^{L1} (\phi_1''^2\ q_1)d\xi_1 \qquad (5\text{-}22b)$$

$$\frac{\partial f}{\partial q_1} = -\phi_1 \qquad (5\text{-}22c)$$

Combining equations (5-22a) through (5-22c), and noting that no external (non-constraint) forces act on the beams, the equation of motion derived with respect to ql becomes;

$$\rho\int_0^{L1} (\phi_1\ddot{X}1)d\xi_1 + \rho\int_0^{L1} (\phi_1^2\ddot{q}_1)d\xi_1 + EI\int_0^{L1} (\phi_1''^2\ q_1)d\xi_1 = -\phi_1\lambda \qquad (5\text{-}23)$$

Likewise for q2;

$$-\rho\int_0^{L2} (\phi_2\ddot{X}_2)d\xi_2 + \rho\int_0^{L2} (\phi_2^2\ddot{q}_2)d\xi_2 + EI\int_0^{L2} (\phi_2''^2\ q_2)d\xi_2 = -\phi_2\lambda \qquad (5\text{-}24)$$

The fifth equation of motion is determined by differentiating the constraint equation twice with respect to time. This gives an equation relating the second derivatives of the generalized coordinates with respect to time. Differentiating equation (5-18) once yields;

$$\dot{X}2-\dot{X}1-\dot{\phi}_1\ q_1-\phi_1\ \dot{q}_1-\dot{\phi}_2\ q_2-\phi_2\ \dot{q}_2=0$$

After a second differentiation and rearrangement;

$$\ddot{X}2-\ddot{X}1-\phi_1\ \ddot{q}_1-\phi_2\ \ddot{q}_2=\ddot{\phi}_1\ q_1+\ddot{\phi}_2\ q_2+2(\dot{\phi}_1\ \dot{q}_1+\dot{\phi}_2\ \dot{q}_2) \quad (5\text{-}25)$$

Equations (5-20), (5-21), (5-23), (5-24) and (5-25) are the equations of motion describing the dynamical system of Figure 5-16.

These equations can be greatly simplified by making the following substitutions:

$$PHI1=\phi_1 \quad ; \quad PHI2=\phi_2$$

$$IPHI1=\rho\int_0^{L1}\phi_1 d\xi_1 \quad ; \quad IPHI2=\rho\int_0^{L2}\phi_2 d\xi_2$$

$$\rho\int_0^{L1}\phi_1{}^2 d\xi_1=1 \quad ; \quad \rho\int_0^{L2}\phi_2{}^2 d\xi_2=1$$

$$I2PHI1=EI\int_0^{L1}\phi_1''{}^2 d\xi_1 \quad ; \quad I2PHI2=EI\int_0^{L2}\phi_2''{}^2 d\xi_2$$

$$F(q_1,q_2,\phi_1,\phi_2)=\ddot{\phi}_1\ q_1+\ddot{\phi}_2\ q_2+2(\dot{\phi}_1\ \dot{q}_1+\dot{\phi}_2\ \dot{q}_2)$$

(see Appendix 5 for developments concerning these simplifications). The equations can then be written in matrix from in terms of the second derivatives and as;

$$[A]\{\bar{X}\}=\{\bar{B}\} \quad (5\text{-}26)$$

where;

$$[A] = \begin{bmatrix} (M1+MB1) & 0 & IPHI1 & 0 & 1 \\ 0 & M2+MB2 & 0 & -IPHI2 & -1 \\ IPHI1 & 0 & 1 & 0 & PHI1 \\ 0 & -IPHI2 & 0 & 1 & PHI2 \\ -1 & 1 & -PHI1 & -PHI2 & 0 \end{bmatrix}$$

$$\{\bar{\ddot{X}}\} = \begin{Bmatrix} \ddot{X}2 \\ \ddot{X}1 \\ \ddot{q}1 \\ \ddot{q}2 \\ \lambda \end{Bmatrix} \quad \text{and} \quad \{\bar{B}\} = \begin{Bmatrix} -P \\ P \\ -I2PHI*q1 \\ -I2PHI2*q2 \\ F(q1,q2,\phi1,\phi2) \end{Bmatrix}$$

The only differences between equations (5-26) and the equation of motion for the massless beam system (equation (5-11)) are the inertial terms. These are; $\ddot{X}1*IPHI1$, $\ddot{X}2*IPHI2$, and the terms involving $\ddot{q}1$ and $\ddot{q}2$. By eliminating the inertial terms from matrix [A], the resulting equations describe the massless beam system. Appendix 6 includes the analysis and results from this test.

The initial conditions governing the system described by equations (5-26) are chosen such that the massless beam system is emulated. When chosing the initial conditions, there are two sets of parameters which must be considered. The first set consists of the four position variables X1, X2, q1 and q2. In section (5.1.1) it is stated that the beams assume a static orientation at the beginning of the load cycle. Thus, by chosing q1 and q2 as;

$$q1(0) = \frac{P*PHI1}{I2PHI1}$$

$$q2(0) = \frac{P*PHI2}{I2PHI2} \qquad (5\text{-}27)$$

and X1(0) equal to zero as before, the deflection X2(0) is determined from the constraint equation as;

$$X2(0) = q1(0)PHI1 + q1(0)PHI2 \qquad (5\text{-}28)$$

This same reasoning can be applied to the first derivatives of the generalized coordinates, $\dot{X}1$, $\dot{X}2$, $\dot{q}1$ and $\dot{q}2$. Previously, the initial velocities of the foundation masses were determined such that $\dot{X}2-\dot{X}1=0$ at time equal zero. For this case, the same effect is obtained by forcing;

$$\begin{aligned} \dot{X}1(0) &= 0.0 \\ \dot{X}2(0) &= 0.0 \\ \dot{q}1(0) &= 0.0 \end{aligned} \qquad (5\text{-}29)$$

Then, using the first derivative of the constraint equation the value of $\dot{q}2(0)$ is determined from;

$$\dot{X}2 - \dot{X}1 = \dot{q}_1*PHI1 + q_2*DlPHI1 + \dot{q}_2*PHI2 + q_2*DlPHI2$$

where at time equal to zero, all terms are zero except for those in equation (5-30);

$$\dot{q}_2(0) = (-q_1*DlPHI1 - q_2*DlPHI2)/PHI2 \qquad (5\text{-}30)$$

where DlPHI1, DlPHI2 and PHI2 are evaluated at the beginning of the load cycle and q1 and q2 are taken from equations (5-27).

With the initial conditions described by equations (5-27) through (5-30), the dynamic response of the system described in equations (5-26) is determined.

For each time step during the load cycle, the system of

equations (5-26) is inverted to determine the column matrix $\{\ddot{X}\} = \{\ddot{X}1\ \ddot{X}2\ \ddot{q}1\ \ddot{q}2\ \lambda\}^T$ in terms of the current values of $\{\bar{B}\}$ on the right hand side. At the beginning of the load cycle $\{\ddot{X}\}$ is determined for those initial conditions set forth previously, along with the right hand side $\{\bar{B}\}$. The values of $\{\ddot{X}\}$ are then used with the first derivatives of the generalized coordinates (initially equations (5-29) and (5-30)) as input for a Runge-Kutta integration routine which integrates for the desired solution parameters X1, X2, q1 and q2. It also determines the new $\dot{X}1$, $\dot{X}2$, $\dot{q}1$ and $\dot{q}2$ which are in turn used for the next integration step. The algorithm containing the Runge-Kutta (RKGS) and matrix inversion (SIMQ) subroutines along with the parameters describing equations (5-26) is included in Appendix 7. Therein lies a detailed description of the programming steps for the solution of equations (5-26) using the aforementioned initial conditions.

(5.2.2) Dynamic Response Results: Foundation Mass = 1.0 lbs

As stated in section (5.2.1), only the first material mode of vibration is included when determining the dynamic response of the meshing cantilever beams where the inertia of the beams is included. One would then think that the system whose dynamic response is composed of a single mode shape would be somewhat stiffer than the same configuration where the beam deflection is determined from elasticity theory. However, comparing Figures 5-7 to 5-11, with A6-1 to A6-5, it is seen that the difference in deflections is negligible.

In this analysis, with the beam inertia included, the dynamic response is compared to the massless beam problem. At slow moving, constant speed loads, the dynamic response consists of quasi-static deflection with the moving load response superimposed over it (see Figure 5-20). (Results for moving load speed of 1.0 in/sec were not obtainable due to lack of convergence in the Runge-Kutta integration routine). Continuing to increase the moving load speed causes an increase in the response as the resonant frequency is further excited as shown in Figure 5-21 and 5-22. Increasing the moving load speed above the system resonant frequency produces a much smoother response as illustrated in Figure 5-23. Now, examination of Figures 5-20 through 5-23 compared to Figures 5-7 through 5-11 shows that for values of the foundation masses of 1.0 lbs and moving load speeds of 5.0, 10.0, 20.0 and 40.0 in/sec, the responses of the two cantilever beam systems are essentially the same. The same conclusions are drawn when examining Figures 5-24 through 5-27 as compared to Figures 5-13 through 5-16. Here, the initial conditions are changed such that the beams experience an impact load at the beginning of the load cycle. From the figures it can be seen that the responses of the two systems are again, very much the same.

As done for the massless beam configuration, the speed of the moving loads is allowed to vary linearly from zero to a maximum value during the load cycle. This analysis serves as a useful check since the initial conditions are easily defined due to a stationary load. The results from this analysis are contained in Appendix 4.

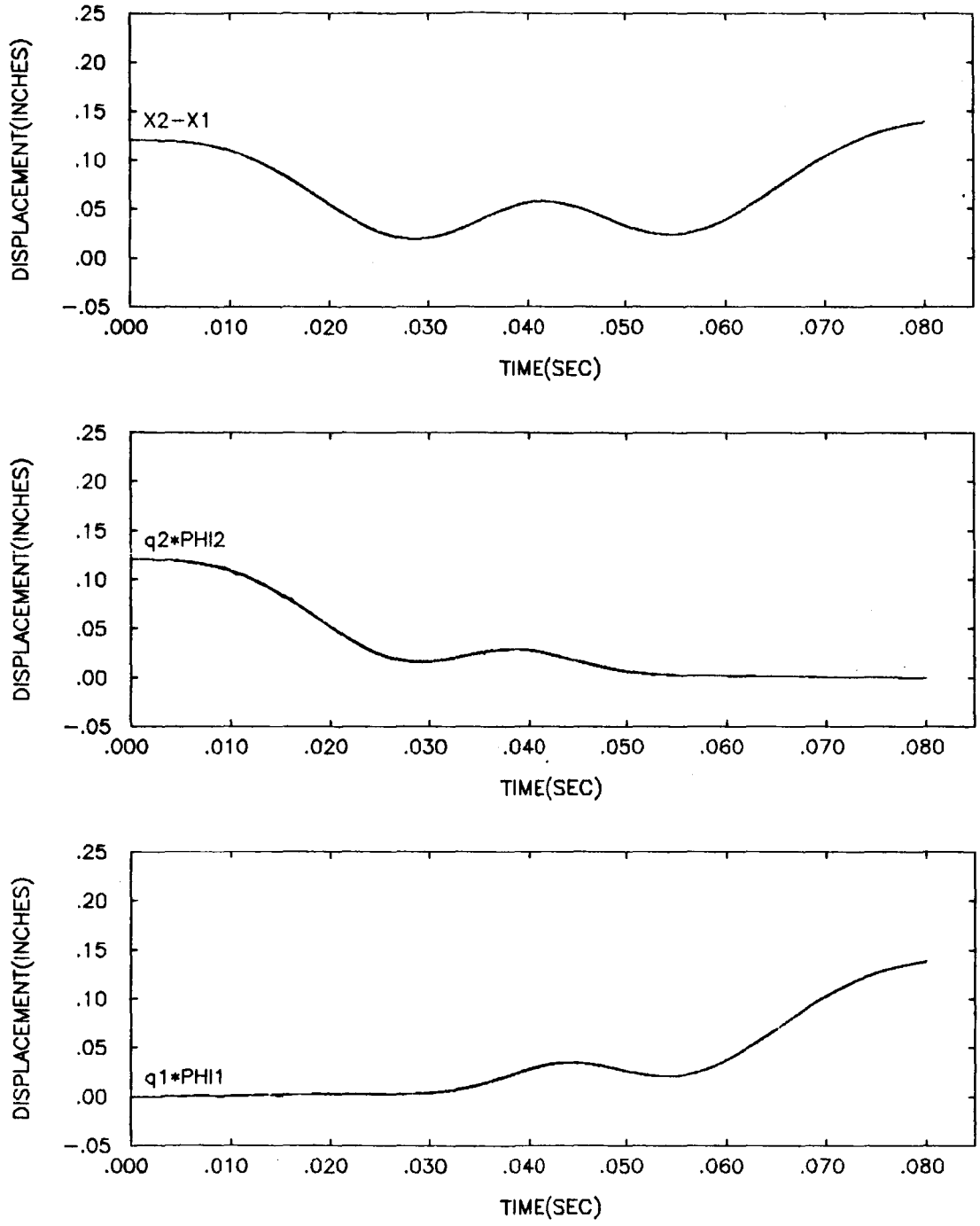

VEL= 5.0 IN/SEC ; MASS= 1.0 ; BEAM LENGTH= 0.5 IN

DYNAMIC RESPONSE OF MESHING CANTILEVER BEAMS, WITH INERTIA (VEL=CONST)

Figure 5-20

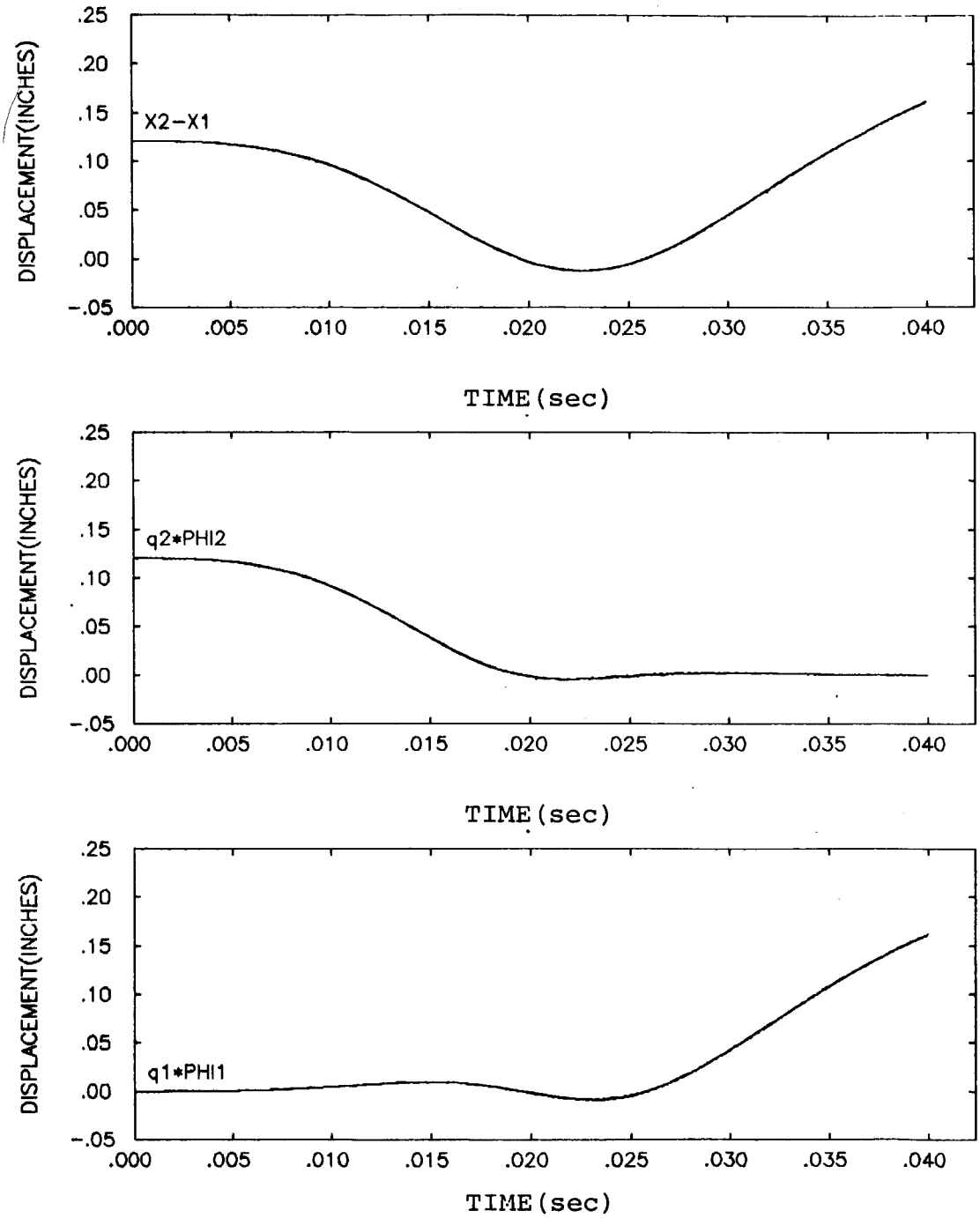

DYNAMIC RESPONSE OF MESHING CANTILEVER BEAMS, WITH INERTIA (VEL=CONST)

Figure 5-21

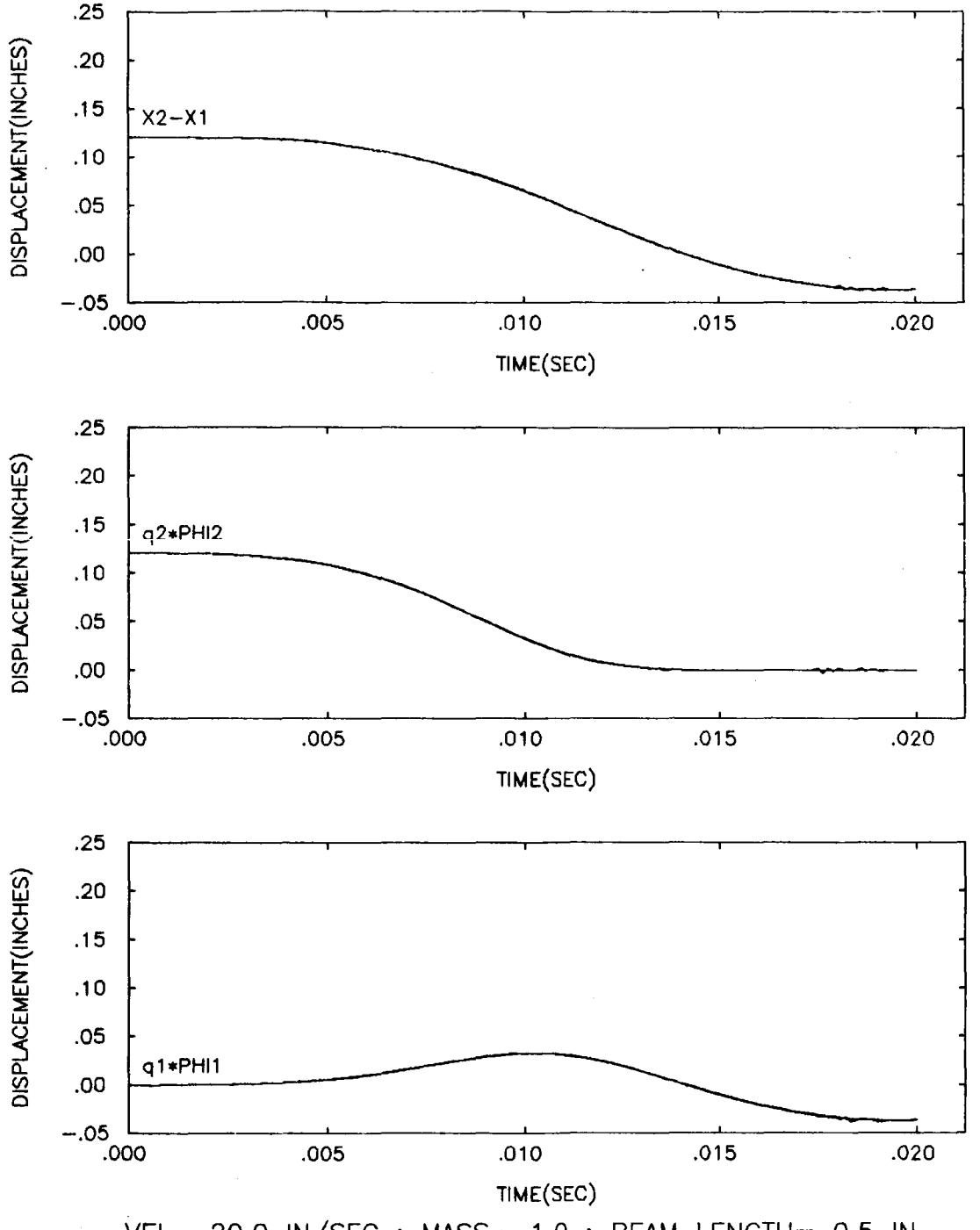

VEL= 20.0 IN/SEC ; MASS= 1.0 ; BEAM LENGTH= 0.5 IN

DYNAMIC RESPONSE OF MESHING CANTILEVER BEAMS, WITH INERTIA (VEL=CONST)

Figure 5-22

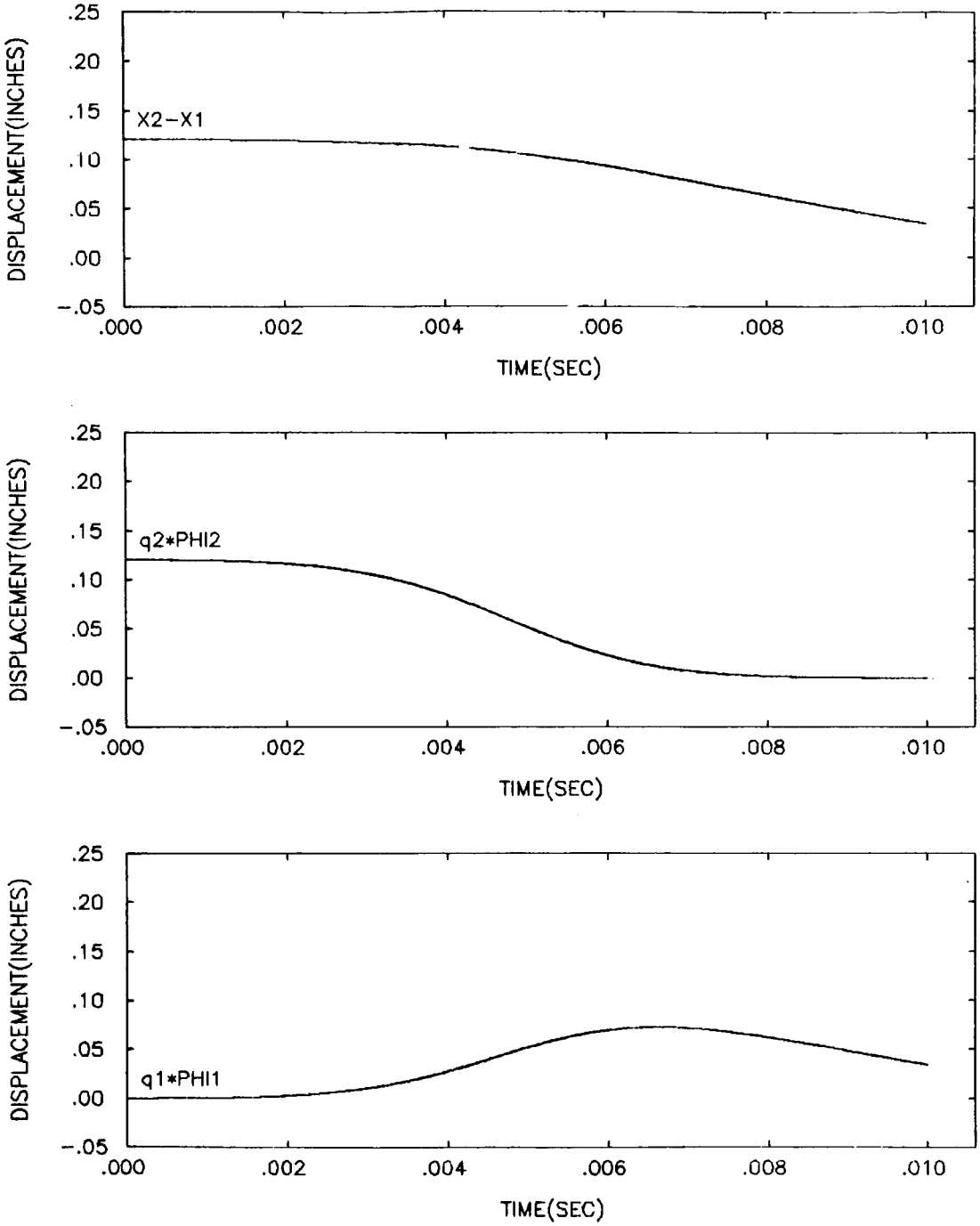

VEL= 40.0 IN/SEC ; MASS= 1.0 ; BEAM LENGTH= 0.5 IN

DYNAMIC RESPONSE OF MESHING CANTILEVER BEAMS, WITH INERTIA (VEL=CONST)

Figure 5-23

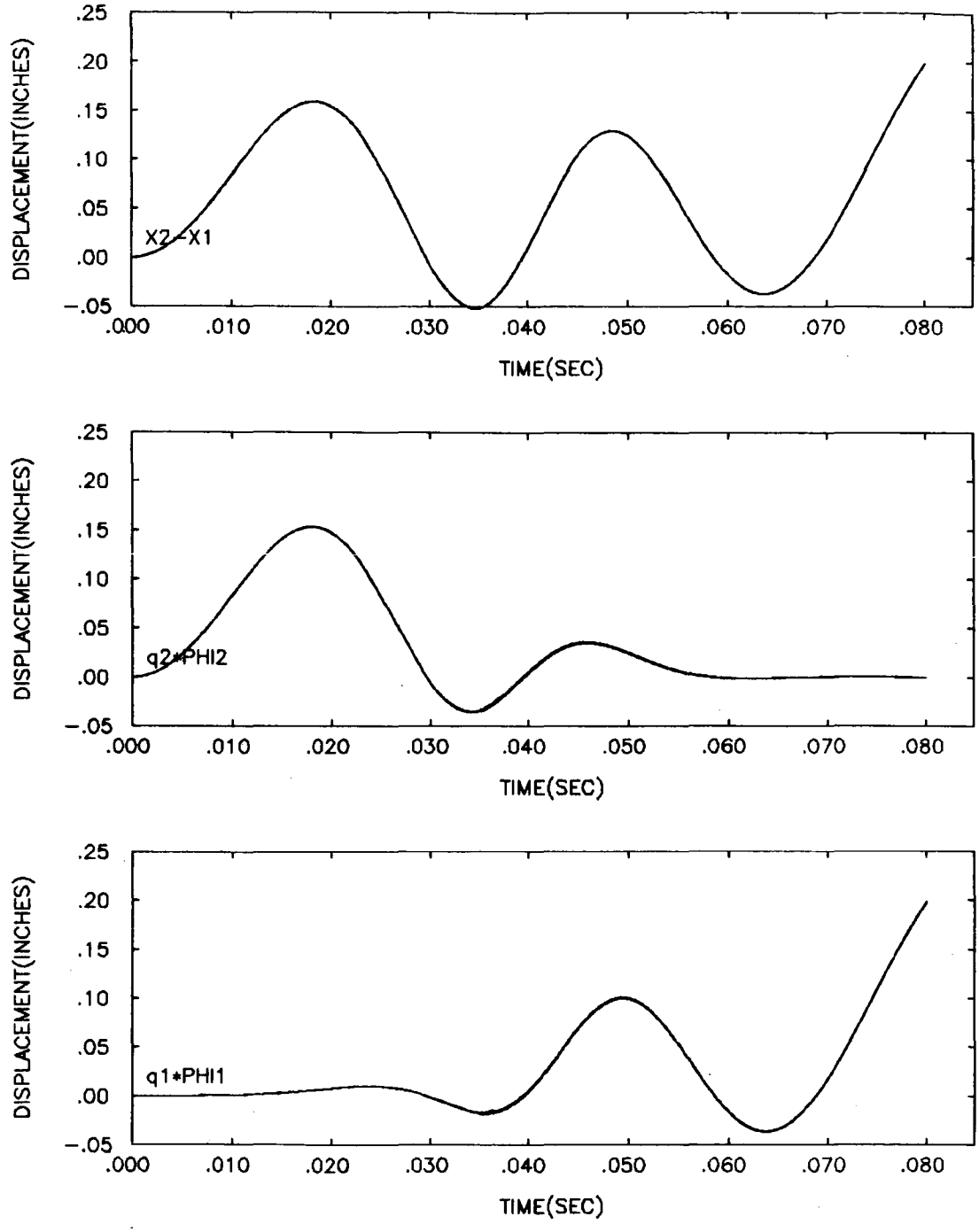

DYNAMIC RESPONSE OF MESHING CANTILEVER BEAMS, WITH INERTIA (VEL=CONST)

Figure 5-24

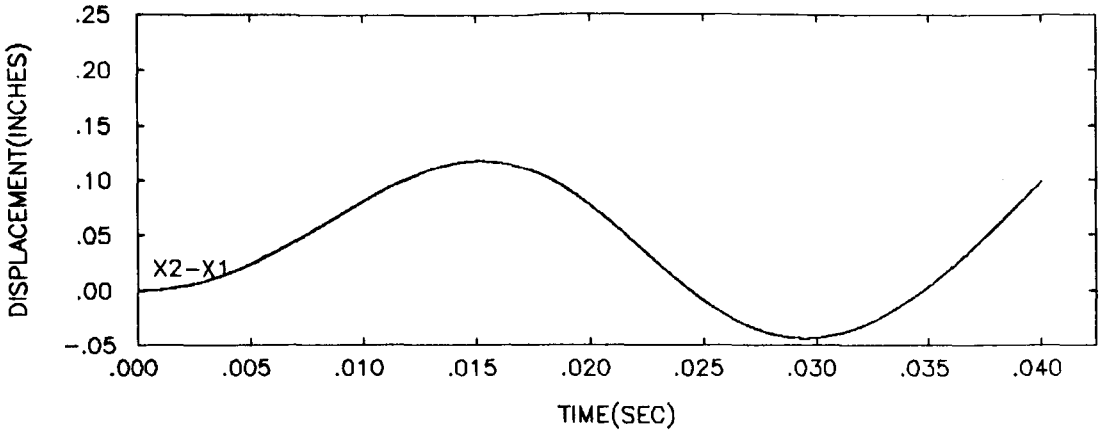

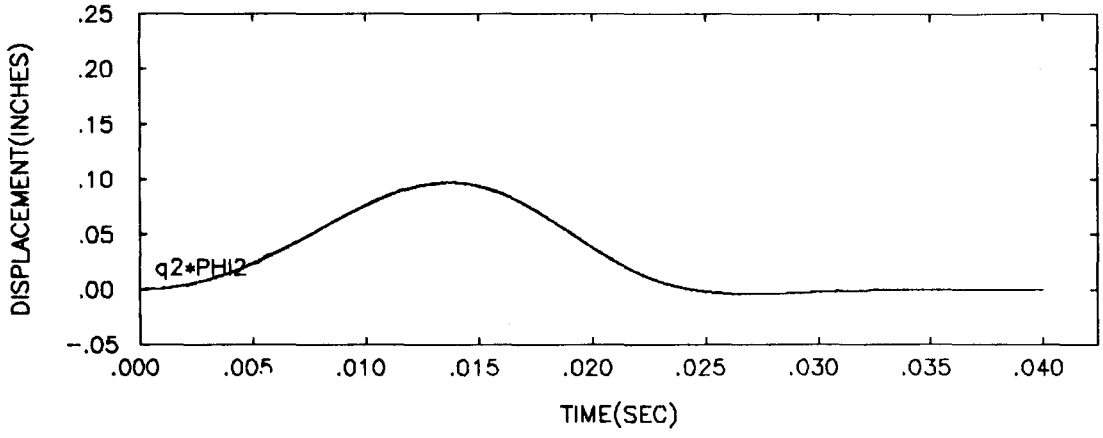

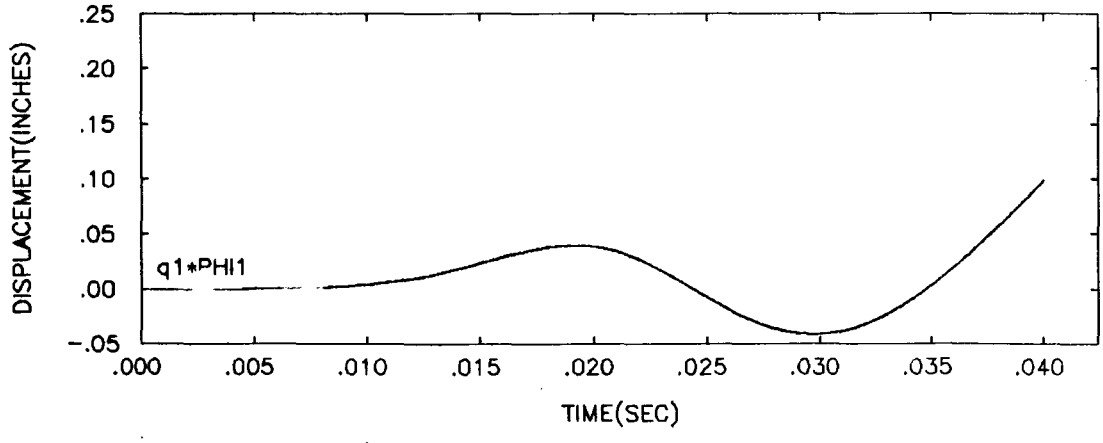

VEL= 10.0 IN/SEC ; MASS= 1.0 ; BEAM LENGTH= 0.5 IN

DYNAMIC RESPONSE OF MESHING CANTILEVER BEAMS, WITH INERTIA (VEL=CONST)

Figure 5-25

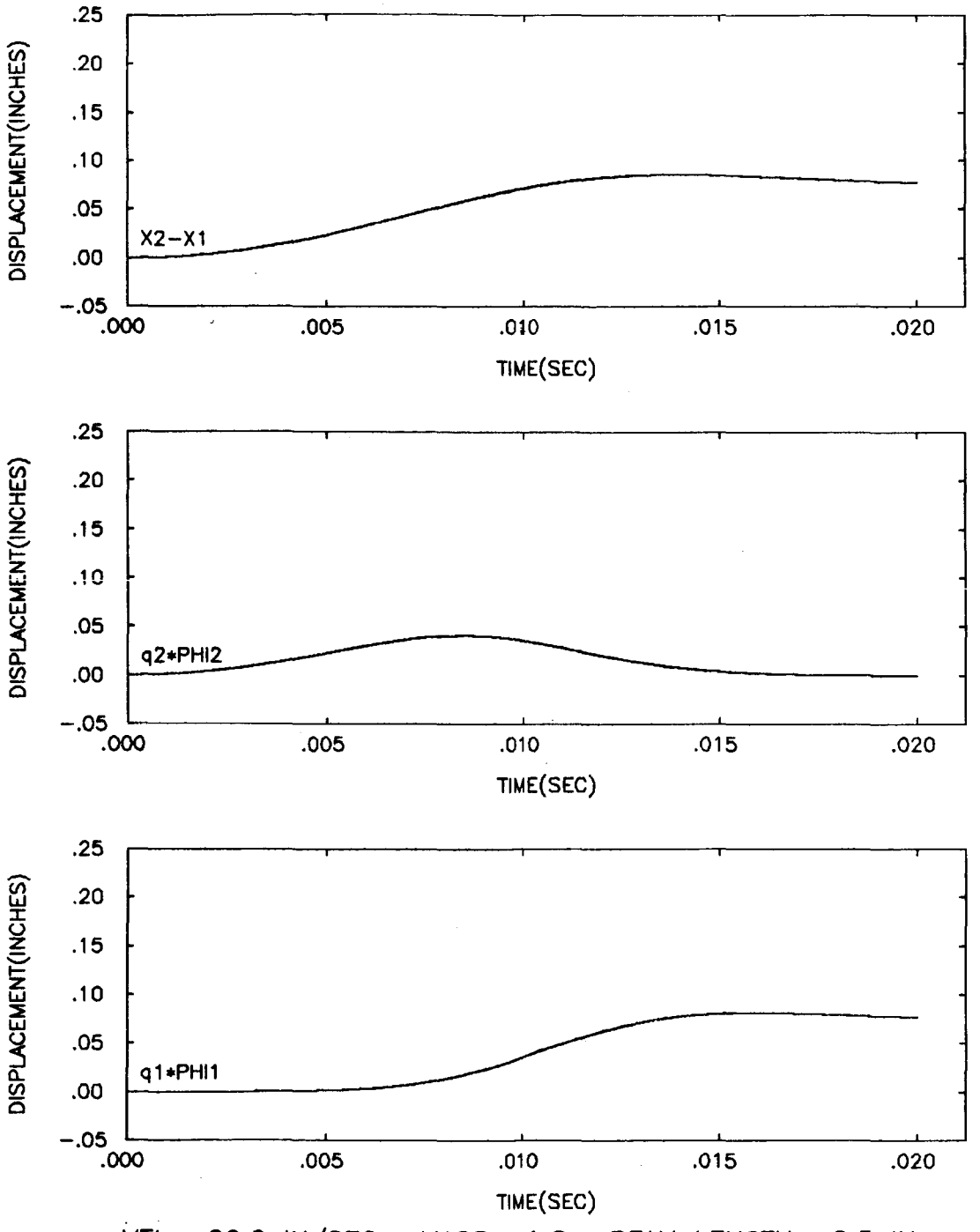

VEL= 20.0 IN/SEC ; MASS= 1.0 ; BEAM LENGTH= 0.5 IN

DYNAMIC RESPONSE OF MESHING CANTILEVER BEAMS, WITH INERTIA (VEL=CONST)

Figure 5-26

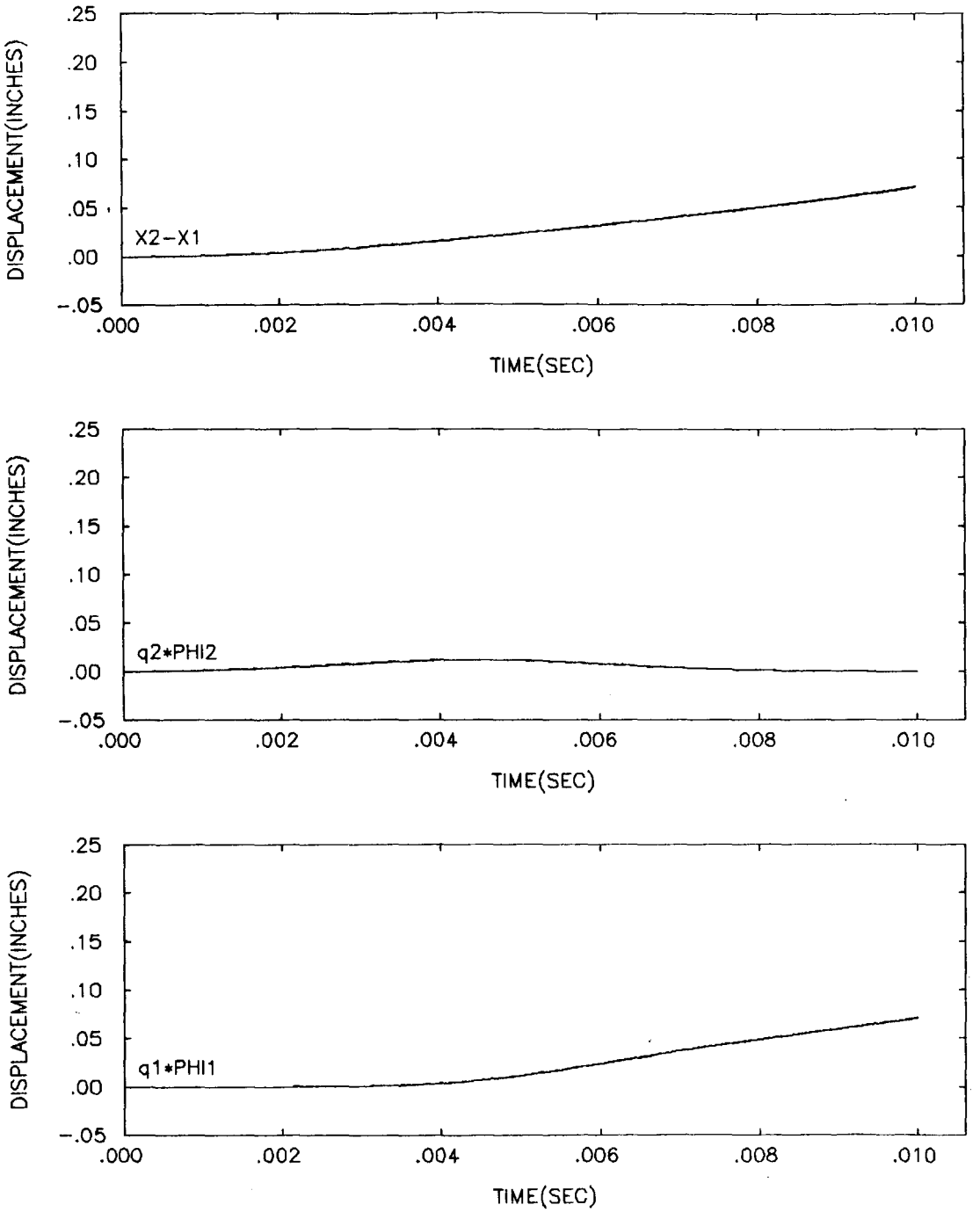

VEL= 40.0 IN/SEC ; MASS= 1.0 ; BEAM LENGTH= 0.5 IN

DYNAMIC RESPONSE OF MESHING CANTILEVER BEAMS, WITH INERTIA (VEL=CONST)

Figure 5-27

(5.2.3) Dynamic Response Results:
Foundation Mass = 1.0E-4 lbs.

In order to substantiate the conclusion that the dynamic response is not dependent on the mass of the beam, both the massless beam and inertial beam configurations are analyzed again with a decrease in the difference between the values of the beam and foundation masses. Of course the mass of the beam is not included in the massless beam analysis. Previously the mass of the foundation was 1.0 lbs and the total mass of the beam was approximately 3.6E-6 lbs. In this analysis, the foundation mass is decreased to 1.0E-4 lbs while the mass of the beam remains the same. Since the overall mass of the system is greatly decreased, the corresponding resonant frequency is much larger. Using an approximation of the resonant frequency using a single mass and the load at the midpoint of the beam yields an approximate resonant frequency of;

$$\omega = \sqrt{\frac{K}{M}} \Rightarrow \sqrt{\frac{48000}{1.E-4}} \quad (\frac{1}{2\pi}) \cong 3500 \text{ cycle/sec.}$$

and a cycle period of approximately 2.875E-4 sec. Therefore, in order to provide an adequate range of moving load speeds such that the system resonance is bracketed, speeds of 100., 500., 1000., 1500. and 2000. in/sec are used. (Approximately one oscillation cycle occurs at 1700 in/sec). To facilitate comparisons of respective systems, the results are presented in a parallel fashion. Figures 5-28 and 5-29 show the respective responses for a moving load speed of 500 in/sec. As seen from the plots, the responses are virtually the same. The results are similar for the other moving load speeds (see Figure 5-30 through 5-35).

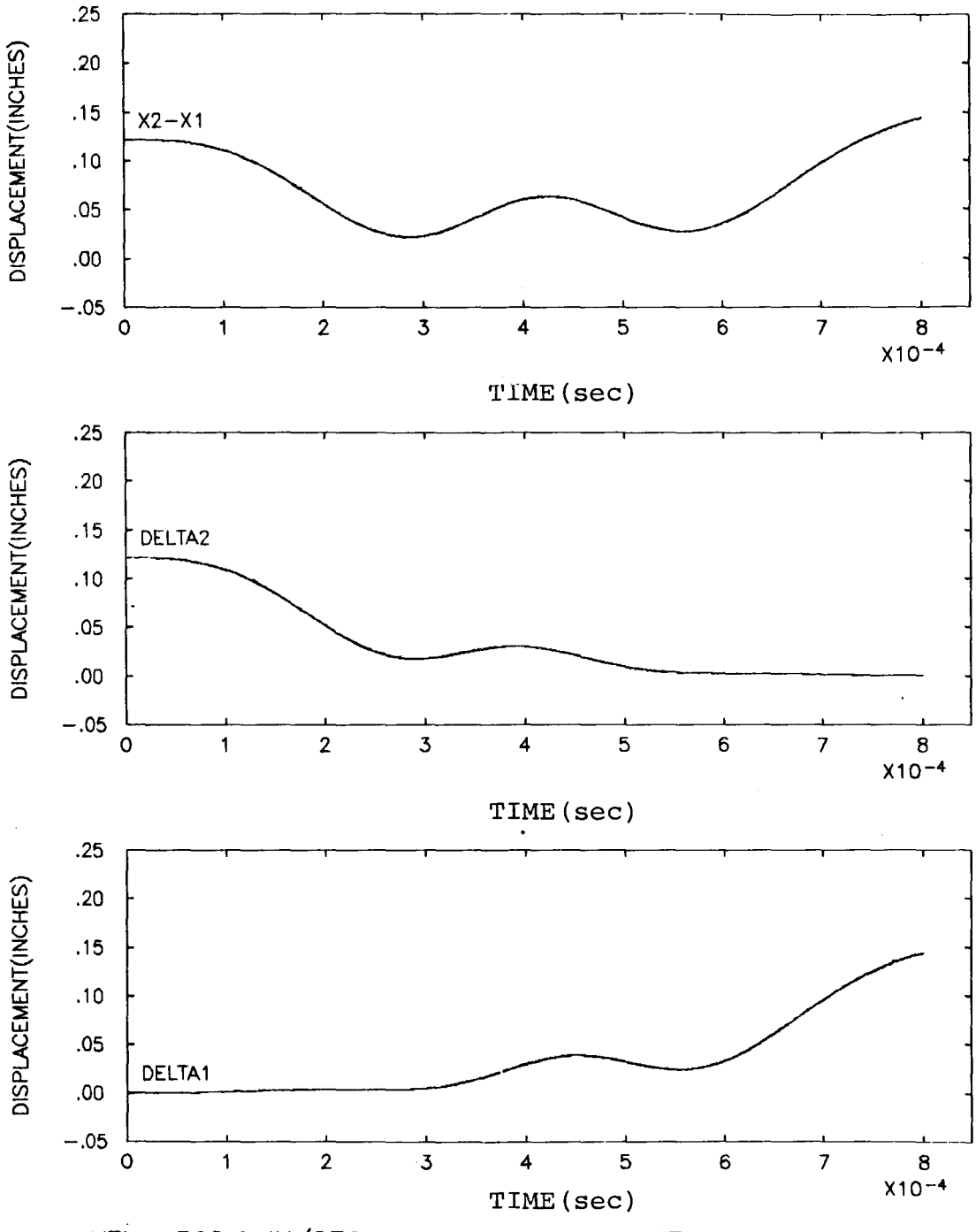

DYNAMIC RESPONSE OF MASSLESS MESHING CANTILEVER BEAMS (VEL=CONST)

Figure 5-28

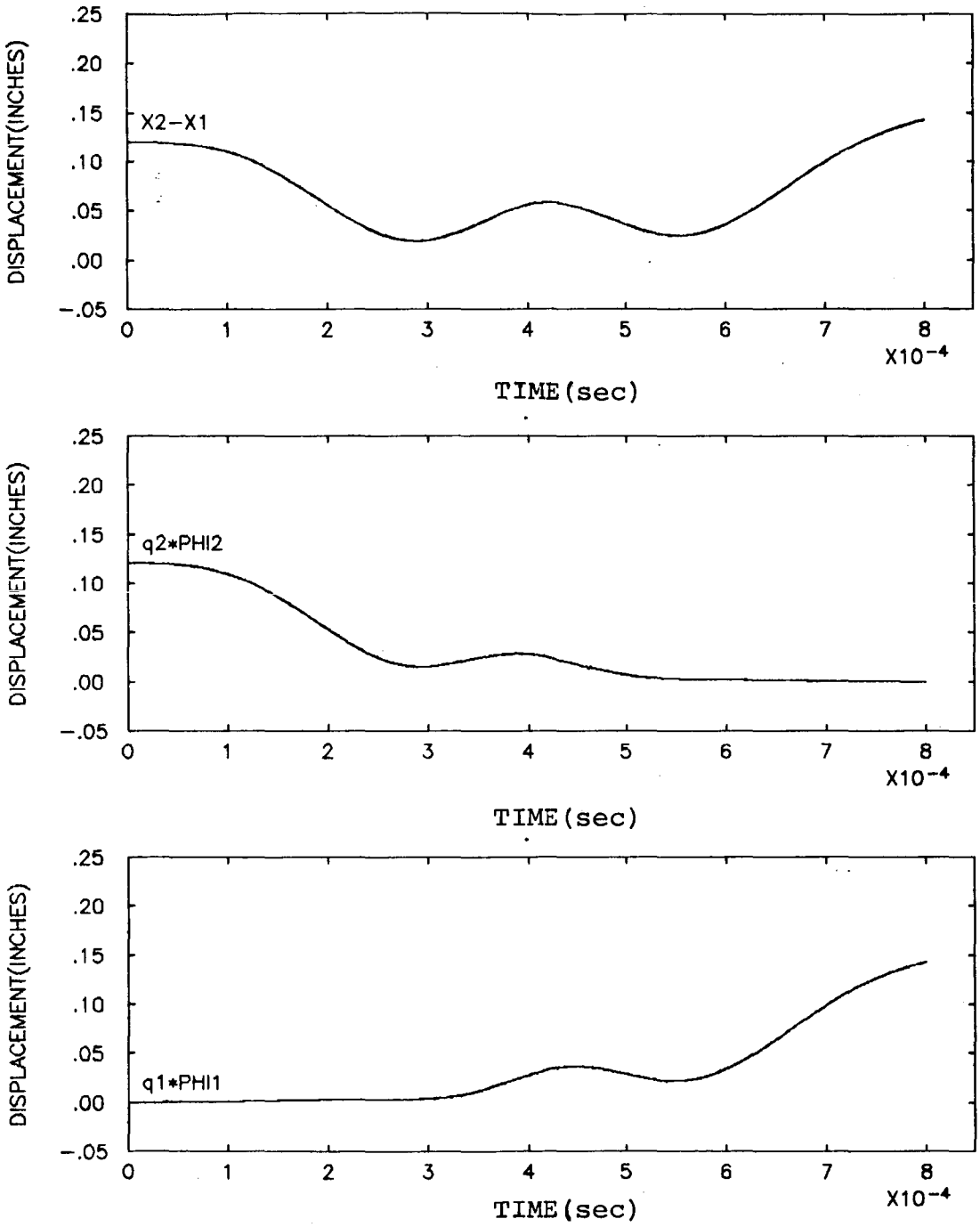

DYNAMIC RESPONSE OF MESHING CANTILEVER BEAMS, WITH INERTIA (VEL=CONST)

Figure 5-29

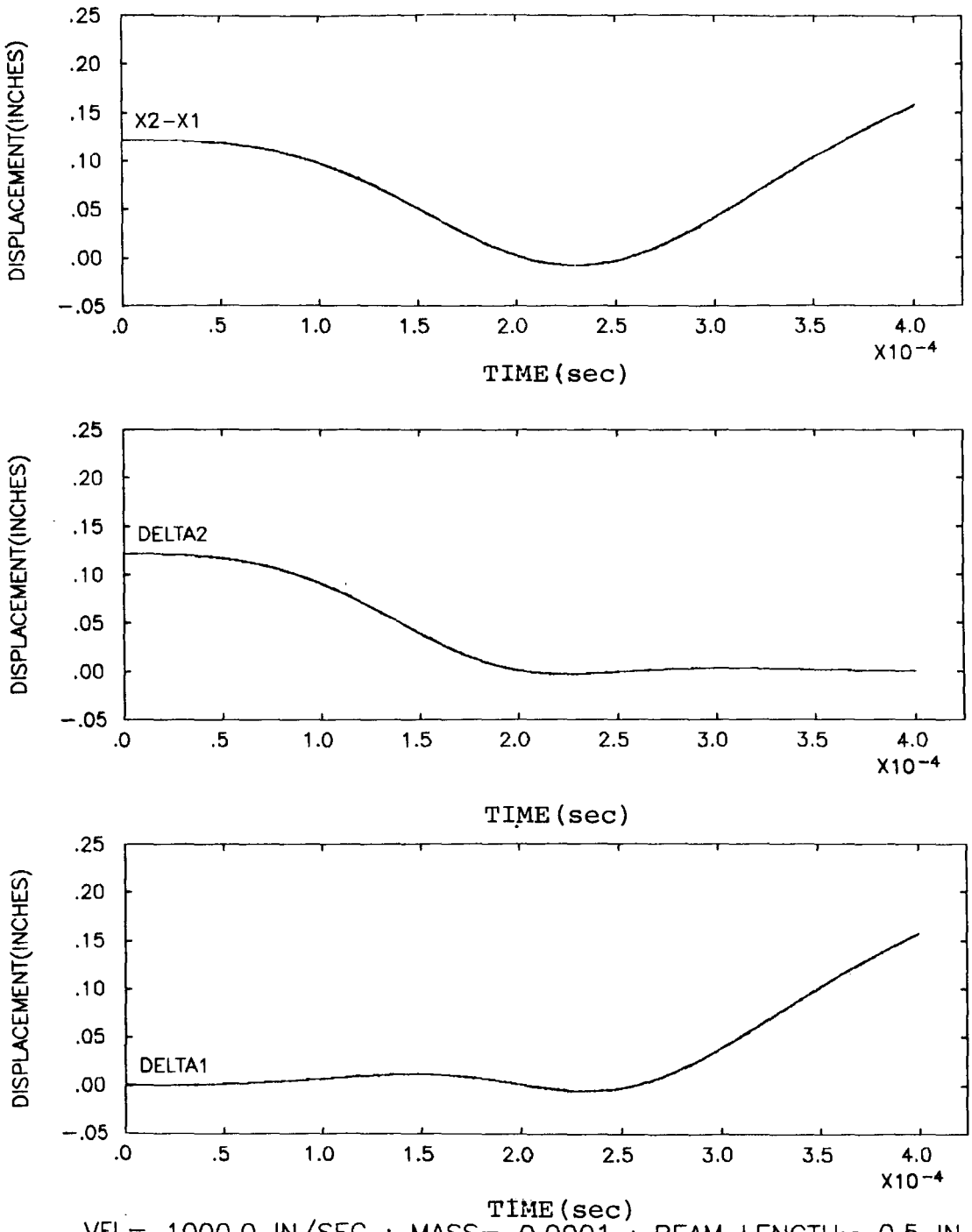

DYNAMIC RESPONSE OF MASSLESS MESHING CANTILEVER BEAMS (VEL=CONST)

Figure 5-30

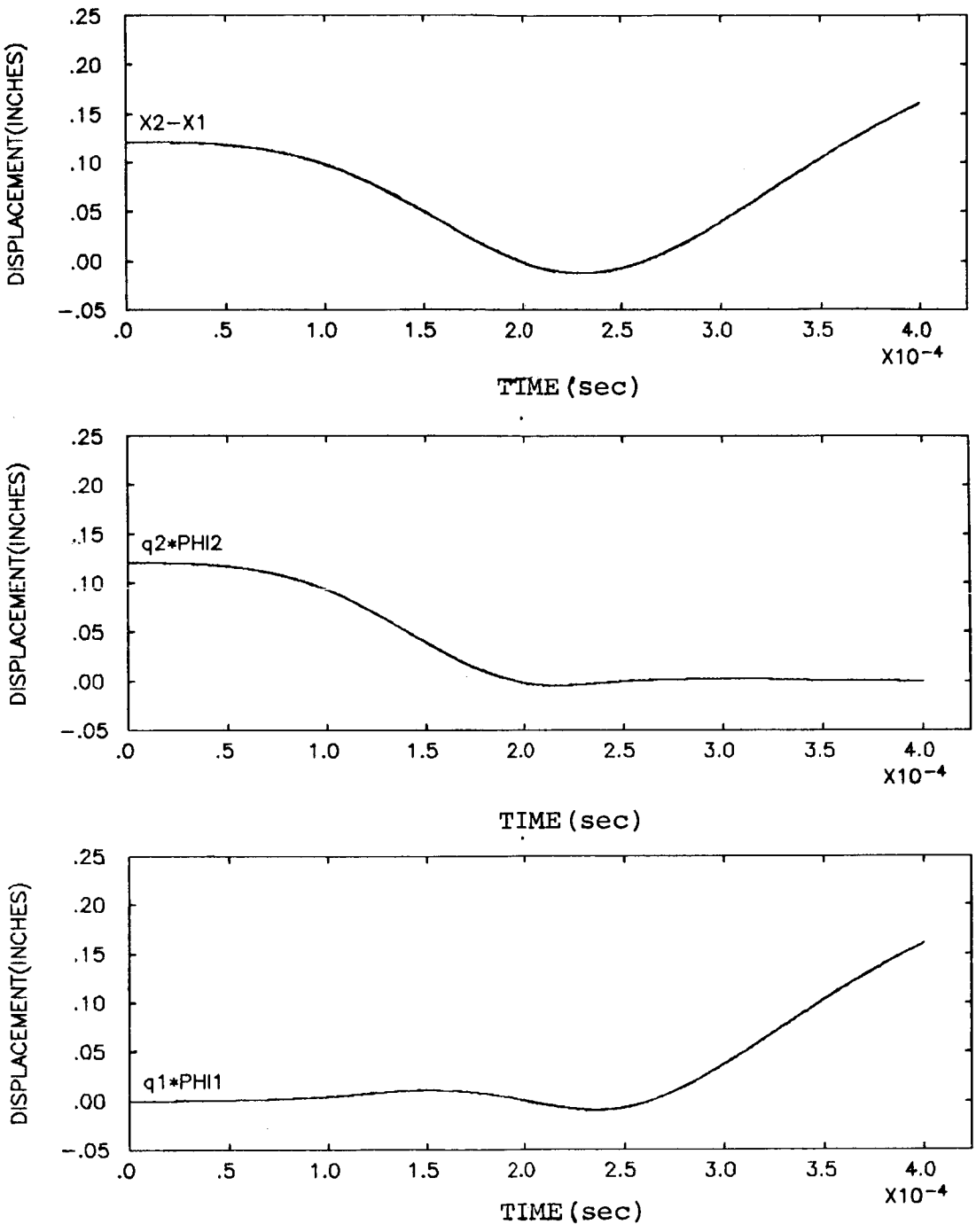

VEL= 1000.0 IN/SEC ; MASS= 0.0001 ; BEAM LENGTH= 0.5 IN

DYNAMIC RESPONSE OF MESHING CANTILEVER BEAMS, WITH INERTIA (VEL=CONST)

Figure 5-31

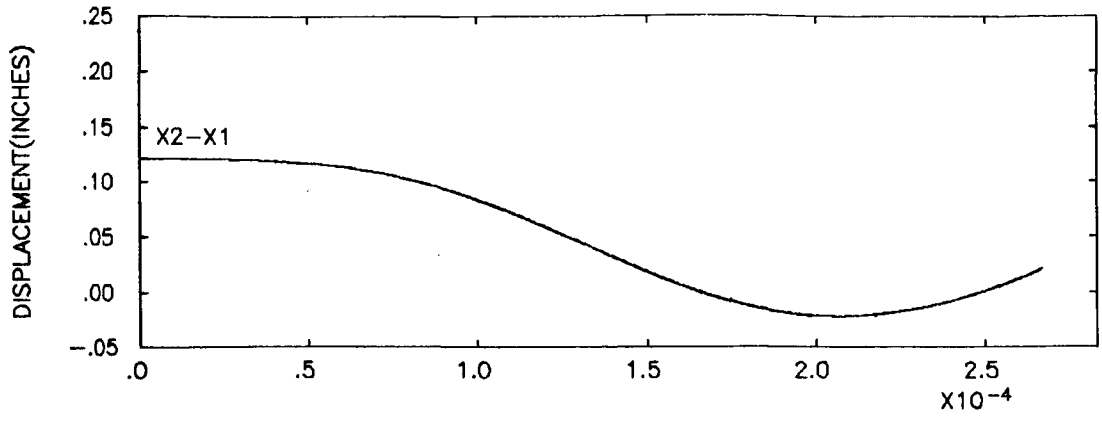

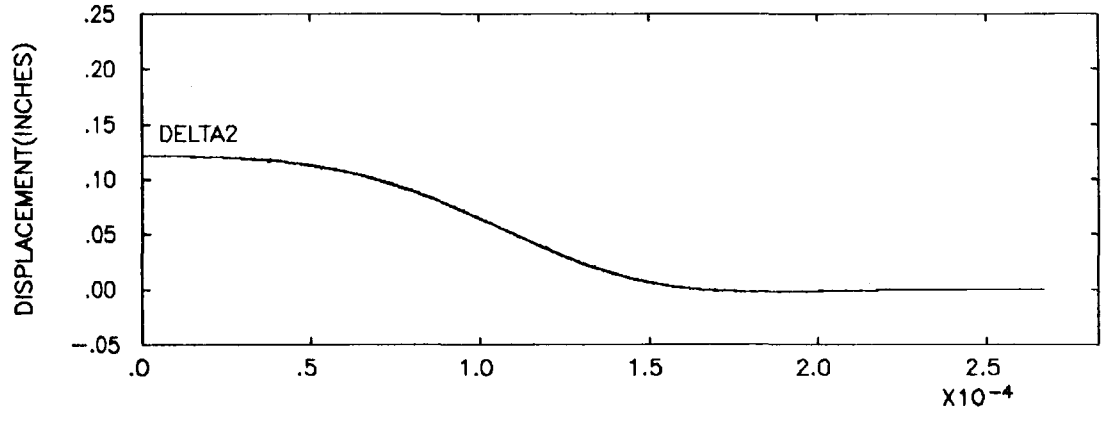

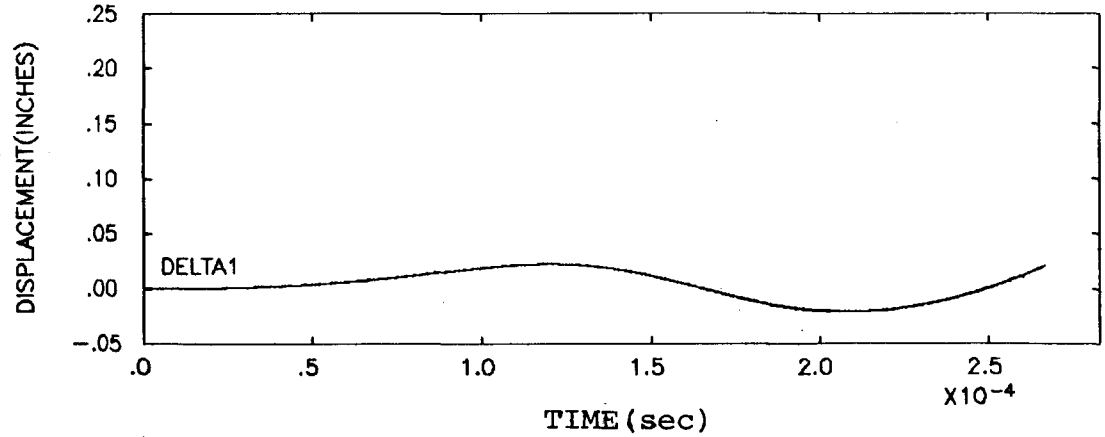

VEL= 1500.0 IN/SEC ; MASS= 0.0001 ; BEAM LENGTH= 0.5 IN

DYNAMIC RESPONSE OF MASSLESS MESHING CANTILEVER BEAMS (VEL=CONST)

Figure. 5-32

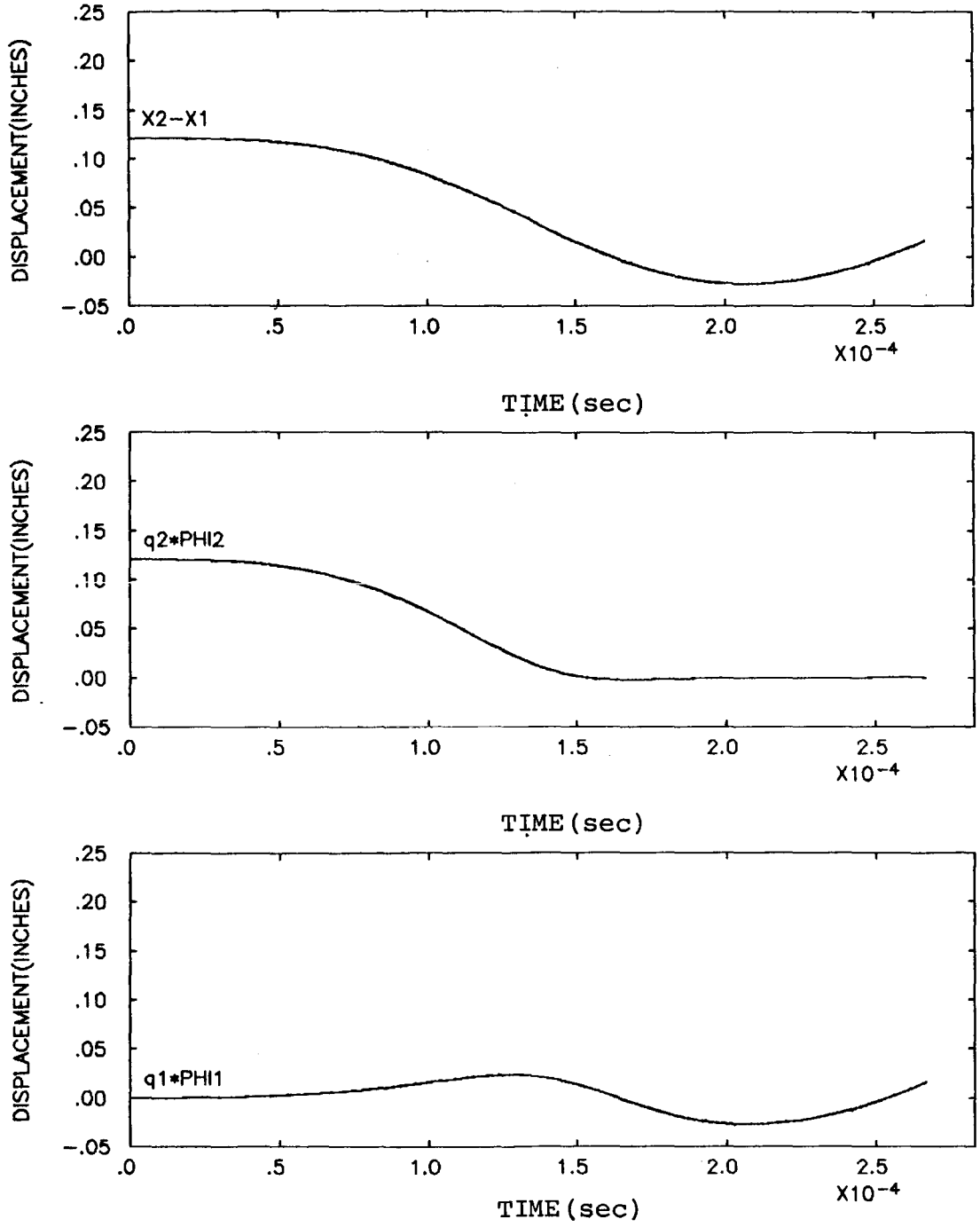

DYNAMIC RESPONSE OF MESHING CANTILEVER BEAMS, WITH INERTIA (VEL=CONST)

Figure 5-33

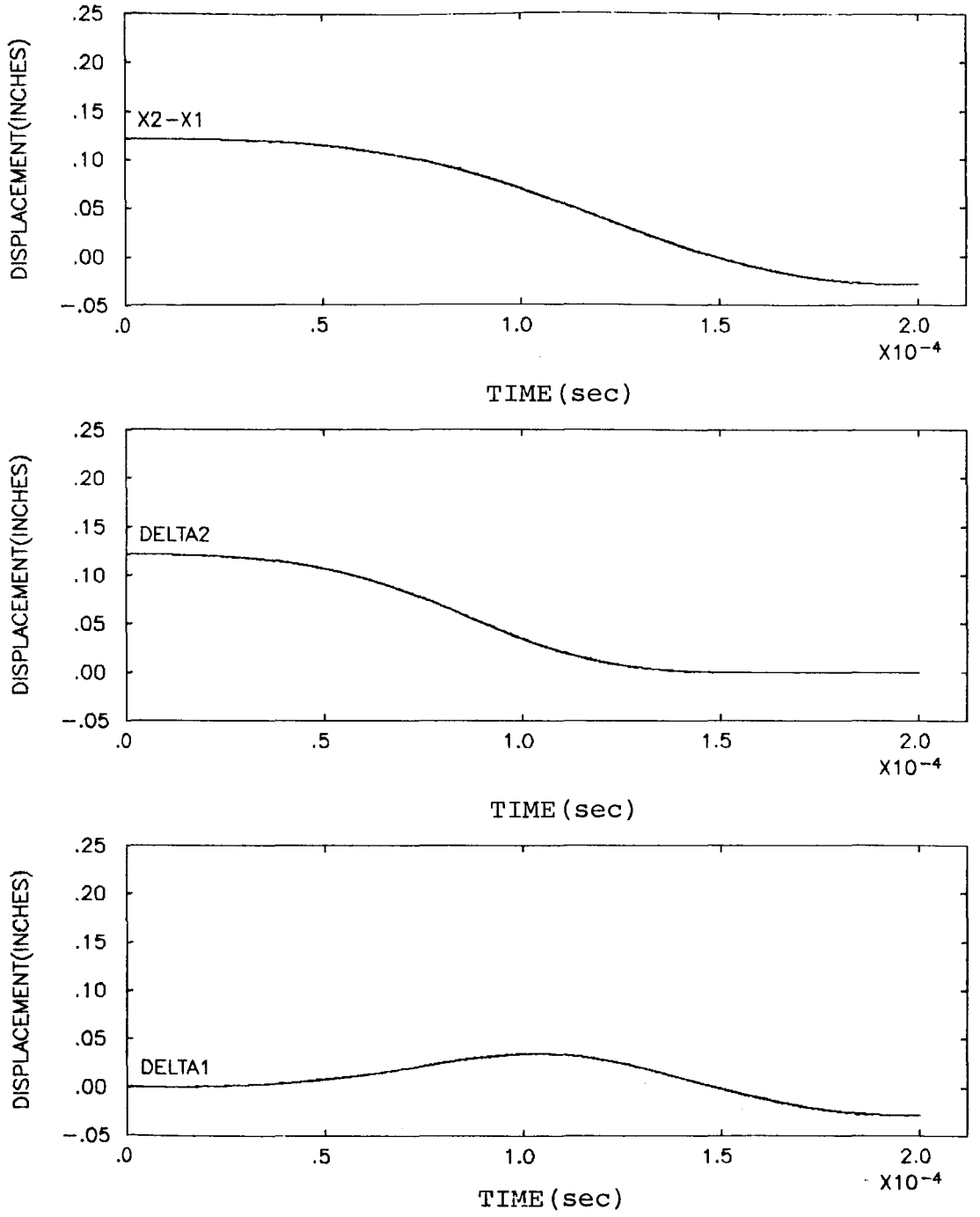

DYNAMIC RESPONSE OF MASSLESS MESHING CANTILEVER BEAMS (VEL=CONST)

Figure 5-34

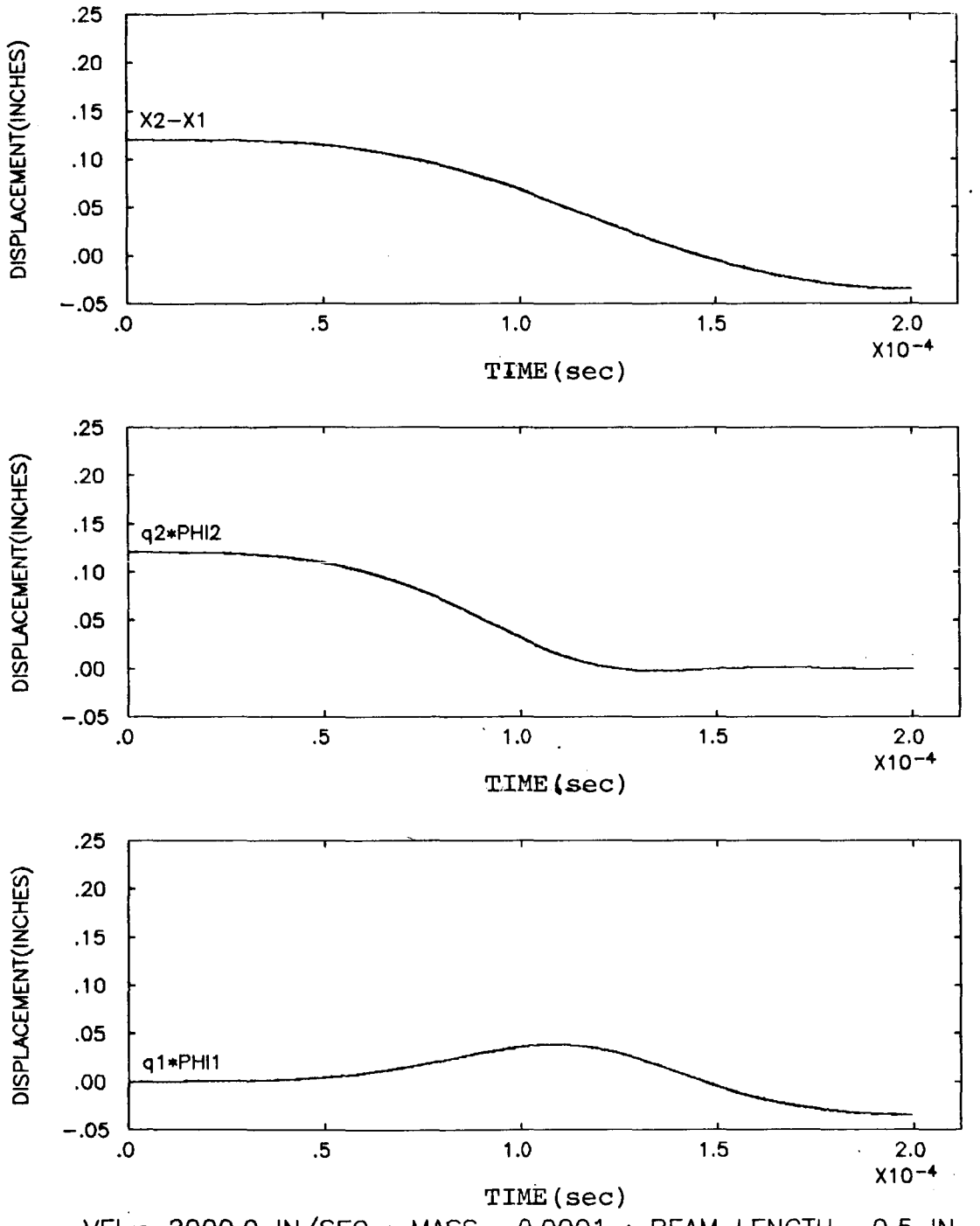

DYNAMIC RESPONSE OF MESHING CANTILEVER BEAMS, WITH INERTIA (VEL=CONST)

Figure 5-35

6. CONCLUSIONS

The objectives of this analysis were twofold. First, the dynamic response of a single spur gear tooth subject to moving loads was studied to determine the effect of the speed of movement of the load. A spur gear tooth, modelled using finite element techniques, was used in the analysis. From this analysis it was found that the dynamic response of a single gear tooth is not dependent on the speed of the moving load, but rather on the type of load engagement experienced at the beginning of the load cycle. Including the rim in the analysis added flexibility to the system but did not change the overall response.

The second objective was to determine whether or not the mass (inertial forces) of the tooth can be neglected when small compared to the mass of the gear hub. A simplified analysis using meshing cantilever beams was used. For the range of speeds tested, it was found that the inertia forces of the tooth are small and therefore, the mass of the tooth can be neglected when determining the dynamic response of a meshing gear system.

BIBLIOGRAPHY

[1] Cornell, R.W. and Westervelt, W.W., "Dynamic Tooth Loads and Stressing for High Contact Ratio Spur Gears", ASME, J. Mech. Des., Vol. 100, No. 1, Jan. 1978.

[2] Wang, K.L. and Cheng, H.S., "A Numerical Solution to the Dynamic Load, Film Thickness, and Surface Temperatures in Spur Gears, Part I - Analysis", ASME, J. Mech. Des., Vol. 103, Jan. 1981.

[3] Wang, K.L. and Cheng, H.S., "A Numerical Solution to the Dynamic Load, Film Thickness, and Surface Temperatures in Spur Gears, Part II - Results", ASME, J. Mech. Des. Vol. 103, Jan. 1981.

[4] Richardson, H.H., "Static and Dynamic Load, Stress, and Deflection Cycles in Spur Gearing", Sc. D. Thesis, Dept. of Mech. Eng., MIT Cambridge, Mass, 1958.

[5] Kasuba, R. and Evans, J.W., "An Extended Model for Determining Dynamic Loads in Spur Gearing", ASME, J. Eng. Ind., Vol. 103, No. 2, Apr. 1981.

[6] Attia, A.Y., "Deflection of Spur Gear Teeth Cut in Thin Rims", ASME, J. Eng. Ind., Vol. 86, No. 4, Nov. 1964.

[7] Nagaya, K. and Uematsu, S., "Effects of Moving Load Speeds of Dynamic Loads on the Deflections of Gear Teeth", ASME, J. Mech. Des., Vol. 103, No. 2, Apr. 1981.

[8] Karas, F., "Elastiche Formanderung und Lasterverteilung heim Doppleleingriff geroder Stirnradzahne", V.D.I. Forschh. Vol. 406, 1941.

[9] Wallace, D.B. and Seireg, A., "Computer Simulation of Dynamic Stress, Deformation, and Fracture of Gear Teeth", ASME, J. Eng. Ind., Vol. 95, 1973.

[10] Cornell, R.W., "Compliance and Stress Sensitivity of Spur Gear Teeth", ASME, J. Mech. Des., Vol. 103, No. 2, Apr. 1981.

[11] Chang, S.H., Huston, R.L. and Coy, J.J., "A Finite Element Stress Analysis of Spur Gears Including Fillet Radii and Rim Thickness Effects", ASME, J. Mech. Des., Paper No. 82-WA/DE-35, 1982.

[12] Weber, C., "The Deformations of Loaded Gears and the Effect on Their Load Carrying Capacity", Sponsored Research (Germany), British Dept. of Scientific and Industrial Research, Report No. 3, 1949.

[13] Segerlind, L.J., Applied Finite Element Analysis, John Wiley and Sons, Inc., New York, 1976.

[14] Cook, R.D., Concepts and Applications of Finite Element Analysis, 2nd Ed., John Wiley & Sons, New York, 1981.

[15] Meirovitch, L., Analytical Methods in Vibrations, MacMillan Comp., New York, 1967.

[16] Meirovitch, L., Methods of Analytical Dynamics, McGraw-Hill Inc., New York, 1970.

[17] Clough, R.W. and Penzien, J., Dynamics of Structures, McGraw-Hill, New York, 1975.

[18] Craig, R.R., Structural Dynamics an Introduction to Computer Methods, John Wiley and Sons, New York, 1981.

[19] Budynas, R.G., Advanced Strength and Applied Stress Analysis, McGraw-Hill, New York, 1977.

[20] Shigley, J.E., Mechanical Engineering Design, 3rd Ed., McGraw-Hill, New York, 1977.

[21] Merritt, H.E., Gear Engineering, Halsted Press, New York, 1971.

[22] Fryba, L., Vibration of Solids and Structures Under Moving Loads, Noordhoff International Publishing, Groningen, The Netherlands, 1972.

APPENDIX 1

1. Finite Element Model Generation Program

2. Moving Load Generation Program Using Wallace-Seireg Load History

```
C     ****************************************
C     *                                      *
C     *    SPUR GEARTOOTH PROFILE GENERATOR  *
C     *                                      *
C     *       WRITTEN BY  LYLE W. SHUEY      *
C     *                                      *
C     * THIS PROGRAM GENERATES A FINITE ELEMENT *
C     * MESH FOR EITHER A HIGH CONTACT RATIO  *
C     * GEAR OR A LOW CONTACT RATIO GEAR, IN- *
C     * CLUDING THE FOUNDATION AND RIM IN THE *
C     * MODEL.                               *
C     * A MINIMUN OF INPUT PARAMETERS ARE NEEDED*
C     * TO DESCRIBE THE GEAR GEOMETRY.       *
C     * THEY ARE;                            *
C     *          PRESSURE ANGLE   :PANG      *
C     *          PITCH RADIUS     :RP        *
C     *          ADDENDUM         :AD        *
C     *          DEDENDUM         :DED       *
C     *          CIRCULAR PITCH   :CIRP      *
C     *          BACKLASH         :BACKL     *
C     *          FILLET RADIUS    :RF        *
C     *          RIM THICKNESS    :RTH       *
C     *                                      *
C     ****************************************
C
C
C******  THE PROGRAM READS THE INPUT VARIABLES
C******  USING THE PROCEEDING STATEMENTS.
C
      DIMENSION DUMY(20),YPRF(20),XPRF(20)
      DIMENSION XX(40),YY(40),XN(400),YN(400)
      DIMENSION XANG(9,9),XADA(9),XINC(9)
      PI=3.141592654
      READ(5,*) PANG
      WRITE(6,*) 'PRESSURE ANGLE:      ',PANG
      PANG=PANG*PI/180.
      READ(5,*) RP
      WRITE(6,*) 'PITCH RADIUS:        ',RP
      READ(5,*) AD
      WRITE(6,*) 'ADDENDUM:            ',AD
      READ(5,*) DED
      WRITE(6,*) 'DEDENDUM:            ',DED
      READ(5,*) CIRP
      WRITE(6,*) 'CIRCULAR PITCH:      ',CIRP
      READ(5,*) RF
      WRITE(6,*) 'FILLET RADIUS:       ',RF
      READ(5,*) BACKL
      WRITE(6,*) 'BACKLASH:            ',BACKL
      READ(5,*) RTH
      WRITE(6,*) 'RIM THICKNESS:       ',RTH
      RB=RP*COS(PANG)
      THP=((RP*RP-RB*RB)/(RB*RB))**.5
      CIRTH=CIRP/2.-BACKL
      WRITE(6,*) 'CIRTH:               ',CIRTH
      AL=THP-ATAN(THP)+CIRTH/(RP*2.)
      DP=PI/CIRP
      WRITE(6,*) 'DIAMETRAL PITCH:     ',DP
      RR=RP-DED
      RO=RP+AD
```

```
      N=27
C     ******************************************
C     *  THIS SECTION CALCULATES POINTS ON THE  *
C     *  INVOLUTE SURFACE, FOUNDATION, AND RIM  *
C     *  WHICH WILL LATER BE USED TO GENERATE   *
C     *  NODAL COORDINATES. (BOTH HCRG AND LCRG)*
C     ******************************************
C
C******  GENERATING POINTS ON THE INVOLUTE PROFILE
C
      DO 5 I=1,11
        IA=1+(I-1)
        HH=(RO-RB)/10.
        H=RO-HH*(I-1)
        ANG=((H*H-RB*RB)/(RB*RB))**.5
        X=-RB*(SIN(ANG)-ANG*COS(ANG))
        Y=RB*(COS(ANG)+ANG*SIN(ANG)-1)
        ANGF=ATAN(SIN(ANG)/COS(ANG))-AL
        ANGF=ANGF*180./PI
        XP=RB*SIN(AL)+X*COS(AL)+Y*SIN(AL)
        YP=RB*COS(AL)-X*SIN(AL)+Y*COS(AL)
        XX(IA)=XP
        YY(IA)=YP
        WRITE(6,*) 'XP:',XP,'YP:',YP,'THETA:',ANGF
5     CONTINUE
C
C******  CHECK IF GEAR IS LCRG OR HCRG
C
      CHECK=RR*RR+2.*RR*RF
      ITAN=2
      IF(CHECK.LT.RB*RB) ITAN=1
      IF(ITAN.NE.1) GO TO 15
C
C******  STRAIGHT LINE TANGENT TO INVOLUTE (HCRG)
C
      DD=(-2.*RR+(4.*RR*RR+4.*2.*RF*RR)**.5)/2.
      D=RB-(RR+DD)
      DDD=RB-RR
      XTAN=(D/DDD)
      XFILL=(DD/DDD)
      LTAN=INT(XTAN*8.)
      LFILL=INT(XFILL*8.)+1
      WRITE(6,*) 'DD:       ',DD
      WRITE(6,*) 'D:        ',D
      WRITE(6,*) 'DDD:      ',DDD
      WRITE(6,*) 'XTAN:      ',XTAN
      WRITE(6,*) 'XFILL:     ',XFILL
      WRITE(6,*) 'LFILL:      ',LFILL
      WRITE(6,*) 'LTAN:       ',LTAN
      DRI=D/LTAN
      DR=0.0
      DO 10 I=1,LTAN
        IA=12+(I-1)
        XP=XP-(((RB-DR)*SIN(AL))-((RB-DRI)*SIN(AL)))
        YP=YP-(((RB-DR)*COS(AL))-((RB-DRI)*COS(AL)))
        DR=DRI
        DRI=DRI+D/LTAN
        XX(IA)=XP
        YY(IA)=YP
```

```
10     CONTINUE
C
C*********   FILLET RADIUS SECTION (HCRG)
C
       BETA=ATAN((RR+RF)/RF)
       BETA=BETA/LFILL
       DO 11 I=1,LFILL
         IA=(12+LTAN)+(I-1)
         X=RF-RF*COS(BETA*I)
         Y=-RF*SIN(BETA*I)
         XP=(RB-D)*SIN(AL)+X*COS(AL)+Y*SIN(AL)
         YP=(RB-D)*COS(AL)-X*SIN(AL)+Y*COS(AL)
         XX(IA)=XP
         YY(IA)=YP
11     CONTINUE
       GO TO 21
C
C******  GENERATING POINTS FOR FILLET RADIUS (LCRG)
C
15     DD=RB-RR
       RF=((DD*DD)+(2.*DD*RR))/(2.*RR)
       WRITE(6,*) 'NEW FILLET RADIUS    ',RF
       BETA=ATAN((RR+DD)/RF)
       WRITE(6,*)'BETA:',BETA*180./PI
       BETA=BETA/8.0
       DO 20 I=1,8
         IA=12+(I-1)
         X=RF-RF*COS(BETA*I)
         Y=-RF*SIN(BETA*I)
         XP=RB*SIN(AL)+X*COS(AL)+Y*SIN(AL)
         YP=RB*COS(AL)-X*SIN(AL)+Y*COS(AL)
         XX(IA)=XP
         YY(IA)=YP
         WRITE(6,*) 'XP:',XP,'YP:',YP
20     CONTINUE
C
C******  GENERATING POINTS ON OUTER RIM SURFACE
C
21     ADA=ASIN((XP+CIRTH)/RR)-ASIN(XP/RR)
       DADA=ADA/6.
       ADA1=ASIN(XP/RR)
       WRITE(6,*)'ADA:',ADA*180./PI
       DO 30 I=1,4
         IA=20+(I-1)
         DUMY(I)=10.
         XP=XP+RR*(SIN(ADA1+DADA)-SIN(ADA1))
         YP=YP-RR*(COS(ADA1)-COS(ADA1+DADA))
         XX(IA)=XP
         YY(IA)=YP
         WRITE(6,*) 'XP:',XP,'YP:',YP
         DADA=ADA/4.
         ADA1=ADA1+DADA
30     CONTINUE
C
C******  GENERATING POINTS ON RADIAL PORTION OF RIM
C
       DELTA=ASIN(XP/RR)
       RIM=RR-RTH
       DRTH=RTH/4.
```

```
      DX=RR*SIN(DELTA)-RIM*SIN(DELTA)
      DDX=DX/4.0
      DO 40 I=1,4
        IA=24+(I-1)
        XPRF(I)=XP-DDX
        YPRF(I)=YP-DRTH
        XX(IA)=XPRF(I)
        YY(IA)=YPRF(I)
        DRTH=DRTH+RTH/4.
        DDX=DDX+DX/4.0
        WRITE(6,*) 'XP:',XPRF(I),'YP:',YPRF(I)
40    CONTINUE
      XP=XPRF(4)
      YP=YPRF(4)
C
C******  GENERATING POINTS ON INNER RIM SURFACE
C
      DELTA=ATAN(XP/YP)
      XLEG=((XP*XP)+(YP*YP))**.5
      DELTA1=DELTA/4.0
      DO 50 I=1,4
        IA=28+(I-1)
        DELTA=DELTA-DELTA1
        XPRF(I)=XLEG*SIN(DELTA)
        YPRF(I)=XLEG*COS(DELTA)
        XX(IA)=XPRF(I)
        YY(IA)=YPRF(I)
        WRITE(6,*) 'XP:',XPRF(I),'YP:',YPRF(I)
50    CONTINUE
C
C     ****************************************
C     *  THIS SECTION USES COORDINATES FROM   *
C     *  THE PREVIOUS SECTIONS TO CALCULATE   *
C     *  NODAL NUMBERS AND COORDINATES. THERE *
C     *  ARE 319 NODES USED IN THIS MODEL.    *
C     ****************************************
C
C******  GENERATING NODES 1-121
C
      II=0
      DO 60 I=1,11
        IA=1+(I-1)*11
        YA=YY(I)
        XA=XX(I)
        AZ=XA*.15
        BZ=XA*.30
        CZ=XA*.50
        DZ=XA*.75
        XN(IA)=-XA
        XN(IA+10)=XA
        XN(IA+1)=-XA+AZ
        XN(IA+9)=XA-AZ
        XN(IA+2)=-XA+BZ
        XN(IA+8)=XA-BZ
        XN(IA+3)=-XA+CZ
        XN(IA+7)=XA-CZ
        XN(IA+4)=-XA+DZ
        XN(IA+6)=XA-DZ
        XN(IA+5)=0.0
```

```
        DO 60 J=1,11
          II=II+1
          YN(II)=YA
60    CONTINUE
C
C******  GENERATING NODES 122-209
C
      DANG=2.5
      SANG=10.0
      DO 70 I=1,8
        DXANG=SANG
        DO 75 J=1,4
         XANG(I,J)=DXANG
         DXANG=DXANG-DANG
          WRITE(6,*) XANG(I,J)
          XANG(I,J)=XANG(I,J)*PI/180.
75      CONTINUE
        DANG=DANG+2.5
        SANG=SANG+10.
70    CONTINUE
       DO 71 I=1,8
        XANG(I,4)=0.0
71    CONTINUE
C
      DO 80 I=1,8
        IA=122+(I-1)*11
        XA=XX(11+I)
        YA=YY(11+I)
        AZ=XA*.15
        BZ=XA*.30
        CZ=XA*.50
        DZ=XA*.75
        DZ=DZ*(1.+(I*.02))
        XN(IA)=-XA
        XN(IA+10)=XA
        XN(IA+1)=-XA+AZ*COS(XANG(I,1))
        XN(IA+9)=-XN(IA+1)
        XN(IA+2)=XN(IA+1)+(BZ-AZ)*COS(XANG(I,2))
        XN(IA+8)=-XN(IA+2)
        XN(IA+3)=XN(IA+2)+(CZ-BZ)*COS(XANG(I,3))
        XN(IA+7)=-XN(IA+3)
        XN(IA+4)=XN(IA+3)+(DZ-CZ)*COS(XANG(I,4))
        XN(IA+6)=-XN(IA+4)
        XN(IA+5)=0.0
        IF(I.EQ.7) CZ=CZ*1.1
        IF(I.EQ.8) CZ=CZ*1.15
        YN(IA)=YA
        YN(IA+10)=YA
        YN(IA+1)=YA-AZ*SIN(XANG(I,1))
        YN(IA+9)=YN(IA+1)
        YN(IA+2)=YN(IA+1)-(BZ-AZ)*SIN(XANG(I,2))
        YN(IA+8)=YN(IA+2)
        YN(IA+3)=YN(IA+2)-(CZ-BZ)*SIN(XANG(I,3))
        YN(IA+7)=YN(IA+3)
        YN(IA+4)=YN(IA+3)-(DZ-CZ)*SIN(XANG(I,4))
        YN(IA+6)=YN(IA+4)
        YN(IA+5)=YN(IA+4)
80    CONTINUE
C
```

```
      DZ=DZ/1.16
       CZ=CZ/1.15
C
C******  GENERATING NODES 210-233
C
       DO 85 I=1,3
         J=20+(I-1)
         XINC(I)=ATAN(XX(J)/YY(J))
85     CONTINUE
       DINC=XINC(1)/2.
       DO 90 I=1,3
         IA=210+(I-1)*8
         YA=YY(19+I)
         XA=XX(19+I)
         XN(IA)=-XA
         XN(IA+7)=XA
         XN(IA+1)=XN(IA)+AZ*SIN(XINC(I))
         XN(IA+6)=-XN(IA+1)
         XN(IA+2)=XN(IA+1)+(BZ-AZ)*SIN(XINC(I))
         XN(IA+5)=-XN(IA+2)
         XN(IA+3)=XN(IA+2)+(CZ-BZ)*SIN(XINC(I))
         XN(IA+4)=-XN(IA+3)
         YN(IA)=YA
         YN(IA+7)=YA
         YN(IA+1)=YA-AZ*COS(XINC(I))
         YN(IA+6)=YN(IA+1)
         YN(IA+2)=YN(IA+1)-(BZ-AZ)*COS(XINC(I))
         YN(IA+5)=YN(IA+2)
         YN(IA+3)=YN(IA+2)-(CZ-BZ)*COS(XINC(I))
         YN(IA+4)=YN(IA+3)
90     CONTINUE
C
C******  GENERATING NODES 234-241
C
       DELTA=ATAN(XX(23)/YY(23))
       ALPHA=DELTA-ATAN(XN(206)/YN(206))
       XN(241)=XX(23)
       YN(241)=YY(23)
       XN(234)=-XN(241)
       YN(234)=YN(241)
       XN(240)=XN(241)-AZ*SIN(DELTA)
       YN(240)=YN(241)-AZ*COS(DELTA)
       XN(235)=-XN(240)
       YN(235)=YN(240)
       XN(239)=XN(241)-BZ*SIN(DELTA)
       YN(239)=YN(241)-BZ*COS(DELTA)
       XN(236)=-XN(239)
       YN(236)=YN(239)
       XN(238)=XN(241)-CZ*SIN(DELTA)
       YN(238)=YN(241)-CZ*COS(DELTA)
       XN(237)=-XN(238)
       YN(237)=YN(238)
C
C******  GENERATING NODES 242-319
C
       RIM=(YN(238)-YY(27))/COS(DELTA)
       DRIM=RIM/6.0
       DO 100 I=1,5
         IA=238-(I-1)*8
```

```
        XADA(I)=ATAN(XN(IA)/YN(IA))
        XADA(6)=ATAN(XN(205)/YN(205))
100   CONTINUE
C
      DO 110 I=1,6
        IA=238-(I-1)*8
        IX=254-(I-1)
        IF(I.EQ.6) IA=205
        XN(254)=XN(238)-DRIM*SIN(XADA(1))
        YN(254)=YN(238)-DRIM*COS(XADA(1))
        XRAD=XN(254)/SIN(XADA(1))
        IF(I.EQ.1) GO TO 111
        XN(IX)=XRAD*SIN(XADA(I))
        YN(IX)=XRAD*COS(XADA(I))
111     XN(IX-(14-2*I))=-XN(IX)
        YN(IX-(14-2*I))=YN(IX)
110   CONTINUE
C
      DO 119 J=1,6
        DO 120 I=1,6
        IA=255+(J-1)*13+(I-1)
          XN(IA)=XN(IA-13)+DRIM*SIN(XADA(I))
          YN(IA)=YN(IA-13)-DRIM*COS(XADA(I))
          XN(IA+(14-2*I))=-XN(IA)
          YN(IA+(14-2*I))=YN(IA)
120     CONTINUE
119   CONTINUE
      DO 125 I=1,6
        IA=248+((I-1)*13)
        XN(IA)=0.0
        YN(IA)=YN(IA-1)
125   CONTINUE
C
      DO 130 I=1,319
        WRITE(11,1000) I,XN(I),YN(I)
130   CONTINUE
1000  FORMAT(I10,7X,'0.0',F10.5,F10.5)
C
C******  THIS ENDS THE NODE GENERATION SECTION
C
C
C     ****************************************
C     *  THIS SECTION GENERATES THE ELEMENTS  *
C     *  AND ELEMENT NUMBERS.  TWO-DIMENSIONAL*
C     *  4-NODED ELEMENTS ARE USED.  FOR THIS *
C     *  MODEL THERE ARE 276 ELEMENTS.        *
C     ****************************************
C
C******  GENERATING ELEMENTS 1-183
C
      II=0
      DO 140 I=1,18
        IA=12+(I-1)*11
        IB=13+(I-1)*11
        IC=2+(I-1)*11
        ID=1+(I-1)*11
        DO 145 J=1,10
          II=II+1
          LA=IA+(J-1)
```

```
          LC=IC+(J-1)
          LD=ID+(J-1)
145     WRITE(11,112) II,LA,LB,LC,LD
140   CONTINUE
      WRITE(11,112)181,210,211,200,199
      WRITE(11,112)182,211,212,201,200
      WRITE(11,112)183,212,213,202,201
C
C******   GENERATING ELEMENTS 184-195
C
      II=183
      DO 150 I=1,3
        IA=218+(I-1)*8
        IB=219+(I-1)*8
        IC=211+(I-1)*8
        ID=210+(I-1)*8
        DO 155 J=1,3
          II=II+1
          LA=IA+(J-1)
          LB=IB+(J-1)
          LC=IC+(J-1)
          LD=ID+(J-1)
155     WRITE(11,112)II,LA,LB,LC,LD
150   CONTINUE
      WRITE(11,112)193,214,215,207,206
      WRITE(11,112)194,215,216,208,207
      WRITE(11,112)195,216,217,209,208
C
C******  GENERATING ELEMENTS 196-203
C
      II=195
      DO 160 I=1,3
        IA=222+(I-1)*8
        IB=223+(I-1)*8
        IC=215+(I-1)*8
        ID=214+(I-1)*8
        DO 165 J=1,3
          II=II+1
          LA=IA+(J-1)
          LB=IB+(J-1)
          LC=IC+(J-1)
          LD=ID+(J-1)
165     WRITE(11,112)II,LA,LB,LC,LD
160   CONTINUE
C
C******  GENERATING ELEMENTS 204-213
C
      II=204
      DO 170 I=1,3
        LA=242+(I-1)
        LB=243+(I-1)
        LC=229-(I-1)*8
        LD=237-(I-1)*8
        II=II+1
170   WRITE(11,112)II,LA,LB,LC,LD
      WRITE(11,112)208,245,246,202,213
      WRITE(11,112)209,246,247,203,202
      WRITE(11,112)210,247,248,204,203
```

```
      WRITE(11,112)211,248,249,205,204
      WRITE(11,112)212,249,250,206,205
      WRITE(11,112)213,250,251,214,206
C
C******  GENERATING ELEMENTS 214-276
C
      II=213
      DO 180 I=1,3
        LA=251+(I-1)
        LB=252+(I-1)
        LC=222+(I-1)*8
        LD=214+(I-1)*8
        II=II+1
180   WRITE(11,112)II,LA,LB,LC,LD
      II=216
      DO 190 I=1,5
        IA=255+(I-1)*13
        IB=256+(I-1)*13
        IC=243+(I-1)*13
        ID=242+(I-1)*13
        DO 195 J=1,12
          II=II+1
          LA=IA+(J-1)
          LB=IB+(J-1)
          LC=IC+(J-1)
          LD=ID+(J-1)
195     WRITE(11,112)II,LA,LB,LC,LD
190   CONTINUE
C
112   FORMAT(I5,4X,'8',4I5,23X,'21',4X,'1')
C
C******  THIS ENDS THE ELEMENT GENERATION SECTION
C
      STOP
      DEBUG SUBCHK
      END
```

```
C*************************************************
C                                                 *
C  VARIABLE SPEED/LOAD GENERATION PROGRAM         *
C                                                 *
C  THIS PROGRAM GENERATES THE SAP6 TIME           *
C  FUNCTIONS DESCRIBING THE LOAD MOVING           *
C  OVER THE INVOLUTE OF A GEAR TOOTH. THE         *
C  SPEED OF THE MOVING LOAD ON THE INVOLUTE       *
C  OF A TOOTH VARIES AS                           *
C                                                 *
C          V(T)=RB*OMEGA**2*T                     *
C                                                 *
C  WHERE RB IS THE BASE RADIUS OF THE GEAR        *
C  OMEGA IS THE ANGULAR VELOCITY OF THE GEAR      *
C  AND T IS THE ELLAPSED TIME.  THE LOAD          *
C  FUNCTIONS WERE TAKEN FROM WALLACE, AND ARE     *
C                                                 *
C  F(T)=F0(1-COS(T/ALPHAT))/2     0<T<ALPHAT      *
C                                                 *
C  F(T)=F0              ALPHAT<T<(1-ALPHA)TF       *
C                                                 *
C  F(T)=F0(1-COS(T-ALPHATF)/ALPHATF))/2           *
C                           (1-ALPHA)TF<T<TF      *
C                                                 *
C  WHERE TF IS THE TOTAL TIME, AND ALPHA IS       *
C  A FACTOR DEPENDENT ON THE CONTACT RATIO.       *
C                                                 *
C  THE USER MUST ENTER THE FOLLOWING PARAMETERS   *
C                                                 *
C        PRESSURE ANGLE=PANG                      *
C        PITCH RADIUS  =RP                        *
C        ADDENDEM      =AD                        *
C        CIRCULAR PITCH=CIRP                      *
C        BACKLASH      =BACKL                     *
C        MAX VELOCITY  =VMAX                      *
C                                                 *
C*************************************************
      DIMENSION XX(40),YY(40),FORCE(11,500),TIME(500),T(500)
      DIMENSION XINC(11),DXINC(11),FX(11,500),FY(11,500),XN(15),YN(15)
      PI=3.141592654
      READ(5,*) PANG
      PANG=PANG*PI/180.
      READ(5,*) RP
      READ(5,*) AD
      READ(5,*) CIRP
      READ(5,*) BACKL
      READ(5,*) VMAX
      RB=RP*COS(PANG)
      THP=((RP*RP-RB*RB)/(RB*RB))**0.5
      CIRTH=CIRP/2.-BACKL
      AL=THP-ATAN(THP)+CIRTH/(RP*2.)
      RO=RP+AD
C
C*************************************************
C  THE INVOLUTE COORDINATES AND INVOLUTE NORMALS  *
C  ARE CALCULATED IN THIS SECTION.                *
C*************************************************
C
      DO 5 I=1,11
```

```
        IA=1+(I-1)
        HH=(RO-RB)/10.
        H=RO-HH*(I-1)
        ANG=((H*H-RB*RB)/(RB*RB))**0.5
        Y=RB*(COS(ANG)+ANG*SIN(ANG)-1.)
        X=-RB*(SIN(ANG)-ANG*COS(ANG))
        XP=RB*SIN(AL)+X*COS(AL)+Y*SIN(AL)
        YP=RB*COS(AL)-X*SIN(AL)+Y*COS(AL)
        XX(IA)=XP
        YY(IA)=YP
        XN(I)=-SIN(AL)*SIN(ANG)-COS(AL)*COS(ANG)
        YN(I)=SIN(AL)*COS(ANG)-COS(AL)*SIN(ANG)
5     CONTINUE
C
C*************************************************
C  THE DISTANCE ALONG THE INVOLUTE IS DETERMINED  *
C  FROM WHICH THE TOTAL TIME AND ANGULAR VELOCITY *
C  ARE FOUND.                                     *
C*************************************************
C
      S=0.0
      DO 6 I=1,10
        XL=XX(I+1)-XX(I)
        YL=YY(I)-YY(I+1)
        XINC(I)=(XL**2+YL**2)**0.5
        S=S+XINC(I)
        WRITE(6,*) 'XINC(I)=  ',XINC(I),'  S=  ',S
6     CONTINUE
      TF=2.*S/VMAX
      XOMEGA=(VMAX/(TF*RB))**.5
      WRITE(6,*) 'TF=  ',TF,'  OMEGA=  ',XOMEGA
      TALPHA=0.28*TF
      WRITE(6,*) 'TALPHA=  ',TALPHA,'  (1-ALPHA)*TF=  ',(1.-.28)*TF
C
C*************************************************
C  THE DISTANCE BETWEEN EACH NODE IS DIVIDED UP   *
C  INTO 20 EQUAL INCREMENTS AND THE TIME AND      *
C  AND FORCE VALUES ARE DETERMINED FOR EACH.      *
C*************************************************
C
      DIST=0.0
      DO 10 I=1,10
        DXINC(I)=XINC(I)/20.
        DO 15 J=1,20
          JJ=J+20*(I-1)
          DIST=DIST+DXINC(I)
          TIME(JJ)=(2.*DIST/(RB*XOMEGA**2))**0.5
          T(JJ)=TIME(JJ)
          IF(TIME(JJ).GT.TALPHA) GO TO 11
          FORCE(I,J)=(FO/2.)*(1.-COS(PI*TIME(JJ)/TALPHA))
      GO TO 15
11        IF(TIME(JJ).GT.(TF-TALPHA)) GO TO 12
          FORCE(I,J)=FO
      GO TO 15
12        FORCE(I,J)=(FO/2.)*(1.-COS(PI*(TF-TIME(JJ))/TALPHA))
15      CONTINUE
10    CONTINUE
C
      DO 20 I=1,1
```

```
        DO 30 J=1,20
          JJ=J+20*(I-1)
       FX(I,J+20)=FORCE(I,J)*((XINC(I)-(RB*(XOMEGA**2)/2.)
      $*TIME(JJ)**2)/XINC(I))*XN(I)
       FY(I,J+20)=FORCE(I,J)*((XINC(I)-(RB*(XOMEGA**2)/2.)
      $*TIME(JJ)**2)/XINC(I))*YN(I)
          FACT=(RB*(XOMEGA**2)/2.)*(TIME(JJ+180)**2-TIME(180)**2)
          FX(11,J)=FORCE(10,J)*(FACT/XINC(10))*XN(11)
          FY(11,J)=FORCE(10,J)*(FACT/XINC(10))*YN(11)
30      CONTINUE
20    CONTINUE
      DO 25 I=2,10
        DO 35 J=1,20
          JJ=J+20*(I-2)
          XTIME1=TIME((I-1)*20)
          IF(I.NE.2) GO TO 36
          XTIME=0.0
          GO TO 37
36        XTIME=TIME((I-2)*20)
37        FACT=((RB*(XOMEGA**2))/2.)*(TIME(JJ)**2-XTIME**2)
          FACT1=((RB*(XOMEGA**2))/2.)*(TIME(JJ+20)**2-XTIME1**2)
          FX(I,J)=FORCE(I-1,J)*(FACT/XINC(I-1))*XN(I)
          FY(I,J)=FORCE(I-1,J)*(FACT/XINC(I-1))*YN(I)
       FX(I,J+20)=FORCE(I,J)*((XINC(I)-FACT1)/XINC(I))*XN(I)
       FY(I,J+20)=FORCE(I,J)*((XINC(I)-FACT1)/XINC(I))*YN(I)
35      CONTINUE
25    CONTINUE
C
C*************************************************
C  THE REMAINDER OF THE PROGRAM WRITES THE TIME  *
C  FUNCTION VALUES (TIME,FORCE) TO A FILE FOR    *
C  USE IN A FINITE ELEMENT CODE. THIS PROGRAM    *
C  IS FORMATTED FOR SAP6.                        *
C*************************************************
C
      NFN=22
      WRITE(11,99) NFN
99    FORMAT(3X,I2,4X,'0',4X,'0',3X,'NT',4X,'1',6X,'DPER',7X,'0.0')
      IFN=0
      DO 60 I=1,11
        NP=11+11*(I-1)
        IC=2
        DO 60 J=1,2
          IFN=IFN+1
          WRITE(11,98) NP,IC,IFN
          IC=3
98        FORMAT(I5,4X,I1,I5,4X,'1',7X,'1.0',24X,'0')
60    CONTINUE
      WRITE(11,97)
97    FORMAT(/'    ')
C
C*****  TIME FUNTION DATA     ****
C
      TF=1.0
      T0=0.0
      F0=0.0
C********  TIME FUNCTION FOR NODE 11 *******
C
      NLP=24
```

```
      WRITE(11,101) NLP
101   FORMAT(3X,I2,11X,'TIME FUNCTION',50X,'1')
100   FORMAT(3(E12.6,F12.0))
      WRITE(11,100) T0,F0,T(1),FX(1,21),T(2),FX(1,22)
      DO 200 I=3,18,3
200   WRITE(11,100) T(I),FX(1,I+20),T(I+1),FX(1,I+21),T(I+2),FX(1,I+22)
      WRITE(11,100) TF,F0,TF,F0,TF,F0
      WRITE(11,101) NLP
      WRITE(11,100) T0,F0,T(1),FY(1,21),T(2),FY(1,22)
      DO 201 I=3,18,3
201   WRITE(11,100) T(I),FY(1,I+20),T(I+1),FY(1,I+21),T(I+2),FY(1,I+22)
      WRITE(11,100) TF,F0,TF,F0,TF,F0
C******  TIME FUNCTIONS FOR NODES 22 THRU 110  *****
C
      DO 202 I=2,10
        NLP=45
        WRITE(11,101) NLP
        K=20*(I-2)
        T(0)=0.0
        WRITE(11,100) T0,F0,T(K),F0,T(1+K),FX(I,1)
        DO 203 J=2,38,3
203   WRITE(11,100) T(J+K),FX(I,J),T(J+1+K),FX(I,J+1),T(J+2+K),FX(I,J+2)
      WRITE(11,100) TF,F0,TF,F0,TF,F0
        WRITE(11,101) NLP
        WRITE(11,100) T0,F0,T(K),F0,T(1+K),FY(I,1)
        DO 205 J=2,38,3
205   WRITE(11,100) T(J+K),FY(I,J),T(J+1+K),FY(I,J+1),T(J+2+K),FY(I,J+2)
      WRITE(11,100) TF,F0,TF,F0,TF,F0
202   CONTINUE
C
C**** TIME FUNCTION FOR NODE 121  *******
C
      NLP=24
      WRITE(11,101) NLP
      WRITE(11,100) T0,F0,T(180),F0,T(181),FX(11,1)
      DO 206 I=2,17,3
        K=I+180
206     WRITE(11,100) T(K),FX(11,I),T(K+1),FX(11,I+1),T(K+2),FX(11,I+2)
      WRITE(11,100) T(200),FX(11,20),TF,F0,TF,F0
      WRITE(11,101) NLP
      WRITE(11,100) T0,F0,T(180),F0,T(181),FY(11,1)
      DO 207 I=2,17,3
        K=I+180
207     WRITE(11,100) T(K),FY(11,I),T(K+1),FY(11,I+1),T(K+2),FY(11,I+2)
      WRITE(11,100) T(200),FY(11,20),TF,F0,TF,F0
C
C****  ECHO CHECK  ******
C
      DO 40 I=1,11
        IF(I.NE.1) GO TO 52
        DO 42 J=1,20
          JJ=J+20*(I-1)
          WRITE(12,51) T(JJ),FX(I,J+20)
42      CONTINUE
      GO TO 40
52      IF(I.EQ.11) GO TO 53
        DO 45 J=1,20
          JJ=J+20*(I-2)
          WRITE(12,51) T(JJ),FX(I,J)
```

```
45        CONTINUE
          DO 46 J=1,20
            JJ=J+20*(I-1)
            WRITE(12,51) T(JJ),FX(I,J+20)
46        CONTINUE
          GO TO 40
53        DO 50 J=1,20
            JJ=J+20*(I-2)
            WRITE(12,51) T(JJ),FX(I,J)
50        CONTINUE
40      CONTINUE
51      FORMAT(F12.8,12X,F8.0)
        STOP
        END
```

APPENDIX 2

Contact Point Velocity

Of Meshing Spur Gear Teeth

For a meshing spur gear pair, the speed of the contact point varies with time as it moves from the tip of the tooth to the base circle.

From equations (2-3) and (2-4) and Figure A2-1 the coordinates of a point Bi on the involute are given by;

$$XB_i = -RB(\sin\theta_i - \theta_i\cos\theta_i) \qquad \text{(A2-1)}$$

$$YB_i = RB(\cos\theta_i + \theta_i\sin\theta_i - 1) \qquad \text{(A2-2)}$$

Differentiating (A2-1) and (A2-2) with respect to θ_i;

$$\frac{dXB_i}{d\theta_i} = - RB\,\theta_i\sin\theta_i \qquad \text{(A2-3)}$$

$$\frac{dYB_i}{d\theta_i} = - RB\,\theta_i\cos\theta_i \qquad \text{(A2-4)}$$

and combining to give the resultant;

$$\left(\frac{d\bar{r}}{d\theta_i}\right)^2 = \left(\frac{dXB_i}{d\theta_i}\right)^2 + \left(\frac{dYB_i}{d\theta_i}\right)^2$$

$$= RB^2\,\theta_i^2\ (\sin^2\theta_i + \cos^2\theta_i)$$

$$\left|\frac{d\bar{r}}{d\theta_i}\right| = RB\theta_i \qquad \text{(A2-5)}$$

Multiplying through by $d\,\theta_i = \dot{\theta}_i$, realizing that θ_i and $\bar{r}$ vary with time, we have

$$\frac{d\bar{r}}{dt} = V = RB\theta_i\dot{\theta}_i$$

And if we define $\theta_i = \omega t$;

$$V(t) = RB\omega^2 t \qquad \text{(A2-6)}$$

where;

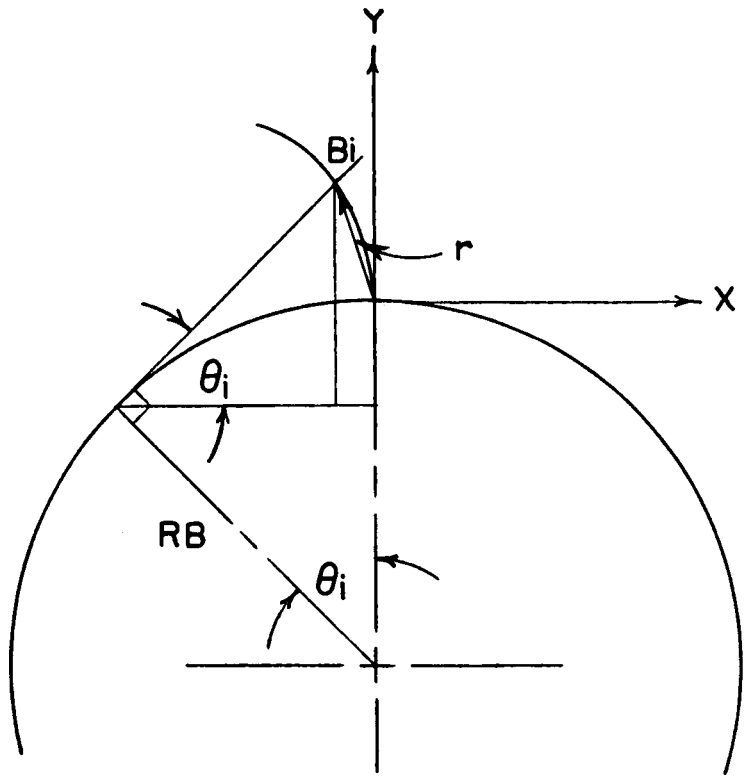

Figure A2-1: Contact point goemetry

$V(t)$ = the speed of the contact point B_i at time t

ω = angular velocity of the gear (rad/sec)

At $t = 0.0$, corresponding to the load at the tip of the tooth, the speed is zero, and at $t = TF$, time corresponding to the load positioned at the base circle, the speed is maximum.

The position of the load as a function of time is found by integrating equation (A2-6) with respect to time. By defining the speed as the first derivative of the position;

$$V(t) = \frac{dS(t)}{dt} = RB\omega^2 t$$

$$dS(t) = RB\omega^2 \int t\, dt$$

$$S(t) = \tfrac{1}{2}RB\omega^2 t^2 + C \qquad \text{(A2-7)}$$

Evaluating the constant of integration for $t = T_i$, the time at the tip of the tooth;

$$S(t_i) = 0.0 = \tfrac{1}{2}RB\omega^2 T_i^2 + C$$

then;

$$C = -\tfrac{1}{2}RB\omega^2 T_i^2 \qquad \text{(A2-8)}$$

The displacement then becomes;

$$S(t) = \tfrac{1}{2}RB\omega^2 t^2 - \tfrac{1}{2}RB\omega^2 T_i^2 \qquad \text{(A2-9)}$$

If we assume that the time at the tip position is zero the constant term vanishes and we are left with only the first term

on the right hand side of equation A2-9 defining the position along the involute.

APPENDIX 3

Deformed Shapes of Gear Tooth

1. Static Loading
2. Modal Analysis
3. Dynamic Response

Static Loading

Timoshenko Beam Constraints

Rim Included

STATIC DEFLECTION ANALYSIS: GEAR #1 (BEAM CONSTR)
UNDEFORMED SHAPE

SEPTEMBER 09, 1983 01:37:07
IAXIS=3 ALPHA= 0.00 BETA= 0.00

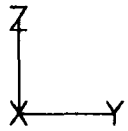

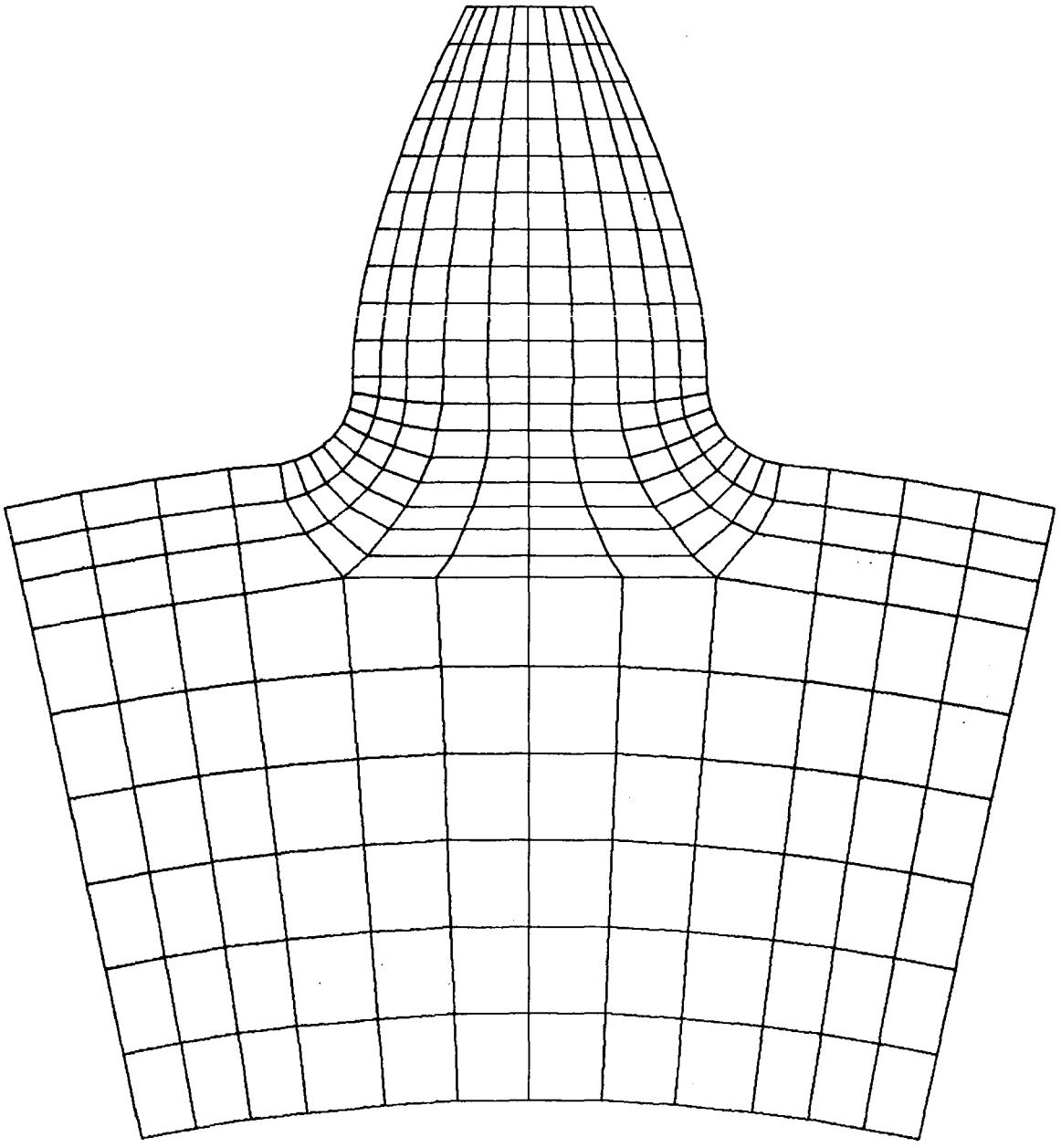

Figure A3-1

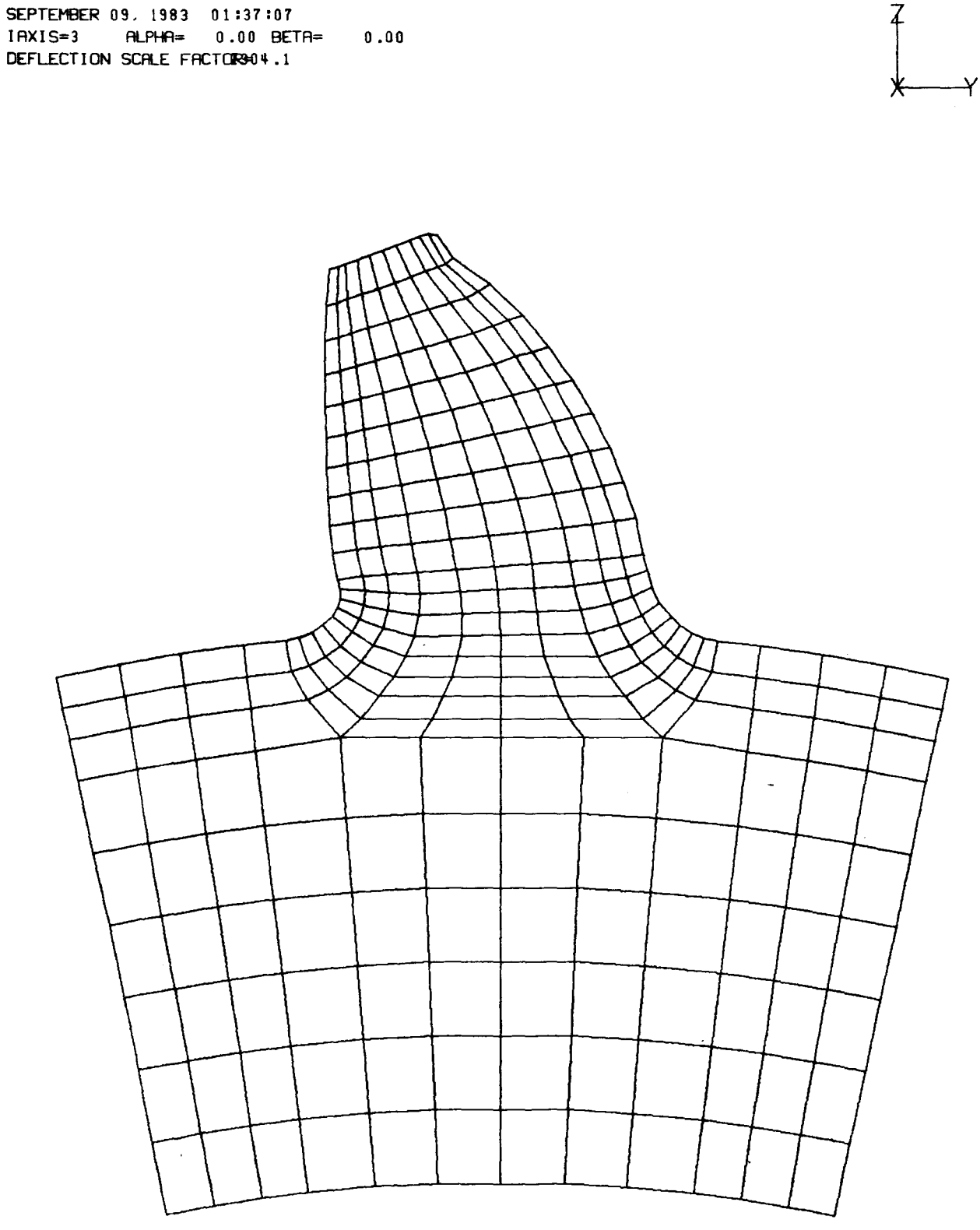
STATIC DEFLECTION ANALYSIS: GEAR #1 (BEAM CONSTR)
STATIC LOAD CASE 1 T = 0.1
SEPTEMBER 09, 1983 01:37:07
IAXIS=3 ALPHA= 0.00 BETA= 0.00
DEFLECTION SCALE FACTOR=4.1
Z
Y

Figure A3-2

STATIC DEFLECTION ANALYSIS: GEAR #1 (BEAM CONSTR)
STATIC LOAD CASE 2 T = 0.3

SEPTEMBER 09, 1983 01:37:07
IAXIS=3 ALPHA= 0.00 BETA= 0.00
DEFLECTION SCALE FACTOR= 88.6

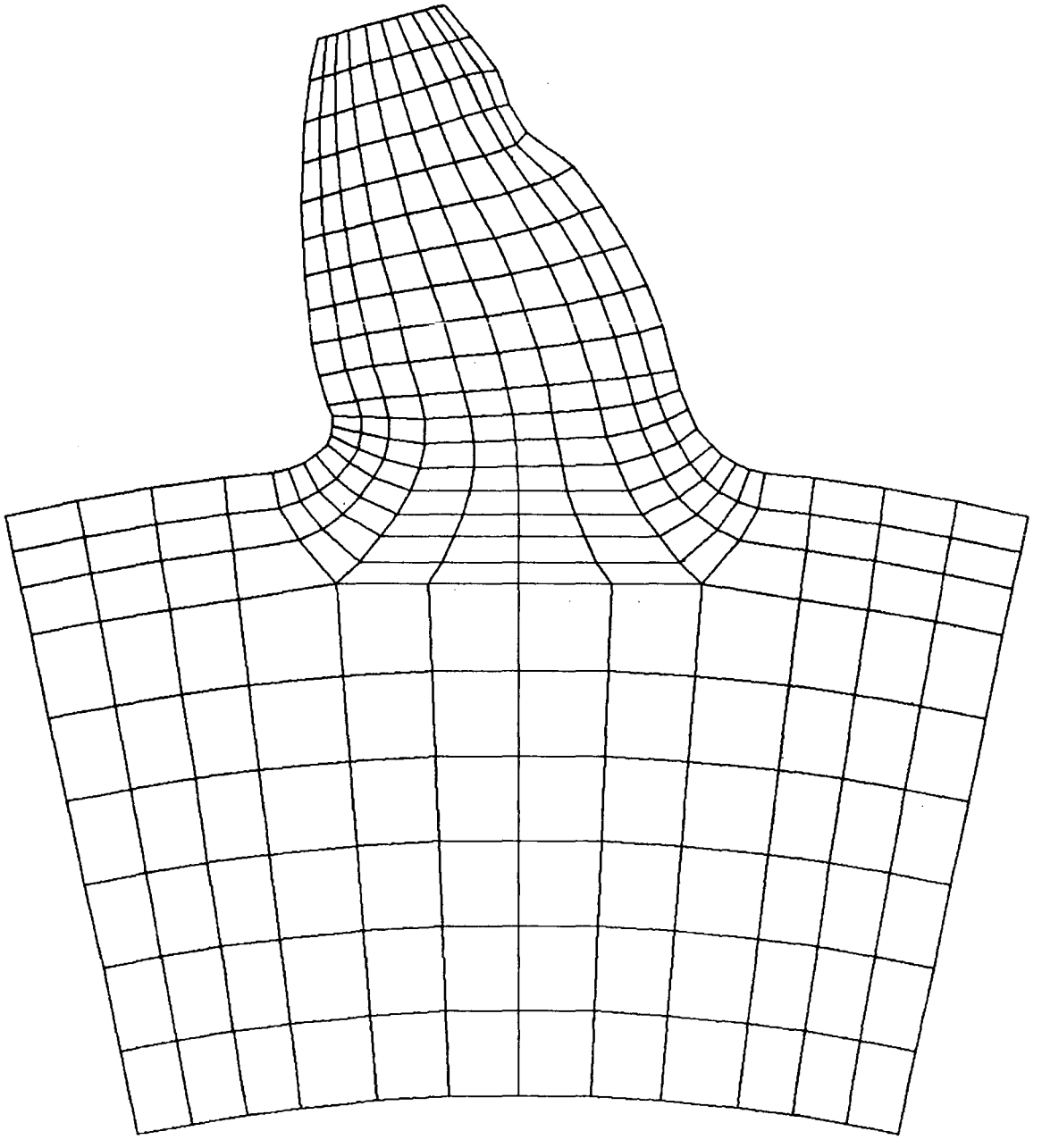

Figure A3-3

STATIC DEFLECTION ANALYSIS: GEAR #1 (BEAM CONSTR)
STATIC LOAD CASE 3 T = 0.5

SEPTEMBER 09, 1983 01:37:07
IAXIS=3 ALPHA= 0.00 BETA= 0.00
DEFLECTION SCALE FACTOR= 57.8

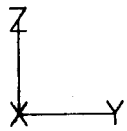

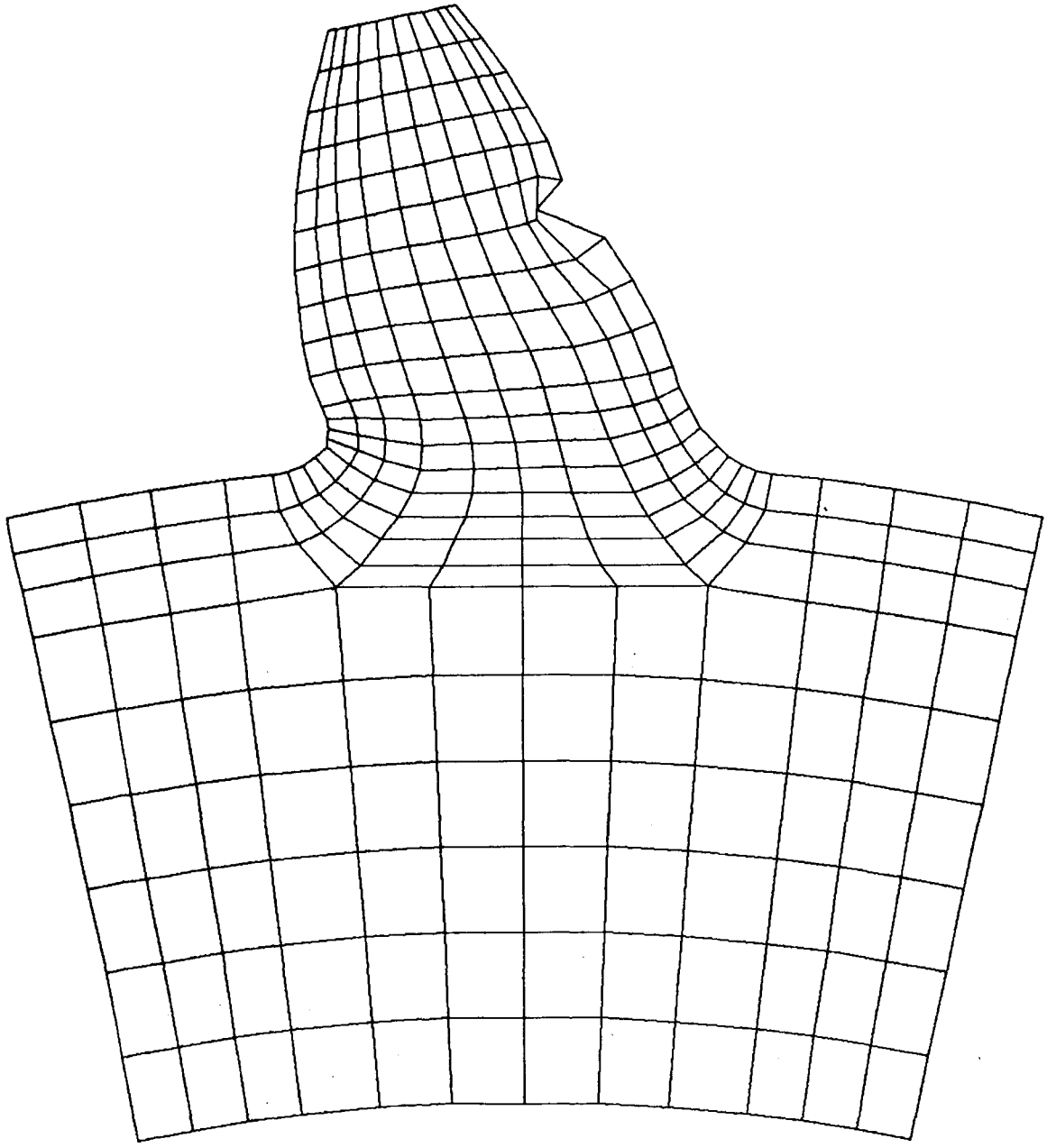

Figure A3-4

STATIC DEFLECTION ANALYSIS: GEAR #1 (BEAM CONSTR)
STATIC LOAD CASE 4 T = 0.8

SEPTEMBER 09, 1983 01:37:07
IAXIS=3 ALPHA= 0.00 BETA= 0.00
DEFLECTION SCALE FACTOR=

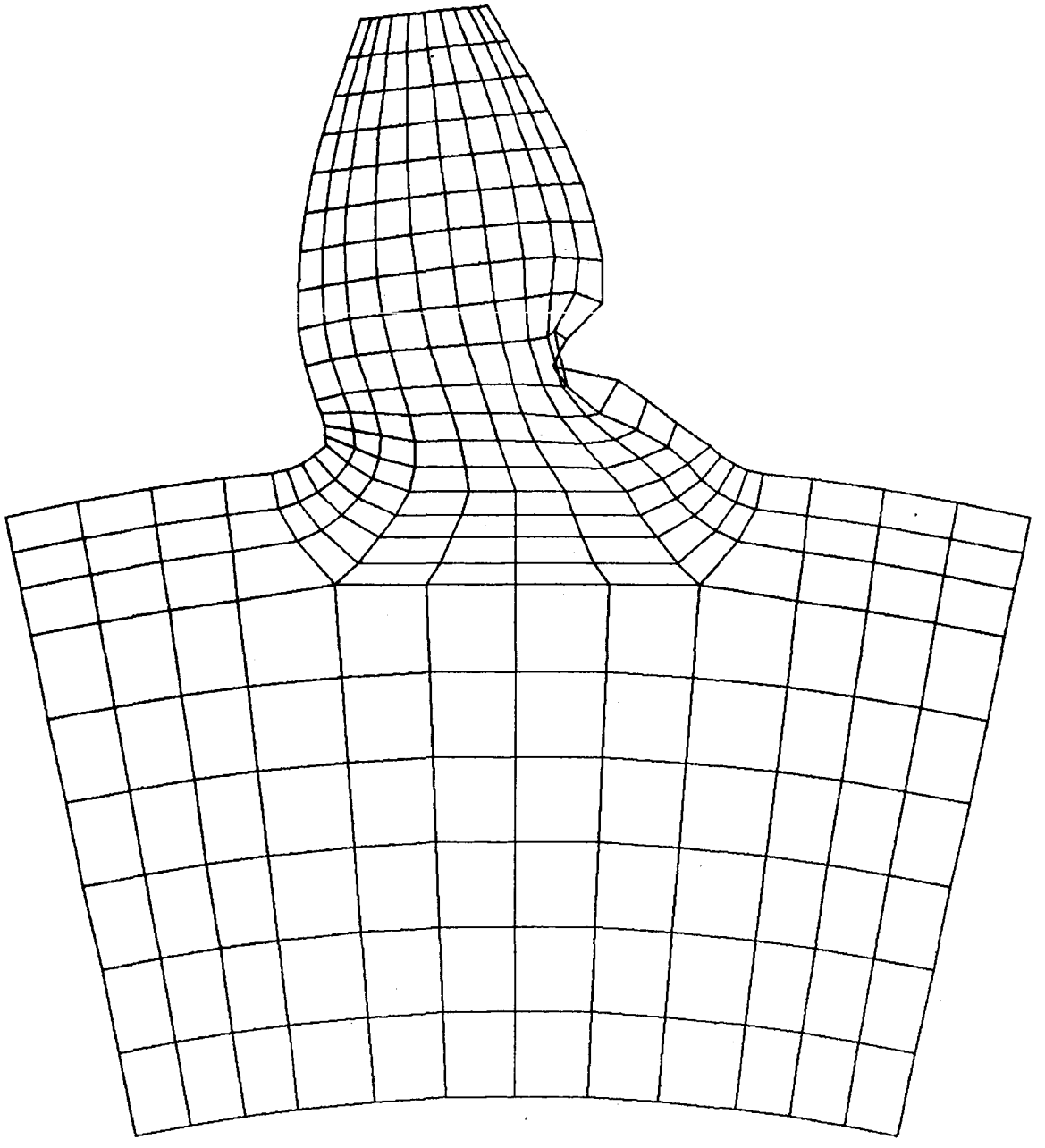

Figure A-5

STATIC DEFLECTION ANALYSIS: GEAR #1 (RIM INCLUDED)
STATIC LOAD CASE 1 T = 0.1

SEPTEMBER 10, 1983 00:10:05
IAXIS=3 ALPHA= 0.00 BETA= 0.00
DEFLECTION SCALE FACTOR= 23.8

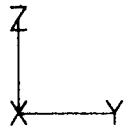

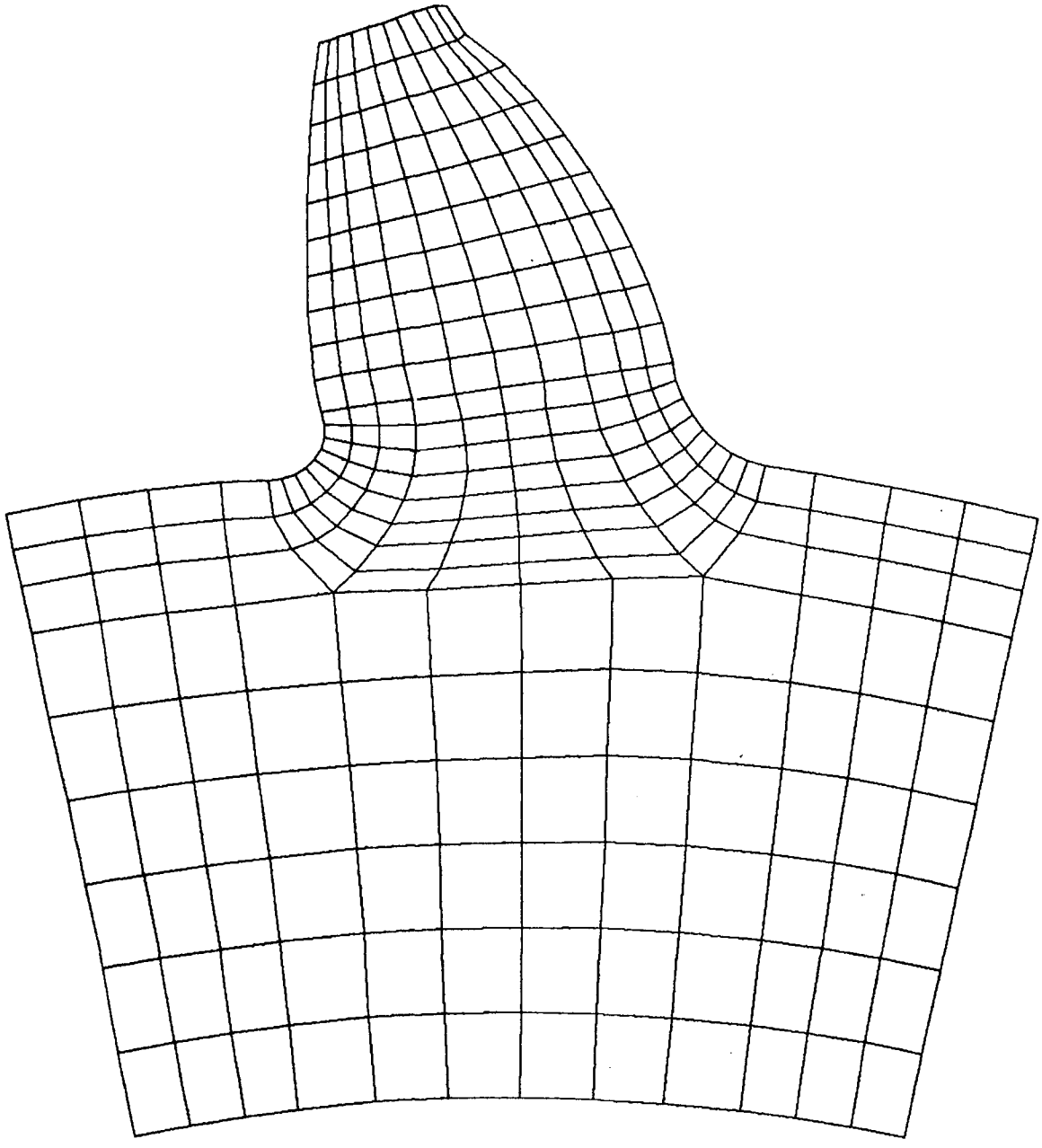

Figure A3-6

STATIC DEFLECTION ANALYSIS: GEAR #1 (RIM INCLUDED)
STATIC LOAD CASE 2 T = 0.3

SEPTEMBER 10, 1983 00:10:05
IAXIS=3 ALPHA= 0.00 BETA= 0.00
DEFLECTION SCALE FACTOR=81.6

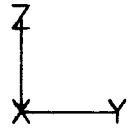

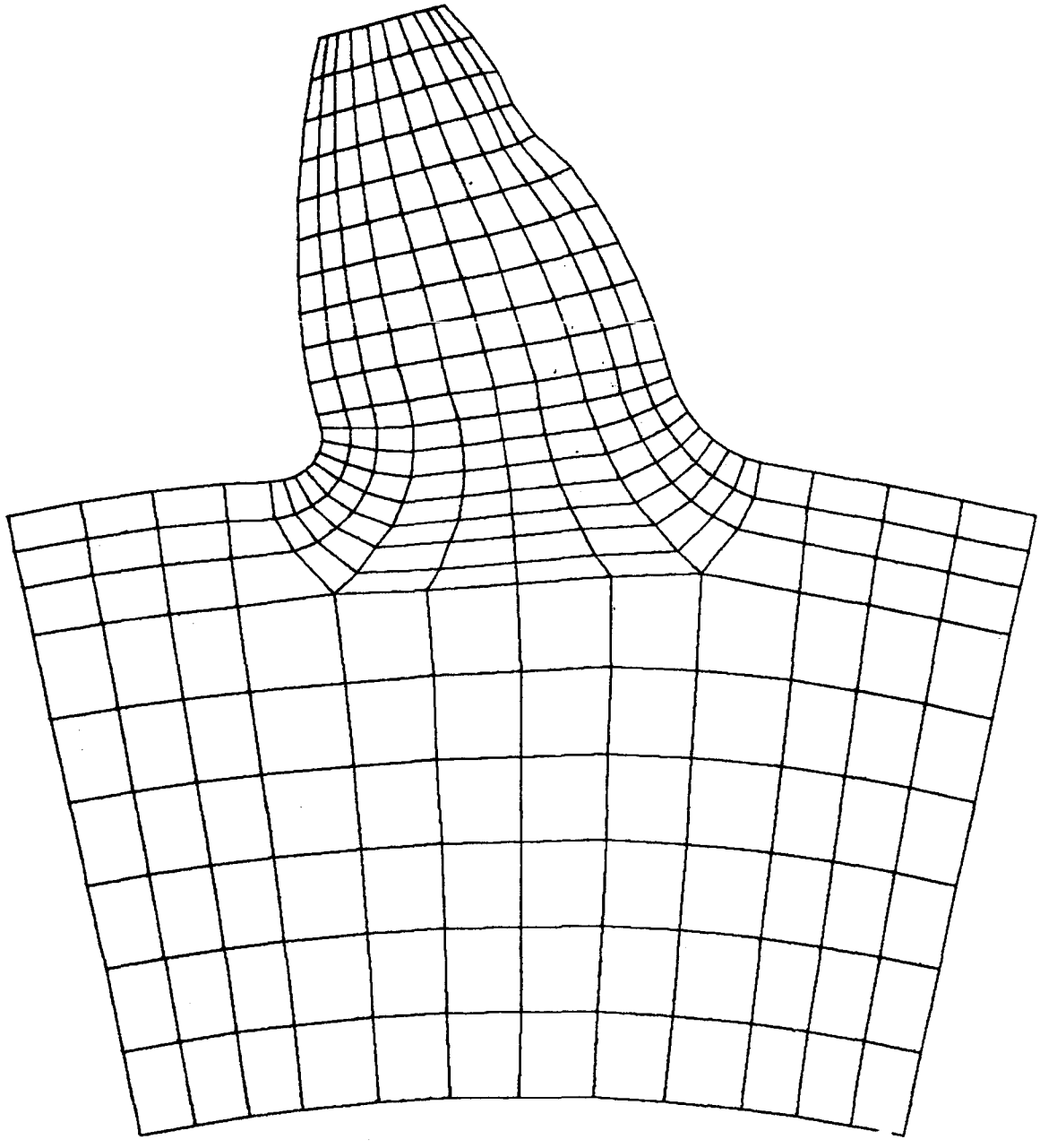

Figure A3-7

STATIC DEFLECTION ANALYSIS: GEAR #1 (RIM INCLUDED)
STATIC LOAD CASE 3 T = 0.5

SEPTEMBER 10, 1983 00:10:05
IAXIS=3 ALPHA= 0.00 BETA= 0.00
DEFLECTION SCALE FACTOR= 7.6

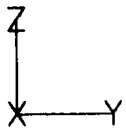

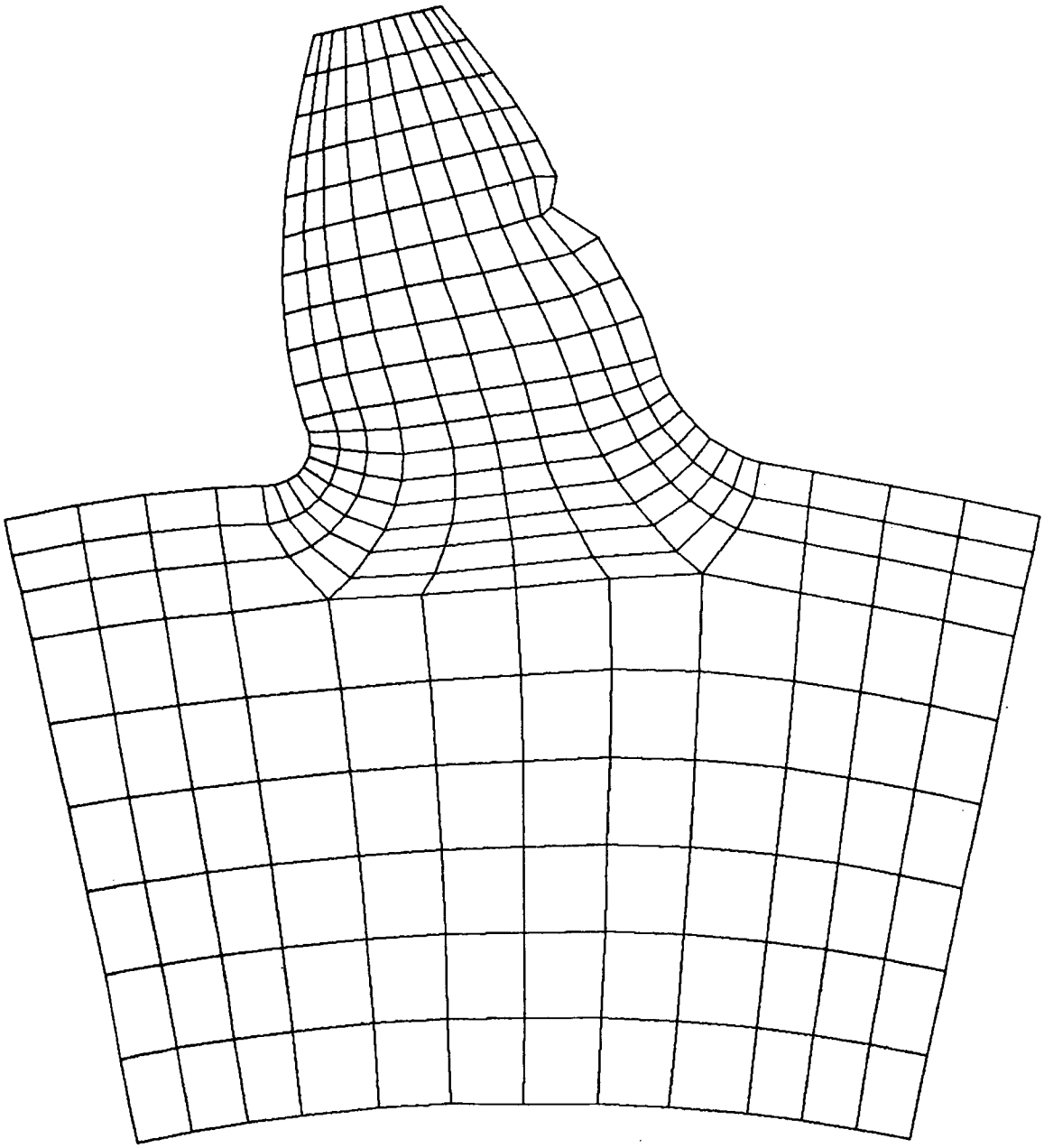

Figure A3-8

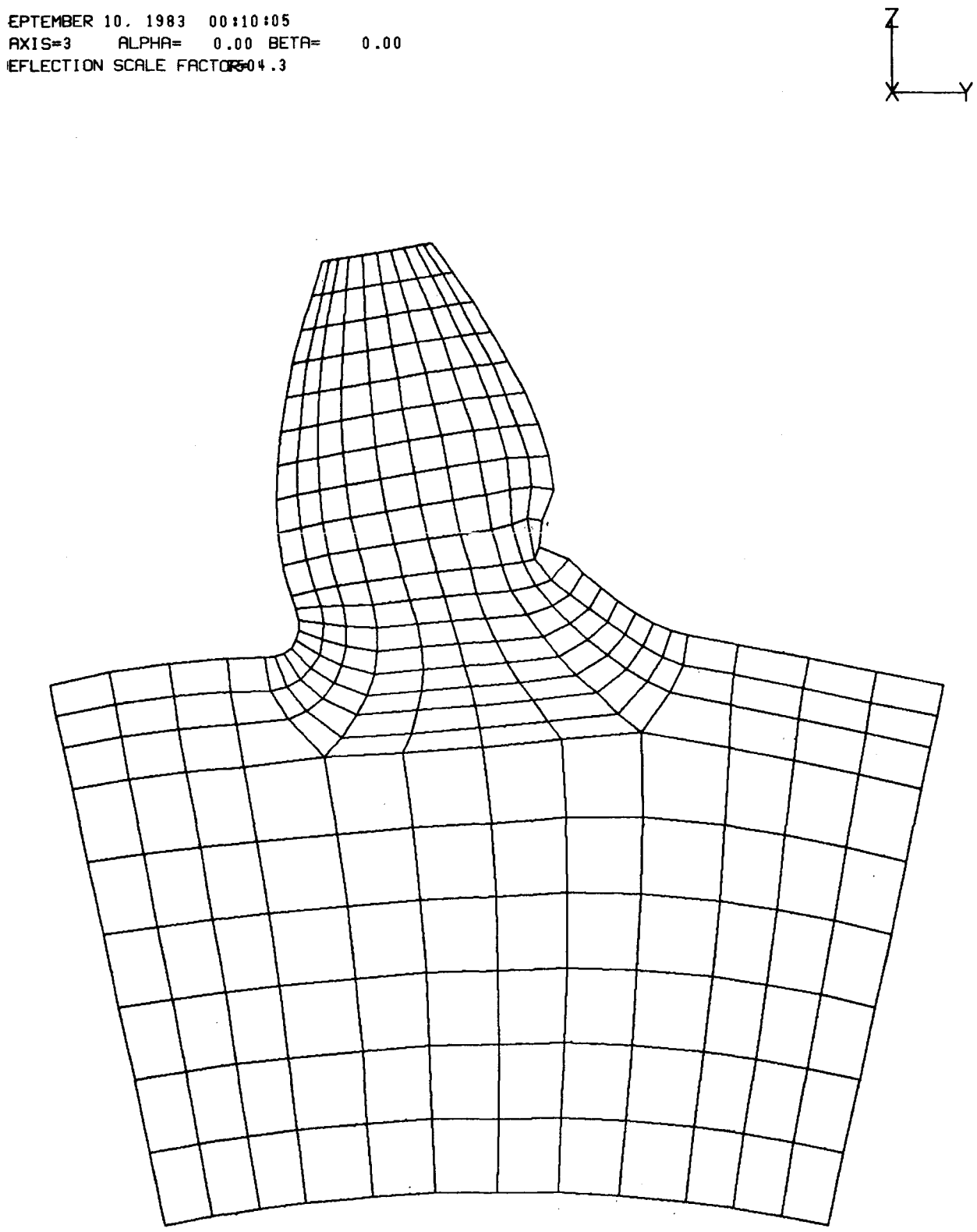
STATIC DEFLECTION ANALYSIS: GEAR #1 (RIM INCLUDED)
STATIC LOAD CASE 4 T = 0.8
EPTEMBER 10, 1983 00:10:05
AXIS=3 ALPHA= 0.00 BETA= 0.00
EFLECTION SCALE FACTOR=4.3
Z
Y
X

Figure A3-9

Modal Analysis

Timoshenko Beam Constraints

Rim Constraints

MODAL ANALYSIS, PLANE STRAIN ELEMENT: GEAR #1
UNDEFORMED SHAPE

UNE 16, 1983 00:10:15
IAXIS=3 ALPHA= 0.00 BETA= 0.00

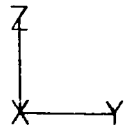

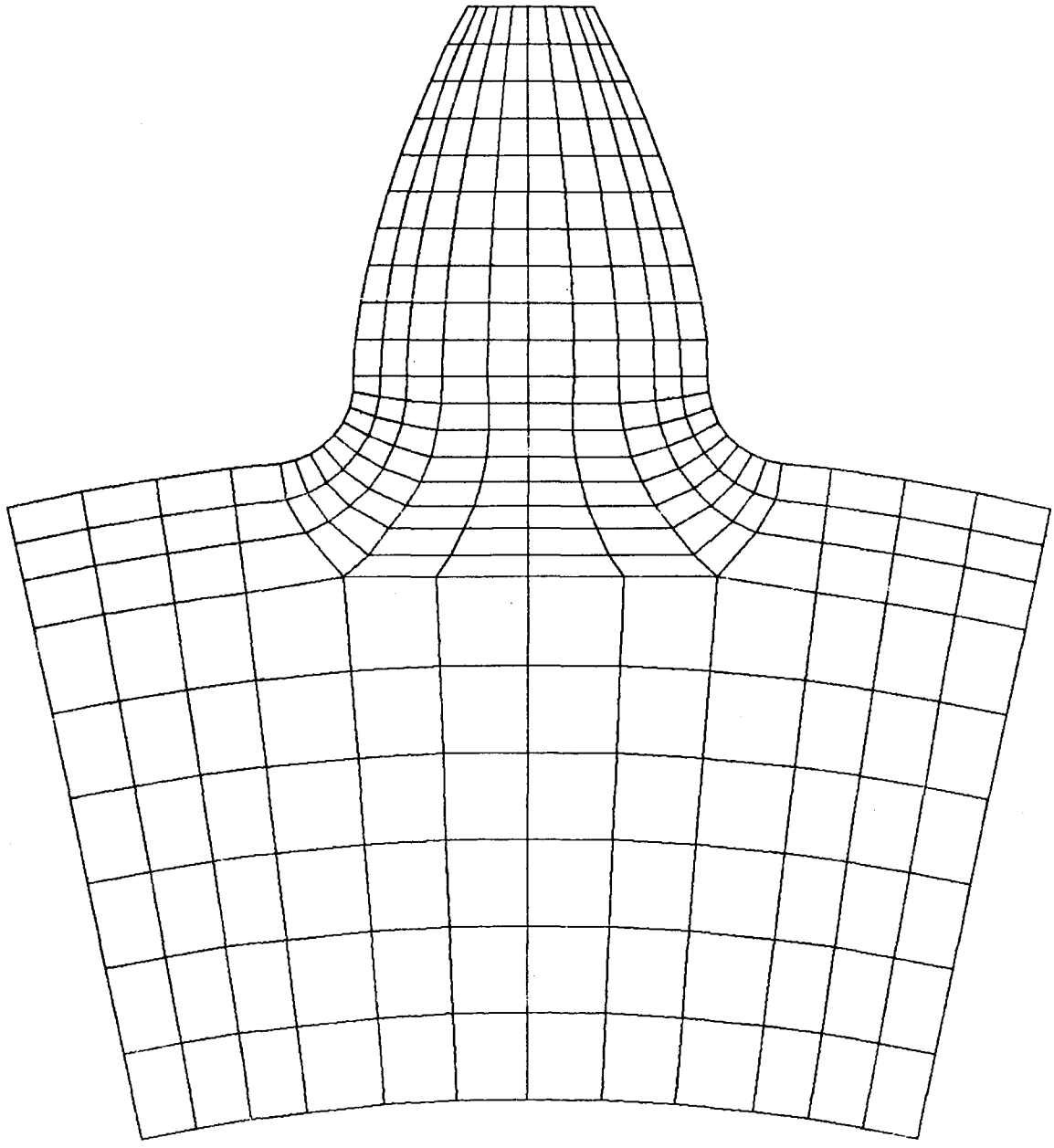

Figure A3-10

MODAL ANALYSIS, PLANE STRAIN ELEMENT: GEAR #1
MODE 1 Freq.= .9101 E5 (CPS)

UNE 10, 1983 19:32:39'
IAXIS=3 ALPHA= 0.00 BETA= 0.00
DEFLECTION SCALE FACTOR= 0.242780E

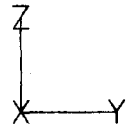

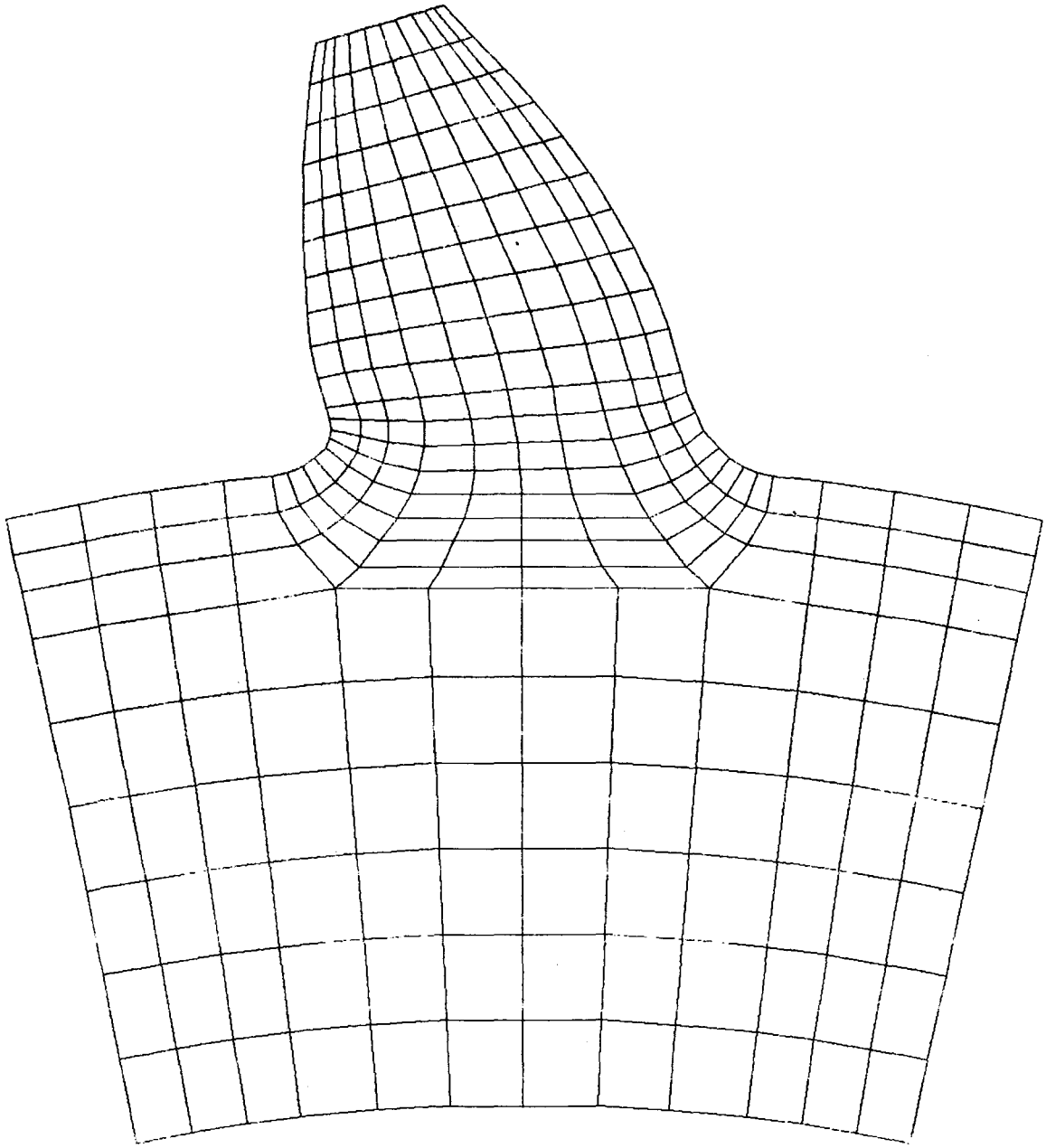

Figure A3-11

MODAL ANALYSIS, PLANE STRAIN ELEMENT: GEAR #1
MODE 2 Freq.= .2159 E6 (CPS)

UNE 10, 1983 19:32:39'
!AXIS=3 ALPHA= 0.00 BETA= 0.00
DEFLECTION SCALE FACTOR= 0.30990E

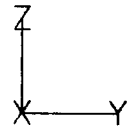

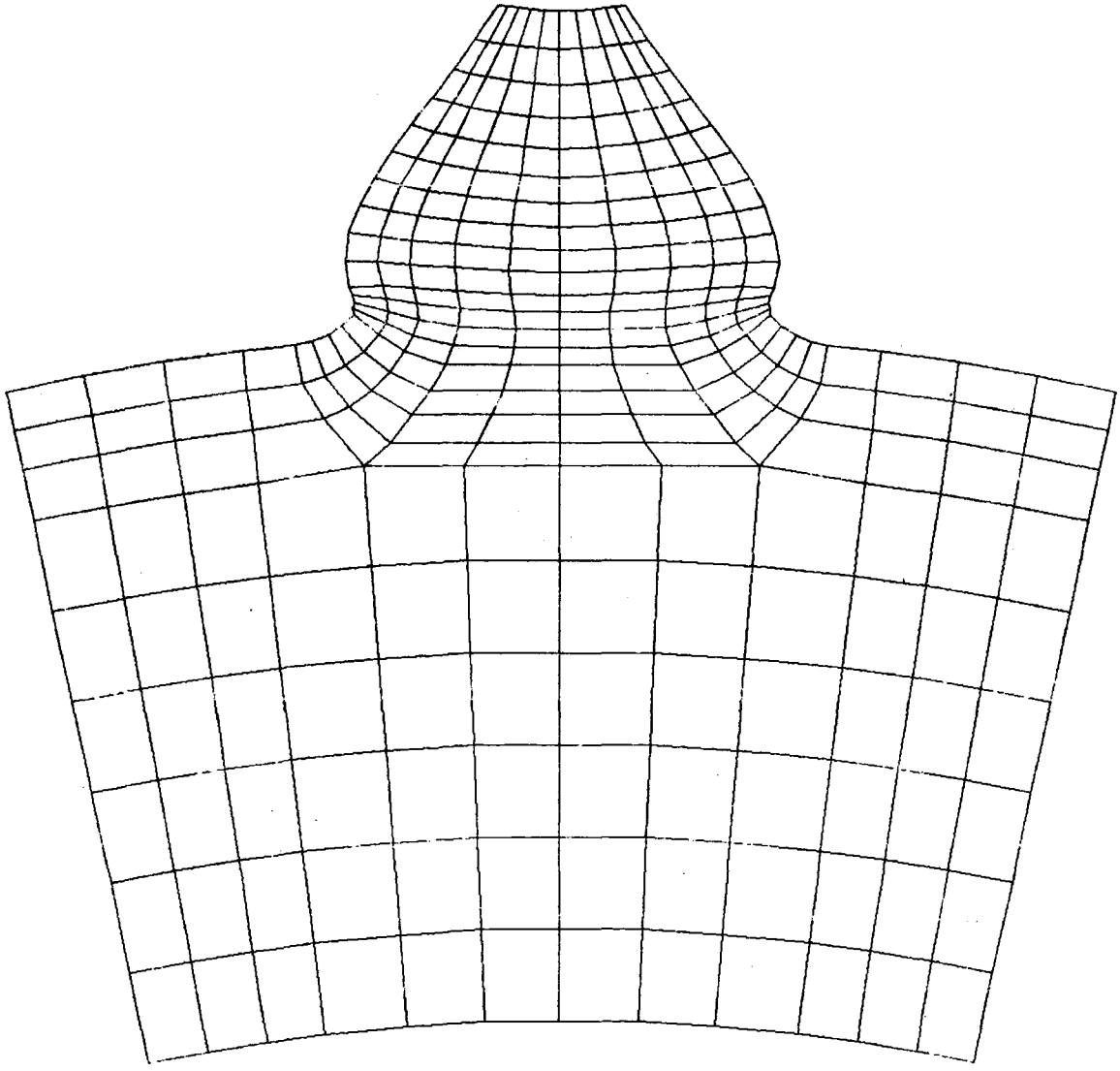

Figure A3-12

MODAL ANALYSIS, PLANE STRAIN ELEMENT: GEAR #1
MODE 3 **Freq.= .2289 E6 (CPS)**

UNE 10, 1983 19:32:39
IAXIS=3 ALPHA= 0.00 BETA= 0.00
DEFLECTION SCALE FACTOR= 0.247566

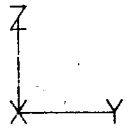

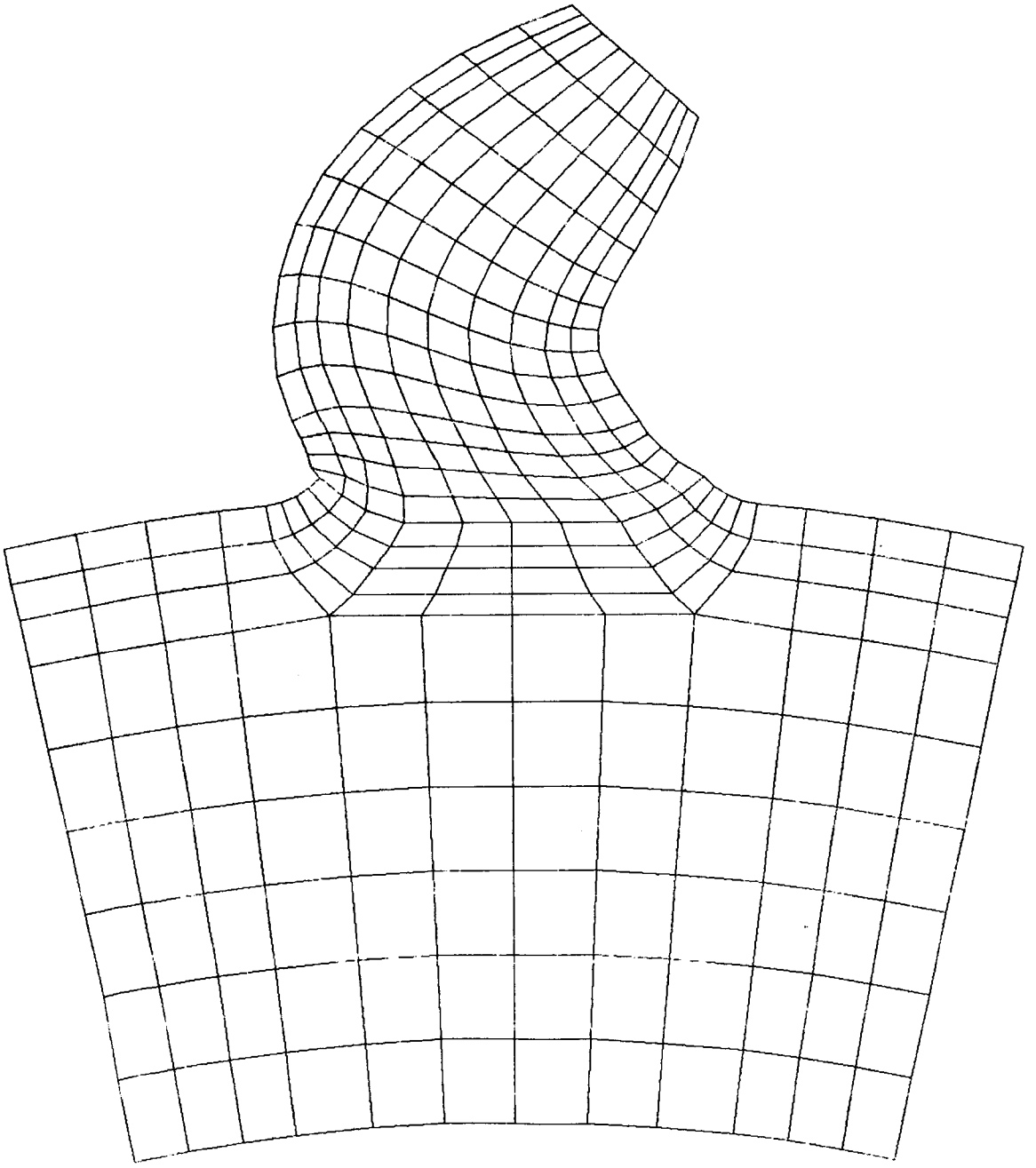

Figure A3-13

MODAL ANALYSIS. PLANE STRAIN ELEMENT: GEAR #1
MODE 4 **Freq.= .4218 E6 (CPS)**

UNE 10. 1983 19:32:39'
IAXIS=3 ALPHA= 0.00 BETA= 0.00
DEFLECTION SCALE FACTOR= 0.21444E

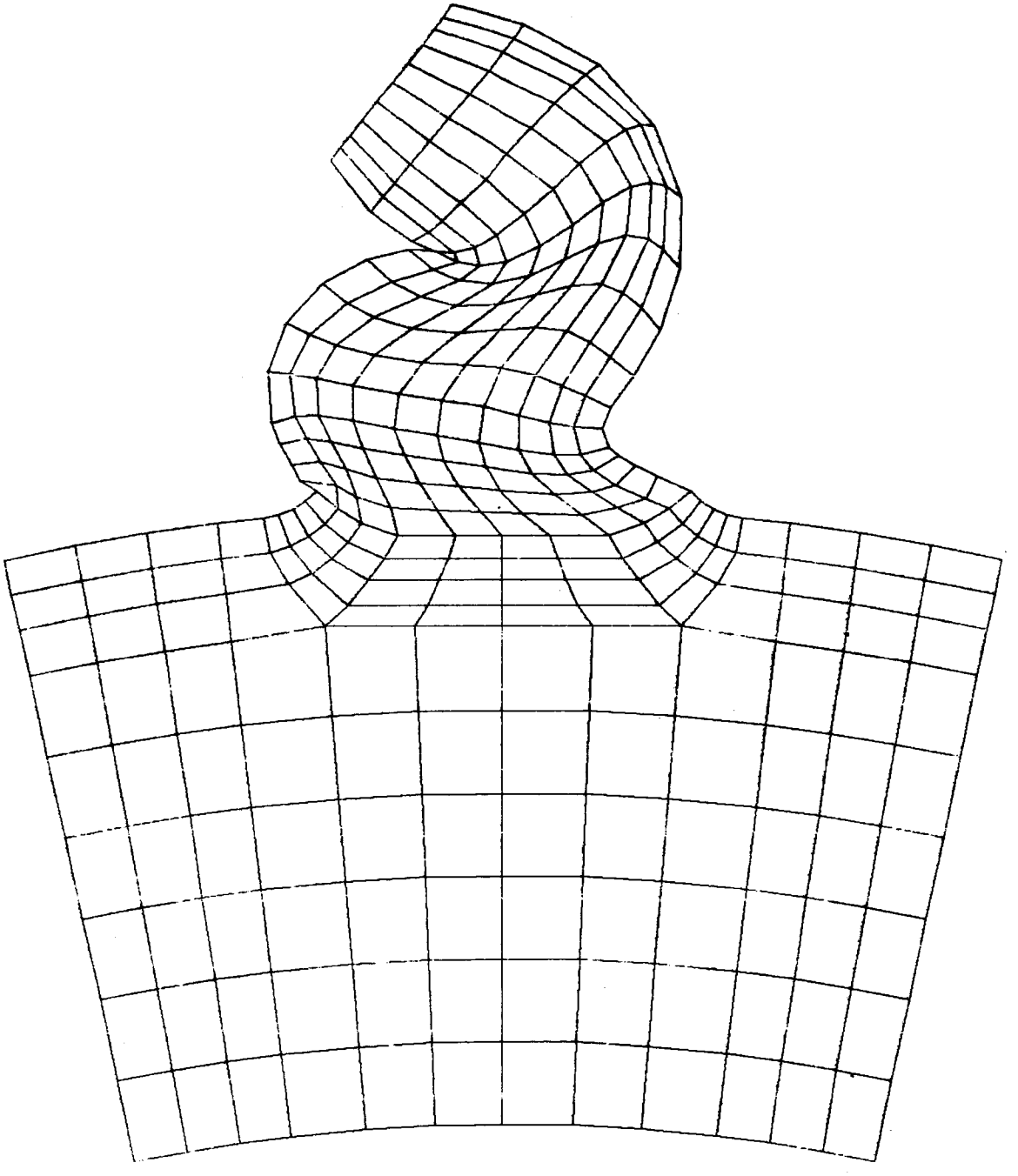

Figure A3-14

MODAL ANALYSIS, PLANE STRAIN ELEMENT: GEAR #1
MODE 5 Freq.= .4794 E6 (CPS)

UNE 10, 1983 19:32:39'
IAXIS=3 ALPHA= 0.00 BETA= 0.00
DEFLECTION SCALE FACTOR= 0.29769E

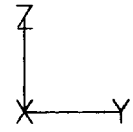

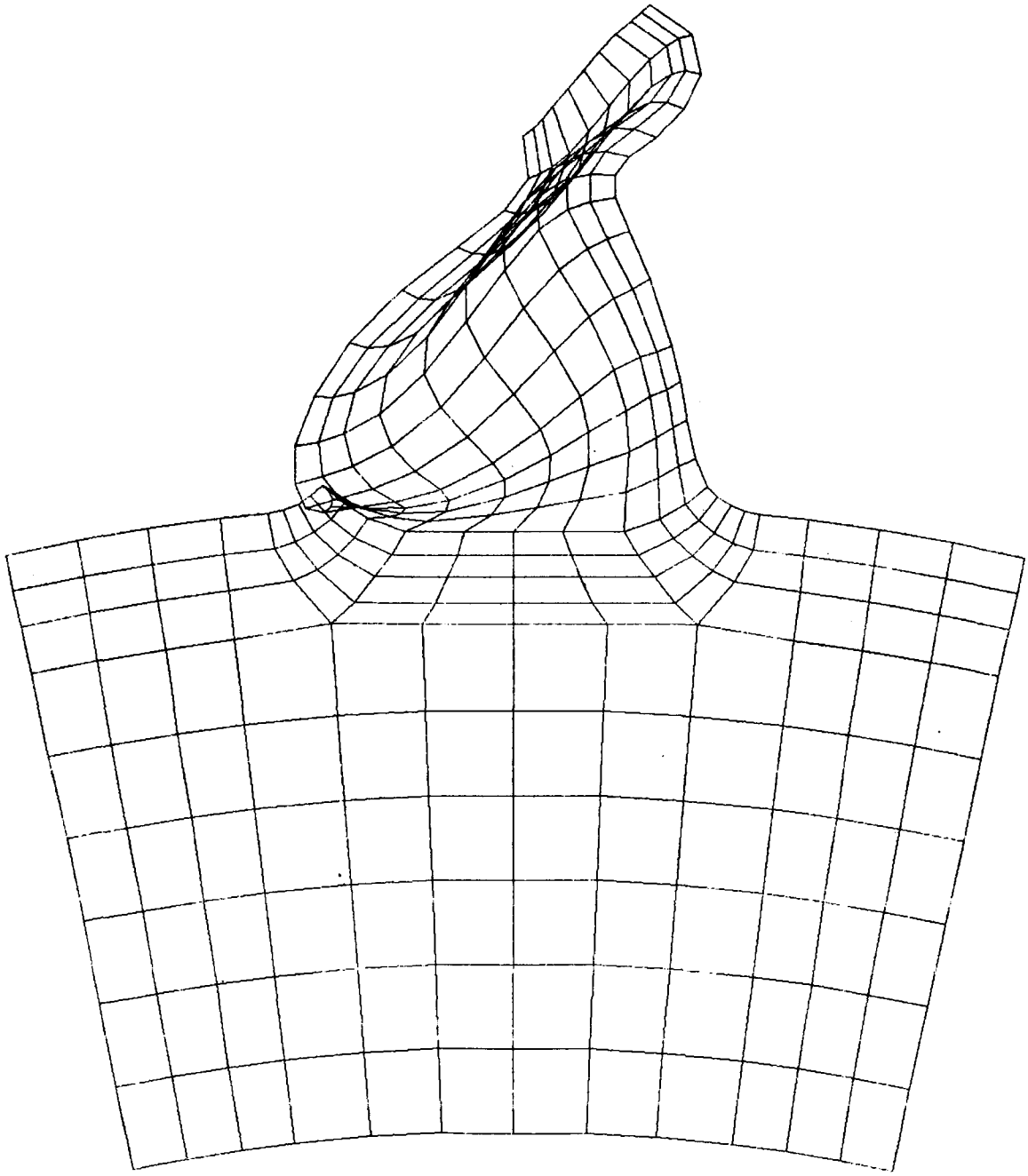

Figure A3-15

MODAL ANALYSIS, PLANE STRAIN ELEMENT: GEAR #1
MODE 1 Freq.= .6545 E5 (CPS)

UNE 16, 1983 00:10:15'
IAXIS=3 ALPHA= 0.00 BETA= 0.00
DEFLECTION SCALE FACTOR= 0.27565E

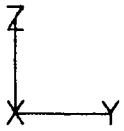

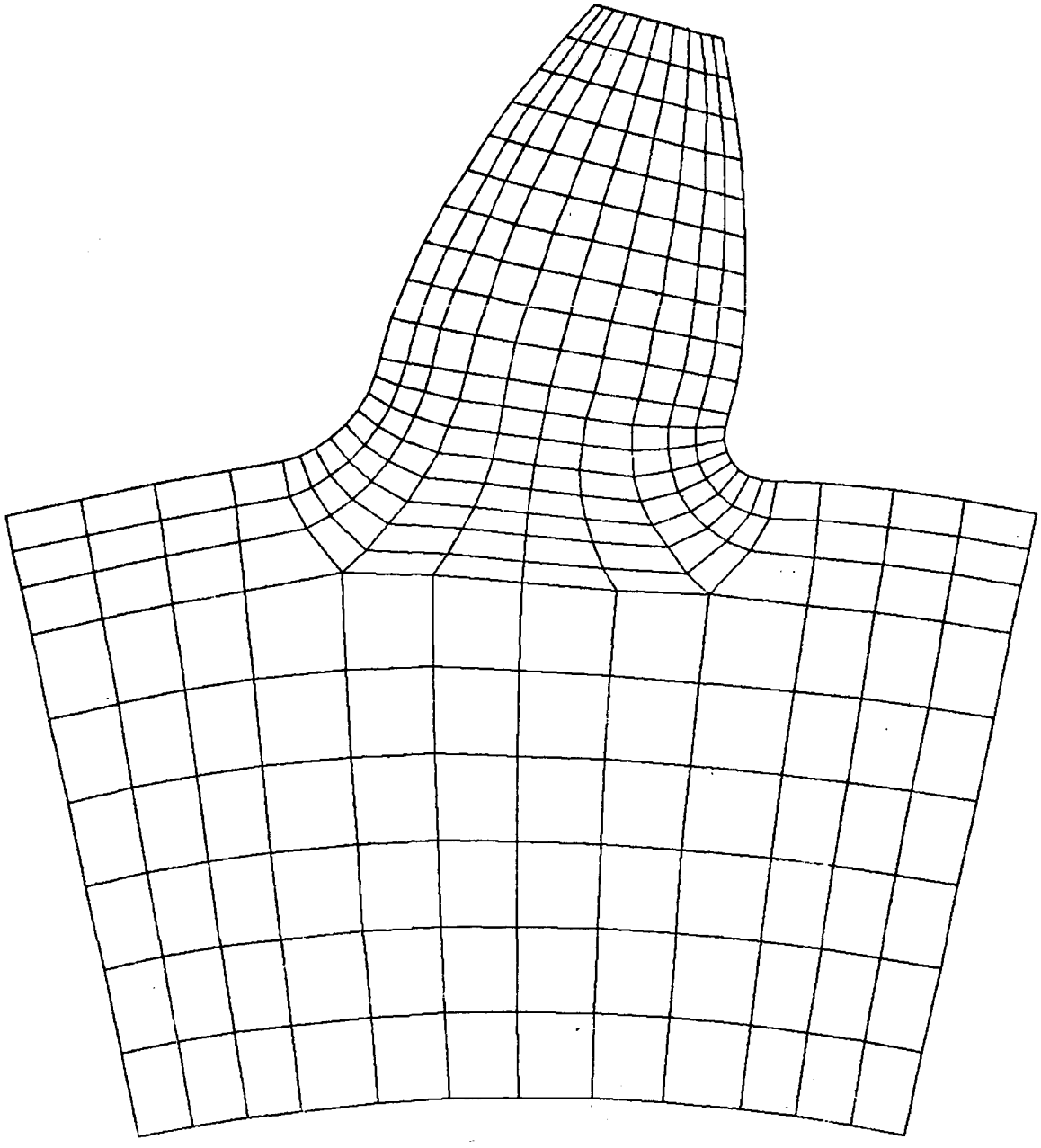

Figure A3-16

MODAL ANALYSIS, PLANE STRAIN ELEMENT: GEAR #1
MODE 2 **Freq.= .1146 E6 (CPS)**

UNE 16, 1983 00:10:15'
IAXIS=3 ALPHA= 0.00 BETA= 0.00
DEFLECTION SCALE FACTOR= 0.5412[illegible]E

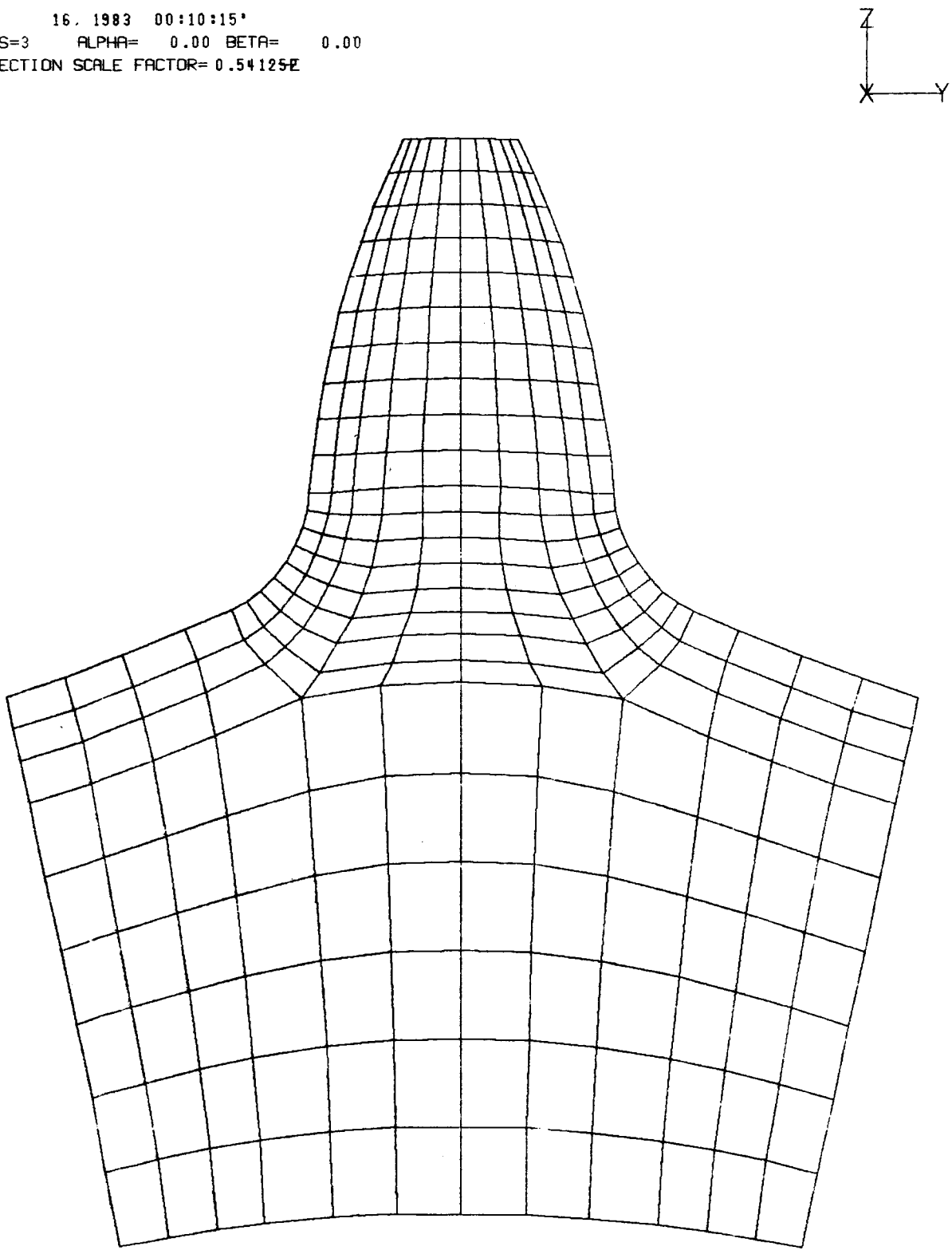

Figure A3-17

MODAL ANALYSIS, PLANE STRAIN ELEMENT: GEAR #1
MODE 3 Freq.= .1517 E6 (CPS)

UNE 16, 1983 00:10:15'
IAXIS=3 ALPHA= 0.00 BETA= 0.00
DEFLECTION SCALE FACTOR= 0.4247+E

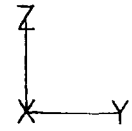

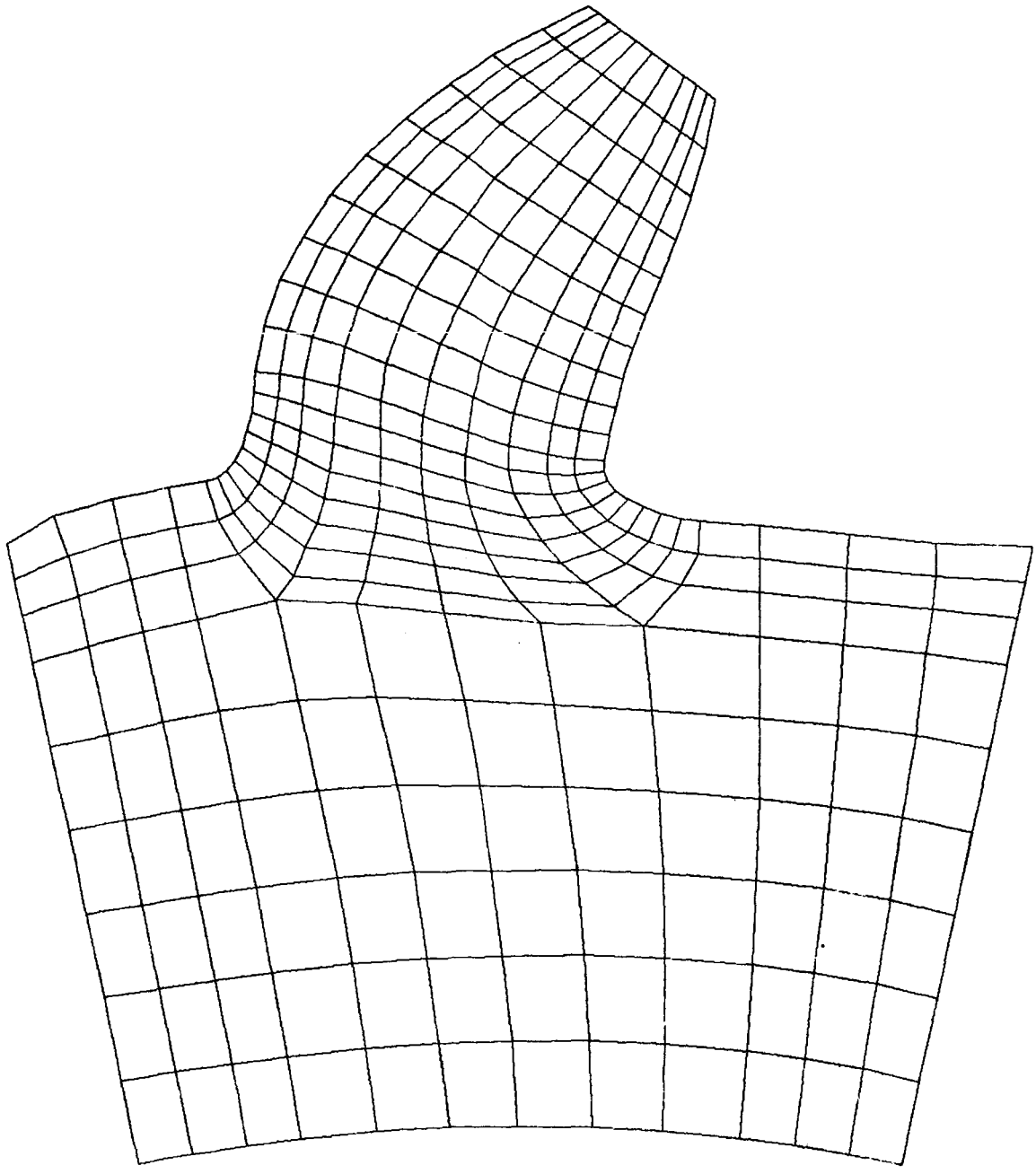

Figure A3-18

MODAL ANALYSIS, PLANE STRAIN ELEMENT: GEAR #1
MODE 4 Freq.= .2034 E6 (CPS)

UNE 16, 1983 00:10:15
IAXIS=3 ALPHA= 0.00 BETA= 0.00
DEFLECTION SCALE FACTOR= 0.42677E

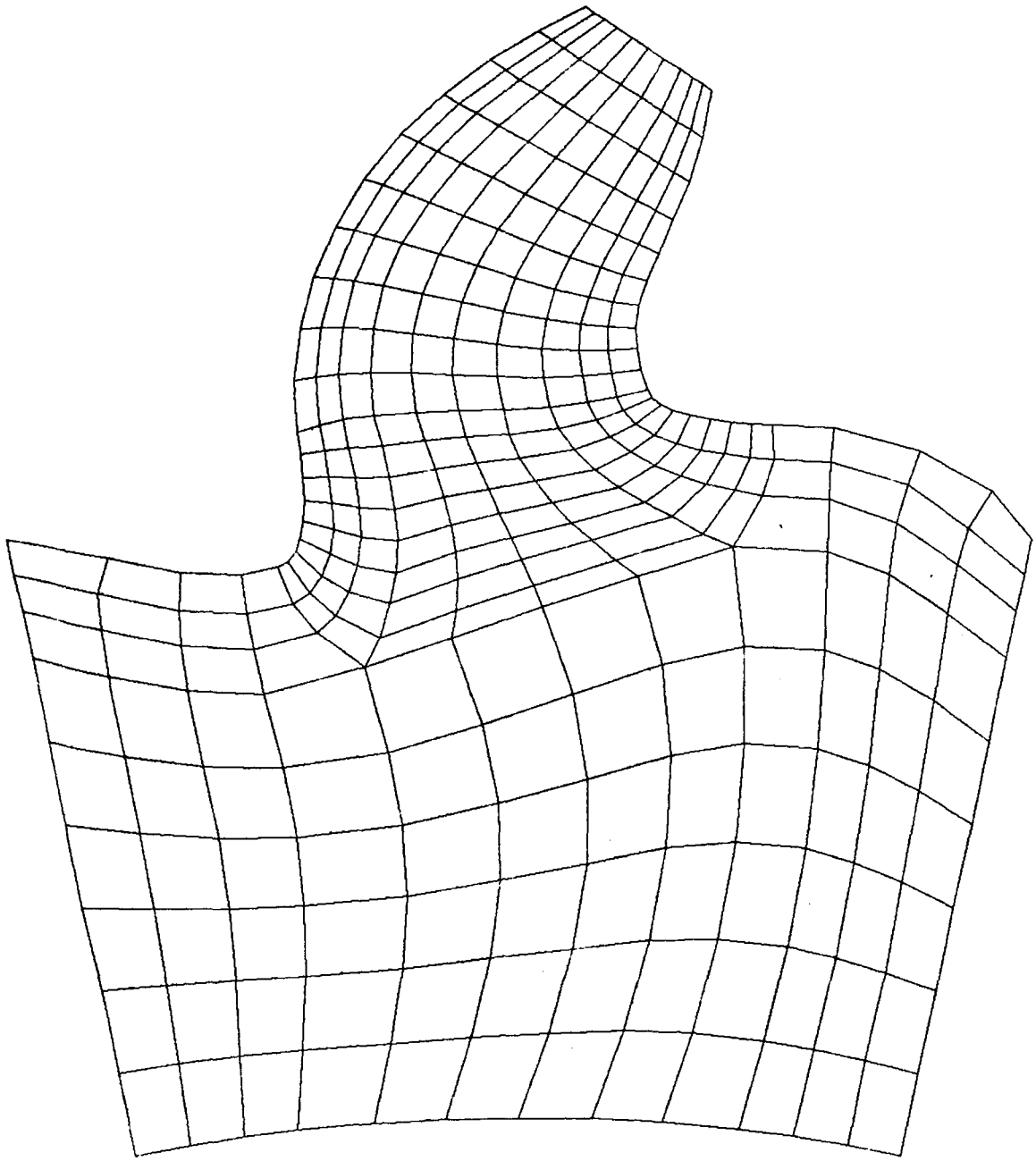

Figure A3-19

MODAL ANALYSIS, PLANE STRAIN ELEMENT: GEAR #1
MODE 5 Freq.= .2319 E6 (CPS)

UNE 16, 1983 00:10:15'
IAXIS=3 ALPHA= 0.00 BETA= 0.00
DEFLECTION SCALE FACTOR= 0.52530E

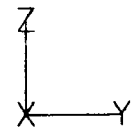

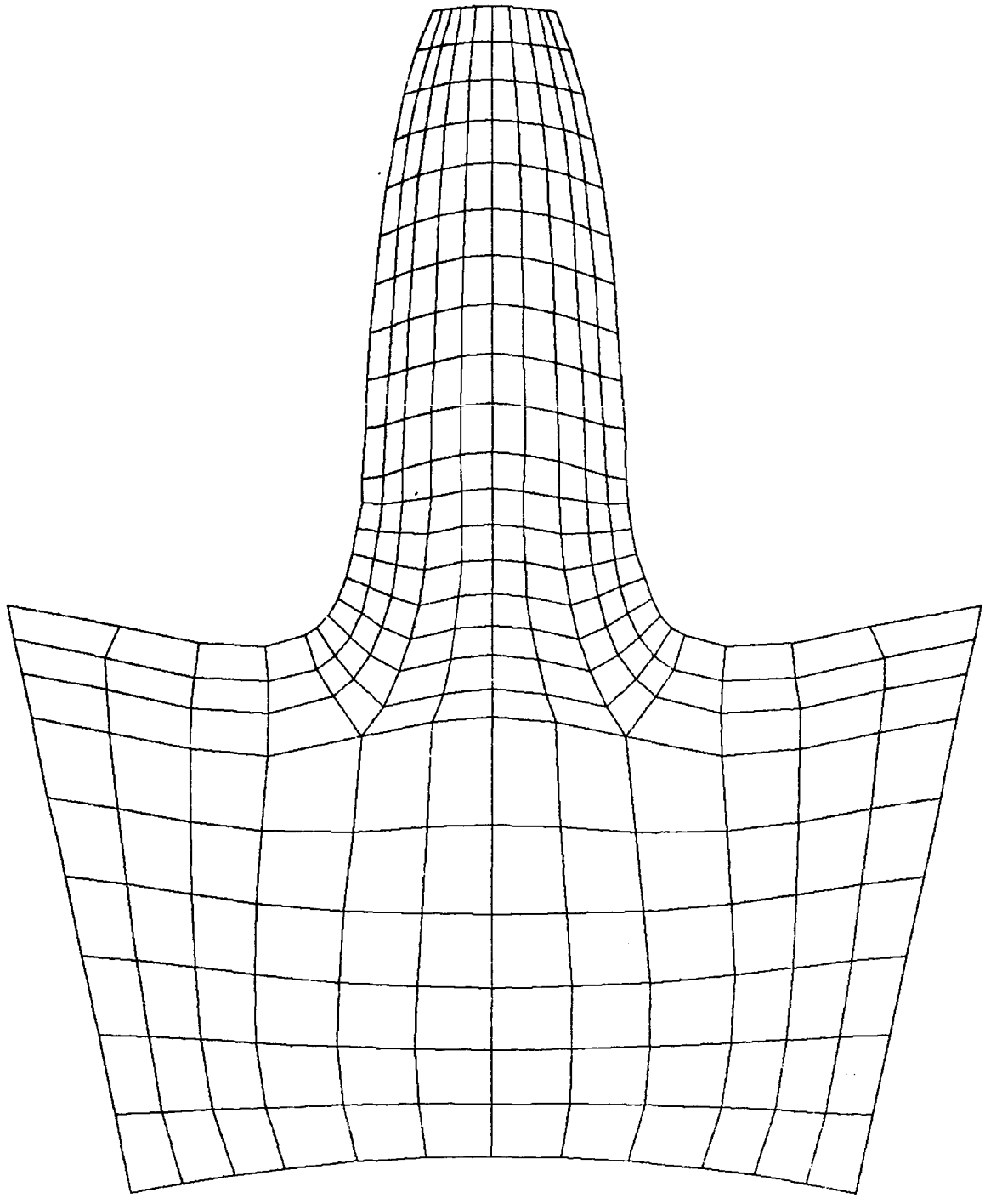

Figure A3-20

Dynamic Response

Gear Tooth Profile Deflections

In the modal response analysis, modal superposition is used to sum the effects of all the included mode shapes producing the desired response. The more modes included, the more accurate the analysis. However, there is a practical limit to the number of modes used dictated by the type of loading used (impact, constant, sinusoidal, etc.) and of course computational efficiency. As previously mentioned, the first ten modes are used for this analysis.

To better comprehend the dynamic deflection phenomena, the deflected state of the tooth profile, subject to the impact loading case, is plotted for different load positions with V*=0.01. Figure A3-21 shows the underformed shape and Figures A3-22 through A3-25 are the various deformed shapes. From the figure(s), one can see those modes which contribute noticeably to the overall deflection of the tooth. It is apparent that only the first three or four have a major effect (see Figure A3-19, T=0.5). Thus the problem of local deformation encountered in the static analysis is not apparent here.

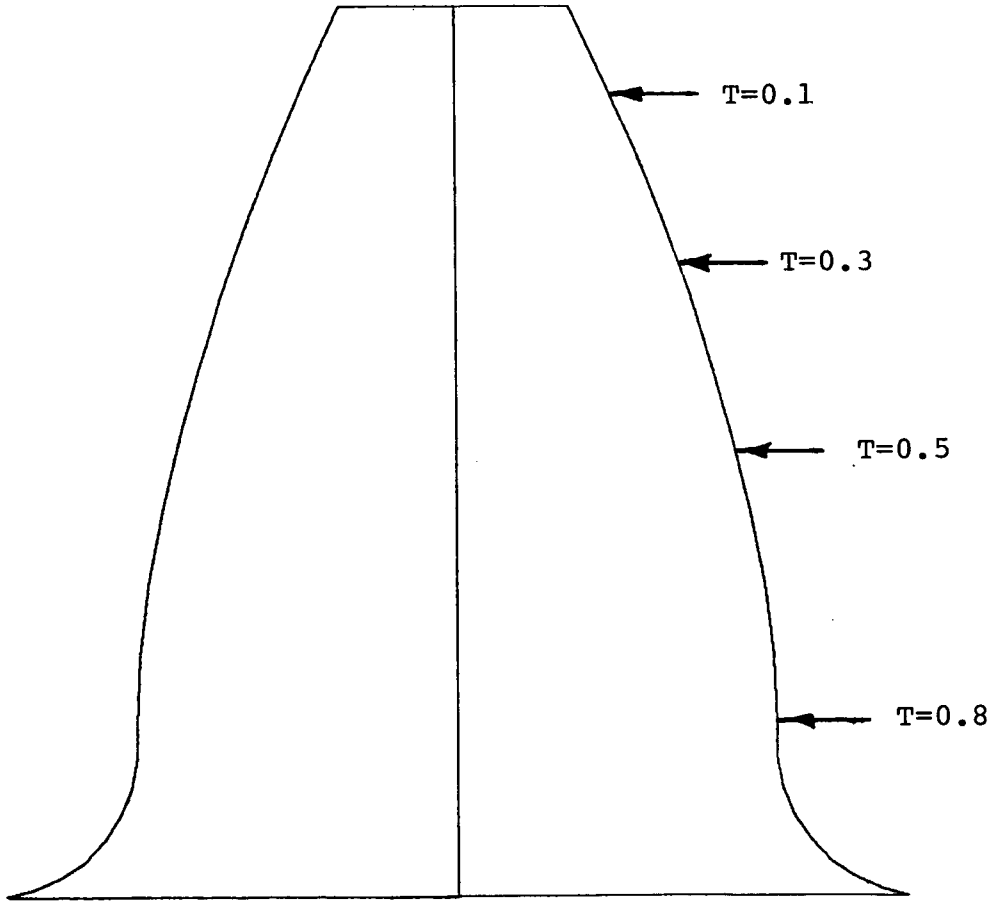

DYNAMIC DEFLECTIONS OF GEAR TOOTH: UNDEFORMED SHAPE

Figure A3-21

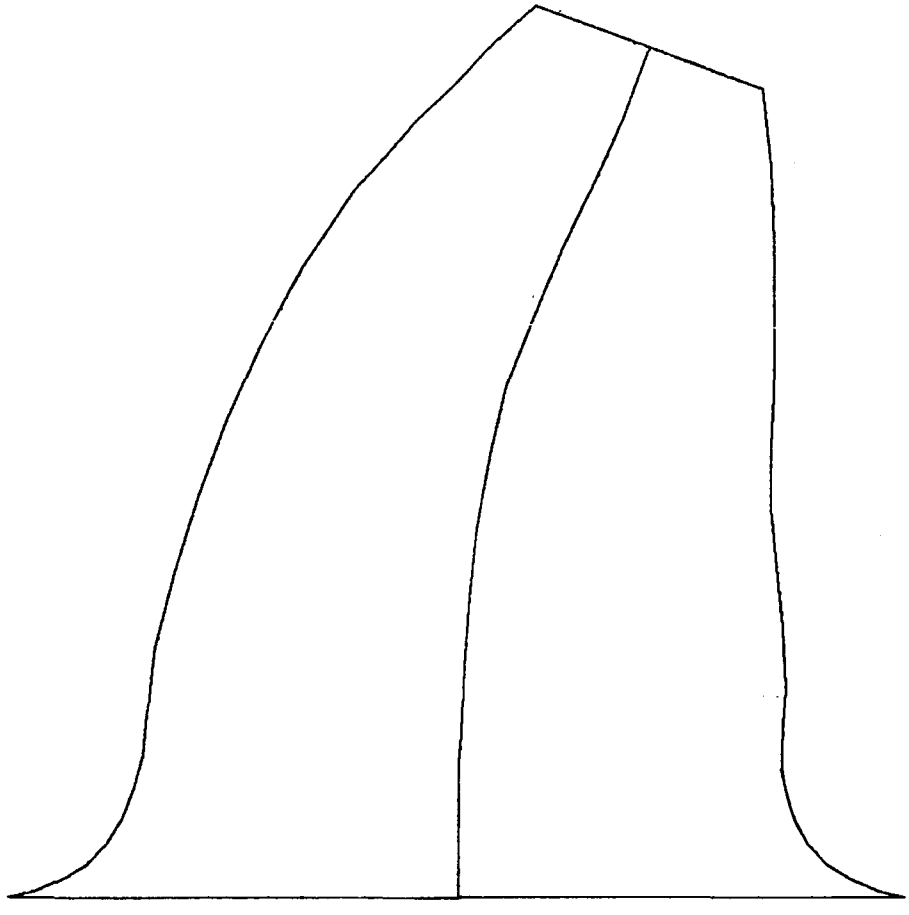

V*=0.01 T=0.1

DYNAMIC DEFLECTIONS OF GEAR TOOTH WITH MOVING LOADS

Figure A3-22

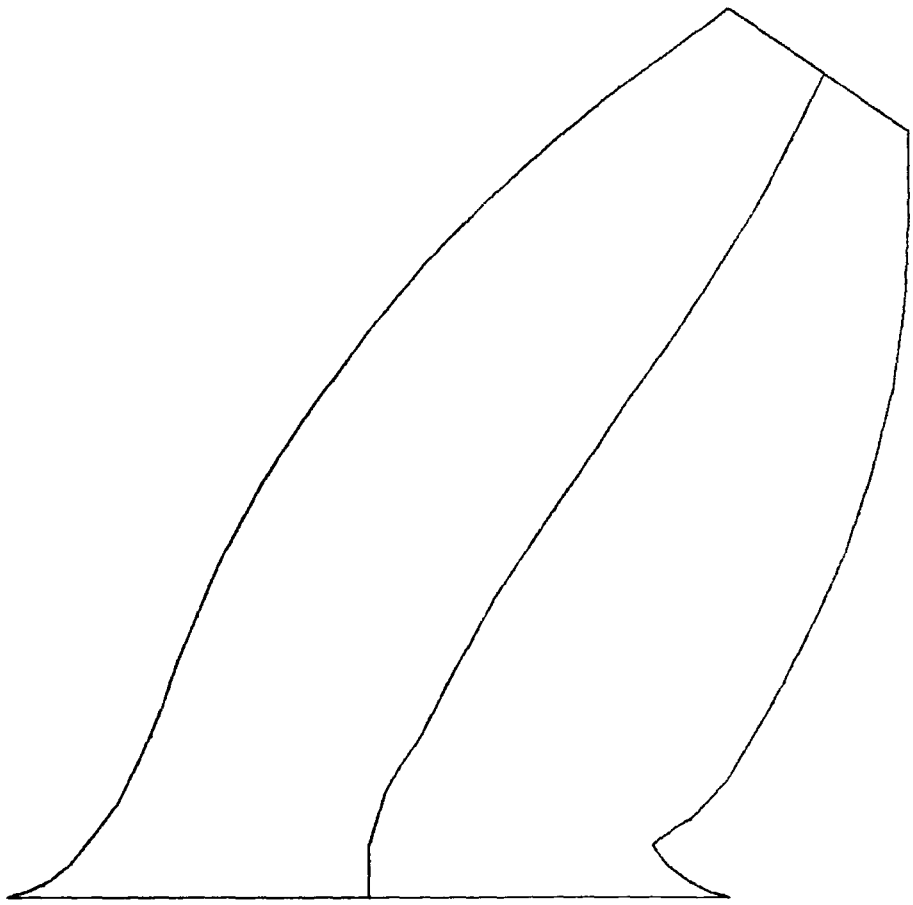

V*=0.01 T=0.3

DYNAMIC DEFLECTIONS OF GEAR TOOTH WITH MOVING LOADS

Figure A3-23

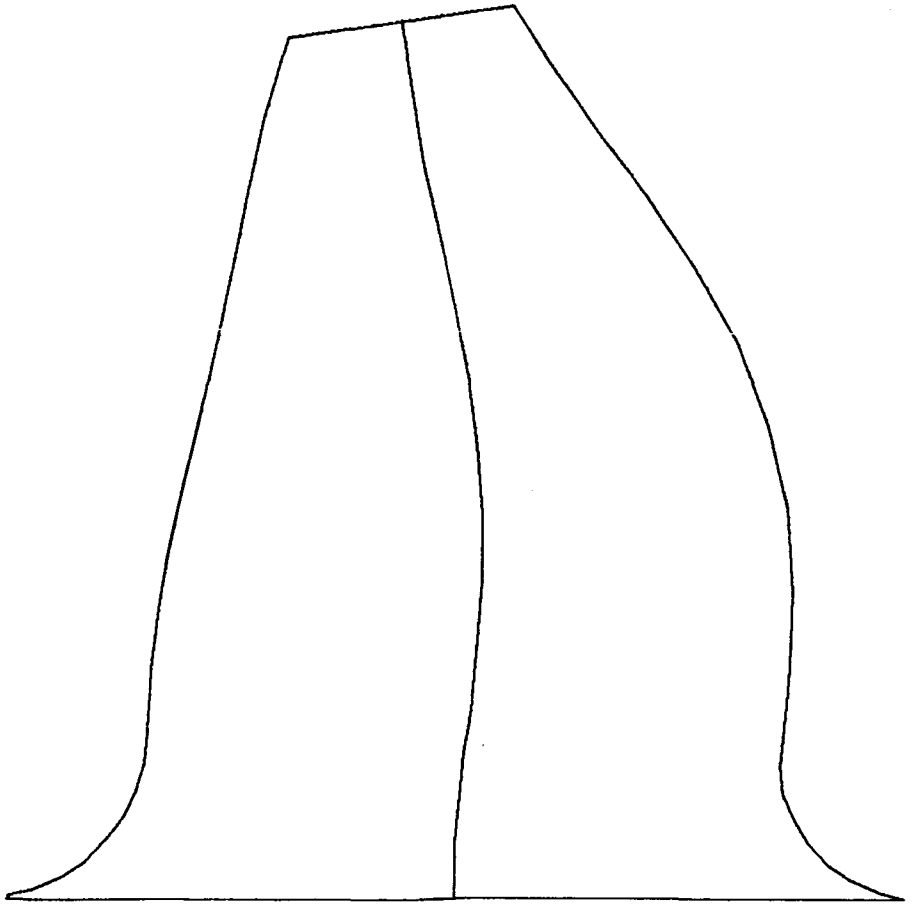

V*=0.01 T=0.5

DYNAMIC DEFLECTIONS OF GEAR TOOTH WITH MOVING LOADS

Figure A3-24

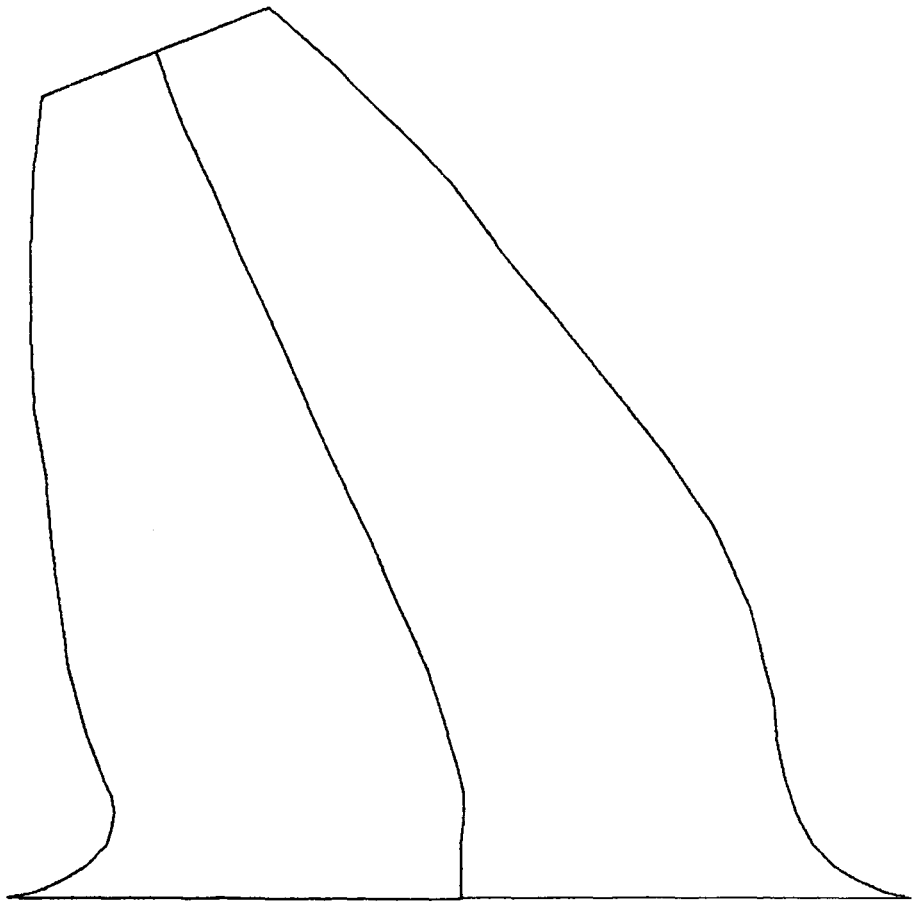

V*=0.01 T=0.8

DYNAMIC DEFLECTIONS OF GEAR TOOTH WITH MOVING LOADS

Figure A3-25

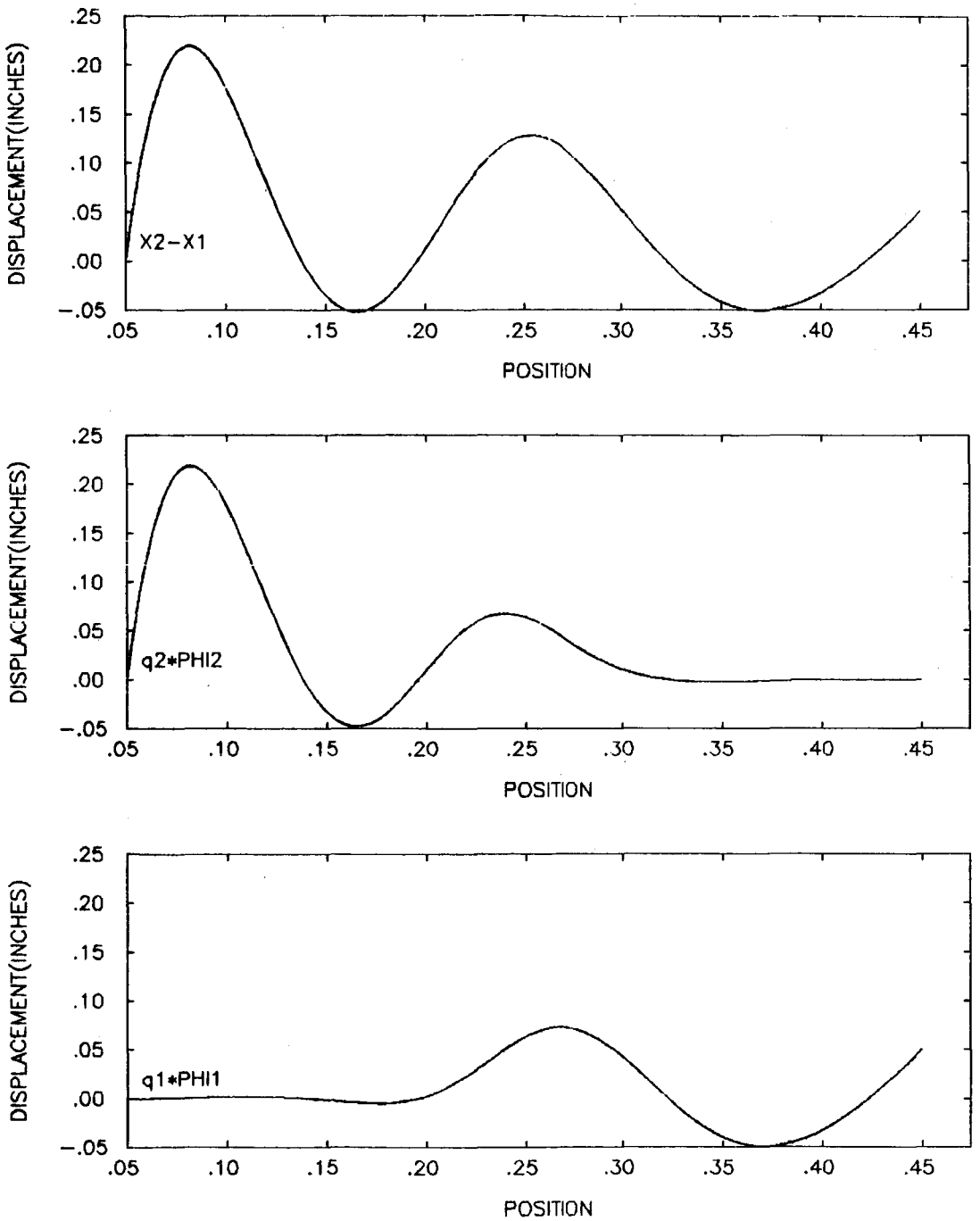

VEL= 10.0 IN/SEC ; MASS= 1.0 ; BEAM LENGTH= 0.5 IN

DYNAMIC RESPONSE OF MESHING CANTILEVER BEAMS, WITH INERTIA (VEL=V(T))

Figure A4-16

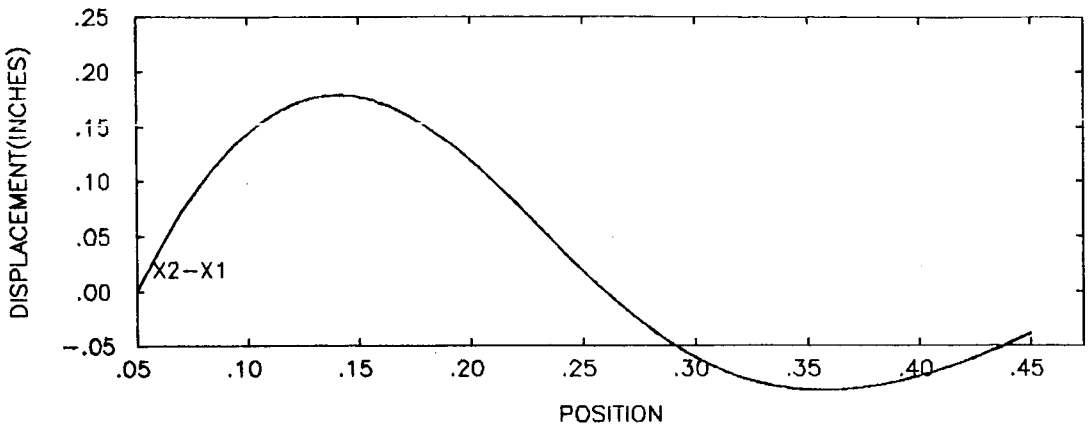

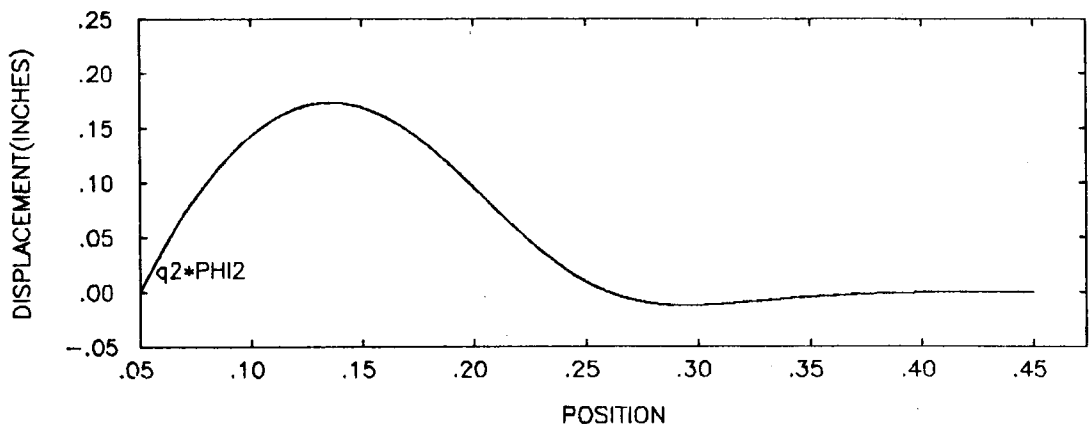

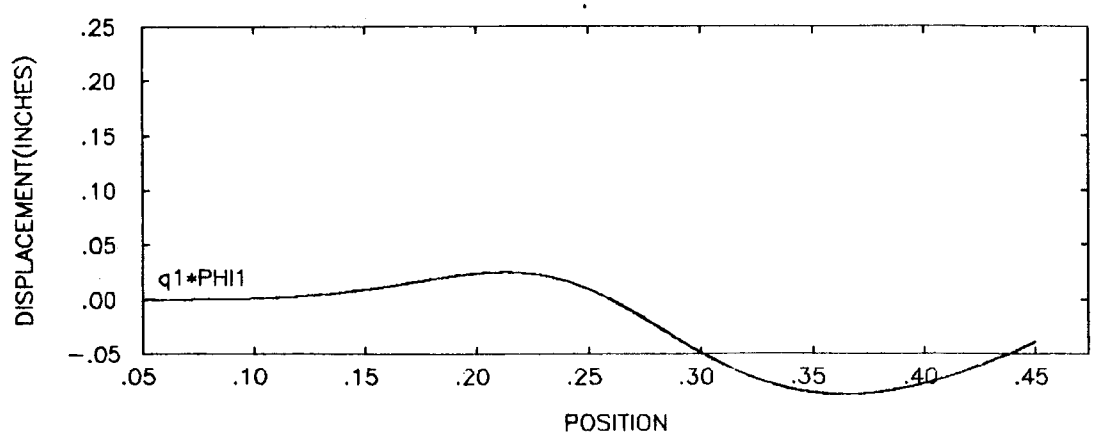

VEL= 20.0 IN/SEC ; MASS= 1.0 ; BEAM LENGTH= 0.5 IN

DYNAMIC RESPONSE OF MESHING CANTILEVER BEAMS, WITH INERTIA (VEL=V(T))

Figure A4-17

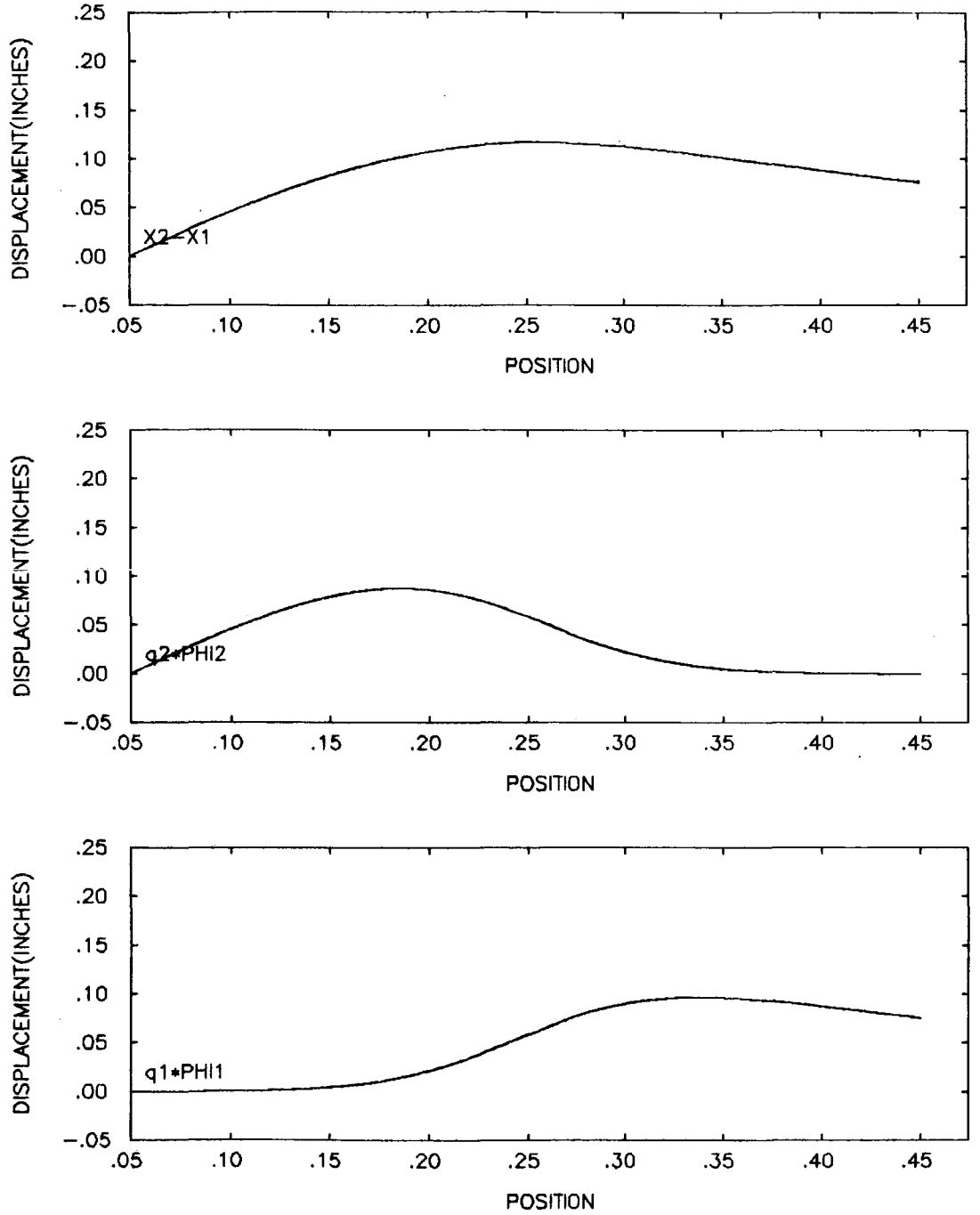

VEL= 40.0 IN/SEC ; MASS= 1.0 ; BEAM LENGTH= 0.5 IN

DYNAMIC RESPONSE OF MESHING CANTILEVER BEAMS, WITH INERTIA (VEL=V(T))

Figure A4-18

C-3

APPENDIX 5

Use of Natural Modes in Equation of Motion for Cantilever Beams

1) Constant of Integration

2) Evaluation of I2PHI1 AND I2PHI2

3) Derivatives of the Mode Shape With Time

1.) Constant of Integration

In order to simplify the solution of the equation of motion (5-26), the constant of integration associated with the mode shape of a cantilever beam is determined such that;

$$\rho\int_0^L \phi^2(\xi)d\xi = 1 \qquad \text{(A5-1)}$$

Since the beams are identical and the integral is over the length of the beam, the constant is the same for both beams.

The first natural mode of vibration for a uniform fixed-free cantilever beam is;

$$\phi(\xi) = C[(\sin\beta L-\sinh\beta L)(\sin\beta\xi-\sinh\beta\xi) + (\cos\beta L+\cosh\beta L)(\cos\beta\xi-\cosh\beta\xi) \qquad \text{(A5-2)}$$

where;

$$\beta^4 = \frac{\omega^2\rho}{EI}$$

Equation (A5-2) is simplified by rewriting with;

$$S1 = \sin\beta L-\sinh\beta L$$

$$S2 = \cos\beta L+\cosh\beta L$$

We then have;

$$\phi(\xi) = C[S1\sin x-S1\sinh x+S2\cos x-S2\cosh x] \qquad \text{(A5-3)}$$

where x is used in place of the argument $\beta\xi$.

Squaring equation (A5-3);

$$\phi^2(\xi) = C^2[Sl^2(\sin^2x+\sinh^2x-2\sin x\sinh x) + S2^2(\cos^2x+\cosh^2x-2\cos x\sinh x) + 2SlS2(\sin x\cos x-\sin x\cosh x-\cos x\sinh x+\sinh x\cosh x)] \quad (A5\text{-}4)$$

We can then solve for the constant C with the following substitution;

$$C = \left(\frac{1}{\rho\int_0^L G(\xi)d\xi}\right)^{\frac{1}{2}} \quad (A5\text{-}5)$$

where $\phi(\xi)=CG(\xi)$. Whenever the relation represented by equation (A5-1) occurs in equations (5-26) it is replaced by 1. Throughout the remainder of equations of motion the constant of integration C is represented by equation (A5-5). This relation is evaluted using Simpson's Rule.

2.) Evaluation of I2PHI1 and I2PHI2

Using the arbitrary constant of integration, C, determined in the previous section, the relationship;

$$I2PHI1 = I2PHI2 = \int_0^L \phi^2(\xi)d\xi \quad (A5\text{-}6)$$

can be evaluated. The integrand represents the second derivative of the mode shape with respect to the length variable, ξ, quantity squared. The first derivative of the mode shape with x again used in place of $\beta\xi$;

$$\frac{d\phi}{d\xi} = C\beta[Slcosx-S2coshx-S2sinx-S2sinhx]$$

and the second derivative;

$$\frac{d^2\phi}{d\xi^2} = C\beta^2[-S1\sin x-S1\sinh x-S2\cos x-S2\cosh x]$$

Squaring this relation and simplifying yields the desired result;

$$\left(\frac{d^2\phi}{d\xi^2}\right)^2 = C^2\beta^4[S1^2(\sin^2 x+\sinh^2 x+2\sin x \sinh x) + S2^2(\cos^2 x+\cosh^2 x+2\cos x \cosh x) + 2S1S2(\sin x \cos x+\sin x \cosh x+\cos x \sinh x+\sinh x \cosh x)] \quad \text{(A5-7)}$$

This relation is then used in equation (A5-6) which is evaluated using Simpson's Rule.

3.) Derivatives of the Mode Shape with Time

When the constraint equation is differentiated, first and second derivatives of the mode shape result where the dependent variable, ξ, must be considered as a function of time. The first derivative of the mode shape with respect to time is;

$$\frac{d\phi(\xi)}{dt} = C\beta\dot{\xi}[S1\cos x-S1\cosh x-S2\sin x-S2\sinh x] \quad \text{(A5-8)}$$

where x is used in place of the argument $\beta\xi$ and $\dot{\xi}$ is the velocity of the moving load. Taking the second derivative, we have;

$$\frac{d^2\phi(\xi)}{dt^2} = C[S1(-\beta^2\dot{\xi}^2(\sin x+\sinh x) + \beta\ddot{\xi}(\cos x-\cosh x)) - S2(\beta^2\dot{\xi}^2(\cos x+\cosh) + \beta\ddot{\xi}(\sin x+\sinh x))] \quad \text{(A5-9)}$$

where $\ddot{\xi}$ is the acceleration of the moving load. For a moving load with constant speed, $\ddot{\xi}$ is of course zero.

APPENDIX 6

Development and Solution of Equations of Motion with Inertial Terms Removed

By eliminating the inertial terms from the first four equations of (5-26), and using the undifferentiated form of the constraint equation (5-18), a new set of equations for the beam-mass system take the form;

$$[A]\{\bar{X}\} = \{\bar{B}\} \qquad \text{(A6-1)}$$

where;

$$[A] = \begin{bmatrix} (M1+MB1) & 0 & 0 & 0 & 1 \\ 0 & (M2+MB2) & 0 & 0 & -1 \\ 0 & 0 & I2PHI1 & 0 & PHI1 \\ 0 & 0 & 0 & I2PHI2 & PHI2 \\ 0 & 0 & -PHI1 & -PHI2 & 0 \end{bmatrix}$$

$$\{\bar{X}\} = \begin{Bmatrix} \ddot{X}1 \\ \ddot{X}2 \\ q1 \\ q2 \\ \lambda \end{Bmatrix} \quad ; \quad \{\bar{B}\} = \begin{Bmatrix} -P \\ P \\ 0 \\ 0 \\ X1-X2 \end{Bmatrix}$$

The initial conditions for this system are determined by arbitrarily chosing three of the four unknowns composing the constraint equation. Letting the beams assume static deflections at time equal to zero, and X1 equal to zero; the initial conditions are;

$$q1(0) = \frac{P*PHI1}{I2PHI2}$$

$$q2(0) = \frac{P*PHI2}{I2PHI2}$$

$$X1(0) = 0.0$$

with;

$$X2(0) = X1 + q1PHI1 + q2PHI2$$

Solving for $\{\bar{X}\}$ in equation (A6-1) by inversion;

$$\{\bar{X}\} = [A]^{-1}\{\bar{B}\}$$

gives the values of the unknowns in terms of X1 and X2. Using these values for $\{\bar{X}\}=\{\ddot{X}1\ \ddot{X}2\ q1\ q2\ \lambda\}^T$, the system is integrated using a Runge-Kutta integration algorithm solving for X1 and X2 and λ. Then equations 3 and 4 of (A6-1) are used to solve for q1 and q2.

Tests were done for constant velocity moving loads of 1.0, 5.0, 10.0, 20.0 and 40.0 inches per second. Plots of X2-X1, q1PHI1 and q2PHI2 are included in Figures (A6-1) through (A6-5). Comparing these to Figures (5-7) to (5-11) show that even though only one vibrational mode is used, the results are very nearly the same as those determined for the massless beams.

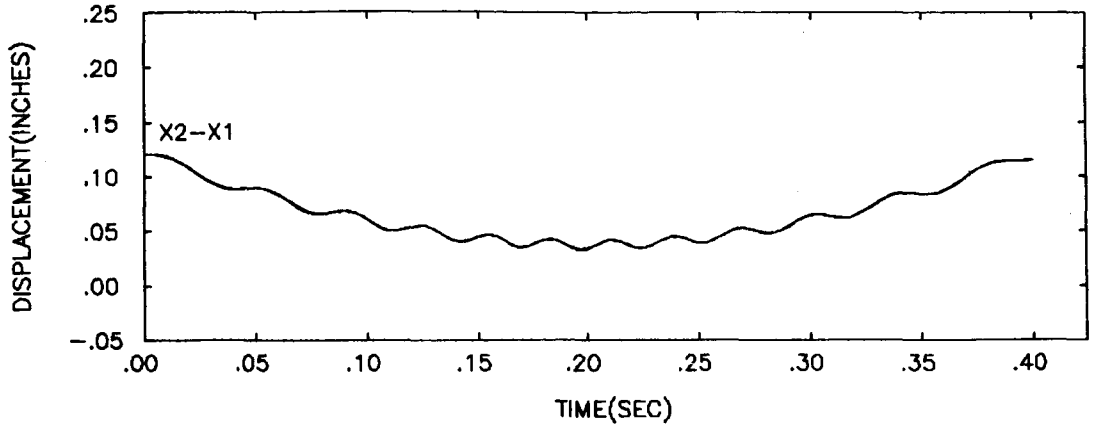

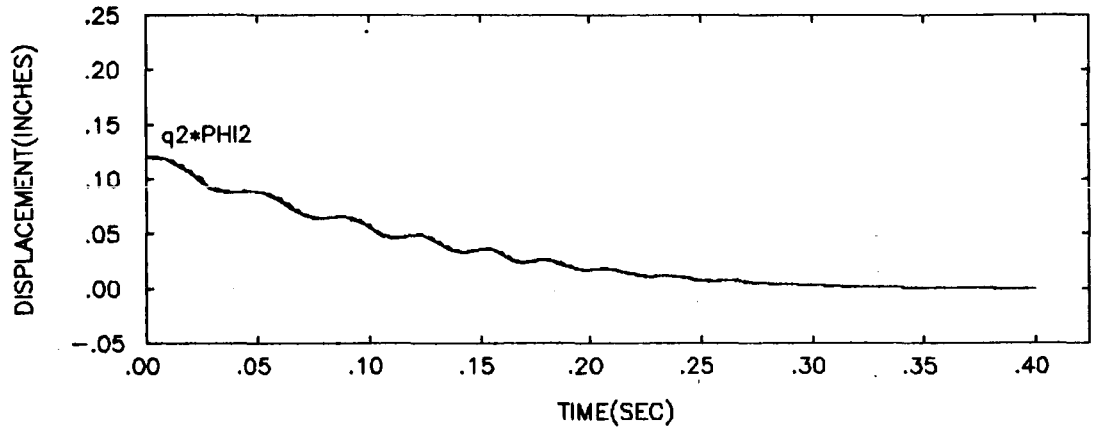

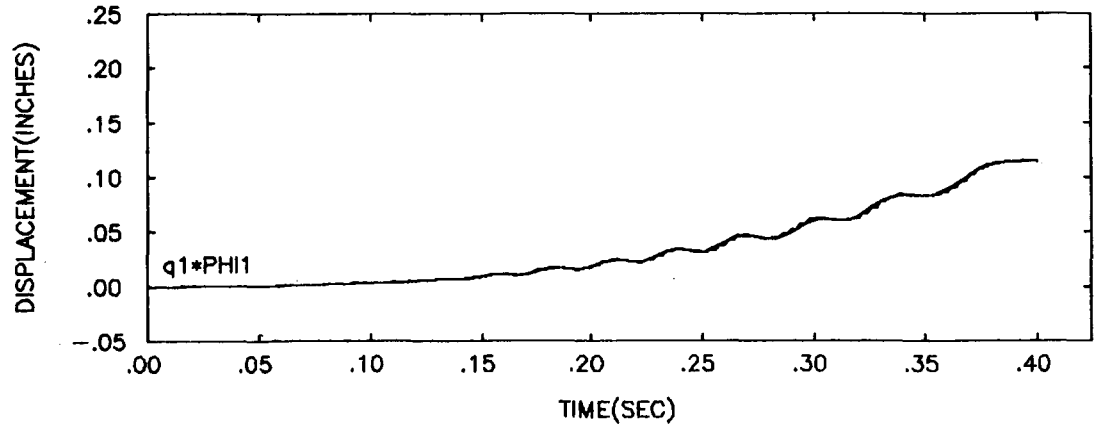

VEL= 1.0 IN/SEC ; MASS= 1.0 ; BEAM LENGTH= 0.5 IN

DYNAMIC RESPONSE OF MESHING CANTILEVER BEAMS, NO INERTIA (VEL=CONST)

Figure A6-1:

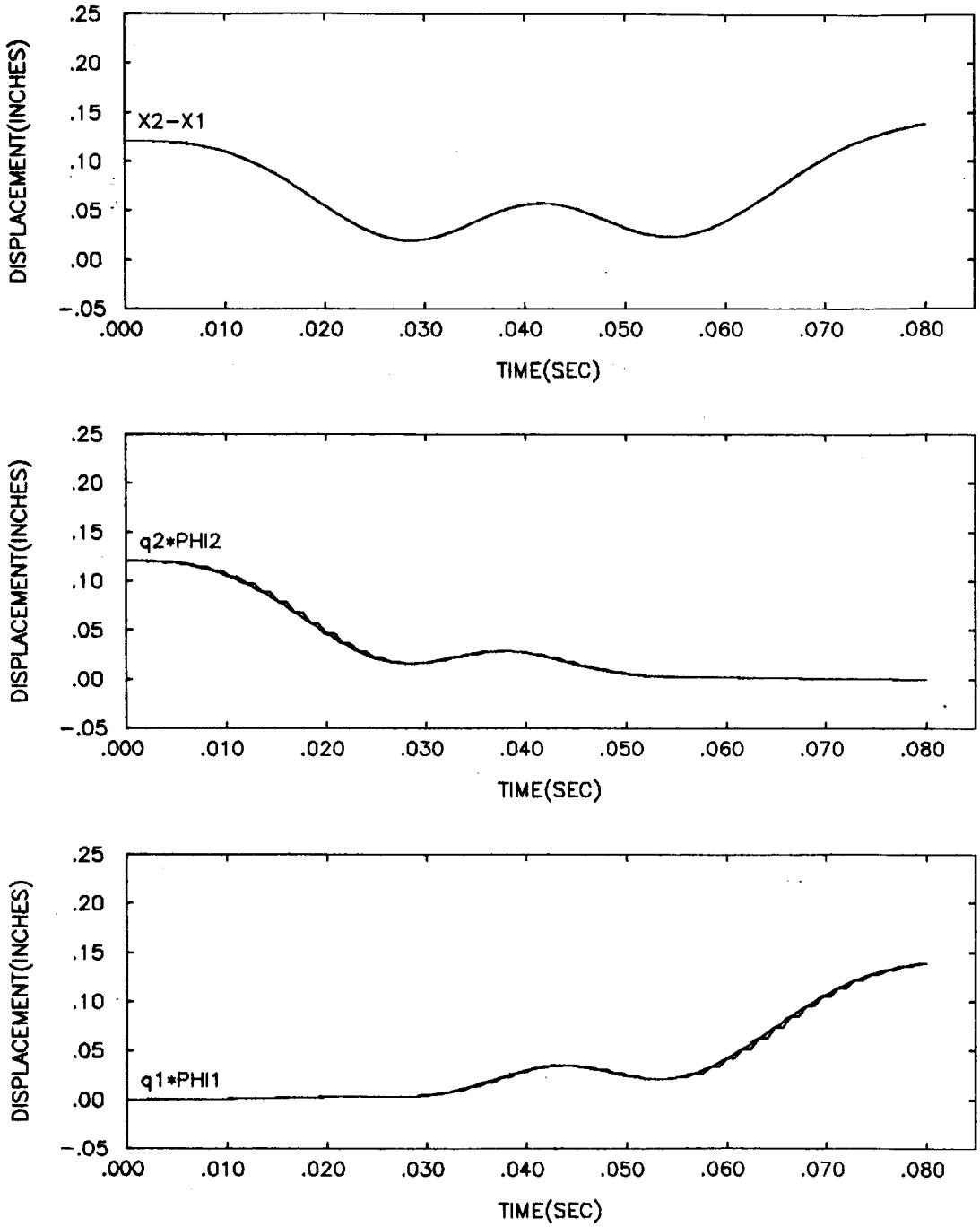

VEL= 5.0 IN/SEC ; MASS= 1.0 ; BEAM LENGTH= 0.5 IN

DYNAMIC RESPONSE OF MESHING CANTILEVER BEAMS, NO INERTIA (VEL=CONST)

Figure A6-2:

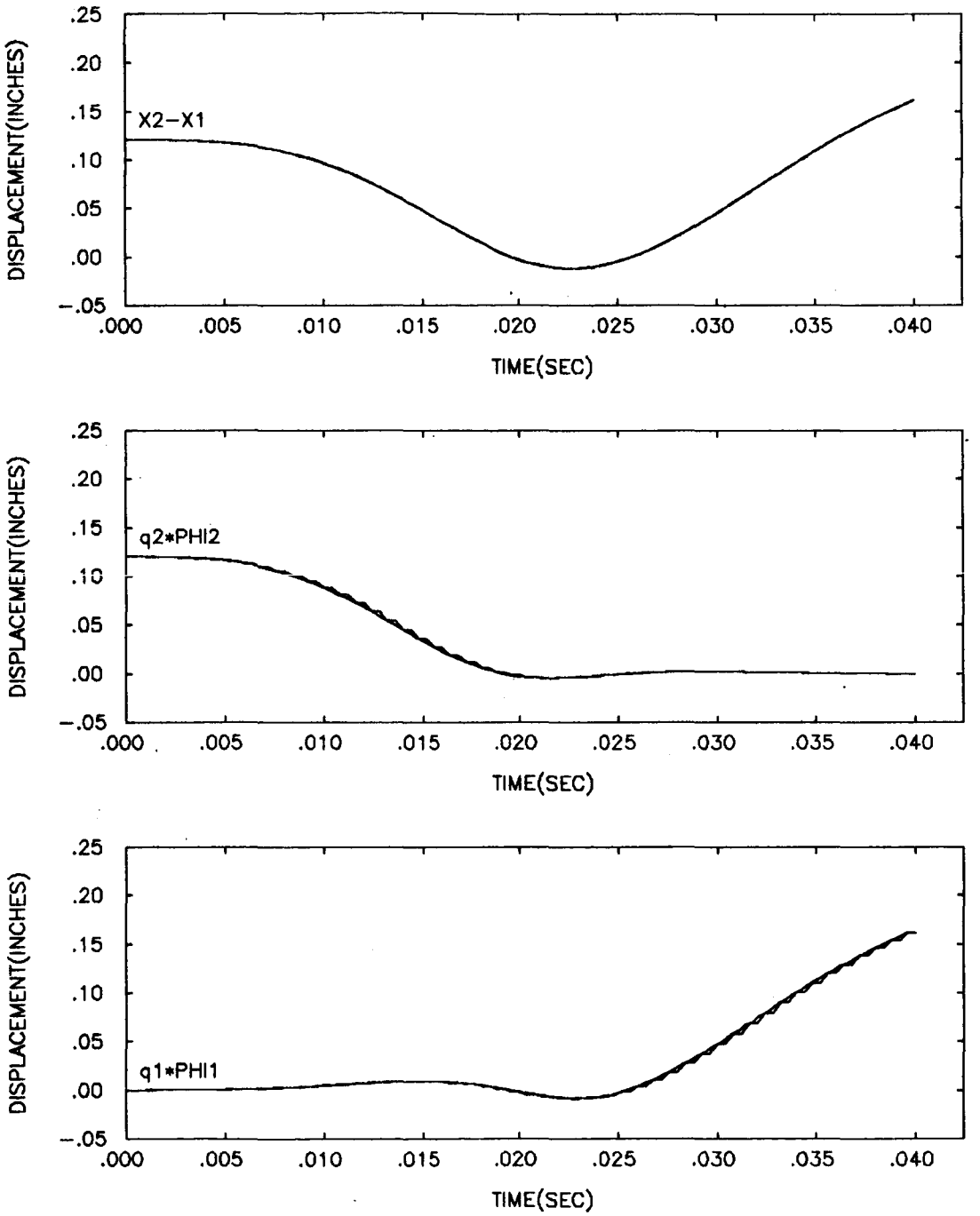

VEL= 10.0 IN/SEC ; MASS= 1.0 ; BEAM LENGTH= 0.5 IN

DYNAMIC RESPONSE OF MESHING CANTILEVER BEAMS, NO INERTIA (VEL=CONST)

Figure A6-3

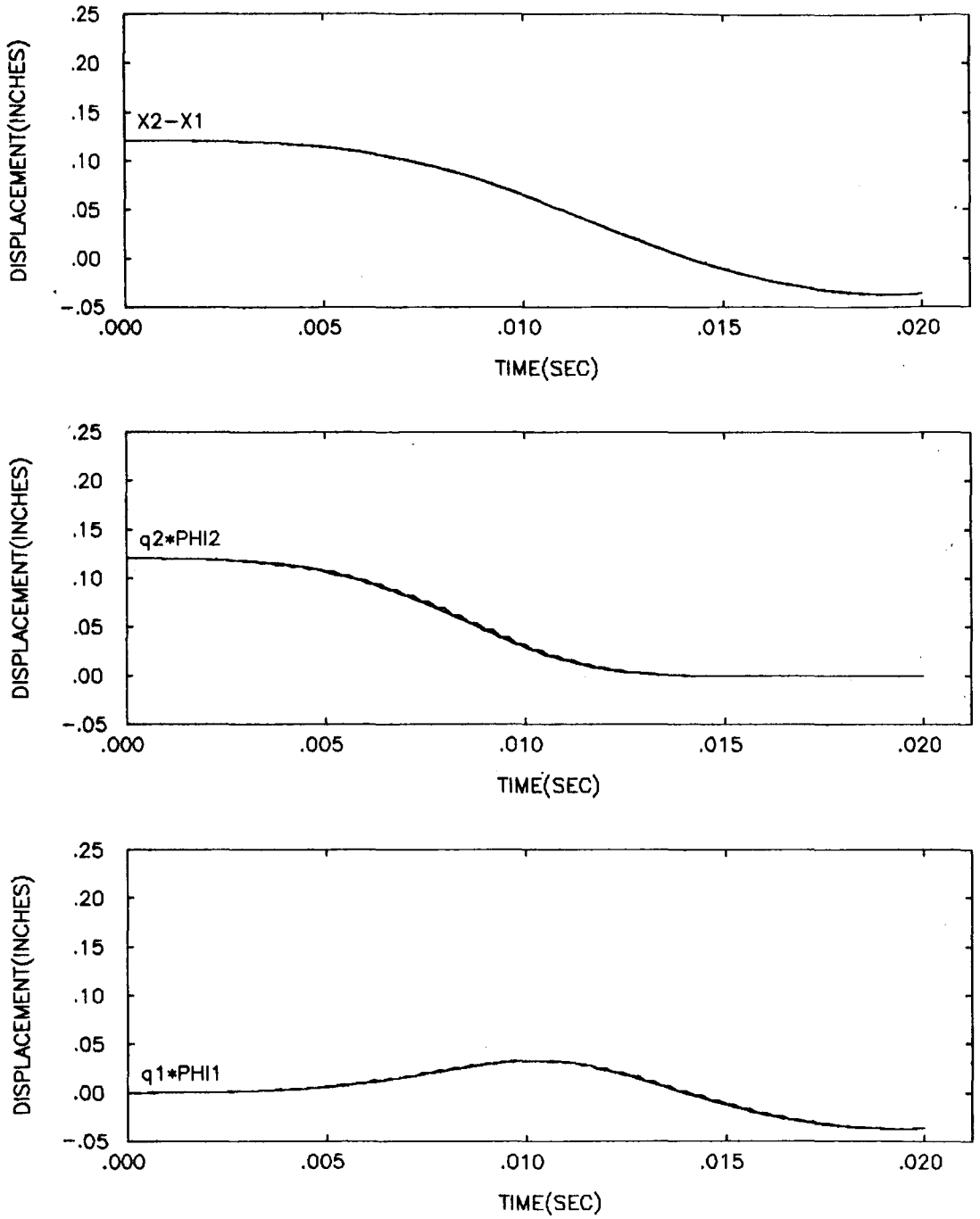

VEL= 20.0 IN/SEC ; MASS= 1.0 ; BEAM LENGTH= 0.5 IN

DYNAMIC RESPONSE OF MESHING CANTILEVER BEAMS, NO INERTIA (VEL=CONST)

Figure A6-4:

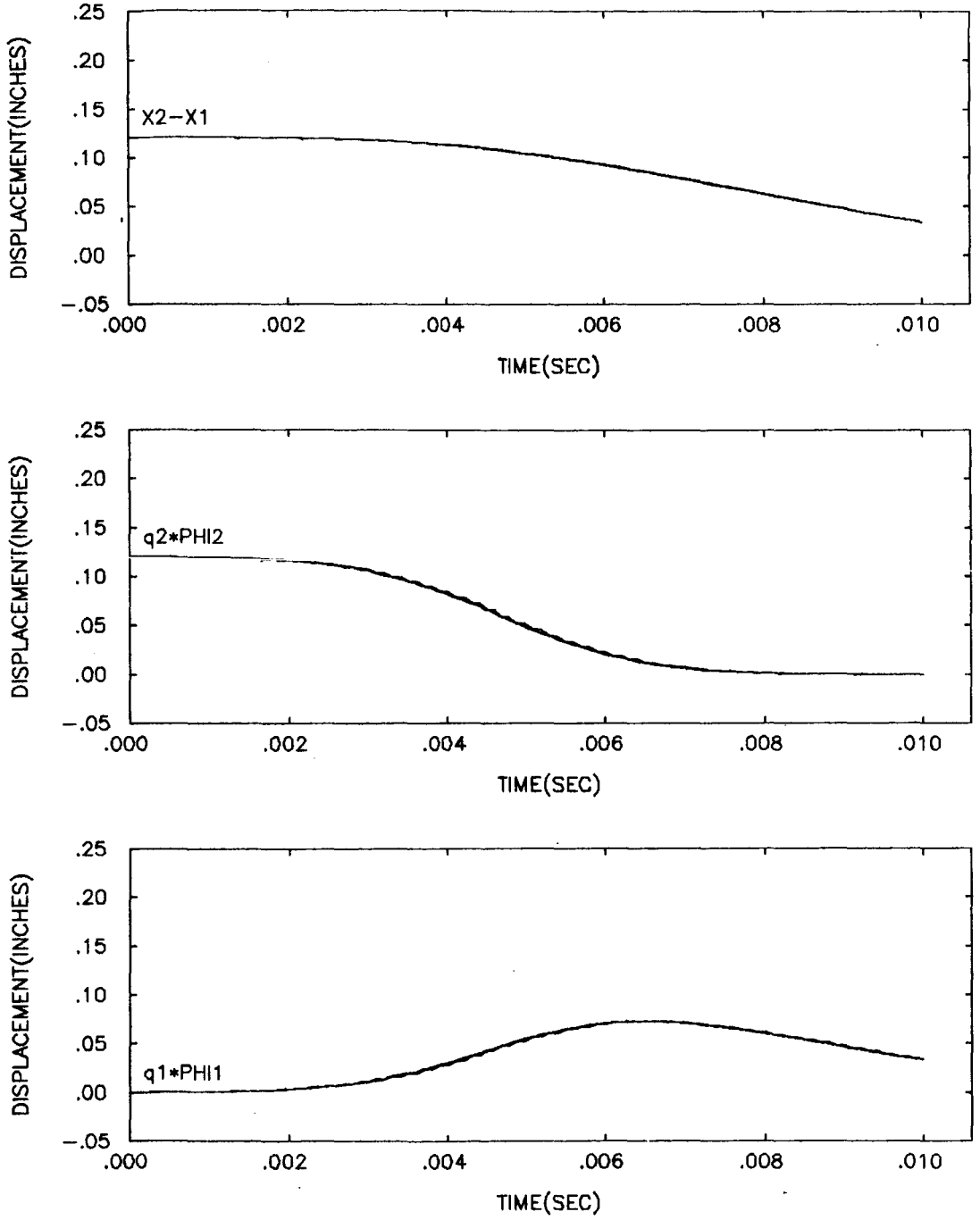

VEL= 40.0 IN/SEC ; MASS= 1.0 ; BEAM LENGTH= 0.5 IN

DYNAMIC RESPONSE OF MESHING CANTILEVER BEAMS, NO INERTIA (VEL=CONST)

Figure A6-5:

APPENDIX 7

Dynamic Response Algorithm for Meshing Cantilever Beam

1. Massless Configuration
2. Inertia of Beam Included

```
C*********************************************
C  THIS PROGRAM SOLVES THE EQUATION OF MOTION  *
C  DESCRIBING A PAIR OF MESHING CANTILEVER     *
C  BEAMS ATTACHED TO MOVEABLE FOUNDATAION      *
C  MASSES.  THE SECOND ORDER DIFFERENTIAL      *
C  EQUATION: M(D2X/DT2) +KX = P   IS WRITTEN   *
C  AS A FIRST ORDER DIFFEQ AND INTEGRATED      *
C  USING A 4TH ORDER "RUNGE-KUTTA" INTEGRA-    *
C  TION ROUTINE.                               *
C*********************************************
      EXTERNAL FCT,OUTP
      DIMENSION Y(4),DERY(4),PRMT(5),AUX(8,4)
      REAL P,L,BA,VEL,M1,M2,MASS,INERT,K1,K2,STIFF,MOD,STIFF1
      COMMON P,L,VEL,MASS,INERT,K1,K2,STIFF,MOD,ZETA1,ZETA2,TF,DENOM
      WRITE(6,*) 'ENTER: APPLIED LOAD, BEAM LENGTH, BASE WIDTH'
      READ(5,*) P,L,BA
      WRITE(6,*) 'ENTER: VELOCITY, MASS#1, MASS#2'
      READ(5,*) VEL,M1,M2
      MOD=30.E6
      INERT=(1./12.)*BA*BA**3
      ZETA1=L/10.
      ZETA2=9.*L/10.
      K1=(3.*MOD*INERT)/(ZETA1**3)
      K2=(3.*MOD*INERT)/(ZETA2**3)
      STIFF=(K1*K2)/(K1+K2)
      STIFF1=STIFF
      WRITE(6,*) 'APPLIED LOAD      :',P
      WRITE(6,*) 'BEAM LENGTH       :',L
      WRITE(6,*) 'BASE WIDTH        :',BA
      WRITE(6,*) 'MASS #1           :',M1
      WRITE(6,*) 'MASS #2           :',M2
      WRITE(6,*) 'VELOCITY          :',VEL
      Y(1)=0.0
      Y(2)=P/STIFF
      DERY(1)=0.5
      DERY(2)=0.5
      PRMT(1)=0.0
      PRMT(2)=(.8*L)/VEL
      PRMT(3)=PRMT(2)/5000.
      WRITE(6,*) 'STARTING TIME:    ',PRMT(1)
      WRITE(6,*) 'ENDING TIME:      ',PRMT(2)
      WRITE(6,*) 'TIME INCREMENT:   ',PRMT(3)
      PRMT(4)=0.0001
      NDIM=2
      MASS=(M1*M2)/(M1+M2)
      TIME=0.0
      CALL RKGS(PRMT,Y,DERY,NDIM,IHLF,FCT,OUTP,AUX)
*********************************************************
*********************************************************
      SUBROUTINE FCT(T,Y,DERY)
      DIMENSION Y(4),DERY(4)
      REAL P,L,BA,VEL,M1,M2,MASS,INERT,K1,K2,STIFF,MOD
      COMMON P,L,VEL,MASS,INERT,K1,K2,STIFF,MOD,ZETA1,ZETA2,TF,DENOM
      ZETA1=(L/10.)+T*VEL
      ZETA2=(9.*L/10.)-T*VEL
      K1=(3.*MOD*INERT)/(ZETA1**3)
      K2=(3.*MOD*INERT)/(ZETA2**3)
      STIFF=(K1*K2)/(K1+K2)
      DERY(1)=(P-STIFF*Y(2))/MASS
```

```
      DERY(2)=Y(1)
      DENOM=1.+(ZETA1**3/ZETA2**3)
      RETURN
      END
*******************************************************
*******************************************************
      SUBROUTINE OUTP(T,Y,DERY,IHLF,NDIM,PRMT)
      DIMENSION Y(4),DERY(4)
      COMMON P,L,VEL,MASS,INERT,K1,K2,STIFF,MOD,ZETA1,ZETA2,TF,DENOM
      DELTA2=Y(2)/DENOM
      DELTA1=Y(2)-DELTA2
      WRITE(15,*) T,Y(2),DELTA1,DELTA2
      RETURN
      END
*******************************************************
*******************************************************
C  THE SUBROUTINE "RKGS" (RUNGE-KUTTA) IS INCLUDED
C  IN THE NEXT PROGRAM
C                                                                      RKG
C     ................................................................RKG
C                                                                      RKG
C        SUBROUTINE RKGS                                               RKG
C                                                                      RKG
C        PURPOSE                                                       RKG
C           TO SOLVE A SYSTEM OF FIRST ORDER ORDINARY DIFFERENTIAL     RKG
C           EQUATIONS WITH GIVEN INITIAL VALUES.                       RKG
C                                                                      RKG
C        USAGE                                                         RKG
C           CALL RKGS (PRMT,Y,DERY,NDIM,IHLF,FCT,OUTP,AUX)             RKG
C           PARAMETERS FCT AND OUTP REQUIRE AN EXTERNAL STATEMENT.     RKG
C                                                                      RKG
C        DESCRIPTION OF PARAMETERS                                     RKG
C           PRMT   - AN INPUT AND OUTPUT VECTOR WITH DIMENSION GREATER RKG
C                    OR EQUAL TO 5, WHICH SPECIFIES THE PARAMETERS OF  RKG
C                    THE INTERVAL AND OF ACCURACY AND WHICH SERVES FOR RKG
C                    COMMUNICATION BETWEEN OUTPUT SUBROUTINE (FURNISHED RKG
C                    BY THE USER) AND SUBROUTINE RKGS. EXCEPT PRMT(5)  RKG
C                    THE COMPONENTS ARE NOT DESTROYED BY SUBROUTINE    RKG
C                    RKGS AND THEY ARE                                 RKG
C           PRMT(1)- LOWER BOUND OF THE INTERVAL (INPUT),              RKG
C           PRMT(2)- UPPER BOUND OF THE INTERVAL (INPUT),              RKG
100:>TERVAL (INPUT),                RKGS 220
C           PRMT(2)- UPPER BOUND OF THE INTERVAL
```

```
C*********************************************
C  THIS PROGRAM SOLVES A SYSTEM OF 5 LINEAR   *
C  DIFFERENTIAL EQUATIONS DESCRIBING THE      *
C  DYNAMIC RESPONSE OF TWO COUPLED CANTILEVER *
C  BEAMS WITH A MOVING LOAD BETWEEN THEM.     *
C*********************************************
C
      EXTERNAL FCT,OUTP
      DIMENSION FUNC(10),Y(8),DERY(8),PRMT(5),AUX(8,8),A(5,5)
      REAL MOD,INERT,M1,M2,MB1,MB2,S1,S2,OMEG,IPHI1,IPHI2
      REAL I2PHI1,I2PHI2,LAMBDA,LENG
      COMMON IPHI1,IPHI2,BETA,CONST,S1,S2,M1,M2,MB1,MB2,VEL
     $,LAMBDA,ZETA1,ZETA2,I2PHI1,I2PHI2,LENG,PHI1,PHI2,DZZ
      WRITE(6,*) 'ENTER APPLIED LOAD(lbs),AND SPEED OF MOVING LOAD'
      READ(5,*) P,VEL
      WRITE(6,*) 'ENTER BEAMLENGTH(in),AND BASE THICKNESS(in)'
      READ(5,*) LENG,THICK
      WRITE(6,*) 'ENTER MASSES: M1,M2, AND DENSITY OF BEAM(lbs/in3)'
      READ(5,*) M1,M2,DENS
      MOD=30.E6
      LC=0
      INERT=(1./12.)*THICK**4
      DENS=(DENS/386.4)*THICK**2
      WRITE(6,*) 'APPLIED LOAD:  ',P
      WRITE(6,*) 'VELOCITY    :  ',VEL
      WRITE(6,*) 'BEAM LENGTH :  ',LENG
      WRITE(6,*) 'THICKNESS   :  ',THICK
      WRITE(6,*) 'MASS/UNIT   :  ',DENS
C
C****  ONE TERM OF THE NATURAL MODE SERIES IS USED  ******
C
      OMEG=(1.875**2)*(MOD*INERT/(DENS*LENG**4))**0.5
      BETA=(((OMEG**2)*DENS)/(MOD*INERT))**0.25
      WRITE(6,*) 'OMEGA=',OMEG,'  BETA=',BETA
C
C****  EVALUATE THE CONSTANT TERMS IN MODE EQUATION  ******
C
      X=BETA*LENG
      S1=SIN(X)-SINH(X)
      S2=COS(X)+COSH(X)
      WRITE(6,*) 'S1=',S1,'  S2=',S2
C
C****  EVALUATE CONSTANT OF INTEGRATION OF MODE EQUATION ****
C****  INTEGRATE USING SIMPSON'S RULE - 100 INCREMENTS*****
C
      XINC=LENG/100.
      ZETA=0.0
      XFACT=0.0
      DO 10 I=2,100,2
        DO 20 J=1,3
          ZETA=XINC*(I-2)+XINC*(J-1)
          X=BETA*ZETA
          FUNC(J)=S1**2*(SIN(X)**2+SINH(X)**2-2.*SIN(X)*SINH(X))
     $+S2**2*(COS(X)**2+COSH(X)**2-2.*COS(X)*COSH(X))
     $+2.*S1*S2*(SIN(X)*COS(X)-SIN(X)*COSH(X)-COS(X)*SINH(X)
     $+SINH(X)*COSH(X))
20      CONTINUE
        XFACT=XFACT+(XINC/3.)*(FUNC(1)+4.*FUNC(2)+FUNC(3))
10    CONTINUE
```

```
      CONST=-(1./(DENS*XFACT))**0.5
      WRITE(6,*) 'CONST=',CONST
C
C****  EVALUATE INTEGRAL OF MODE SHAPE: IPHI1=IPHI2****
C
      XINC=LENG/100.
      ZETA=0.0
      XFACT=0.0
      DO 30 I=2,100,2
        DO 40 J=1,3
          ZETA=XINC*(I-2)+XINC*(J-1)
          X=ZETA*BETA
          FUNC(J)=(S1*(SIN(X)-SINH(X))+S2*(COS(X)-COSH(X)))
40      CONTINUE
        XFACT=XFACT+(XINC/3.)*(FUNC(1)+4.*FUNC(2)+FUNC(3))
30    CONTINUE
      IPHI1=DENS*XFACT*CONST
      IPHI2=IPHI1
      WRITE(6,*) 'IPHI1=IPHI2=',IPHI1
C
C****  EVALUATE INTEGRAL OF (D2PHI/DZETA2)**2: I2PHI  ****
C
      XINC=LENG/100.
      ZETA=0.0
      XFACT=0.0
      DO 50 I=2,100,2
        DO 60 J=1,3
          ZETA=XINC*(I-2)+XINC*(J-1)
          X=ZETA*BETA
          FUNC(J)=(S1**2*(SIN(X)**2+SINH(X)**2
     $+2.*SIN(X)*SINH(X))+S2**2*(COS(X)**2+COSH(X)**2
     $+2.*COS(X)*COSH(X))+2.*S1*S2*(SIN(X)*COS(X)+SIN(X)*COSH(X)
     $+COS(X)*SINH(X)+COSH(X)*SINH(X)))
60        CONTINUE
        XFACT=XFACT+(XINC/3.)*(FUNC(1)+4.*FUNC(2)+FUNC(3))
50    CONTINUE
      I2PHI1=XFACT*MOD*INERT*CONST**2*BETA**4
      I2PHI2=I2PHI1
      WRITE(6,*) 'I2PHI1=I2PHI2=',I2PHI1
C
      MB1=DENS*LENG
      MB2=MB1
      ZETA1=LENG/10.
      ZETA2=.9*LENG
      X1=ZETA1*BETA
      X2=ZETA2*BETA
      PHI1=CONST*(S1*(SIN(X1)-SINH(X1))+S2*(COS(X1)-COSH(X1)))
      PHI2=CONST*(S1*(SIN(X2)-SINH(X2))+S2*(COS(X2)-COSH(X2)))
      WRITE(6,*) 'PHI1=',PHI1,' PHI2=',PHI2
      DZ=VEL
      DZZ=0.0
      D1PHI1=CONST*BETA*DZ*(S1*(COS(X1)-COSH(X1))
     $-S2*(SIN(X1)+SINH(X1)))
      D1PHI2=CONST*BETA*(-DZ)*(S1*(COS(X2)-COSH(X2))
     $-S2*(SIN(X2)+SINH(X2)))
C
C**** DEFINE THE INITIAL VALUES OF THE DEPENDENT VARIABLES **
C
      Y(3)=P*PHI1/I2PHI1
```

```
      Y(4)=P*PHI2/I2PHI2
      Y(1)=0.0
      Y(2)=Y(1)+PHI1*Y(3)+PHI2*Y(4)
      Y(7)=0.0
      Y(8)=0.0
      Y(5)=0.0
      Y(6)=Y(5)+Y(3)*D1PHI1+Y(4)*D1PHI2
      WRITE(6,*) 'Y(1)=',Y(1)
      WRITE(6,*) 'Y(2)=',Y(2)
      WRITE(6,*) 'Y(3)=',Y(3)
      WRITE(6,*) 'Y(4)=',Y(4)
      DO 55 I=1,8
        DERY(I)=1./8.
55    CONTINUE
      PRMT(1)=0.0
      PRMT(2)=.8*LENG/(VEL)
      PRMT(3)=(PRMT(2)-PRMT(1))/100.
      PRMT(4)=0.0001
      NDIM=8
      CALL RKGS(PRMT,Y,DERY,NDIM,IHLF,FCT,OUTP,AUX)
*********************************************
*********************************************
      SUBROUTINE FCT(T,Y,DERY)
      DIMENSION Y(8),DERY(8),A(5,5),B(5)
      REAL MOD,INERT,M1,M2,MB1,MB2,S1,S2,OMEG,IPHI1,IPHI2
      REAL I2PHI1,I2PHI2,LAMBDA,LENG
      COMMON IPHI1,IPHI2,BETA,CONST,S1,S2,M1,M2,MB1,MB2,VEL
     $,LAMBDA,ZETA1,ZETA2,I2PHI1,I2PHI2,LENG,PHI1,PHI2,DZZ
      ZETA1=(LENG/10.)+VEL*T
      ZETA2=(.9*LENG)-VEL*T
      X1=ZETA1*BETA
      X2=ZETA2*BETA
C
C****  EVALUATE MODE SHAPE EQUATIONS AT EACH LOAD POSITION  ***
C
      PHI1=CONST*(S1*(SIN(X1)-SINH(X1))+S2*(COS(X1)-COSH(X1)))
      PHI2=CONST*(S1*(SIN(X2)-SINH(X2))+S2*(COS(X2)-COSH(X2)))
C
      IF(LC.GT.10) GO TO 71
      WRITE(6,*) '**********TIME=',T
C****  EVALUATE DERIVATIVES OF MODE SHAPE EQUATIONS  ****
C
71    DZ=VEL
      DZZ=0.0
      D1PHI1=CONST*BETA*DZ*(S1*(COS(X1)-COSH(X1))
     $-S2*(SIN(X1)+SINH(X1)))
      D1PHI2=CONST*BETA*(-DZ)*(S1*(COS(X2)-COSH(X2))
     $-S2*(SIN(X2)+SINH(X2)))
      D2PHI1=CONST*BETA*(S1*(-BETA*DZ**2*SIN(X1)+DZZ*COS(X1)
     $-BETA*DZ**2*SINH(X1)-DZZ*COSH(X1))-S2*(BETA*DZ**2*COS(X1)
     $+DZZ*SIN(X1)+BETA*DZ**2*COSH(X1)+DZZ*SINH(X1)))
      D2PHI2=CONST*BETA*(S1*(-BETA*DZ**2*SIN(X2)+DZZ*COS(X2)
     $-BETA*DZ**2*SINH(X2)-DZZ*COSH(X2))-S2*(BETA*DZ**2*COS(X2)
     $+DZZ*SIN(X2)+BETA*DZ**2*COSH(X2)+DZZ*SINH(X2)))
C
C****  DEFINE MATRIX COEFFICIENTS  A[5,5]  ****
C
      A(1,1)=M1+MB1
      A(2,1)=0.0
```

```
      A(3,1)=IPHI1
      A(4,1)=0.0
      A(5,1)=-1.
      A(1,2)=0.0
      A(2,2)=M2+MB2
      A(3,2)=0.0
      A(4,2)=-IPHI2
      A(5,2)=1.0
      A(1,3)=IPHI1
      A(2,3)=0.0
      A(3,3)=1.0
      A(4,3)=0.0
      A(5,3)=-PHI1
      A(1,4)=0.0
      A(2,4)=-IPHI2
      A(3,4)=0.0
      A(4,4)=1.0
      A(5,4)=-PHI2
      A(1,5)=1.0
      A(2,5)=-1.0
      A(3,5)=PHI1
      A(4,5)=PHI2
      A(5,5)=0.0
C
C****  DEFINE RIGHT HAND SIDE  B[5]  *******
C
      B(1)=-P
      B(2)=P
      B(3)=-I2PHI1*Y(3)
      B(4)=-I2PHI2*Y(4)
      B(5)=D2PHI1*Y(3)+D2PHI2*Y(4)+2.*D1PHI1*Y(7)+2.*D1PHI2*Y(8)
      IF(LC.GT.10) GO TO 1
      DO 63 I=1,5
63    WRITE(6,*) A(I,1),A(I,2),A(I,3),A(I,4),A(I,5),B(I)
1     LC=LC+1
      N=5
      CALL SIMQ(A,B,N,KS)
      IF(KS.EQ.1) WRITE(6,*) 'NO SOLUTION!!!!!!'
      IF(LC.GT.10) GO TO 64
      WRITE(6,*) 'BACK FROM SIMQ [B]'
      DO 64 I=1,5
      WRITE(6,*) B(I)
64    CONTINUE
      DERY(1)=Y(5)
      DERY(2)=Y(6)
      DERY(3)=Y(7)
      DERY(4)=Y(8)
      DERY(5)=B(1)
      DERY(6)=B(2)
      DERY(7)=B(3)
      DERY(8)=B(4)
      LAMBDA=B(5)
      IF(LC.GT.10) GO TO 62
      DO 61 I=1,8
61    WRITE(6,*) 'Y(',I,')=',Y(I)
62    RETURN
      END
**************************************************
**************************************************
```

```
      SUBROUTINE OUTP(T,Y,DERY,IHLF,NDIM,PRMT)
      DIMENSION Y(8),DERY(8),PRMT(5)
      REAL MOD,INERT,M1,M2,MB1,MB2,S1,S2,OMEG,IPHI1,IPHI2
      REAL I2PHI1,I2PHI2,LAMBDA,LENG
      COMMON IPHI1,IPHI2,BETA,CONST,S1,S2,M1,M2,MB1,MB2,VEL
     $,LAMBDA,ZETA1,ZETA2,I2PHI1,I2PHI2,LENG,PHI1,PHI2,DZZ
      ZETA1=(LENG/10.)+VEL*T
      ZETA2=(.9*LENG)-VEL*T
      X1=ZETA1*BETA
      X2=ZETA2*BETA
      PHI1=CONST*(S1*(SIN(X1)-SINH(X1))+S2*(COS(X1)-COSH(X1)))
      PHI2=CONST*(S1*(SIN(X2)-SINH(X2))+S2*(COS(X2)-COSH(X2)))
      WRITE(15,*) T,Y(2)-Y(1),Y(3)*PHI1,Y(4)*PHI2
      WRITE(6,*) 'ACCEL=',DZZ
      RETURN
      END
***********************************************
***********************************************
C
C ..............................................................
C
C  SUBROUTINE SIMQ
C
C  PURPOSE
C     OBTAIN SOLUTION OF A SET OF SIMULTANEOUS LINEAR EQUATIONS,
C     AX=B
C
C  USAGE
C     CALL SIMQ(A,B,N,KS)
C
C  DESCRIPTION OF PARAMETERS
C     A - MATRIX OF COEFFICIENTS STORED COLUMNWISE.  THESE ARE
C         DESTROYED IN THE COMPUTATION.  THE SIZE OF MATRIX A IS
C         N BY N.
C     B - VECTOR OF ORIGINAL CONSTANTS (LENGTH N). THESE ARE
C         REPLACED BY FINAL SOLUTION VALUES, VECTOR X.
C     N - NUMBER OF EQUATIONS AND VARIABLES. N MUST BE .GT. ONE.
C     KS - OUTPUT DIGIT
C          0 FOR A NORMAL SOLUTION
C          1 FOR A SINGULAR SET OF EQUATIONS
C
C  REMARKS
C     MATRIX A MUST BE GENERAL.
C     IF MATRIX IS SINGULAR , SOLUTION VALUES ARE MEANINGLESS.
C     AN ALTERNATIVE SOLUTION MAY BE OBTAINED BY USING MATRIX
C     INVERSION (MINV) AND MATRIX PRODUCT (GMPRD).
C
C  SUBROUTINES AND FUNCTION SUBPROGRAMS REQUIRED
C     NONE
C
C  METHOD
C     METHOD OF SOLUTION IS BY ELIMINATION USING LARGEST PIVOTAL
C     DIVISOR. EACH STAGE OF ELIMINATION CONSISTS OF INTERCHANGING
C     ROWS WHEN NECESSARY TO AVOID DIVISION BY ZERO OR SMALL
C     ELEMENTS.
C     THE FORWARD SOLUTION TO OBTAIN VARIABLE N IS DONE IN
C     N STAGES. THE BACK SOLUTION FOR THE OTHER VARIABLES IS
C     CALCULATED BY SUCCESSIVE SUBSTITUTIONS. FINAL SOLUTION
C     VALUES ARE DEVELOPED IN VECTOR B, WITH VARIABLE 1 IN B(1),
```

```
C     VARIABLE 2 IN B(2),....., VARIABLE N IN B(N).
C     IF NO PIVOT CAN BE FOUND EXCEEDING A TOLERANCE OF 0.0,
C     THE MATRIX IS CONSIDERED SINGULAR AND KS IS SET TO 1. THIS
C     TOLERANCE CAN BE MODIFIED BY REPLACING THE FIRST STATEMENT.
C
C ..................................................................
C
      SUBROUTINE SIMQ(A,B,N,KS)
      DIMENSION A(1),B(1)
C
C        FORWARD SOLUTION
C
      TOL=0.0
      KS=0
      JJ=-N
      DO 65 J=1,N
      JY=J+1
      JJ=JJ+N+1
      BIGA=0
      IT=JJ-J
      DO 30 I=J,N
C
C        SEARCH FOR MAXIMUM COEFFICIENT IN COLUMN
C
      IJ=IT+I
      IF(ABS(BIGA)-ABS(A(IJ))) 20,30,30
   20 BIGA=A(IJ)
      IMAX=I
   30 CONTINUE
C
C        TEST FOR PIVOT LESS THAN TOLERANCE (SINGULAR MATRIX)
C
      IF(ABS(BIGA)-TOL) 35,35,40
   35 KS=1
      RETURN
C
C        INTERCHANGE ROWS IF NECESSARY
C
   40 I1=J+N*(J-2)
      IT=IMAX-J
      DO 50 K=J,N
      I1=I1+N
      I2=I1+IT
      SAVE=A(I1)
      A(I1)=A(I2)
      A(I2)=SAVE
C
C        DIVIDE EQUATION BY LEADING COEFFICIENT
C
   50 A(I1)=A(I1)/BIGA
      SAVE=B(IMAX)
      B(IMAX)=B(J)
      B(J)=SAVE/BIGA
C
C        ELIMINATE NEXT VARIABLE
C
      IF(J-N) 55,70,55
   55 IQS=N*(J-1)
      DO 65 IX=JY,N
```

```
      IXJ=IQS+IX
      IT=J-IX
      DO 60 JX=JY,N
      IXJX=N*(JX-1)+IX
      JJX=IXJX+IT
   60 A(IXJX)=A(IXJX)-(A(IXJ)*A(JJX))
   65 B(IX)=B(IX)-(B(J)*A(IXJ))
C
C        BACK SOLUTION
C
   70 NY=N-1
      IT=N*N
      DO 80 J=1,NY
      IA=IT-J
      IB=N-J
      IC=N
      DO 80 K=1,J
      B(IB)=B(IB)-A(IA)*B(IC)
      IA=IA-N
   80 IC=IC-1
      RETURN
      END


C
C.....................................................................
C
C   SUBROUTINE RKGS
C
C   PURPOSE
C      TO SOLVE A SYSTEM OF FIRST ORDER ORDINARY DIFFERENTIAL
C      EQUATIONS WITH GIVEN INITIAL VALUES.
C
C   USAGE
C      CALL RKGS (PRMT,Y,DERY,NDIM,IHLF,FCT,OUTP,AUX)
C      PARAMETERS FCT AND OUTP REQUIRE AN EXTERNAL STATEMENT.
C
C   DESCRIPTION OF PARAMETERS
C      PRMT   - AN INPUT AND OUTPUT VECTOR WITH DIMENSION GREATER
C               OR EQUAL TO 5, WHICH SPECIFIES THE PARAMETERS OF
C               THE INTERVAL AND OF ACCURACY AND WHICH SERVES FOR
C               COMMUNICATION BETWEEN OUTPUT SUBROUTINE (FURNISHED
C               BY THE USER) AND SUBROUTINE RKGS. EXCEPT PRMT(5)
C               THE COMPONENTS ARE NOT DESTROYED BY SUBROUTINE
C               RKGS AND THEY ARE
C      PRMT(1)- LOWER BOUND OF THE INTERVAL (INPUT),
C      PRMT(2)- UPPER BOUND OF THE INTERVAL (INPUT),
C      PRMT(3)- INITIAL INCREMENT OF THE INDEPENDENT VARIABLE
C               (INPUT),
C      PRMT(4)- UPPER ERROR BOUND (INPUT). IF ABSOLUTE ERROR IS
C               GREATER THAN PRMT(4), INCREMENT GETS HALVED.
C               IF INCREMENT IS LESS THAN PRMT(3) AND ABSOLUTE
C               ERROR LESS THAN PRMT(4)/50, INCREMENT GETS DOUBLED.
C               THE USER MAY CHANGE PRMT(4) BY MEANS OF HIS
C               OUTPUT SUBROUTINE.
C      PRMT(5)- NO INPUT PARAMETER. SUBROUTINE RKGS INITIALIZES
C               PRMT(5)=0. IF THE USER WANTS TO TERMINATE
C               SUBROUTINE RKGS AT ANY OUTPUT POINT, HE HAS TO
C               CHANGE PRMT(5) TO NON-ZERO BY MEANS OF SUBROUTINE
```

```
C               OUTP. FURTHER COMPONENTS OF VECTOR PRMT ARE
C               FEASIBLE IF ITS DIMENSION IS DEFINED GREATER
C               THAN 5. HOWEVER SUBROUTINE RKGS DOES NOT REQUIRE
C               AND CHANGE THEM. NEVERTHELESS THEY MAY BE USEFUL
C               FOR HANDING RESULT VALUES TO THE MAIN PROGRAM
C               (CALLING RKGS) WHICH ARE OBTAINED BY SPECIAL
C               MANIPULATIONS WITH OUTPUT DATA IN SUBROUTINE OUTP.
C     Y       - INPUT VECTOR OF INITIAL VALUES.  (DESTROYED)
C               LATERON Y IS THE RESULTING VECTOR OF DEPENDENT
C               VARIABLES COMPUTED AT INTERMEDIATE POINTS X.
C     DERY    - INPUT VECTOR OF ERROR WEIGHTS.  (DESTROYED)
C               THE SUM OF ITS COMPONENTS MUST BE EQUAL TO 1.
C               LATERON DERY IS THE VECTOR OF DERIVATIVES, WHICH
C               BELONG TO FUNCTION VALUES Y AT A POINT X.
C     NDIM    - AN INPUT VALUE, WHICH SPECIFIES THE NUMBER OF
C               EQUATIONS IN THE SYSTEM.
C     IHLF    - AN OUTPUT VALUE, WHICH SPECIFIES THE NUMBER OF
C               BISECTIONS OF THE INITIAL INCREMENT. IF IHLF GETS
C               GREATER THAN 10, SUBROUTINE RKGS RETURNS WITH
C               ERROR MESSAGE IHLF=11 INTO MAIN PROGRAM. ERROR
C               MESSAGE IHLF=12 OR IHLF=13 APPEARS IN CASE
C               PRMT(3)=0 OR IN CASE SIGN(PRMT(3)).NE.SIGN(PRMT(2)-
C               PRMT(1)) RESPECTIVELY.
C     FCT     - THE NAME OF AN EXTERNAL SUBROUTINE USED. THIS
C               SUBROUTINE COMPUTES THE RIGHT HAND SIDES DERY OF
C               THE SYSTEM TO GIVEN VALUES X AND Y. ITS PARAMETER
C               LIST MUST BE X,Y,DERY. SUBROUTINE FCT SHOULD
C               NOT DESTROY X AND Y.
C     OUTP    - THE NAME OF AN EXTERNAL OUTPUT SUBROUTINE USED.
C               ITS PARAMETER LIST MUST BE X,Y,DERY,IHLF,NDIM,PRMT.
C               NONE OF THESE PARAMETERS (EXCEPT, IF NECESSARY,
C               PRMT(4),PRMT(5),...) SHOULD BE CHANGED BY
C               SUBROUTINE OUTP. IF PRMT(5) IS CHANGED TO NON-ZERO,
C               SUBROUTINE RKGS IS TERMINATED.
C     AUX     - AN AUXILIARY STORAGE ARRAY WITH 8 ROWS AND NDIM
C               COLUMNS.
C
C   REMARKS
C      THE PROCEDURE TERMINATES AND RETURNS TO CALLING PROGRAM, IF
C      (1) MORE THAN 10 BISECTIONS OF THE INITIAL INCREMENT ARE
C          NECESSARY TO GET SATISFACTORY ACCURACY (ERROR MESSAGE
C          IHLF=11),
C      (2) INITIAL INCREMENT IS EQUAL TO 0 OR HAS WRONG SIGN
C          (ERROR MESSAGES IHLF=12 OR IHLF=13),
C      (3) THE WHOLE INTEGRATION INTERVAL IS WORKED THROUGH,
C      (4) SUBROUTINE OUTP HAS CHANGED PRMT(5) TO NON-ZERO.
C
C   SUBROUTINES AND FUNCTION SUBPROGRAMS REQUIRED
C      THE EXTERNAL SUBROUTINES FCT(X,Y,DERY) AND
C      OUTP(X,Y,DERY,IHLF,NDIM,PRMT) MUST BE FURNISHED BY THE USER.
C
C   METHOD
C      EVALUATION IS DONE BY MEANS OF FOURTH ORDER RUNGE-KUTTA
C      FORMULAE IN THE MODIFICATION DUE TO GILL. ACCURACY IS
C      TESTED COMPARING THE RESULTS OF THE PROCEDURE WITH SINGLE
C      AND DOUBLE INCREMENT.
C      SUBROUTINE RKGS AUTOMATICALLY ADJUSTS THE INCREMENT DURING
C      THE WHOLE COMPUTATION BY HALVING OR DOUBLING. IF MORE THAN
C      10 BISECTIONS OF THE INCREMENT ARE NECESSARY TO GET
```

```
C       SATISFACTORY ACCURACY, THE SUBROUTINE RETURNS WITH
C       ERROR MESSAGE IHLF=11 INTO MAIN PROGRAM.
C       TO GET FULL FLEXIBILITY IN OUTPUT, AN OUTPUT SUBROUTINE
C       MUST BE FURNISHED BY THE USER.
C       FOR REFERENCE, SEE
C       RALSTON/WILF, MATHEMATICAL METHODS FOR DIGITAL COMPUTERS,
C       WILEY, NEW YORK/LONDON, 1960, PP.110-120.
C
C.....................................................................
C
      SUBROUTINE RKGS (PRMT,Y,DERY,NDIM,IHLF,FCT,OUTP,AUX)
C
C
      DIMENSION Y(1),DERY(1),AUX(8,1),A(4),B(4),C(4),PRMT(1)
      DO 1 I=1,NDIM
    1 AUX(8,I)=.06666667*DERY(I)
      X=PRMT(1)
      XEND=PRMT(2)
      H=PRMT(3)
      PRMT(5)=0.
      CALL FCT(X,Y,DERY)
C
C     ERROR TEST
      IF(H*(XEND-X))38,37,2
C
C     PREPARATIONS FOR RUNGE-KUTTA METHOD
    2 A(1)=.5
      A(2)=.2928932
      A(3)=1.707107
      A(4)=.1666667
      B(1)=2.
      B(2)=1.
      B(3)=1.
      B(4)=2.
      C(1)=.5
      C(2)=.2928932
      C(3)=1.707107
      C(4)=.5
C
C     PREPARATIONS OF FIRST RUNGE-KUTTA STEP
      DO 3 I=1,NDIM
      AUX(1,I)=Y(I)
      AUX(2,I)=DERY(I)
      AUX(3,I)=0.
    3 AUX(6,I)=0.
      IREC=0
      H=H+H
      IHLF=-1
      ISTEP=0
      IEND=0
C
C
C     START OF A RUNGE-KUTTA STEP
    4 IF((X+H-XEND)*H)7,6,5
    5 H=XEND-X
    6 IEND=1
C
C     RECORDING OF INITIAL VALUES OF THIS STEP
    7 CALL OUTP(X,Y,DERY,IREC,NDIM,PRMT)
```

```
      IF(PRMT(5))40,8,40
    8 ITEST=0
    9 ISTEP=ISTEP+1
C
C
C     START OF INNERMOST RUNGE-KUTTA LOOP
      J=1
   10 AJ=A(J)
      BJ=B(J)
      CJ=C(J)
      DO 11 I=1,NDIM
      R1=H*DERY(I)
      R2=AJ*(R1-BJ*AUX(6,I))
      Y(I)=Y(I)+R2
      R2=R2+R2+R2
   11 AUX(6,I)=AUX(6,I)+R2-CJ*R1
      IF(J-4)12,15,15
   12 J=J+1
      IF(J-3)13,14,13
   13 X=X+.5*H
   14 CALL FCT(X,Y,DERY)
      GOTO 10
C     END OF INNERMOST RUNGE-KUTTA LOOP
C
C
C     TEST OF ACCURACY
   15 IF(ITEST)16,16,20
C
C     IN CASE ITEST=0 THERE IS NO POSSIBILITY FOR TESTING OF ACCURACY
   16 DO 17 I=1,NDIM
   17 AUX(4,I)=Y(I)
      ITEST=1
      ISTEP=ISTEP+ISTEP-2
   18 IHLF=IHLF+1
      X=X-H
      H=.5*H
      DO 19 I=1,NDIM
      Y(I)=AUX(1,I)
      DERY(I)=AUX(2,I)
   19 AUX(6,I)=AUX(3,I)
      GOTO 9
C
C     IN CASE ITEST=1 TESTING OF ACCURACY IS POSSIBLE
   20 IMOD=ISTEP/2
      IF(ISTEP-IMOD-IMOD)21,23,21
   21 CALL FCT(X,Y,DERY)
      DO 22 I=1,NDIM
      AUX(5,I)=Y(I)
   22 AUX(7,I)=DERY(I)
      GOTO 9
C
C     COMPUTATION OF TEST VALUE DELT
   23 DELT=0.
      DO 24 I=1,NDIM
   24 DELT=DELT+AUX(8,I)*ABS(AUX(4,I)-Y(I))
      IF(DELT-PRMT(4))28,28,25
C
C     ERROR IS TOO GREAT
   25 IF(IHLF-10)26,36,36
```

```
   26 DO 27 I=1,NDIM
   27 AUX(4,I)=AUX(5,I)
      ISTEP=ISTEP+ISTEP-4
      X=X-H
      IEND=0
      GOTO 18
C
C     RESULT VALUES ARE GOOD
   28 CALL FCT(X,Y,DERY)
      DO 29 I=1,NDIM
      AUX(1,I)=Y(I)
      AUX(2,I)=DERY(I)
      AUX(3,I)=AUX(6,I)
      Y(I)=AUX(5,I)
   29 DERY(I)=AUX(7,I)
      CALL OUTP(X-H,Y,DERY,IHLF,NDIM,PRMT)
      IF(PRMT(5))40,30,40
   30 DO 31 I=1,NDIM
      Y(I)=AUX(1,I)
   31 DERY(I)=AUX(2,I)
      IREC=IHLF
      IF(IEND)32,32,39
C
C     INCREMENT GETS DOUBLED
   32 IHLF=IHLF-1
      ISTEP=ISTEP/2
      H=H+H
C       TO STOP AT INPUT DELT: IF(IHLF) 4,33,33
      IF(IHLF) 4,33,33
   33 IMOD=ISTEP/2
      IF(ISTEP-IMOD-IMOD)4,34,4
   34 IF(DELT-.02*PRMT(4))35,35,4
   35 IHLF=IHLF-1
      ISTEP=ISTEP/2
      H=H+H
      GOTO 4
C
C
C     RETURNS TO CALLING PROGRAM
   36 IHLF=11
      CALL FCT(X,Y,DERY)
      GOTO 39
   37 IHLF=12
      GOTO 39
   38 IHLF=13
   39 CALL OUTP(X,Y,DERY,IHLF,NDIM,PRMT)
   40 RETURN
      END
```

★U.S GOVERNMENT PRINTING OFFICE: 1 9 8 7-7 4 8-1 2 0/6 0 4 0 7

NASA
National Aeronautics and Space Administration

Report Documentation Page

1. Report No.	2. Government Accession No.	3. Recipient's Catalog No.
NASA CR-179643 AVSCOM TR-87-C-23		

4. Title and Subtitle

An Investigation of the Dynamic Response of Spur Gear Teeth With Moving Loads

5. Report Date

August 1987

6. Performing Organization Code

7. Author(s)

C.E. Passerello and L.W. Shuey

8. Performing Organization Report No.

None

10. Work Unit No.

1L161102AH45
505-63-51

9. Performing Organization Name and Address

Michigan Technological University
Department of Mechanical Engineering and Engineering Mechanics
Houghton, Michigan 49931

11. Contract or Grant No.

NAG 3-344

13. Type of Report and Period Covered

Contractor Report
Final

12. Sponsoring Agency Name and Address

U.S. Army Aviation Research and Technology Activity - AVSCOM, Propulsion Directorate, Lewis Research Center, Cleveland, Ohio 44135 and NASA Lewis Research Center, Cleveland, Ohio 44135

14. Sponsoring Agency Code

15. Supplementary Notes

Project Manager, John J. Coy, Propulsion Directorate, U.S. Army Aviation Research and Technology Activity - AVSCOM, Lewis Research Center, Cleveland, Ohio 44135.

16. Abstract

In this investigation, two concepts relating to gear dynamics were studied. The first phase of the analysis involved the study of the effect of the speed of a moving load on the dynamic deflections of a gear tooth. A single spur gear tooth modelled using finite elements was subjected to moving loads with variable velocities. The tooth tip deflection time histories were plotted, from which it was seen that the tooth tip deflection consisted of a quasistatic response with an oscillatory response superimposed on it whose amplitude was dependent on the type of load engagement. Including the rim in the analysis added flexibility to the model but did not change the general behavior of the system. The second part of the analysis involved an investigation to determine the effect on the dynamic response of the inertia of the gear tooth. A simplified analysis using meshing cantilever beams was used. In one case, the beams were assumed massless, in the other, the mass (inertia) of the beams were included. From this analysis it was found that the inertia of the tooth did not affect the dynamic response of meshing cantilever beams.

17. Key Words (Suggested by Author(s))	18. Distribution Statement
Gears; Vibration; Noise; Machine design; Finite element analysis	Unclassified - unlimited STAR Category 37

19. Security Classif. (of this report)	20. Security Classif. (of this page)	21. No of pages	22. Price*
Unclassified	Unclassified	237	A11

NASA FORM 1626 OCT 86

*For sale by the National Technical Information Service, Springfield, Virginia 22161